THE ALIGNMENT OF FERROELECTRIC LIQUID CRYSTALS AND ITS AFFECT ON DEVICE ~~PERFORMANCE~~ CHARACTERISTICS

Submitted by

CAROLYN BOWRY

to University College London
as a thesis for the degree of
Doctor of Philosophy

June 1989

Dedicated to:
My Grandfather, Father and Sister
who led the way
and to my Mother.

CONTENTS

ABSTRACT

This thesis explores the problem of uniformly aligning Ferroelectric Liquid Crystals (FLCs) over large areas whilst retaining bistability. A novel high tilt alignment (HTA) is presented and its electro-optic performance is compared to the traditional surface stabilised (SS) alignment using three different devices; test cells, displays and all-fibre optic devices.

Evidence is presented to show that the SS alignment has a small surface pretilt of the director which reduces the number of zig-zag defects in parallel aligned cells. This is related to the layer structure and a review of the latest proposed structures of SS devices is presented. The HTA device is shown to have many advantages over the SS device; no zig-zag defects, excellent bistability in up to 6 μm thick cells, good mechanical stability and excellent viewing characteristics when multiplexed. These properties are explored and culminate in the production of two FLC displays, one HTA and one SS aligned. The properties of these displays are compared.

In order to improve the appearance and frame time of the displays, multiplexing schemes were investigated, including a novel two slot scheme that was successfully used to drive both displays. It was found that the SS display could be driven in a reverse contrast mode by taking advantage of the relaxation process. This decreased the line address time and produced a higher contrast display.

A nematic LC all-fibre optic polariser was produced with excellent extinction ratio (45 dB) and low loss (0.2 dB) using evanescent field

coupling. A nematic LC modulator was then demonstrated using a novel electrode arrangement. A modulation depth of 28 dB was achieved using low voltages (~10V) but with <100 Hz modulation frequency. By using a FLC modulator this was increased to >10 kHz but the modulation depth was poor (8.2 dB) because of the unsuitable refractive indices. The potential and uses of LC all-fibre optic devices are discussed.

ACKNOWLEDGEMENTS

I would like to thank many people for their help and contributions to this work. I particularly wish to thank Dr Garath Parry for the continued guidance, enthusiasm and motivation he has given me. He has encouraged me to develop links with the University that have enabled me to gain much more out of this work than just a thesis.

I am grateful to Prof. Mike Clark and Prof. Cyril Hilsum who started me on this course. I particularly thank Prof. Mike Clark for his continued support and contributions throughout. I am also grateful to my colleagues at GEC Hirst Research Centre who have contributed to this work; Drs. Beatrice Nicholas and Alan Mosley for their advice on alignment, multiplexing and displays, Pat Rundle for all the electronics he has built for the project, Marie Bunce and David Grant for fabricating the test cells and displays, and Dr Mike Wiltshire for his advice on optics modelling.

My work with Zachos Ioannidis has been particularly enjoyable and I thank him for all the help he has given me on fibre optics. I also thank Dr Ian Giles for allowing me to do this work at University College London.

I would like to thank Tony Bowry and Nicola Bowry for building the electronics that enabled the FLC displays to be produced and for their continued personal support and guidance. I am especially grateful to Nicola for patiently drawing the figures for me. I am indebted to Lynda Ball who has cheerfully typed this thesis. Finally, I thank GEC for allowing me to do this work and for their financial support.

CHAPTER 1

INTRODUCTION

The expansion of the electronics market in the last twenty years has created a need for large area flat panel displays. The increasing complexity of electronic products necessarily dictates a more complex human-machine interface. The interactive display is perceived not only as simplifying the process of putting information into machines, but also as becoming an integral part of the machine. These displays must therefore have the ability to change information, be compact, have a low power consumption, be lightweight yet rugged and withstand extreme environmental conditions. The liquid crystal display (LCD) is at present the only display capable of meeting all these requirements.

It is this need for flat panel displays that has been the driving force behind the recent research into liquid crystals (LC). Small area devices have, of course, been available for many years. One of the major problems in liquid crystal research has been the scaling up of the small area devices. For the standard nematic displays the relaxation of the director coupled with an rms response to voltage means that the contrast and viewing angle decreases rapidly as the display becomes more complex. This can be overcome by adding memory to each pixel using a thin film transistor (TFT) to capacitively hold the voltage across the pixel for the required time. The 'active matrix' technology is successful and such displays are currently being marketed. However, the production of a large area array of TFTs is a complex and expensive process. The ideal solution is to find a LC material with inherent memory. Such materials are found in the class of LCs which are

ferroelectric. The bistability of ferroelectric liquid crystals (FLC), coupled with the fast response times enables complex, large area displays to be produced without the need for TFT arrays, making the display simpler and less expensive. It is these properties which motivate the research into FLCs for use in displays. It has also been realised that such a material with a large electro-optic coefficient, bistability and fast switching can also be used in other electro-optic devices, for example in shutters, spatial light modulators, nonlinear optics, fibre optic switches, fibre optic polarisers and beam deflectors. The promise of sub-microsecond switching in such devices using the electroclinic effect has also revived research interest in this effect.

This thesis addresses the important problem of aligning ferroelectric liquid crystals over large areas. When this work started in 1985, FLC materials had been studied for over ten years, but very few room temperature materials were available. A 'surface stabilised' (SS) device had been demonstrated five years previously but the difficulty in producing good alignment over large areas had been limiting the production of displays. Although the SS device was bistable it always relaxed to an intermediate state when the voltage was removed. This created problems in driving FLC displays and in understanding the device.

The availability of FLC materials that align well increased dramatically once it was realised that the helical pitch had to be fully unwound at the smectic-nematic transition. Such materials have been used in this work to investigate the affect of the material properties and the aligning agent, on the bistability, switching speed and display

performance. In order to improve the bistability a new alignment was proposed by Professor M G Clark which I have referred to as the high tilt alignment (HTA) (Chapter 3). This alignment has been investigated for device applications and compared with the traditional surface stabilised (SS) alignment (Chapter 4).

In 1985 there was still no demonstration of a large area FLC display. Not only was good alignment and bistabilty of the display difficult to achieve but multiplexing FLC to produce fast switching and a good contrast was not as easy as it had first appeared. A few multiplexing drive schemes existed but they only worked with certain materials and alignments and even then the contrast was not good. In order to make a FLC display it was necessary to analyse how the material and alignment (both SS and HTA) affected the multiplexing of the display and to generate improved multiplexing schemes for driving the display (Chapter 5). The best scheme was then used in the demonstration of two 6 cm x 6 cm, 92 x 92 line FLC displays, one based on the SS alignment and the other based on the HTA. The performance of the two displays has been compared.

The current state-of-the-art in FLC displays has been the production of 2 μm thick, A4, 600 x 400 pixel displays by companies such as Seiko and Toshiba using the traditional SS alignment. At present these have a poor contrast and do not work at video frame rate. To improve the display appearance of SS devices it is necessary to produce 1.5 μm thick cells. A5 displays at 1.5 μm have been produced by Leti and STC using etched pillars as spacers rather than the more common method of randomly scattered fibre spacers. These displays do look better and can produce

video frame rates although they need to work at elevated temperatures (>30°C). However the best contrast demonstrated using a FLC has been in an HTA display.

The use of FLC in devices other than displays is also important. The electro-optic properties of FLCs have been exploited in this work to produce a FLC fibre optic modulator (Chapter 6). Prior to this work all liquid crystal fibre optic modulators that had been reported had used nematics with unsuitable refractive indices and complex electrode patterns. A new nematic material with well suited refractive indices has been used in this work to demonstrate a low loss polariser. A simple ITO electrode structure was then used to create a nematic modulator. Two FLC devices were then demonstrated using the SS and HTA alignments. These show that fast switching could be achieved but due to the high refractive indices of the FLC material the modulation depth was small. The potential and limitations of such devices are discussed.

Since the number of applications is increasing, the need to know more about the fundamental properties of FLC materials and devices is growing. One of the most important areas, which is highlighted by this work, is the need to analyse the director and layer structure of the LC in different alignments. At present there are many techniques being used; X-ray diffraction to analyse the layer structure, surface plasmon coupling and second harmonic generation are being used to study surfaces and dielectric and optical studies are being used to analyse the director configuration. All these methods help to build up an overall picture of the device structure. It is an exciting time to be working

in FLCs since an increased fundamental understanding coupled with improved manufacturing techniques should bring FLC displays and switching devices into the market within the next two years.

CHAPTER 2

PROPERTIES OF FERROELECTRIC LIQUID CRYSTALS

In order to realise the importance of ferroelectric liquid crystals (FLC) it is necessary to understand the phenomenon of liquid crystallinity and the phenomenon of ferroelectricity. Although FLCs are essentially another class of liquid crystal material and are therefore more related to these than crystal ferroelectrics, measurement techniques are taken from both subjects.

Ferroelectricity was first observed by Valasek [1920] who discovered that when an electric field was applied to Rochelle salt (potassium tartrate tetrahydrate, $NaKC_4H_4O_6.4H_2O$) there was an hysteresis effect due to a polarisation reversal. This polarisation reversal induced an electric current which was originally called Seignette electricity after the chemist who first made Rochelle salt [Lines and Glass 1977]. The polarisation arose from the spontaneous alignment of the permanent dipoles, the movement of which were limited by the crystal lattice to produce bistability. This alignment occurs below a particular temperature which is called the Curie temperature, T_C. A material is defined as being ferroelectric when it has two or more stable orientational states in the absence of an electric field and can be switched between these states by an electric field.

Ferroelectric materials are a subset of a larger class of materials that are called piezoelectric. Piezoelectricity was discovered forty years prior to ferroelectricity by J and P Curie [1880] and is the production of an electric current by the application of stress. The applied stress

disrupts the permanent dipoles along a particular direction inducing a moving dipole moment with its associated dipole current. When the stress is thermally induced the phenomenon is called pyroelectricity.

Rochelle salt remained the only example of ferroelectricity until 1935 when Busch and Scherrer [1935] produced the first series of ferroelectric materials from phosphates and arsenates, the most common being potassium dihydrogen phosphate (kH_2PO_4 abbreviated to KDP). Other ferroelectric materials remained elusive for such a long time because of the formation of differently oriented domains in the crystals which produced a zero overall dipole. These domains form to reduce the overall energy of the crystal sample and have to be aligned in the same direction to observe a bulk ferroelectric effect. Where two different oriented domains meet, a domain wall is formed with its own internal energy. It was not until the 1950s that materials with dielectric anomalies were looked at for their ferroelectric properties. This exposed many new materials as being ferroelectric and the interest in this phenomenon grew accordingly.

In 1955 it was realised that materials could also have the permanent dipoles aligned antiparallel rather than parallel. These materials are called antiferroelectrics. The ammonium salt ADP ($NH_4.H_2PO_4$) is antiferroelectric and although it has no ferroelectricity it has very strong piezoelectric properties. Its 30% electro-mechanical coupling efficiency at room temperature makes it an excellent transducer and it was used as the principal sound transducer and submarine detector in world war II.

The large polarisabilities, dielectric constant and piezoelectric constant of ferroelectric crystals initially made them candidates for a variety of applications; sonar detectors, transducers, pickups, non-linear optics, infrared detection and imaging, switches, memory devices and displays. However, the practical problems of using these materials have made them unattractive for most applications. Ferroelectric crystals are not only difficult to prepare but they can also be unreliable and they have very complex microscopic processes that are difficult to control. In addition they also need a large voltage to switch the dipoles between states, despite having a large polarisation. The main area that ferroelectric crystals are still used is in non-linear optics because of their large hyperpolarisabilities, e.g. electro-optic switches for telecommunications and frequency doubling of lasers. Other types of ferroelectric materials such as semiconductors, ceramics, polymers and liquid crystals, can have properties more suited to widespread applications. In particular ceramics such as PLZT are used because they are easier to make and use than their crystal counterparts.

The phenomenon of liquid crystallinity has been known longer than ferroelectricity, in fact since 1888 when Reinitzer [1888] discovered optical activity in cholesterol benzoate. However it was not until 1975 that Meyer et al [1975] predicted from symmetry considerations that a ferroelectric liquid crystal (FLC) could exist and the first FLC material, DOBAMBC, was synthesised. There were previous reports of nematic liquid crystals with electrical properties similar to ferroelectricity but these were just anomalous dielectric effects [Williams and Heilmeier 1966]. It took five more years before the

potential of these new materials as a display device was demonstrated by Clark and Lagerwall [1980] which sparked off the large research interest that now exists.

The potential of these materials stems from the low voltage required to reverse the spontaneous polarisation (P_S), the bistability and the large electro-optic effect that is induced. They are also cheap and easy to make compared with other ferroelectric materials. FLCs are therefore ideal candidates for large area electro-optic devices such as flat panel displays, shutters and spatial light modulators. The disadvantage FLCs have is that they switch a thousand times more slowly than crystal ferroelectrics because the switching is molecular rather than electronic. Also the order parameter of liquid crystals is less than crystals which causes the P_S to be smaller (a thousand times less than for crystals). This makes FLCs less interesting for replacement crystal devices in non-linear optical applications and ceramic devices such as transducers. However the switching speed of ferroelectric liquid crystals is a thousand times faster than nematic liquid crystals and FLCs have the additional advantage of bistability. This enables FLCs to improve on many existing liquid crystal applications.

2.1 Classification of Liquid Crystals

A liquid crystal, or mesomorphic, is a state of matter that exists between a solid and an isotropic liquid. The material has a degree of order which gives it crystalline properties such as birefringence and anisotropic dielectric constant but the molecules are free to move with respect to each other giving flowing liquid properties. Liquid crystal (LC) phases form in materials which under certain conditions co-operatively align to form a director. The director is the time

average direction of the optic axes of the molecules and the order parameter S indicates the degree of alignment of the molecules in this direction. In an isotropic liquid $S=0$, in a crystal $S=1$, and in a liquid crystal $0<S<1$. The order parameter is represented by

$$S = \frac{1}{2} <3\cos^2\theta - 1>$$

where θ is the angle between the long axes of the molecule and the director [Saupe 1972].

There are two types of liquid crystals, thermotropic which form the mesomorphic state within a certain temperature range and lyotropic which form the mesophase at a certain concentration of the molecules in a solvent. Amphillic lyotropics are organic molecules containing a hydrophillic and hydrophobic part such as a soap. For example as the concentration of soap in water increases it changes from a suspension, to a liquid crystal then to a solid. Other lyotropics are found in disc shape structures such as chromoniums [Cox et al 1971] which are dye molecules and rod shape structures such as the tobacco mosaic virus [Luzzati 1963]. The importance of lyotropics is in the large scale manufacture of some organic compounds (e.g. soaps) and in biological systems where they occur in abundance [Small 1969].

Thermotropic liquid crystals are the type used in electro-optic devices. There are many types of thermotropics, the most common being rod shape organic molecules made from a rigid aromatic core and flexible carbon chain end groups. Other types of thermotropics include:

(i) Discotic phases [Chandrasekhar 1983]; these are disc shape molecules that can either align with the discs in the same plane or form columnar phases where the discs pile on top of each other into columns which become the director

(ii) Polymer LCs [For a review see Ciferri et al 1982]; these have the electro-optic properties of low molar mass LC but also have the handling properties of polymers, so that free standing films can be made. There are two types of LC polymer, main chain polymers that are used to make high tensile strength materials such as Kevlar, and side chain polymers which are mainly being investigated for optical storage and non-linear optics using the thermo-optic and aligning properties of these materials.

(iii) Hydrocarbon oil based products [Byrne et al 1987]; when small chain hydrocarbons are heated they can change from an isotropic liquid to a LC. This is opposite to the more common LC thermotropic materials and is caused by cross linking occurring as the material is heated making the molecules larger and more rod like, therefore allowing a LC phase to form.

Thermotropics were classified into three classes by Friedel [1922]: nematic, cholesteric and smectic (Figure 2.1). Nematics (N) have a director but the centres of gravity of the molecules are randomly placed. The term nematic means thread like and originated from the thready textures seen in nematics when viewed through crossed polarisers. When a nematic has optical activity the material develops a spontaneous helical structure normal to the director with a

Figure 2.1: The classification of liquid crystals

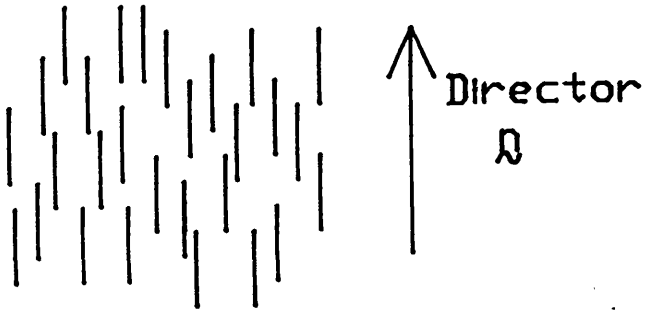

The arrangement of molecules in the nematic mesophase.

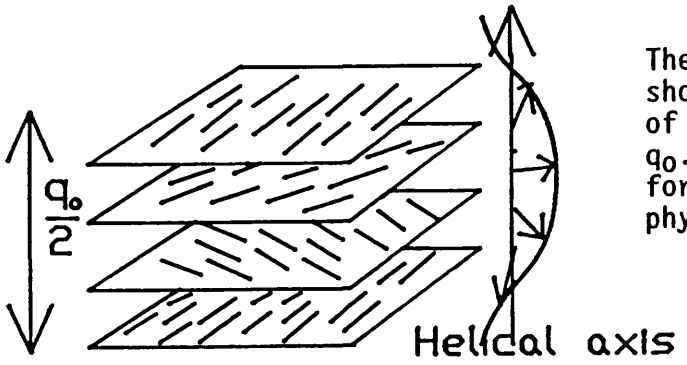

The cholesteric mesophase showing the helical rotation of the director with a pitch q_o. (The planes are drawn for clarification but have no physical meaning).

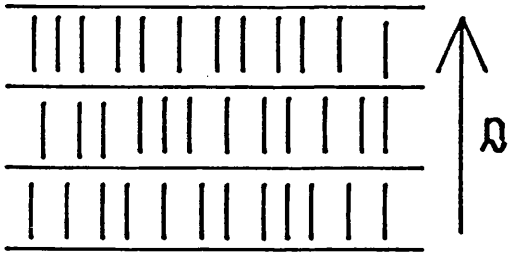

An orthogonal smectic phase (the layers are not distinct as shown but are mass density waves).

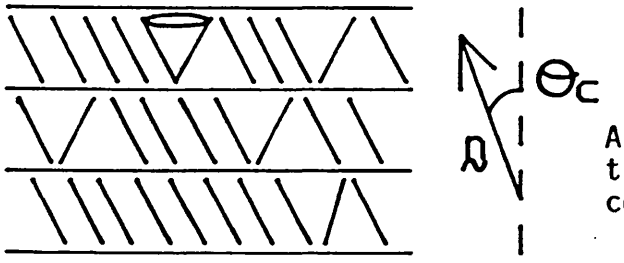

A tilted smectic phase with tilt angle θ_c showing the cone of possible rotation.

characteristic pitch q_0. This is the cholesteric phase (N*) which derives its name from the first material observed with this property, cholesterol benzoate.

As the LC becomes more ordered layers develop in the form of a mass density wave. This is called the smectic phase. The name is the Greek word for 'soap' and was derived from the soapy appearance of the first known smectic materials. There are many different types of smectic phases which are classified from A to K [Gray and Goodby 1984] where A is the least ordered and K is the most ordered (Figure 2.2). Materials G,H,J and K have sufficient order to be classified as plastic crystals rather than liquid crystals.

There are two types of smectic phases; orthogonal and tilted. The orthogonal phases have the director perpendicular to the layers and follow a sequence,

I-N-S_A-S_B-S_E-crystal

The S_A phase has no positional order within the layers whereas the S_B and S_E phases have a two dimensional hexagonal packing within the layers. The tilted phases have the director at a temperature dependent angle to the layers and follow a sequence

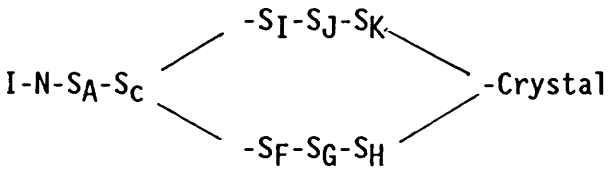

Figure 2.2: Classification of smectic liquid crystals [Gray and Goodby 1984]

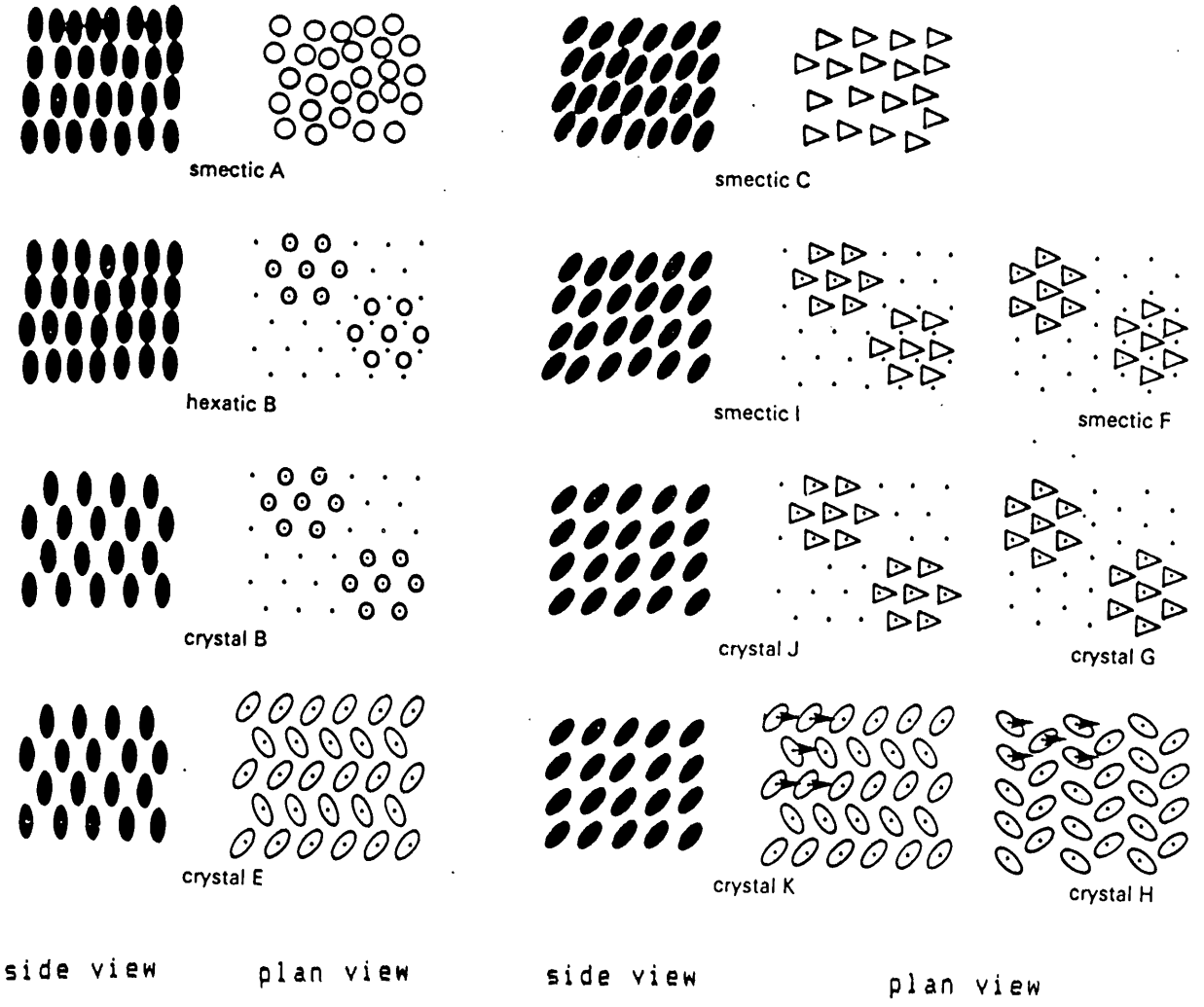

In analogy to the orthogonal phases, the S_C phase has no positional order within the layers and the S_I and S_F phases have a more ordered 2D hexagonal packing within the layers. The S_J, S_K, S_G and S_H can be considered to have a 3D packing with an order parameter less than one. The director in the tilted phases precesses around a cone with half angle θ_C from the layer normal.

Any given material can possess more than one mesophase, these are called polymesomorphic. A polymesomorph (or polymorph) must follow the order of the sequence shown above (although phases can be skipped) unless it has a re-entrant phase (e.g. I-N-S_A-N-S_B) which occurs in some mixtures of materials [Prost 1980].

There is one other identified smectic phase, the S_D that exists between the S_A and S_C phase. This does not have a layered structure but has a three dimensional structure while not being viscous. This has been reported [Etherington et al 1986] to have a cubic structure but with a poor order parameter, although there may be some miscellar or discotic behaviour. The true nature of this phase is not yet known and it may be another class of liquid crystal.

The tilted phases can also be optically active and therefore possess a helical structure. It is these chiral tilted smectic phases that have monoclinic symmetry producing ferroelectricity. Of these ferroelectric phases it is the S_C* phase that has created the most interest for its use in FLC displays. This material is the least ordered and has the lowest viscosity, and therefore has the fastest switching time.

2.2 The symmetry of ferroelectric liquid crystal phases

Ferroelectricity occurs when there is a finite average electric dipole throughout the phase. The material requires that no symmetry operations exist that can remove this dipole. The tilted smectic phases can be considered, in crystallographic terms, as having monoclinic symmetry (C_2h) containing a two fold rotation axis, a mirror plane and a centre of inversion (Figure 2.3). In the non-chiral phases all these operations are allowed so that dipoles can exist in opposite directions cancelling out any overall dipole. To make the material ferroelectric the mirror plane and centre of inversion must be removed. This is achieved by removing one of the enantiomorphs therefore making the material chiral and leaving the phase with a C_2 symmetry. A possible reason for the removal of the centre of inversion is shown in Figure 2.4 (proposed by Raynes [1987]). The inverted molecule distorts the molecular arrangement in the layer which costs energy. The more favoured position is when there is a uniform layer with no inverted molecules. Rotation about the two fold rotation axis (x-axis) does not need to be removed because there is no steric hindrance and the dipole can remain in the same direction allowing the material to have a spontaneous polarisation (P_S).

The chirality of the ferroelectric phases induces a precession of the director about the cone with a characteristic pitch P_0 (Figure 2.5). The axis of the helical pitch is parallel to the layer normal which is perpendicular to the pitch in the cholesteric phase. This also rotates the molecular dipole which cancels out the P_S. To create a permanent polarisation the pitch must be unwound by an electric or magnetic field, by shearing or, more commonly, by surface forces (surface forces are

Figure 2.3: The allowed symmetry operations (C_2h) in tilted smectic phases. In ferroelectric phases (C_2) only the two fold rotation axis can remain.

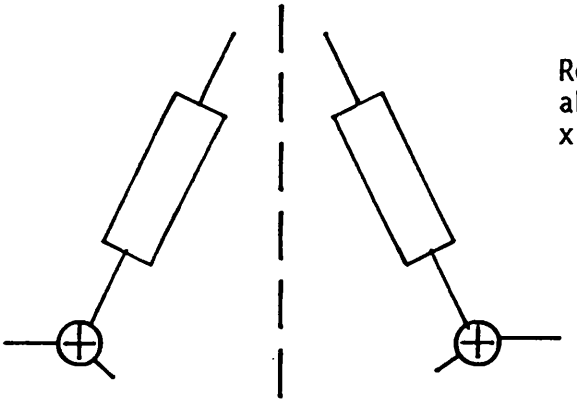

Mirror plane
(removed by inducing chirality)

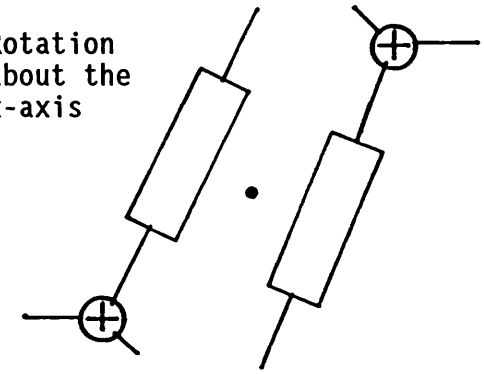

Two fold rotation axis
(remains in ferroelectric phases)

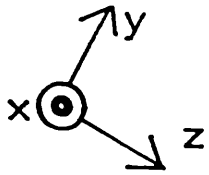

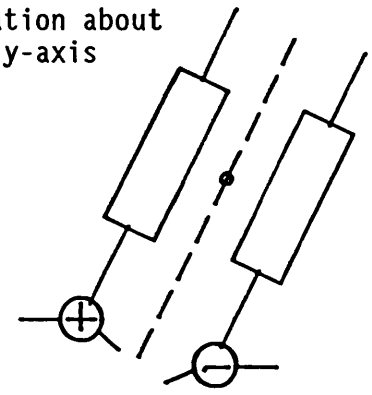

Centre of inversion
(removed in chiral phases)

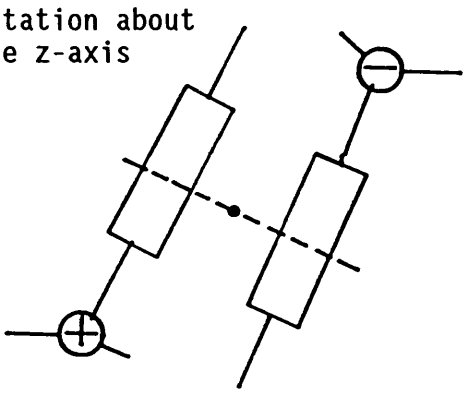

Centre of inversion
(removed in chiral phases)

Figure 2.4: Loss of inversion in ferroelectric phases [Raynes 1987]

A centre of inversion causes distortion of the layers due to steric hindrance.

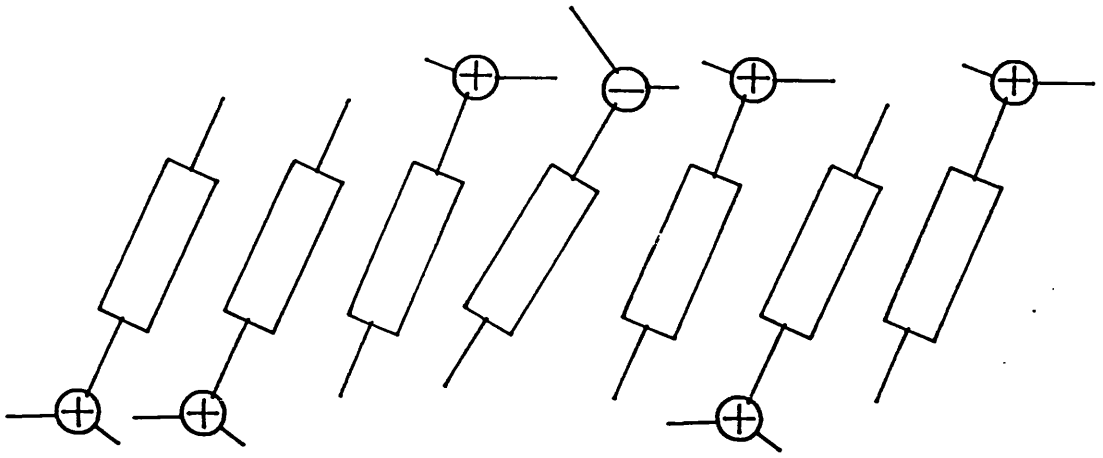

Figure 2.5: The pitch (P_0) in chiral smectic phases

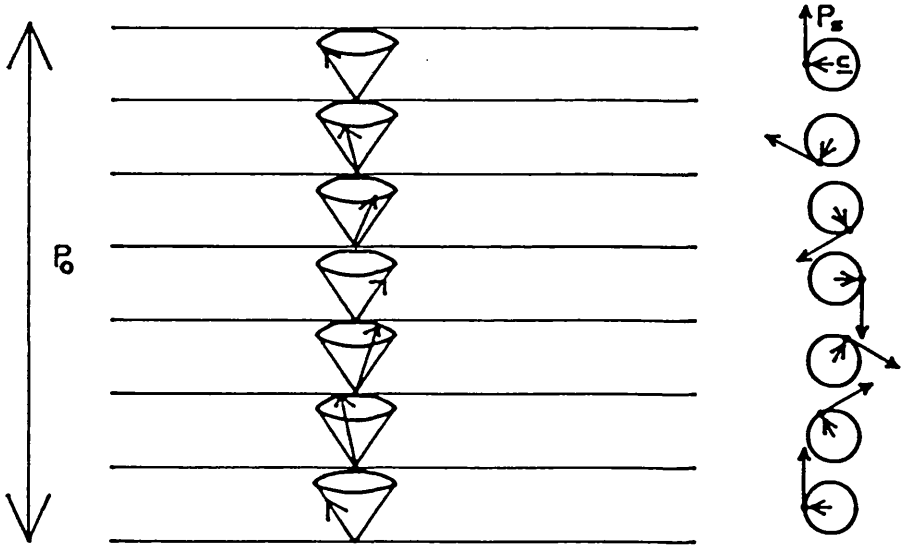

Position of director $\underline{n}$ on cone

Position of $\underline{c}$ vector and P_S dipole on cone (2π rotation).

also used to induce bistability). According to De Gennes [1974] the period of the pitch is given as $2\pi/P_o$, not π/q_o as in cholesterics, since $\underline{c} \neq -\underline{c}$. The $\underline{c}$ director is orthogonal to the P_S and the layer normal axis z, it therefore rotates by 2π during one precession of the director around the cone. The period is much larger than the interlayer distance and need not be commensurate.

FLCs are unlike crystal ferroelectrics because they have a pitch which must be removed before a P_S can be produced. There is also a continuous degeneracy of the director around the cone (i.e. an easy plane) which means that there is no need for domain walls to form whereas crystal ferroelectrics have a discrete manifold of easy axes which ensure that domains form. To obtain discrete states in FLCs boundary conditions must be imposed. The influence of surface forces is generally used which induces bistability and domains. A 2 μm thick sample is the maximum thickness used in traditional SS devices in order that the surface forces are strong enough.

The comparison between crystal ferroelectrics and FLCs leads to several other conclusions. (1) The transition S_A-S_C* is a second order Curie point. (2) FLCs are improper ferroelectrics because the transition is driven by intermolecular forces inducing the tilt and is not driven by the dipole coupling. This is demonstrated by the similarity of the transition temperature T_C of the chiral and racemic versions of the same material [Meyer 1975]. This is fundamentally different from crystal ferroelectrics which are spontaneously aligned by dipole interactions. (3) The molecular tilt fluctuations at the transition are analogous to soft optical phonons in crystals. This is known as the soft mode. (4) The rotation of the director about the cone is the

goldstone mode. (5) Piezoelectric effects can easily be observed above the Curie point. When a shear force is applied to the S_A phase (especially near the S_A-S_C* transition) a tilt is induced which produces a polarisation transverse to the shear [Pieranski et al 1975]. Conversely, an electric field in the plane of the layers induces a polarization which couples to the field and tilts the director normal to the field. This is the electroclinic effect first shown by Meyer et al [1975] and studied further by Garoff and Meyer [1977] and has recently received much attention for fast switching devices [Bahr and Heppke 1987, Nishiyama et al 1987].

2.3 Ferroelectric Liquid Crystal Materials

The ability to produce marketable devices using LCs stems from the discovery by Gray et al [1973] of a family of stable (both chemically and photochemically), non-toxic, nematic liquid crystal materials, called the cyanobiphenyls (Figure 2.6). The stability comes from the lack of a linking group between the two phenyls which prior to 1972 had been present in all LC materials synthesised, in particular the unstable Stilbene linkage (-O-CH=CH-). It is well understood that nematic phases can form from rod like molecules with a rigid core and flexible end groups. Modifying the properties of the liquid crystal is achieved by changing the chain lengths, the type of groups on the molecules and the core itself. It is extremely difficult to predict the affect on the LC phase that the modification will have. The first S_C* material was reported by Meyer et al [1975], and was called p-decyloxybenzylidene p'-amino 2-methyl butyl cinnamate (DOBAMBC) (Figure 2.7). This material was far from ideal not least because of the unstable stilbene linkage.

Figure 2.6: A typical family of cyanobiphenyls that exhibit nematic behaviour

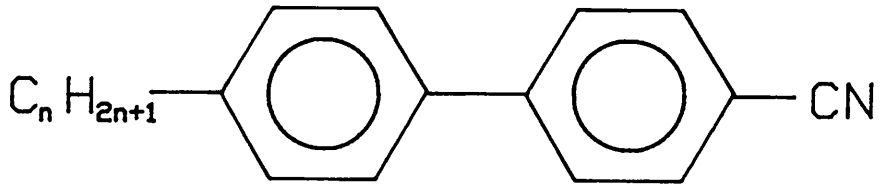

Figure 2.7: The structure of the first ferroelectric liquid crystal material, DOBAMBC (p-decyloxybenzylidene p'-amino 2-methyl butyl cinnamate)

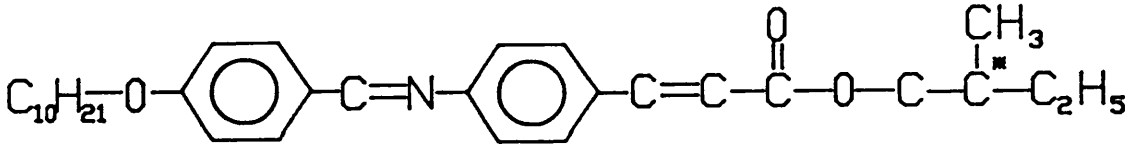

Figure 2.8: An MBF ester. The rigid core structure with alkyl chains at both ends plus a lateral dipole moment are required to form a tilted smectic phase.

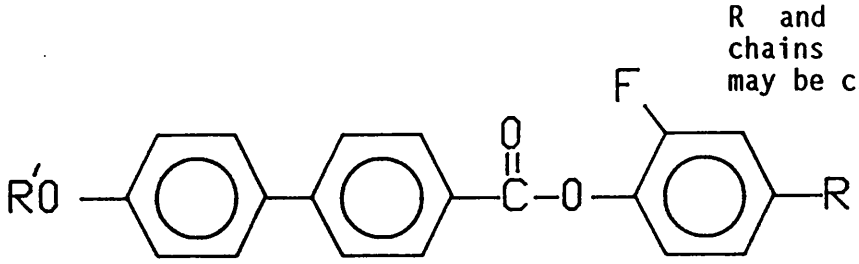

McMillan [1973] proposed that to make a material with an S_C phase a centre of symmetry was required and a large antiparallel terminal outboard dipole moment. Alternatively Wulf [1975] proposed that a zig-zag shaped molecule was required for S_C phase formation. Gray and Goodby [1976] studied esters to conclude that although large terminal outboard dipoles aided S_C formation they are not a necessity and the phases were more stable if asymmetrical chain lengths were used along with branched terminal groups. However the zig-zag model still seemed to apply reasonably well. They also found that complex core structures favour the S_C phase and 2 alkyl chains are needed at either end of the core. A suitable stable S_C LC material is a laterally fluorinated ester such as the MBF esters used by BDH [Bishop et al 1986] as shown in Figure 2.8. It has two alkyl chains either end and two outboard dipoles from the fluorine and the oxygen atoms. Other materials that are in common use and commercially available are pyrimidines [Zaschke 1975], NCBs [Eidenschink et al 1986] as used by Merck and fluoro-terphenyls currently being investigated by BDH [Chan et al 1988] (Figure 2.9).

Using liquid crystals for device applications requires the phase to exist between a certain temperature range, generally -10°C to +60°C. It is not usual for pure materials to have the required temperature range whilst retaining other desirable properties, it is therefore necessary to make mixtures. The most commonly used nematic material, E7, is a eutectic mixture of three cyanobiphenyls and a cyanoterphenyl. At the eutectic point the nematic phase is extended beyond the temperature range of both starting materials. Commercial S_C* materials are also eutectic mixtures the usual temperature range being -20°C to +60°C but the chemical formulas and compositions are not disclosed.

Most ferroelectric liquid crystal materials are polymesomorphic, the phase sequence of which is very important for aligning FLC devices. There are four possible sequences for an S_C^* material:

1. I-S_C^*. This is not polymorphic and is not desirable. It is very difficult to align because the layers and director must be aligned at the same time. Not many of these materials exist and there are none with a suitable temperature range.

2. I- S_A-S_C^*. This is also difficult to align because both the layer and director must align at the I-S_A transition.

3. I-N*-S_A-S_C^*. This is the most commonly used sequence of phases and is the easiest to align. The director aligns in the N* phase, the layers form in the S_A phase and the director tilts in the S_C^* phase in a continuous second order transition. Although these types of materials are the easiest to align they are also very temperature dependent.

4. I-N*-S_C^*. This is also difficult to align because although the director is fixed in the N^* phase, the layers must form and the director must tilt with respect to the layers at the N*-S_C^* transition (first order) and two layer directions can form. It will be shown later (Chapter 3) that this material can be used in certain alignments and may be an advantage because the cone angle, θ_C, is less temperature dependent in this type of material than in type 3.

To obtain good alignment it is also important to have a long pitch in both the N^* and S_C^* phases. Bradshaw et al [1986] showed that to align S_C^* materials a compensated N* pitch (i.e. $q_o = \infty$) near the N* - Smectic transition is more important than a large S_C^* pitch as long as the S_C^* pitch is >4d (d=thickness). Chirality is induced by including an optically active carbon atom in the molecule. A chiral carbon atom has four different groups attached and is identified by a '*' (Figure 2.7). It is common for the chirality to be induced in a stable S_C material by adding a small percentage (e.g. 10%) of a chiral dopant, (such as chiral octanol (Figure 2.10) which has a large P_S but unsuitable phase stability. This makes it easier to have the required stability and large pitch whilst retaining a large P_S. The pitch of a chiral material can easily be increased by adding suitable quantities of a similar material with a pitch of the opposite sense until the compensation point is reached when the pitch is infinite. It is difficult to adjust both the S_C^* and N* pitches of the same material to the required values, it is therefore usual for the N* phase to be compensated rather than the S_C^* phase. The S_C^* phase is more difficult to compensate because of the need for a large P_S, if two opposite enantiomorphs are mixed to an infinite pitch in the S_C^* phase then the P_S also becomes zero. This can be overcome in three ways.

1. Mix a cholesteric material in with the S_C^* material that has an opposite pitch sense. [Brunet and Williams 1978]. The S_C^* pitch can be increased and although the P_S is reduced it does remain finite.

Figure 2.9: Some typical host materials used in S_C^* mixtures

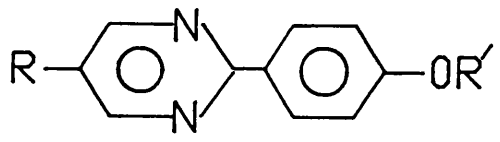

A pyrimidine

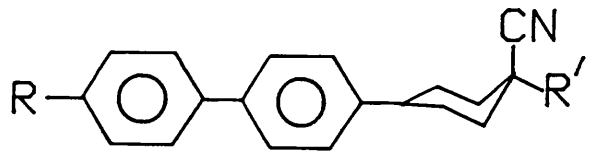

A NCB

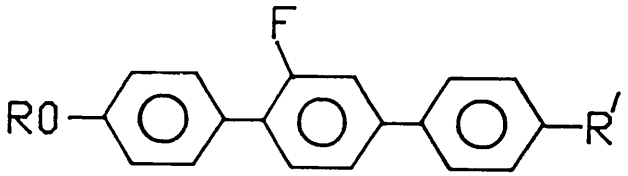

A fluoroterphenyl

R and R′ are alkyl chains one of which may be chiral

Figure 2.10: Some typical dopant materials used in S_C^* mixtures

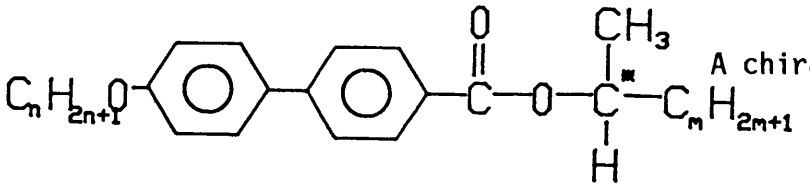

A chiral octanol dopant

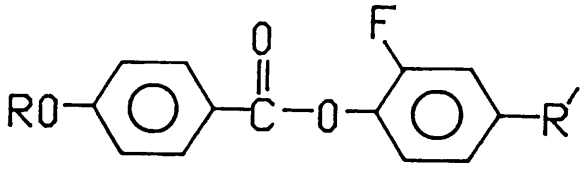

A cyano-alkyl dopant

2. Mix two S_C^* materials with opposite pitch sense but with the same P_S [Beresnev et al 1982]. Although it is difficult to find two appropriate materials to do this with it is possible to compensate the S_C^* pitch totally whilst retaining a P_S.

3. Mix two S_C^* materials with opposite pitch and opposite P_S where one has a higher P_S value. At the compensation point there will still be a finite P_S. This is the most common method because suitable materials are easier to find [Bradshaw et al 1986].

For the material to have a large P_S it not only requires a large polar group normal to the long axis of the molecule but the chiral group needs to be as close as possible to the central dipole and the core of the molecule [Goodby 1983] (which unfortunately also reduces the temperature range of the S_C phase). This reduces rotation of the dipole about the molecule therefore increasing the percentage of the dipole that contributes to the P_S. A FLC will have approximately 7-10% of the total molecular dipole moment contributing to the P_S. S_C materials have been reported with a P_S greater than 200nC/cm^2 [Dijon and Ebel 1988, Sakurai et al 1988] but then 10% is mixed into the eutectic S_C material to produce a P_S of ~20 nC/cm^2. The maximum P_S values obtained in useable S_C^* materials are ~40 nC/cm^2, this should be compared with values of 10 μC/cm^2 for crystal ferroelectrics.

Once a stable S_C^* material has been produced with the appropriate temperature range, a large N* pitch and a large P_S, then other properties can be improved upon. Some properties like the elastic and viscosity coefficients are extremely difficult to adjust for S_C^*

materials since not enough is understood about what is required and how to molecularly engineer changes. Other properties that can be controlled are the optical and dielectric constants which are both anisotropic.

The dielectric anisotropy, $\Delta\epsilon$, is mainly determined by the polar groups on the core of the molecule. If the polar group is along the axis of the molecule it has a positive $\Delta\epsilon$ such as the cyanobiphenyls. If the polar group is perpendicular to the molecular axis then the material will have a negative $\Delta\epsilon$ as long as the dielectric permittivity due to the core is less than that due to the polar group. Most FLCs have an outboard dipole moment giving a small negative $\Delta\epsilon$ between one and two.

The birefringence Δn, comes from the anisotropic polarisability of the phenyl rings in the molecule. This can be reduced by substituting the phenyl rings for less anisotropic rings such as cyclohexanes. This has been demonstrated in nematics but not in S_C^* materials as yet. Most S_C^* materials have a Δn between 0.12 and 0.2. For an S_C^* device to have maximum transmission it must satisfy the equation:-

$$\frac{\Delta n d}{\lambda} = \frac{1}{2}$$

where d is the thickness and λ is the wavelength, so for d = 2 μm and λ= 0.5 μm, Δn= 0.125. This is about the lowest value of the current S_C^* mixtures. If thicker devices are to be used then a lower birefringence will be required.

2.4 Liquid Crystal Textures

The term texture was used by Friedel [1922] to designate the picture of

a thin layer of LC observed under a microscope in polarised light. The textures seen are due to defects in the LC structure such as dislocations and disclinations (discontinuities in the director configuration). Defects in liquid crystals are larger than in solid crystals because of the elastic nature of the material and are therefore observable under a polarising microscope. Each liquid crystal phase has a distinguishing texture; Nematics form thready textures called Schlieren textures (Figure 2.11a and b) and smectics tend to form focal conics (Figure 2.11c and d) with each type of smectic phase having distinguishing focal conic features [Gray and Goodby 1984] (For more detailed information refer to Chandrasekhar [1977] and De Gennes [1974]). The S_C phase can also form a Schlieren texture if a nematic Schlieren texture exists above it. If a S_A phase is above the S_C phase then focal conics will form. Some of the basic types of defects that can occur in smectic LCs are shown in Figure 2.12. The first five defects are two dimensional and the tores and cyclide defects are three dimensional. The Schlieren texture is a combination of two dimensional disclinations and the focal conics are the three dimensional disclinations (mainly Dupin cyclides since tores are rare).

Focal conics are the textures seen when Dupin cyclides exist. The Dupin cyclide satisfies the condition that the layer thickness and parallelism must be preserved. A special case of a Dupin cyclide is a torus which are not common in liquid crystals. The layers in a Dupin cyclide are arranged in a torus so that the curvature remains the same for any one layer. The layers form a family of cyclides encasing each other (Figure 2.13) [Hartshorne and Stuart 1970, Gray and Goodby 1984].

Figure 2.11: Textures of S_C^*

Schlieren Texture

(a) Natural

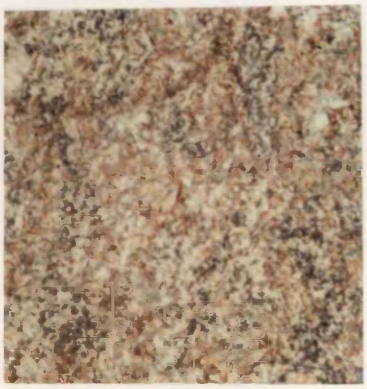

(b) Only centres with four brushes appear

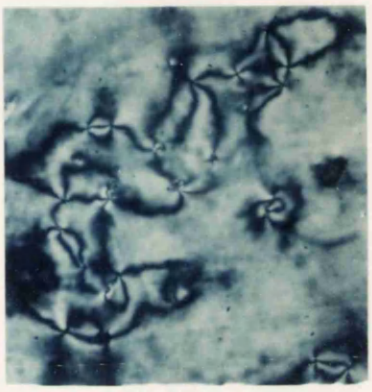

Focal Conics

(c)

(d) Banded due to pitch

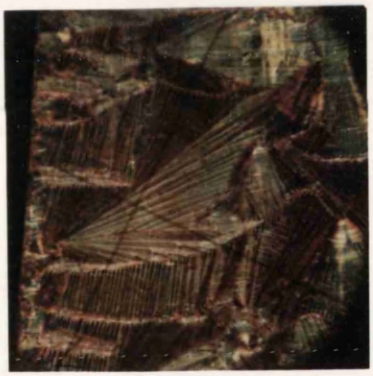

Partially Aligned (Elongated Focal Conics)

(e)

(f)

Figure 2.12: The defects found in smectics.

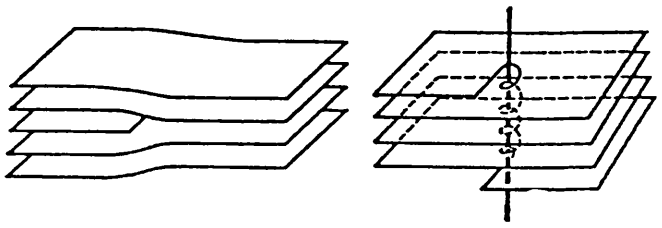

Edge dislocation Screw dislocation

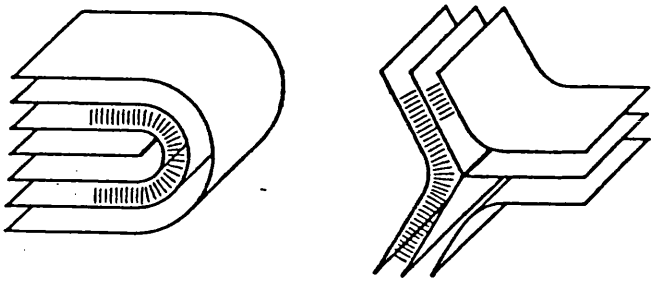

+π disclination -π disclination

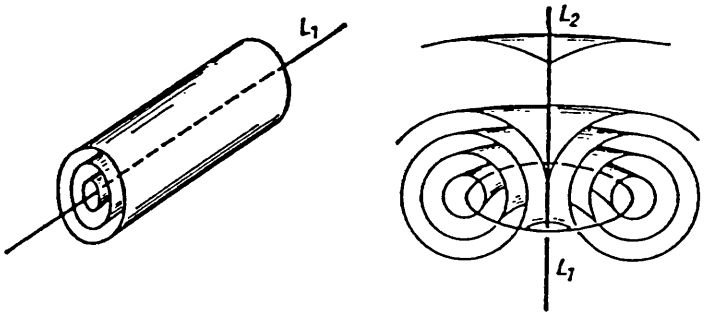

+2 π disclination Tores

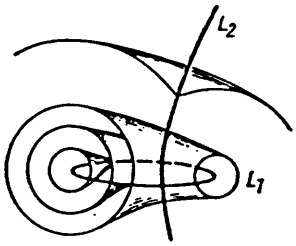

Dupin cylides

Figure 2.13: The arrangment of layers in a focal conic
[Hartshorne and Stuart 1970, Gray and Goodby 1984]

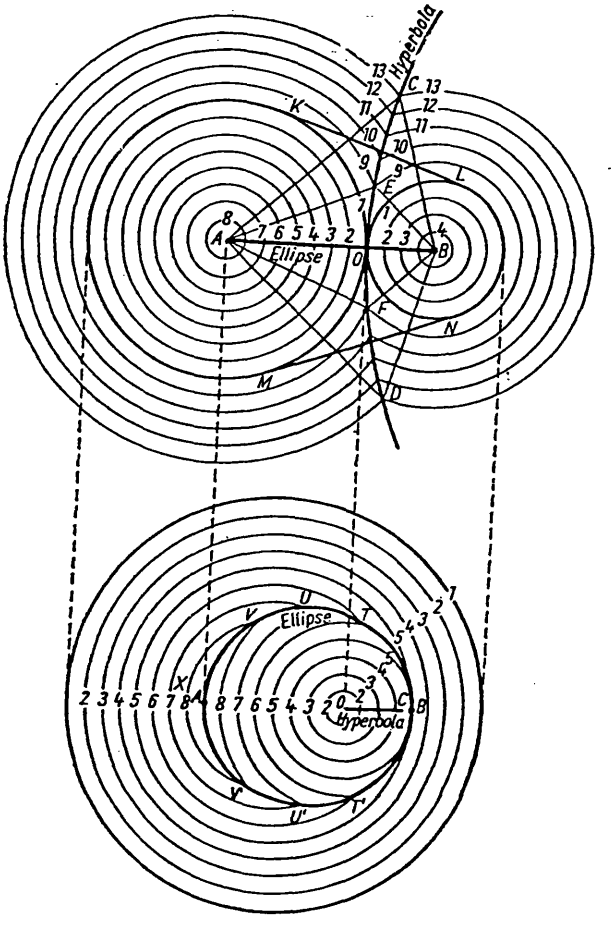

a. Vertical cross-section through the set of cyclides (section parallel to the hyperbola plane)

b. Plan of the dupin cyclides (section parallel to the ellipse plane)

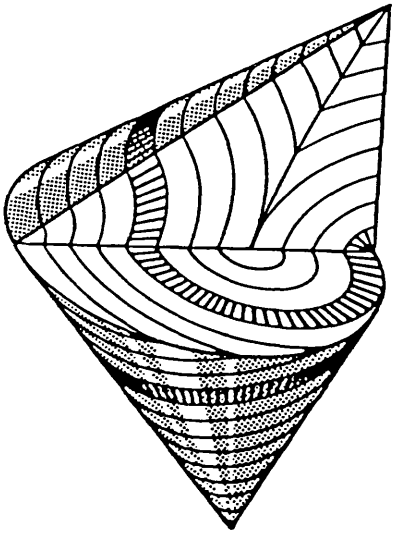

c. A focal conic domain

As the cross sectional diameter increases the central hole gets smaller until it reaches a point when there is no hole then a disclination is formed where two layers meet. This disclination forms a hyperbolae if the cyclide is looked at in plan view. As the cross sectional diameter decreases the cyclides become a cresent and an ellipse is formed by the resulting disclination which can be seen when looking at the cyclide in cross section. The ellipse and the hyperbolae are perpendicular to each other and form a pair of focal conics, hence the name. The conic shape seen under the microscope is the section of the cyclide shown in Figure 2.13c. The banded focal conic texture (Figure 2.11d) is seen in chiral smectic phases and is the pitch formation.

The Schlieren texture is a series of point disclinations from which four dark brushes start. These brushes appear when the director is parallel to either the polariser or analyser. When the sample is rotated between crossed polarisers the brushes rotate, the direction of rotation depends on the type of point singularity and is defined by a positive singularity for a rotation of the brushes in the same direction as the sample and negative if its opposite. The type of singularity is also defined by the s number where s = (the number of brushes)/4. There are four possible types of point singularity that can occur in S_C these are shown in Figure 2.12a-d. Neighbouring singularities have opposite signs so over any sample s is approximately zero.

The S_C Schlieren texture generally occurs in homeotropic or tilted homeotropic samples and has the layers parallel to the surface. This is opposite to focal conic textures which occur in homogeneous samples when the layers are perpendicular to the surfaces.

When an S_C material is aligned homogeneously the textures seen are not the natural focal conics or Schlieren textures but are either distorted focal conics such as the elongated focal conics shown in Figure 2.11e and f or new textures. The textures are characteristic of particular alignments and material combinations (see Figures 4.5, 4.6, 4.8 and 4.9). Some of the other textures are shown in Figure 2.14.

The domains that form (Figure 2.14a) are characteristic of all ferroelectric smectic phases and are regions of different azimuthal angle around the cone. The point of contact between these two regions is a domain wall of characteristic width. Figure 2.14b shows domains but these are of different layer directions and are seen in materials with no S_A phase. The zig-zag discontinuity (Figure 2.14c) is specific to aligned tilted smectic phases. The optics either side of a zig-zag defect can be very similar implying that the director configuration is similar. A zig-zag is considered as a boundary between two regions of different layer bending or tilting. Steric interaction between each layer causes the boundary to form as a zig-zag across the layer normal. Reiker et al [1987] has proposed a structure for the zig-zag using a chevron layer structure determined from X-ray diffraction measurements. This is discussed further in Section 3.2.

Figure 2.14d shows another texture seen in materials with no S_A phase called the lined texture (it is not zig-zags). Figure 2.14e shows a typical texture seen for materials with an S_A phase aligned on SiO. This will be discussed further in Chapter 3.

Figure 2.14: Aligned Textures of S_C^*

(a) Pixels on and off with domains surrounding

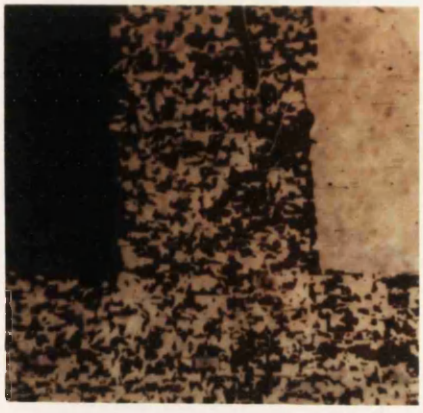

(b) Domains of different layer directions ($I\text{-}N^*\text{-}S_C^*$)

(c) Zigzag defects showing hairpin (thick and smooth) and lightening (thin and jagged) types

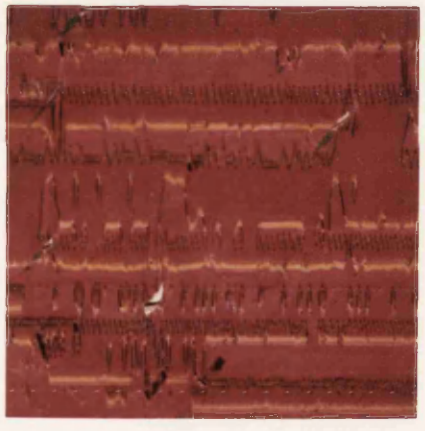

(d) Lined texture ($I\text{-}N^*\text{-}S_C^*$)

(e) Domains when aligned on SiO

CHAPTER 3

THE ALIGNMENT OF FERROELECTRIC LIQUID CRYSTALS

The ability to make electro-optic measurements on any ferroelectric liquid crystal device requires the liquid crystal to be uniformly aligned. The alignment not only produces a uniform optical appearance but it also determines the direction of the spontaneous polarisation dipole (P_S). The P_S needs to be aligned parallel to the applied electric field so that the dipole and therefore the director can be switched. This is achieved by aligning the FLC homogeneously. The first homogeneously aligned display device was demonstrated by Clark and Lagerwall [1980]. This configuration (Figure 3.1) was named the "bookshelf geometry" because it was proposed that the layers were arranged perpendicular to the substrates like books on a shelf. It was claimed by Clark and Lagerwall that the substrates had to be close together (<2 μm) so that the surfaces were strong enough to unwind the intrinsic helical pitch of the ferroelectric liquid crystal and this has led to the more common title of surface stabilised geometry. It is now known that the helical pitch can be unwound in thicker devices although a 2 μm thickness is still necessary in order to induce bistability.

The task of aligning FLC uniformly and homogeneously turned out to be a particularly difficult one, especially over the large areas required for LC displays (A4). Initial experiments used the alignment techniques developed for nematic LC devices such as rubbed polyimide [Nesrullaev et al 1980, Patel et al 1984] and evaporated SiO [Martinot-Lagarde 1977]. A rubbed polymer is a good aligning agent to use for LC displays because it is cheap and is easily used in manufacturing processes. However, it

Figure 3.1: The 'bookshelf' geometry as proposed by Clark and Lagerwall [1980]

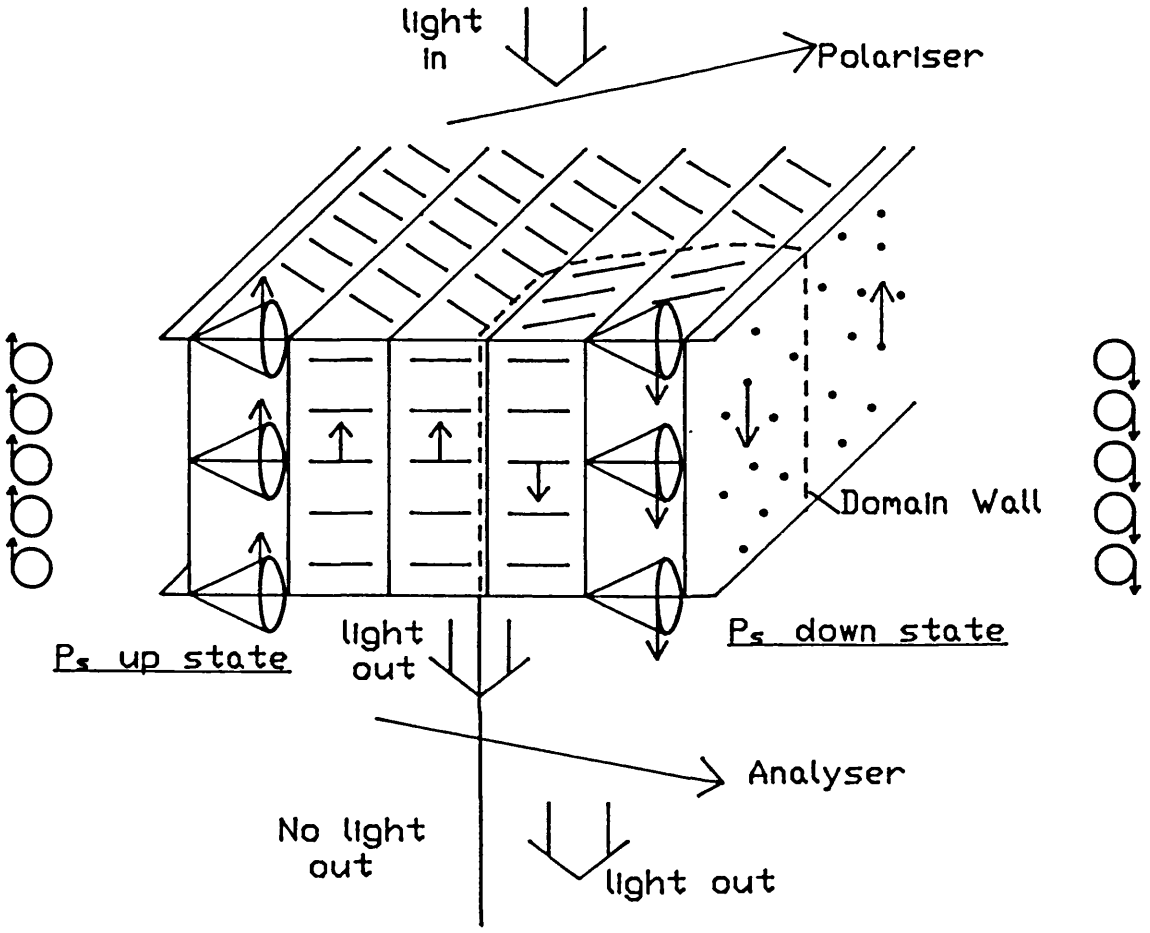

was found that these techniques did not produce good uniform alignment and other aligning techniques were investigated such as applying electric fields [Parmar and Martinot-Lagarde 1978, Uemoto et al 1979] and magnetic fields [Ostrovskii et al 1977] or shear aligning [Pieranski et al 1975]. New techniques were also developed. One technique which is still used for research purposes is the epitaxial growth from a thermal gradient edge [Ishikawa et al 1985]. This takes a long time but can produce good results. As FLC mixtures have improved, the ability to align them has become easier so that now good uniform alignment can be achieved over large areas using rubbed polyimide and SiO as aligning layers. This has enabled large area displays to be produced [Matsumoto et al 1988, Ross 1988].

The problem of alignment is complicated further by the requirement for bistability. The alignment must allow two equally stable states to exist that correspond to a positive or negative field being applied. The bistability reported by Clark and Lagerwall using the surface stabilised geometry does have two states but there is a relaxation such that the states with a field applied (switched states) are different from the states with no field applied (relaxed states). The process of understanding the mechanism for this relaxation has led to a questioning of the proposed bookshelf geometry. Most liquid crystal scientists now agree that the director and layer configuration is more complex than originally perceived. Many other configurations have been proposed but only recently has one model, the chevron structure, started to dominate.

This chapter describes the surface stabilised geometry and other proposed geometries, in particular a novel high tilt alignment that has

been developed by myself and coworkers. The current ideas on the director and layer configuration in a surface stabilised device will be reviewed.

3.1 The Surface Stabilised Alignment

The bookshelf geometry is produced using a homogeneous aligning agent such as a rubbed polyimide (Figure 3.1). Best results have been obtained by using a polymorphic material with the phase sequence I-N^*-S_A-S_C^*, with a large S_C^* pitch compared with the thickness of the device (2 μm) and a compensated pitch in the N^* phase near the N^*-S_A transition. Alignment is best obtained by heating the FLC into the isotropic phase then cooling slowly into the S_C^* phase. On cooling, the director aligns in the nematic phase along the rubbing direction. At the N^*-S_A transition the N^* pitch unwinds and the layers form perpendicularly with respect to the director and the aligning surfaces. At the S_A-S_C^* transition there is a problem. Either the surface director or the layer at the surface needs to move by the cone angle, θ_C, or a combination of both must happen. The assumption of the bookshelf geometry is that the layers stay fixed and the surface director moves by θ_C from the alignment direction but stays parallel to the substrate surfaces. It also assumes that the surface director moves by $2\theta_C$ when a reversing field is applied and since the surface director fixes the direction of the bulk director, the bistability is intrinsic to the device.

The surface stabilised alignment has the director and the normal to the layers, parallel to the bounding surfaces therefore the P_S dipole is perpendicular to these surfaces. This allows an electric field to be applied parallel to the dipole. When the field is reversed the dipole

reverses which moves the director around the cone. The director is moved at the surface by an angle $2\theta_C$ and because the director is uniformly aligned between the bounding surfaces the device can be treated as a birefringent slab. Optical contrast is produced by placing the device between crossed polarisers. When one of the polarisers is aligned parallel to the director a dark state is seen. Reversing the field switches the director by $2\theta_C$ from the polariser axis and coloured light is transmitted with intensity

$$I = I_o \sin^2 4\theta_c . \sin^2 \left(\frac{\pi \Delta n d}{\lambda} \right)$$

where I_0 = input intensity, Δn = birefringence, d = thickness and λ = wavelength. Maximum contrast is obtained with

$$\theta_c = 22.5 \text{ and } \frac{\Delta n d}{\lambda} = \frac{1}{2}$$

It is fortunate that most FLC materials naturally have a cone angle between 20° and 30°.

To prevent any relaxation occurring in SSFLC devices a high frequency a.c. field can be applied which couples to an induced dielectric dipole. Most FLC materials have a negative dielectric anisotropy, $\Delta\epsilon$, so that an a.c. field will align the director parallel to the substrates. The resulting director configuration should be the same as the P_S switched state. If the a.c. field is kept across the device after the d.c. reversing pulse has been applied then the director will not relax and the device will appear bistable. This a.c. stabilisation was

demonstrated by Geary [1985]. It has the advantage that thick cells can be used because the surfaces no longer need to induce bistability. The disadvantages are that the device has a larger power consumption and the electronics is more complex for multiplexed displays.

Materials with the phase sequence I-N^*-S_C^* can also be used in a homogeneously aligned device [Patel and Goodby 1986] but the alignment and device performance is very different from the materials with I-N^*-S_A-S_C^* sequences. Since there is no S_A phase the layers form at the same time as the director tilts by θ_C. Instead of the director moving out of the rubbing direction the layer now forms at an angle θ_C from the rubbing direction. This leads to two layer directions. In practice the layers form at ±10-15° from the rubbing direction rather than $\pm\theta_C$ and the director remains in the rubbing direction. There is no bistability in these devices and the textures formed are very distinctive (see Figure 2.14b and d).

3.2 The Structure of the Surface Stabilised Alignment

At present there is a debate as to the true structure of a surface stabilised (SS) device. This stems from the observation that there is always some relaxation of the liquid crystal director when the electric field is removed. It is generally assumed that the coupling of the permanent dipole to the electric field is strong enough to produce a uniform director configuration throughout the cell except very close to the surfaces. The relaxation implies that the director is not uniform after the field has been removed so the structure cannot be the proposed SS alignment. In order for there to be two stable states in the Clark and Lagerwall structure the surface director has to move out of the rubbing direction when a field is applied to provide a new pinning site

for the bulk of the LC. Moving the director across the surface and out of the rubbing direction is contrary to evidence gained from nematic LCs and this simple picture provides no other reason why the director should move.

The Clark and Lagerwall model requires a uniform director configuration between the surfaces. This demands the spontaneous dipole to be attracted to one surface and repelled by the other. Since SS devices are generally manufactured using two similar surfaces it is obvious that in practice a polarity difference at the surfaces is not obtained and in fact it has been shown by Shimizu et al [1986] that when the surfaces are different the bistability is lost totally. This has led to an alternative model being proposed by Handschy and Clark [1984] called the splayed state (Figure 3.2). Both surfaces have the spontaneous dipole interacting in the same way. The director is therefore at opposite sides of the cone at the two surfaces (i.e. either side of the rubbing direction) and the director uniformly rotates around the cone between the surfaces so that the P_S splays. Although this alignment uses the difference in polarity at the surfaces, it has the problem that there should be no bistability. There should only be one optically distinguishable relaxed state whereas in practice there are always two. It also requires the surface director to move out of the alignment direction and, as discussed earlier, it is preferable not to have to impose this.

The relaxation mechanism can be built into the Clark and Lagerwall model by allowing the surface director to be tilted out of the plane of the

surfaces and moved out of the alignment direction so that it remains on the cone. This was also proposed by Clark and Lagerwall [1984]. They categorised the many possible boundary conditions as

(i) complete conical: circular and anisotropic

(ii) incomplete conical

(iii) polar

(i) A complete conical boundary condition is when the layer is perpendicular to the surface and the projection of the director on the surface, n_s, can be at any angle θ where $-\theta_c \leq \theta \leq +\theta_c$. Complete circular is when there is no preferred direction of n_s and complete anisotropic is when there is a preferred direction of n_s e.g. when using rubbed polyimide.

(ii) An incomplete conical boundary condition is when the layer is not perpendicular to the surface therefore the angle of n_s is limited i.e. n_s can rotate on the surface until a threshold value is reached then it will flip 180° rather than continue rotating. This they claimed would happen for a high surface pre-tilt alignment.

(iii) The polar boundary condition was proposed by Handschy and Clark [1984] as the mechanism for stabilising the splayed state. This is when the spontaneous dipole interacts with the surface so that the director is limited in its position on the cone. Very polar surfaces will make the LC monostable.

Figure 3.2: The splayed state as proposed by Handschy and Clark [1984]

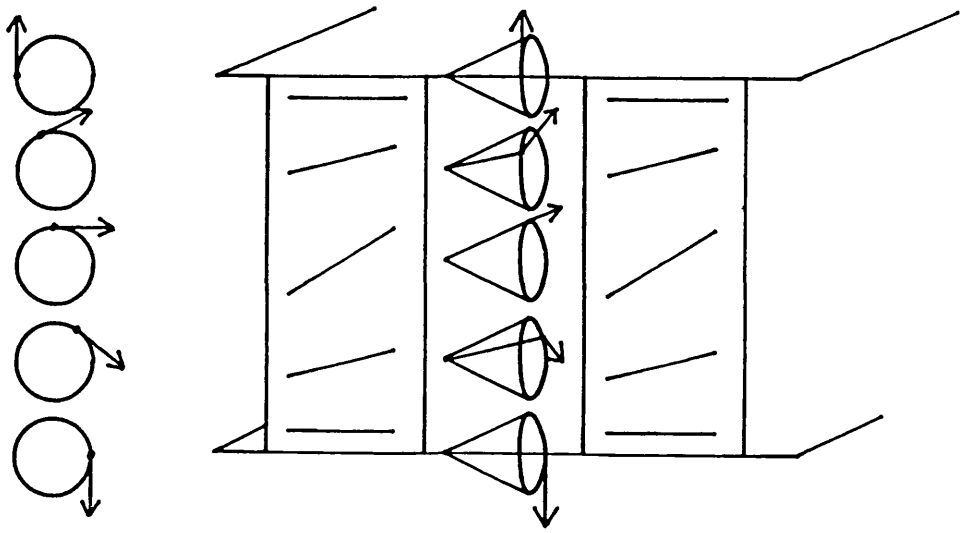

Figure 3.3: The structure of SSFLC proposed by Crossland et al [1987] with a surface pretilt

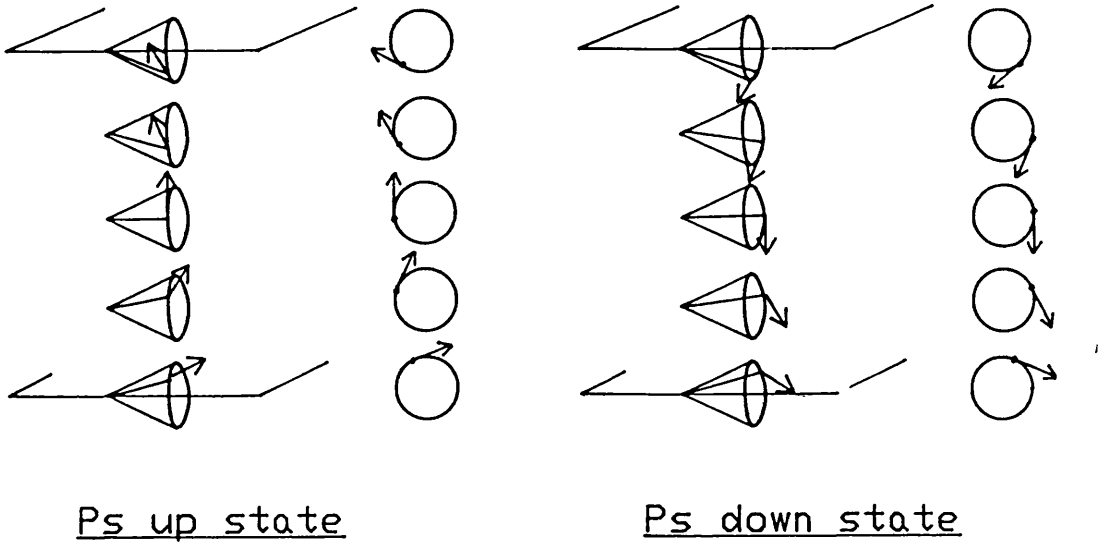

Although all these different configurations exist theoretically, none of them have all the properties required to explain the SS alignment that is produced on rubbed polymers.

Clark and Lagerwall [1984] also proposed a multistate boundary condition such as a crystal ferroelectric or an orientationally plastic surface which could be switched between two states.

In 1987 Crossland et al [1987] deduced from dielectric measurements that there was a pretilt of the director in the cell which he proposed was at the surface (Figure 3.3). When no field is applied the ϵ measured is smaller than with a field. Since the material had a negative $\Delta\epsilon$ Crossland et al interpreted this as a component of $\epsilon_{\perp}$ being measured in the relaxed state therefore an out of plane component of the director existed at the surface. He proposed that the surface director does move out of the rubbing direction when a field is applied and that the relaxation when the field is removed is due to the surface director moving around the cone. The problem with this model is that the surface director has to move.

Most of the models discussed so far have assumed that the layers are straight and perpendicular to the surfaces. However it is possible to model a FLC device by varying the layers (the incomplete conical structure proposed by Clark and Lagerwall is a tilted layer structure). Reiker et al [1987] proposed a chevron layer structure deduced from X-ray diffraction evidence from the layers in SS devices. In the chevron model the director remains in the rubbing direction and parallel to the surfaces and the layer tilts at the surfaces by an angle θ so that the layer pitch at the surface and in the bulk remains constant.

Each surface tilts in the opposite direction so that there must be a discontinuity where they meet in the middle. The layers in the chevron structure are generally tilted by less than θ_C in which case the surface director must move around the cone. In this case the mechanism for movement of the director is the fact that the bulk layer pitch is predetermined in the S_A phase and remains constant throughout the S_C phase and the director moves to remain on the cone and parallel to the surfaces. This produces a uniform director configuration at an angle $<\theta_C$ normally between 8-12° from the alignment direction. The director configuration of the proposed chevron structure is shown in Figure 3.4 for the switched and unswitched cases. Note that the director is pinned at the chevron boundary.

When a high frequency a.c. field is applied across a SS device a dielectric dipole is induced that aligns in the field. This produces an optical state that appears the same as the P_S switched state. FLCs have a negative $\Delta\epsilon$ so will align with the long axes of the molecule perpendicular to the field (parallel to the surfaces). If the FLC is treated as uniaxial then the above proposed model does not agree with experiment because the a.c. field will keep the director in the relaxed state and not the P_S switched state. However, if the FLC is treated as biaxial (for which evidence is beginning to appear [Jones et al 1989]) then an a.c. field will move the director to suit the largest component of ϵ_1, ϵ_2 or ϵ_3. This will be coincident with the P_S component since the two dipoles originate from the same molecule. Therefore an a.c. field will not move the molecules parallel to the surfaces but to the same position on the cone that the P_S component will move the director

Figure 3.4: The director and layer configuration for the chevron structure when switched and unswitched.

a. Unswitched

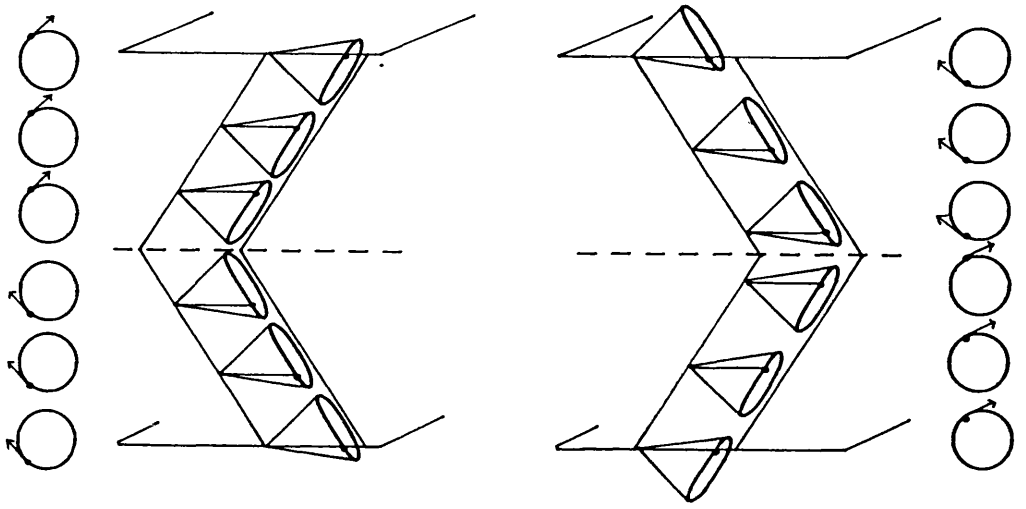

b. Switched

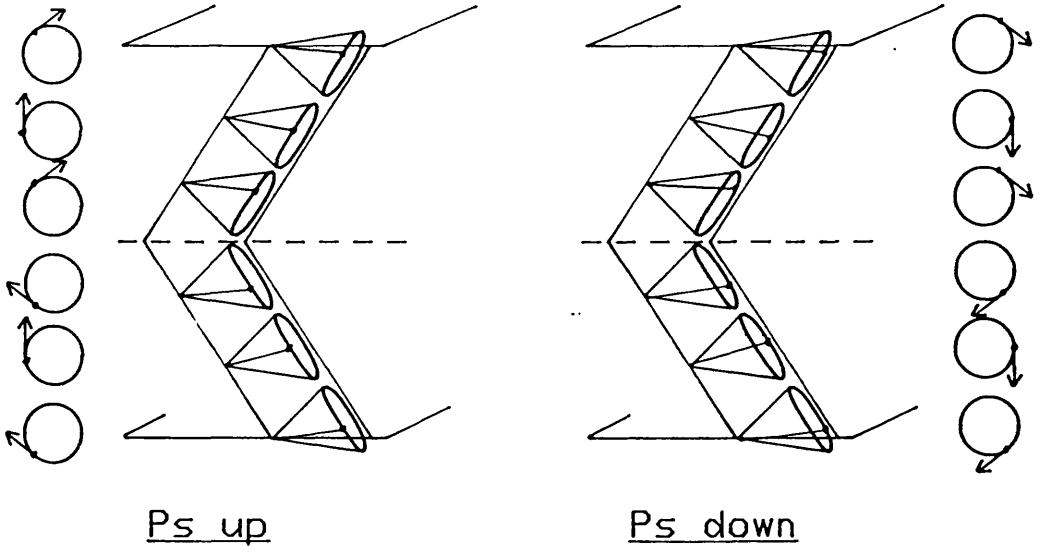

to. Therefore for a biaxial material, such as S_C^*, dielectric switching will move the director to the same state as P_S switching. This can also explain the results of Crossland et al [1987].

The characteristic zig-zag defects that are found in aligned surface stabilised devices can be explained using the chevron layers (although the arguments equally apply for bent layers). The zig is where two chevron layers meet in one direction and the zag is where they meet in the other direction as shown in Figure 3.5. The defect runs at an angle to the layers because of its spatial distribution, the discontinuity in each layer must be slightly shifted relative to the next layer so that they fit together. Since this is a layer discontinuity the director can be the same either side of the zig-zag so that there is little or no optical difference but the centre of the zig-zag will have a rapidly changing director and will appear dark between crossed polarisers. Ouchi et al [1988] and Hiji et al [1988] characterised the zig-zags as lightning or hairpin depending on how the 'zig' and the 'zag' meet, which form loops (Figure 2.14c).

An alternative model proposed by Clark et al [1987] also assumes that the layers move in the bulk but are fixed at the surface. However a bent layer is assumed. If the surface director remains in the rubbing direction in the S_C^* phase then the layers must move to accommodate the cone angle. However, the layers cannot twist since this not only causes the layers to move at the surfaces but also requires a change in the layer pitch within the layers (Figure 3.6). It can also be seen experimentally that the layers do not twist. State a would have the optical axes of the state asymmetrically placed about the rubbing direction whereas it is in fact measured to be symmetrical. State b

Figure 3.5: The structure of the 'zig' and 'zag' layer defects

The 'zig' deformation (hairpin)

The 'zag' deformation (lightning)

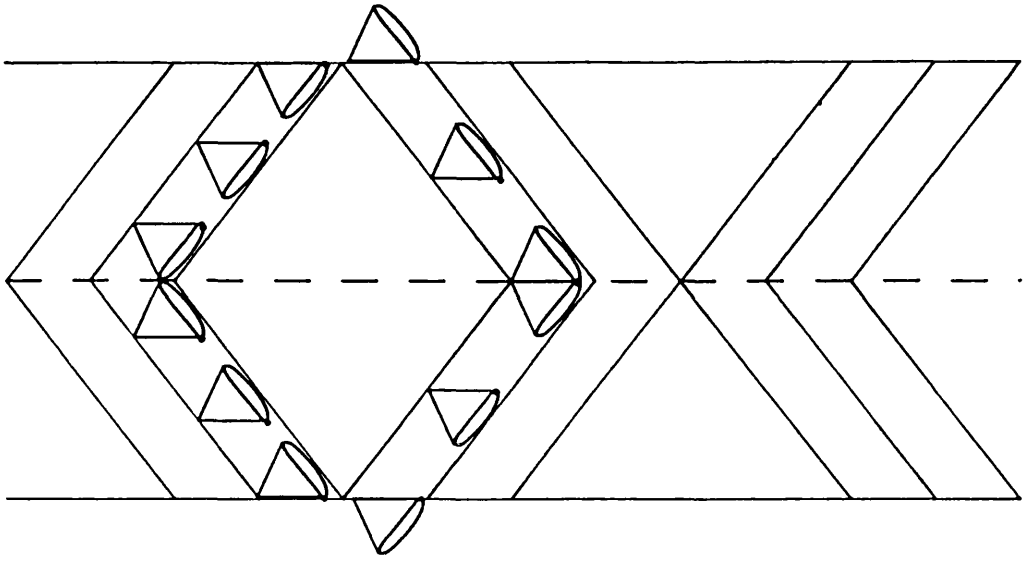

Figure 3.6: Structure of a SSFLC cell if the layer twisted

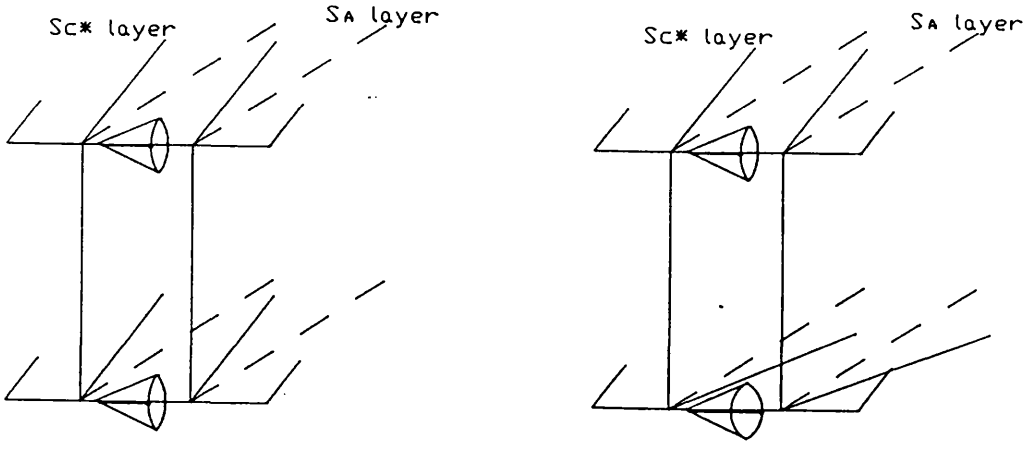

would have a relaxed state whose optical axes was coincident with the rubbing direction whereas they are measured to be approximately ±7-12° from the rubbing direction. Therefore neither state is experimentally observed.

If the layers tilt from the surface there are four possible combinations of movement as shown in Figure 3.7. The states shown in Figure 3.7 a and b have the layers tilted by θ_C. This requires the layers to move at the surfaces which would violate the hydrodynamic no-slip condition. Experimentally these states would be monostable and have the optical axes of the relaxed state coincident with the rubbing direction. Since this is not observed it can be assumed that these states do not form.

There are only two possible states left which are shown in Figures 3.7 c and d. These states have the director either at the top or bottom of the cone only and the director and layers remain fixed at the surface. These two states have all the experimentally observed properties. There are two relaxed stable states whose optical axes are symmetrical about the rubbing direction but will be less than θ_C and by applying a field the optical axes will go to θ_C. The spontaneous dipole is parallel to the surface and therefore is effectively neutral with the surface unlike the proposed bookshelf geometry but in the centre of the cell the P_S is perpendicular to the surface so that is is switchable. When the director switches there will be a discontinuity in the director which gives rise to the observed domain formation. There are two states both with similar director configurations but different layer bends. This can give rise to the observed zig-zag disclinations.

Figure 3.7: Structure of a SSFLC cell if the layers bend

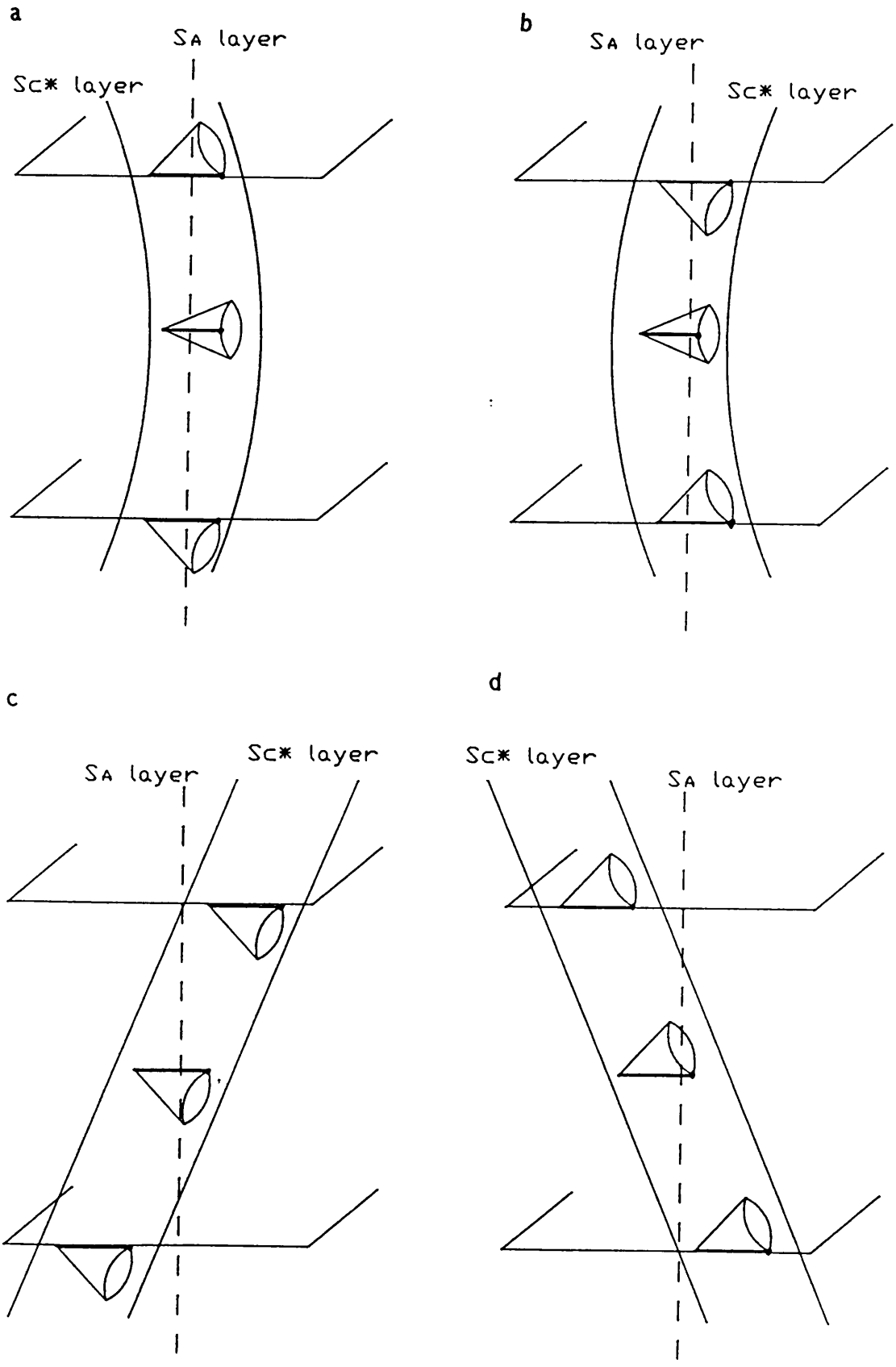

For all the models proposed there must be a discontinuity in the director configuration as it switches from one state to the other. This is the basis of the domain structure in FLC where the domain walls contain the director discontinuities. The study of the nucleation and growth of the domains when switching between states can be used to analyse the internal structures of the device [Handschy and Clark 1982].

Ouchi et al [1987a, 1987b] have used this technique but unfortunately they have analysed their work using only two states, the uniform state (U) which is the original Clark and Lagerwall bookshelf alignment, and the twisted state (T) which is the splayed state proposed by Handschy and Clark [1984]. As discussed earlier these two states are unlikely to be the true states forming. However, following their analysis is useful. There are eight different proposed states, UR, UL, TR1, TR2, TL1, TL2, DR, DL (Figure 3.8) and the disclinations form as the director changes states. Ouchi et al proposed that there are two types of disclination that can form. The first are surface disclinations as proposed by Clark and Lagerwall [1980] which form jagged domain boundaries. These can form disclination loops with $\pm 2\pi$ twist, and wedge disclinations. He also observed smooth domain boundaries which he explained as an internal disclination. As a field is applied, surface and/or internal disclinations appear, the order in which they appear depends on whether the states are changing from U to U, T to T or U to T (e.g. the boundary between two U states consists of two surface and one internal disclination which all change simultaneously when switched). On switching between U states a third type of state appears called the deformed (D) state which is intermediate between the two switched states. There are two D states, one for each U state.

Figure 3.8: The eight states used in the analysis of director switching by Ouchi et al [1987a, 1987b]

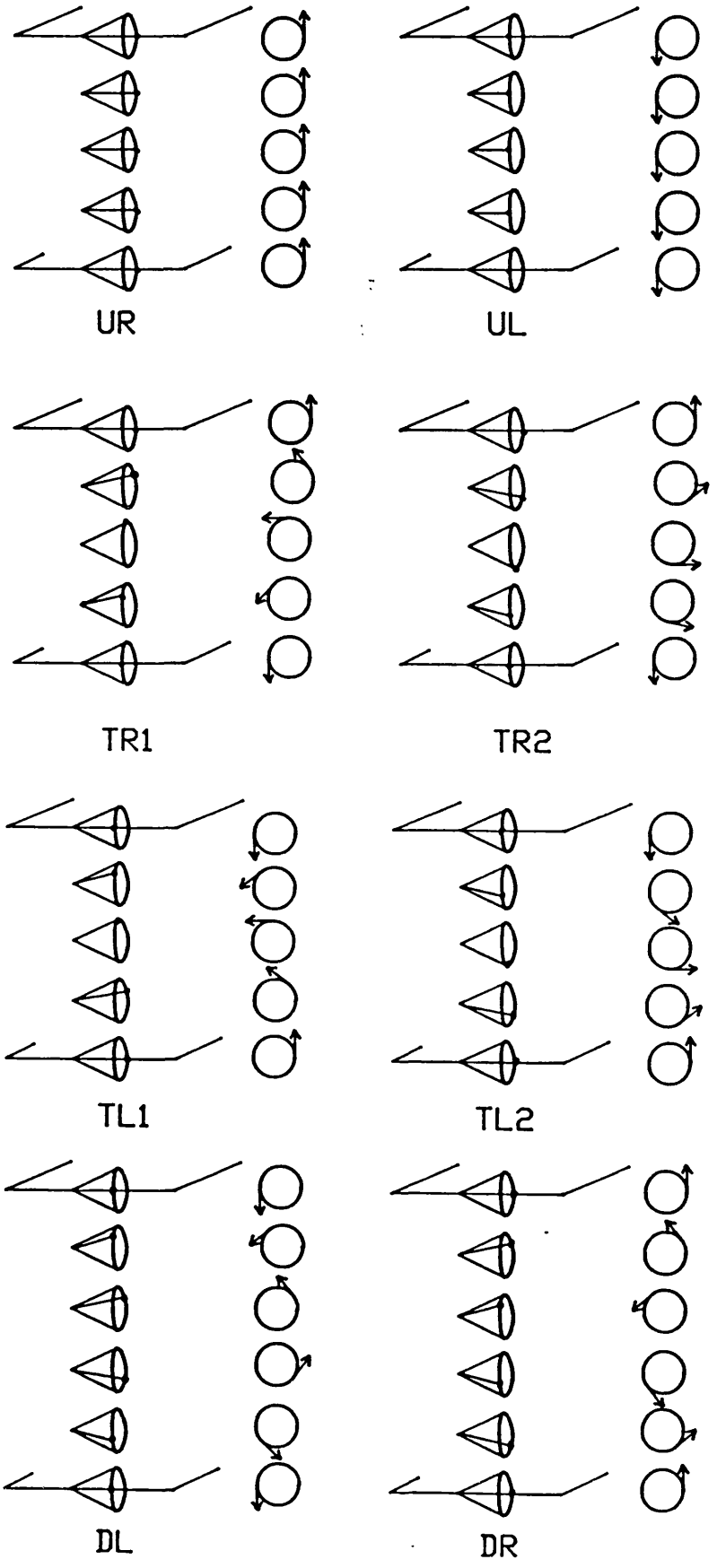

Slow stroboscopic switching showed that the processes that go via internal disclinations are slower than those going via only surface disclinations. This is because the internal disclination only forms when the top and bottom surfaces rotate in opposite directions, i.e. there must be surface movement before an internal disclination can form. Another type of switching was also observed called the co-operative mode which has no nucleation. The director must be able to switch smoothly around the cone with no disclination, therefore the cooperative mode can only occur between T and U states. The non-nucleated processes are faster than the nucleated ones by approximately a hundred times.

The chevron structure of the layers in SS devices is the most favoured alignment at present and there is increasing evidence that the requirement for pitch conservation of the layers in the bulk can also cause the director to move at the surfaces. The chevron discontinuity can be used to explain many effects and is very important in FLC device physics.

3.3 The High Tilt Alignment

The aim of this novel alignment geometry proposed by Professor M G Clark is to allow the surface director to remain fixed at the S_A-S_C^* transition and when a field is applied. It also allows the cell to retain excellent bistability. This is achieved by having a surface pretilt of the director which is equal to the cone angle [Bowry et al 1987a]. The director can be at the top or bottom of the cone allowing the layers to be normal to the surfaces rather than tilted as in the SS case. This configuration also allows the P_S dipole to be parallel to the surfaces therefore minimising the dipole-surface interactions. There are two ways of assembling such a device parallel (↑↑) and antiparallel

Figure 3.9: The two possible geometries for high surface tilt alignments

Antiparallel - The uniform tilt alignment

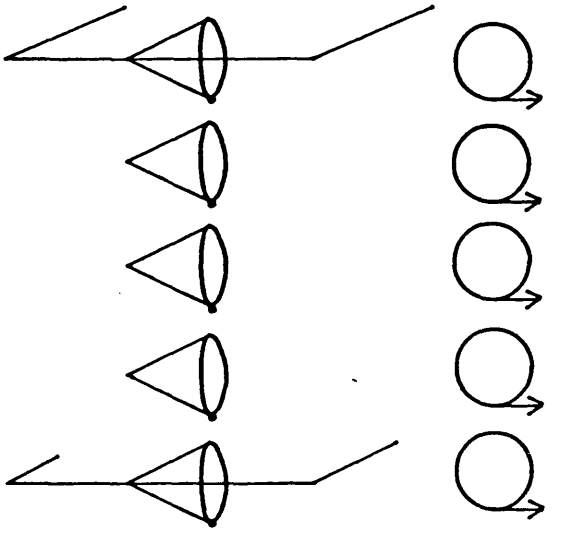

Parallel - The high tilt alignment (HTA)

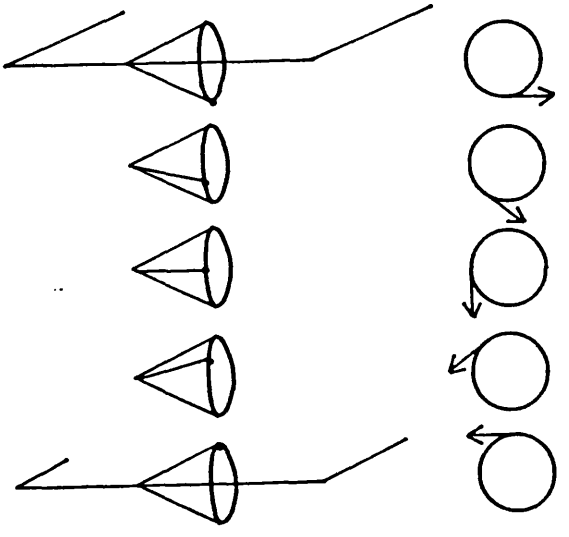

(↑↓) (Figure 3.9). In both cases the layers can form normal to the surfaces but in the antiparallel alignment (uniform tilt alignment) there is only one minimum energy state which should produce a monostable device. However in the parallel alignment the director can vary either way around the cone giving two equally stable states with the P_S up or down. It is this geometry that has been named the high tilt alignment (HTA). The HTA produces a uniform alignment with no zig-zags and it has excellent bistability. This behaviour has also been observed by Bos and Koehler [1988].

A 30° surface pretilt of the director can be obtained by evaporating SiO at a 5° angle with respect to the surface (the alignment will be referred to by the evaporation direction and not the pretilt angle i.e. 5°SiO). In devices with the HTA geometry it is possible to use materials with a phase sequence I-N*-S_C* as well as I-N*-S_A-S_C*. The layer alignment does not need to be defined at a temperature above the S_C* phase because the layers are well defined by the S_C* phase. The extremes of the cone are defined by the two surfaces which results in a very strong layer structure. The optics of the HTA are based on the same principle as the SS device where the optic axis in the HTA is an average of the director which changes through the cell from being in the alignment direction, to θ_C, then back to the alignment direction. The optic axis will be only slightly less than θ_C as long as no guiding occurs (i.e. not in the Mauguin limit pitch >> λ).

Aligning materials in the S_A phase can be difficult for the HTA cell. The high surface pretilt must force the S_A phase to have either a bent or chevron layer structure. A bent layer structure is more likely because in the HTA the chevron layer requires a director discontinuity

(this is not observed in the SS chevron structure). At the S_A-S_C^* transition the layers can either bend further or form straight layers. Since the straight layers have a lower energy than the bent layers and only one layer structure forms because no zig-zags are present it is more likely that the layers are straight.

The pretilt angle of the director at the surface, θ_p, is nominally 30° for SiO evaporated at 5° which does not match exactly the measured cone angle of any of the FLC materials used. There are several possible mechanisms for overcoming this problem. The first and most probable is that the surface pretilt angle is not fixed but can change to accommodate the S_C^* phase. The director may move out of the alignment direction since it is not rigidly fixed or changes its out of plane tilt. The second mechanism is that a small bend may form in the layer to accommodate the pretilt angle. This is shown in Figure 3.10 a and b for the cases when $\theta_C<\theta_p$ and $\theta_C>\theta_p$.

The 5°↑↓ alignment case was predicted to have no bistability therefore it should not be interesting. However because 5°↑↓ alignment only forms one layer structure it gives good uniform alignment with no zig-zags just as for the 5°↑↑ case. Surprisingly it also produces excellent bistability showing that the geometry is not as important as predicted and that the surface properties may be more important in determining bistability. If the FLC material has an N^*-S_C^* phase sequence straight layers can develop perpendicular to the surfaces. If the FLC material has an N^*-S_A-S_C^* phase sequence then the layers in the S_A phase must form tilted with respect to the substrates at an angle equal to the pretilt angle. There is now a problem at the S_A-S_C^* phase transition. If a chevron layer formed as in Figure 3.10 c then there are two

Figure 3.10: Possible structures of high surface tilt alignments when the surface pretilt does not match the cone angle

High tilt alignment

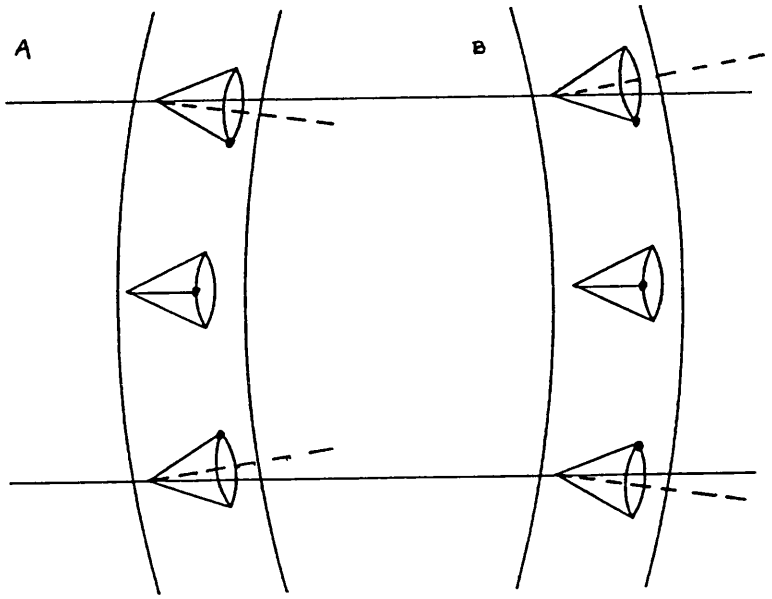

Uniform tilt alignment

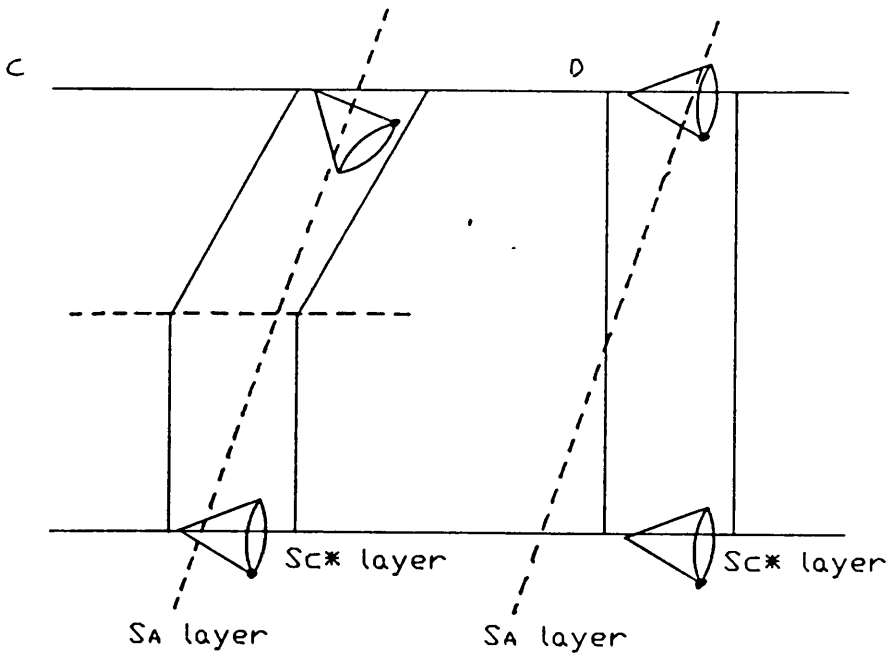

energetically equivalent possibilities and zig-zags would appear. Since no zig-zags are observed these layer structures must not form. The alternative is for the layers to change the tilt angle for example until they are perpendicular to the substrates, Figure 3.10 d.

3.4 The Twisted High Tilt States

The HTA device (5°SiO↑↑) produced four different states. There were two switched states as described in Section 3.3 which were stable for long periods of time after the field had been removed and there were also two other states that appeared which were a pale colour (pale blue in 2 μm cells, Figure 2.14e) that did not extinct at any angle when rotated between crossed polarisers. These states were therefore highly twisted and are referred to as the twisted HTA states. They were also very stable because they formed on cooling the FLC from the S_A or N^* phase and they could also appear a long time after a region had been switched. The 5°SiO↑↓ aligned devices (uniform tilt alignment) also produced a twisted, pale coloured, non-extincting state. Unlike the HTA devices only one such twisted state existed.

There are several possible director configurations that could produce a highly twisted state in the HTA or 5°↑↓ device. These are shown in Figure 3.11. The layer was assumed to be straight and perpendicular to the surfaces. To determine the correct director configuration for these twisted states the transmission spectra were measured at incident angles of 0° and 45° and the results were compared to modelled spectra for each proposed structure. The measured spectra for 2 μm thick ZLI3654 when aligned on the HTA and 5°↑↓ devices are shown in Figure

Figure 3.11: Possible structures of the twisted high surface tilt aligned states

Structure 1

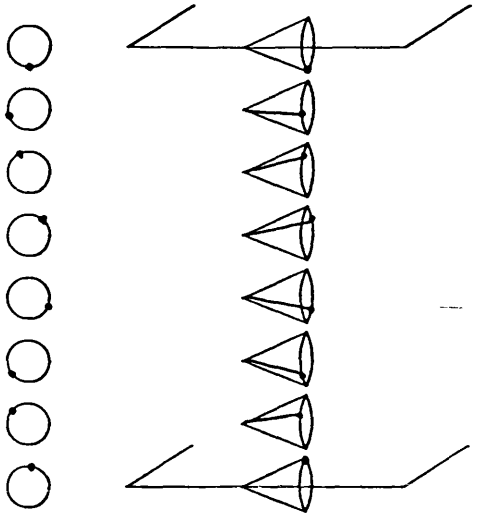

Structure 2

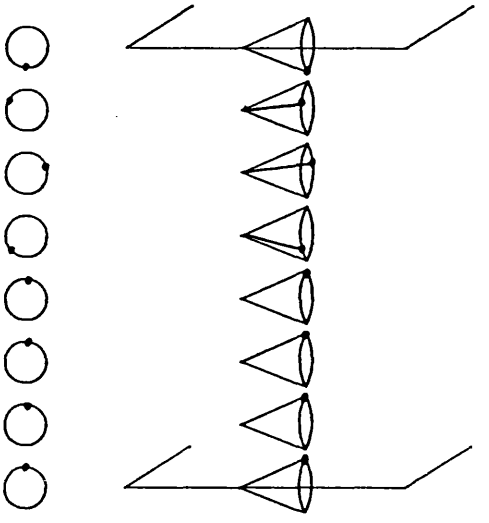

Structure 3

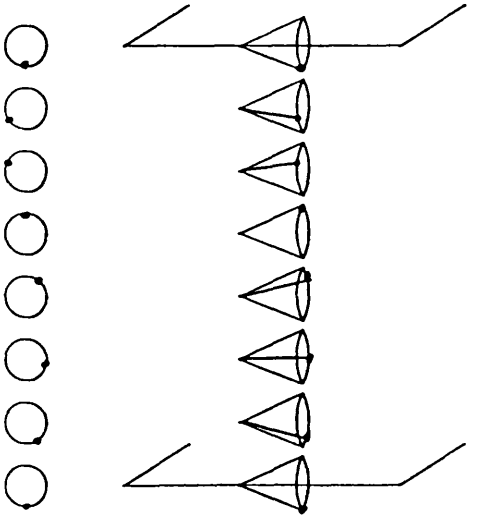

Structure 4

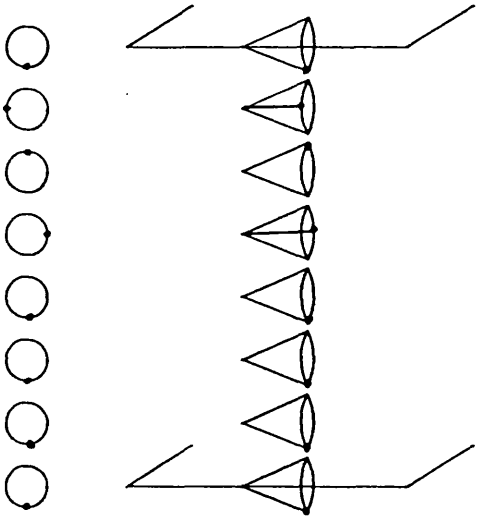

Figure 3.12: Measured transmission spectra of the twisted high tilt states for ZLI3654 aligned on 5°SiO↑↑ and 5°SiO↑↓ for 0° and 45° angle of incidence (θ_i)

5°SiO↑↑, θ_i=0,0

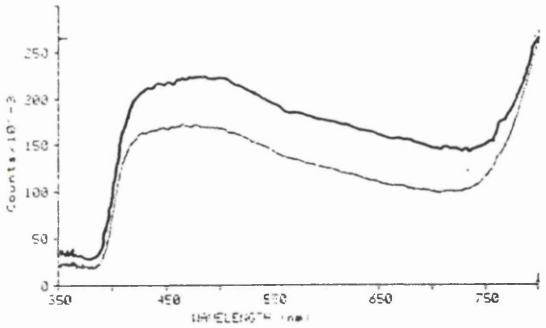

5°SiO↑↑, θ_i=45,0

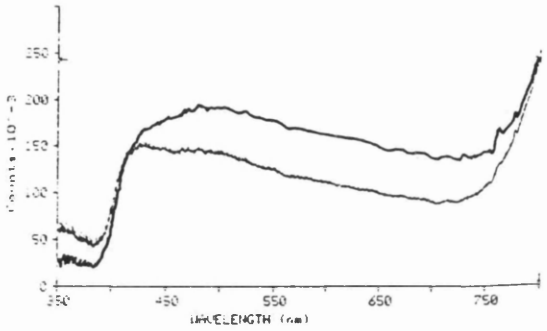

5°SiO↑↑, θ_i=0,90

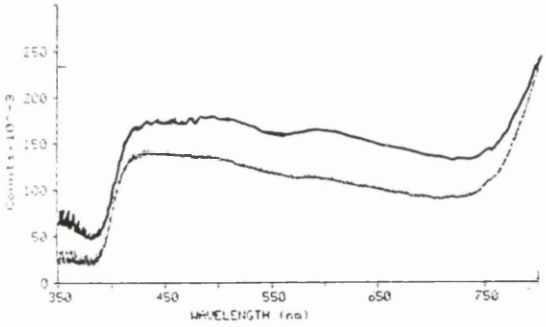

5°SiO↑↑, θ_i=45,90

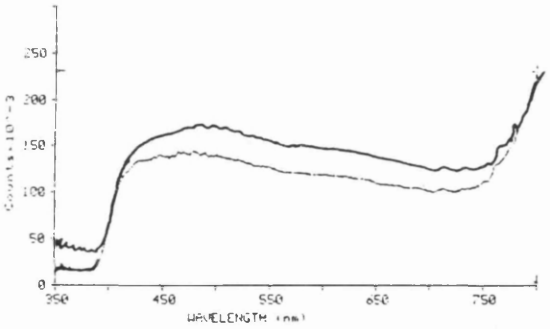

5°SiO↑↓, θ_i=0,0

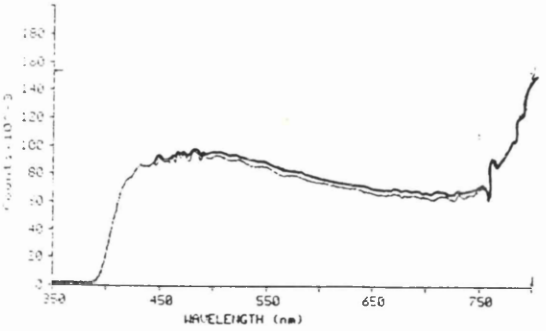

5°SiO↑↓, θ_i=45,0

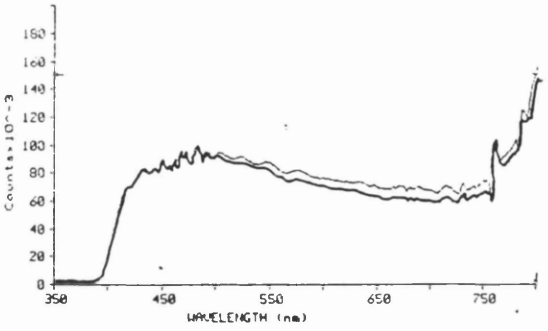

3.12. Some leakage of the lamp spectra could be seen especially at high wavelengths when there was a spike in the lamp spectra. This could be ignored when comparing with the modelled spectra.

The modelling of the transmission spectra was based on the Berreman optics programmes [Berreman 1972, 1983]. This split the LC layer into many homogeneous slabs then used a 4x4 transfer matrix method to calculate the propagation of the light through the multilayer media (which included the polarisers) by solving maxwell's equations.

The director configurations were created by assuming either a uniform director configuration or a sinusoidal twist of the director around the cone. The on configuration had the polarisers at +22.5° to the alignment direction and the off configuration was at -22.5°. The tightness of the twist of the director determined the appearance of the cell. The relaxed HTA cell was a loose twist (i.e. ½ turn through the 2 μm cell) which gave the two distinct on and off states which were almost the same as a uniform slab aligned at 22.5°. As the twist was made tighter within a 2 μm cell the more similar the two states became.

The optics of the HTA states were not symmetrical at an angle of 45° incidence. There was almost a 180° symmetry where 90° and 270° azimuthal angles produced a smaller difference from 0° incidence than the 0° and 180° azimuthal angles. The measured transmission spectra always had a lower percentage transmission than the calculated spectra because light was lost at all the interfaces (glass/air, glass/polariser, SiO/FLC) which were not included in the model.

The calculated spectra for the structures in Figure 3.11 are shown in Figure 3.13, these should be compared to the measured spectra (Figure 3.12). The structure that fitted best were structures 1 and 3 which had a uniform twist between the surfaces (the HTA device had 1½ twists and the 5°↑↓ device had 1 twist). The 5°↑↑ twisted state with ½ twist near the surface and the rest uniformly aligned gave good agreement at 0,0 angle of incidence but gave poor agreement at 45,0 angle of incidence because the two states were clearly on and off in the modelled spectra. The 1½ turn uniformly twisted state agreed fairly closely with the measured spectra. The 45,90 angle of incidence changed the spectra shape very little but reduced the transmission. The 45,0 angle of incidence caused the two curves to cross which was observed to a small extent in the measured spectra. The state with a uniform region with a twist near the surface would have four possible states, one at each surface each with two different twist directions. The two states with similar twist sense at opposite surfaces would look the same. The 5°↑↓ device gave only one twisted state which was symmetrical about the alignment direction. If there was one twist near the surface with the rest uniformly aligned then the on and off states were no longer the same. Also at 45,90 the transmission level dropped enormously and the two states became similar. This was not the observed behaviour. The 1½ turn uniformly twisted state matched the measured spectra qualitatively. At 0,0 angle of incidence the on and off states looked the same. At 45,90 angle of incidence the two states had divided but only slightly and at 45,0 there was a big difference between the two states. Reversing the twist sense produced an identical state which explained why only one state was seen yet the texture could appear like lots of domains.

Figure 3.13a: Calculated spectra for the twisted 5°↑↑ states shown in Figure 3.11

Uniform twist

Twist then uniform

(i) Structure 1

(ii) Structure 2

θ_i=0,0

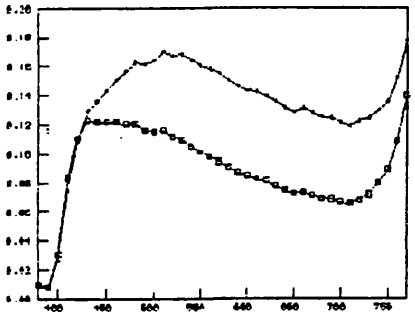

θ_i=0,0

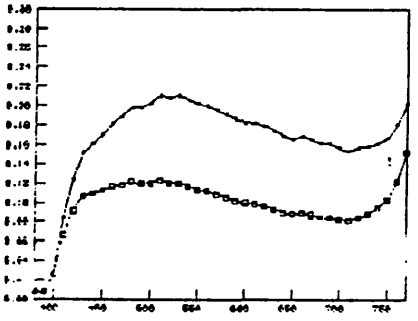

θ_i=45,0

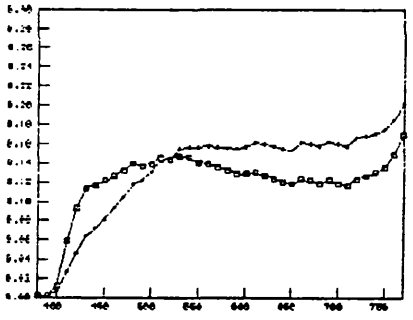

θ_i=45,0

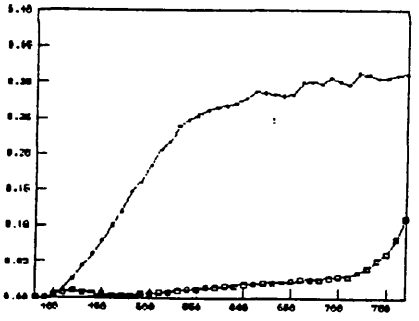

θ_i=45,90

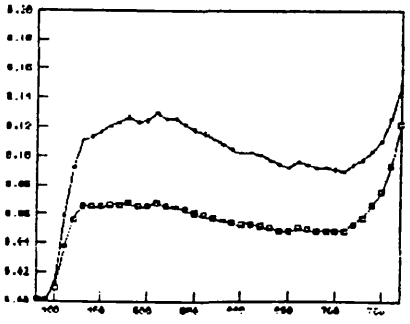

θ_i=45,90

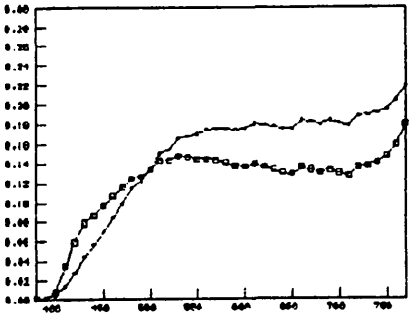

Figure 3.13b: Calculated spectra for the twisted 5°↑↓ states

Uniform twist

(i) Structure 3

θ_i=0,0

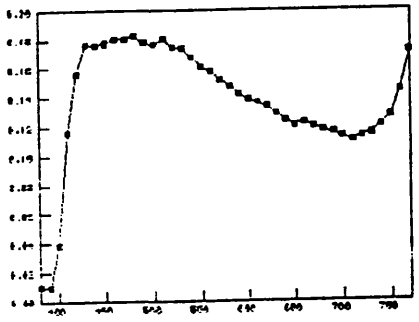

θ_i=45,0

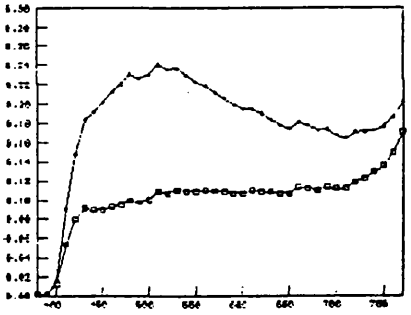

θ_i=45,90

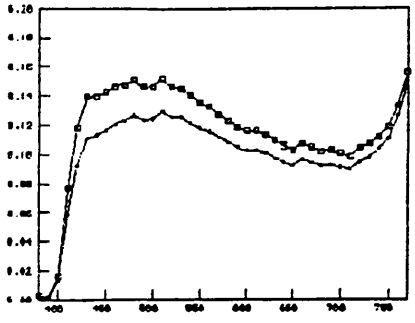

Twist then uniform

(ii) Structure 4

θ_i=0,0

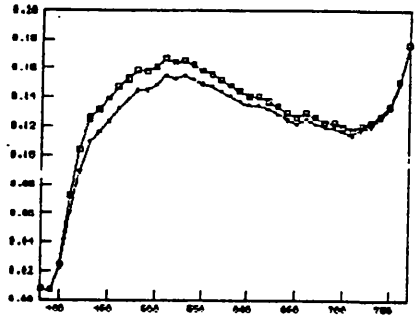

θ_i=45,0

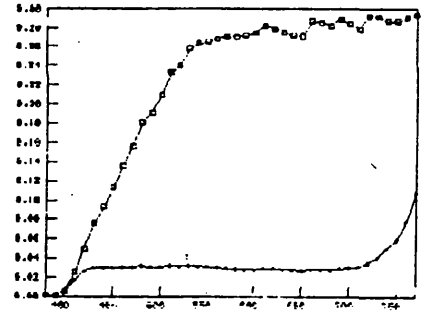

θ_i=45,90

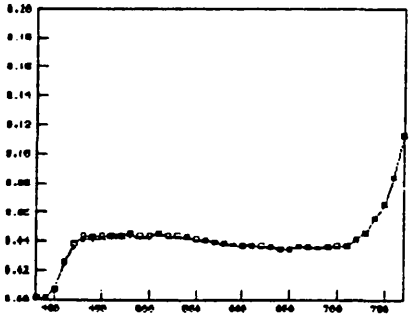

The twisted states could also be seen in SS devices but not as frequently. It is interesting to note that these twisted states are similar to the deformed states discussed by Ouchi [1987a].

CHAPTER 4

THE AFFECT OF ALIGNMENT ON DEVICE PERFORMANCE

This Chapter presents results from studies on the affect of alignment layer on device performance, such as bistability, response time and contrast ratio, for both the surface stabilised (SS) and high tilt aligned (HTA) devices. The aim is to compare the advantages and disadvantages of the traditionally used SS device to the novel HTA device. The most obvious way to do this is to compare a polymer aligned SS device to a 5°SiO HTA device. However, to test the affect of the alignment geometry as opposed to the alignment layer a 5°SiO HTA device has also been compared with a 5°SiO antiparallel aligned device and a SS device using 30°SiO aligning layers. These comparisons have been made in Section 4.3 for four different materials with different phase sequences in order to fully understand the properties of these alignments. An investigation into the affect of surface pretilt on the SS device has also been made in Section 4.2 by varying the polyimide aligning layers used.

The most important property of a device is its alignment quality. Bad alignment produces slow switching, little bistability and a poor contrast. In this work all the cells have been carefully aligned by slowly cooling the FLC from the isotropic phase. The cells have also been aligned by slow cooling with a d.c. field applied. This removes any degeneracy in the device structure to ensure that good alignment is obtained, especially for materials with no S_A phase above the S_C^* phase. A comparison is made between aligning the cells with and without an electric field.

The layer thickness is also a critical parameter for a FLC device because the surfaces determine the alignment quality and induce bistability. This requires thin devices. However, thick devices are easier to manufacture and are therefore preferable. In order to determine the optimum device thickness in terms of ease of manufacture whilst retaining good electro-optic performance, the affect of thickness on alignment and electro-optic properties has been explored in Section 4.4.

Section 4.5 uses the results from this chapter to discuss the material requirements for the best device geometry, alignment and layer thickness required for a display device.

4.1 EXPERIMENTAL TECHNIQUE

4.1.1 Cell construction and alignment

All measurements were made using cells constructed as shown in Figure 4.1. Ordinary soda lime float glass was spluttered with a thin coating of indium tin oxide (ITO) which is a transparent conductor whose resistivity decreases with increasing thickness (200 Å gives 100 Ω/square; 1000 Å gives 20 Ω/square). The ITO was etched to produce the required electrode pattern. The aligning layer, which was deposited over the ITO, was either rubbed polyimide or SiO evaporated at an angle of 5° or 30°. The glass substrates were held at the required thickness apart by plastic fibre spacers which were randomly scattered over the aligning layer. The cell was assembled using a screen printed adhesive seal. The FLC was sucked into the cell via capillary action when the FLC was heated into the N^* or I phase. This was done in a vacuum oven to ensure that the FLC degasses before entering the cell to prevent air bubbles forming. It was also necessary to de-gas absorbed

Figure 4.1: Cell construction

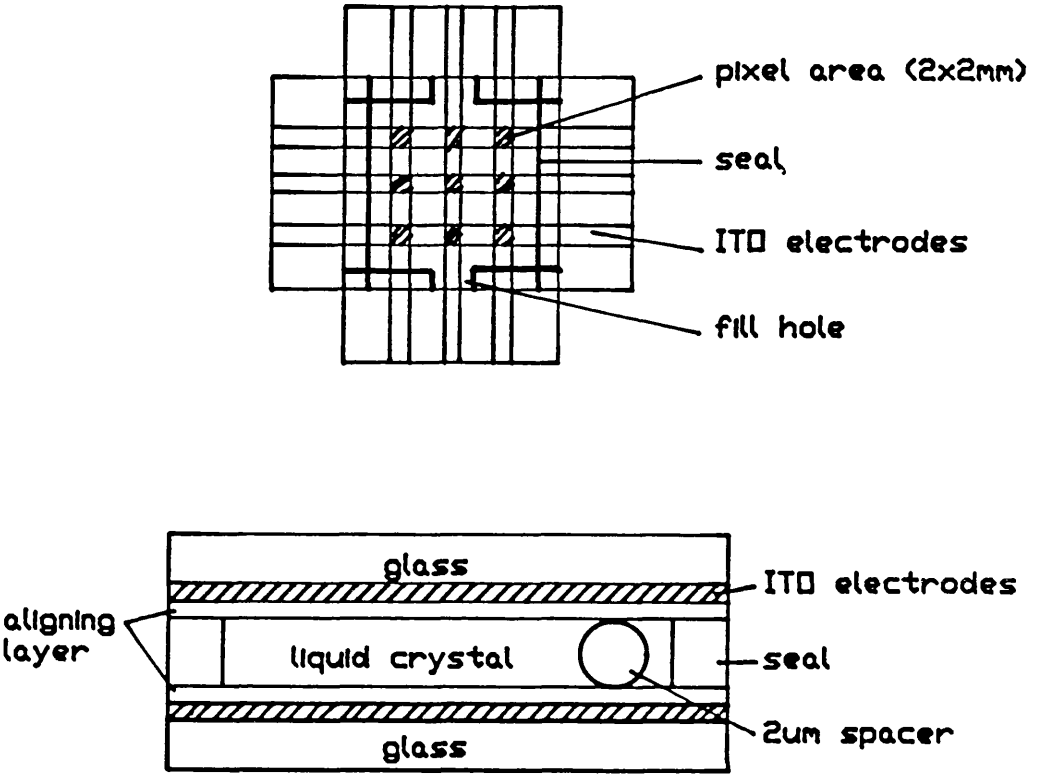

materials from the cells before filling. The side lobes on the seal pattern were to stop FLC being sucked into the area between the seal and outer edge of the glass which would reach the air hole at the other end of the cell before it had filled therefore blocking any further capillary action. Once the cell was full it was sealed using UV curable optical adhesive placed over the fill holes.

The three aligning layers used in this work all have different mechanisms for interacting with the liquid crystal molecules and therefore produce different director pretilt angles at the surfaces. A 30° evaporated SiO layer gives a pretilt angle of 0°, 5° evaporated SiO gives a 30° pretilt angle and rubbed polyimide gives between 0.1° and 5° pretilt angle depending on the curing and rubbing conditions. The mechanism of alignment is not simple (LC alignment can still be considered as a 'black art') and it depends on the surface structure, roughness, dipoles and chemistry. The alignment is referred to by the evaporation direction of the SiO e.g. 5°SiO↑↑ is SiO evaporated at 5° to produce a 30° pre-tilt angle with the evaporation directions aligned parallel.

The rubbed polyimide induces homogeneous alignment of the director along the direction of rubbing [Castellano 1984]. Initially this was thought to be due to a purely mechanical interaction. The polymer is rubbed with a cloth which produces grooves in the surface. The liquid crystal molecules align in the grooves which aligns the bulk of the liquid crystal. However, this does not explain why there is a pretilt angle at the surface which can be varied by curing the polyimide for different lengths of time. An alternative mechanism, proposed by Adamson [1976], is that rubbing the polymer produces a highly localised heating which

leads to melting of either the cloth or the polymer. If the polymer melts it can be aligned by the rubbing and will be quenched into this alignment as it rapidly cools. The liquid crystal then chemically interacts with the aligned polymer. Crossland et al [1976] also showed that the mechanism cannot be purely a mechanical effect due to grooves by showing that rubbed polymers can produce tilted or even homeotropic alignment which depends on the chain length of the LC molecule. Therefore a dipolar interaction must be involved. The true LC/rubbed polymer interaction is probably a combination of mechanical effects and aligned dipoles with the quality of alignment being affected by the surface roughness.

In contrast to the isotropic polyimide which must be rubbed to produce alignment the SiO layers produce an alignment direction due to the crystal structure that grows when evaporated [Jannings 1972]. An evaporation direction of 5° to the substrate surface produces a columnar structure tilted at a 30° angle to the substrate along the evaporation direction [Guyon et al 1973, Goodman et al 1977]. The LC molecules can then align at 30° to the surface in the evaporation direction by lying inbetween the columns. The 5° evaporated SiO is a uniform layer because it is a slowly grown crystalline structure, whereas the polyimide is a rough surface because it is random in nature.

The SiO layer evaporated at 30° to the substrate surface is totally different to the 5°SiO layer. The 30°SiO layer is very smooth with a crystal structure that induces alignment of the LC at 90° to the evaporation direction. The smoothness of the surface implies that the alignment must be a chemical interaction and not mechanical but the 0° pretilt of the LC implies a non-polar interaction.

Understanding the type of aligning layers used and the relative LC/surface interactions is important when analysing the alignment results.

4.1.2 Equipment

The equipment used is shown in Figure 4.2. All experiments were carried out whilst observing the microscopic texture of the FLC devices to ensure that the alignment was good over the whole area that the measurement was taken. A voltage of ±150V with an 8 μs rise time could be applied to the device if necessary using a specially designed amplifier based on a Burr-Brown 354 high voltage amplifier chip. Computer programs were written so that both the Wavetek arbitrary function generator and the Gould 4055 digital storage oscilloscope could be controlled using a BBC microcomputer and data could be stored in the computer or waveforms created on the computer then passed to the instruments.

4.1.3 Measurement techniques

The cone angle of the device was measured by rotating the cell between crossed polarisers until there was extinction of the light, the director was then aligned with the polarisers. If no extinction could be obtained it was because the director had a twisted structure (e.g. the twisted high tilt states). The extinction points were noted for all the stable states when no field was applied which gave the cone angle of the relaxed states (relaxation angle) and were also taken with a positive and negative d.c. field applied which gave the cone angle of the material, θ_C, where θ_C = ½ x (the angle between the two switched extinction points).

Figure 4.2: Equipment for electro-optic measurements

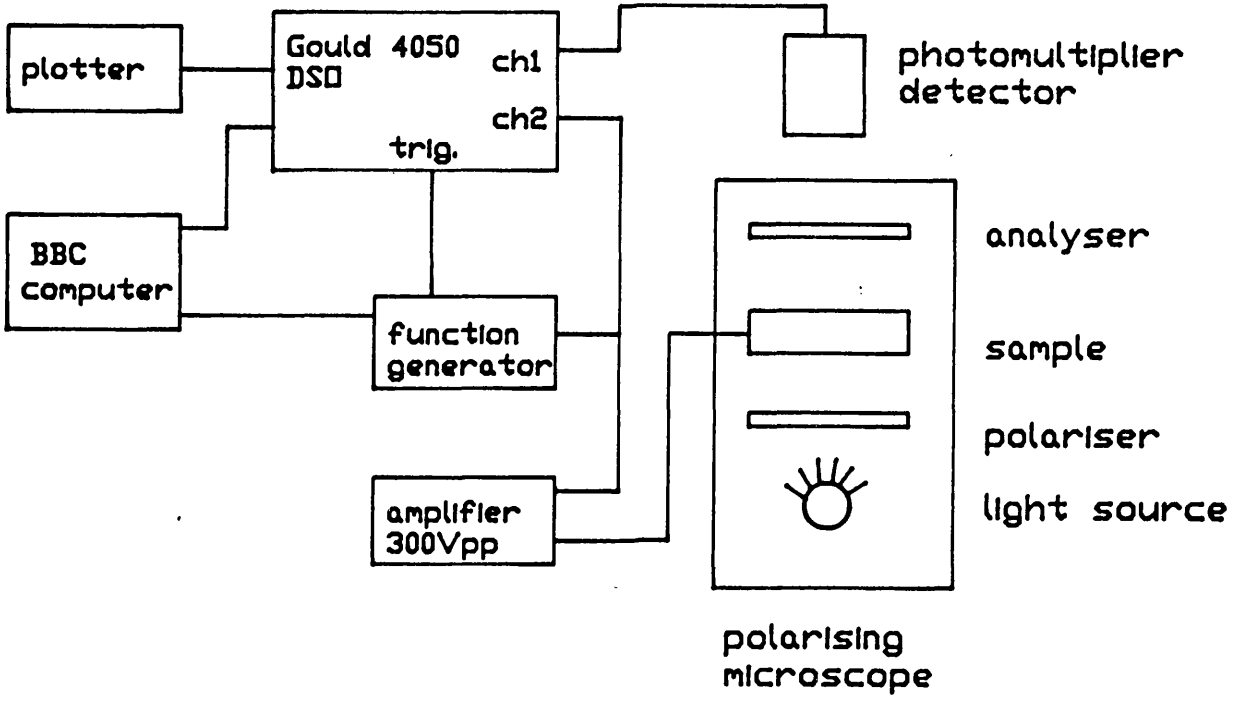

The relaxation of the FLC may have been due to several reasons:

(1) the director moved around the cone to a more stable intermediate position in a continuous process.

(2) an intermediate state was nucleated into.

(3) there could have been only two states (the two switched states) but when the field was removed the other state nucleated into the first causing the overall contrast to be reduced.

By measuring the relaxation angle and simultaneously watching the relaxation process it was possible to distinguish between (1), (2) and (3). In practice the relaxation was mainly due to (1) although sometimes (3) occurred (especially in HTA devices).

The response time (R_t) was taken using two techniques.

1. A 1 kHz 30 Vpp square wave was applied to the device. The R_t was defined as the time taken from the application of the voltage until the transmission level reached 90% (Figure 4.3a). The delay time was defined as the time from the voltage being applied to the 10% transmission point.

2. A second method for measuring R_t was to apply a positive voltage pulse then zero voltage then a negative pulse (Figure 4.3b) with a 1:100 ratio of pulse to gap. The R_t was defined as the minimum pulse time required to retain the transmission level of the latched states. When the cell did not switch fully small domains of an intermediate state started to form between pulses which could be seen through the microscope. This pulsed technique of

Figure 4.3: Definition of response time

a. Using a square wave

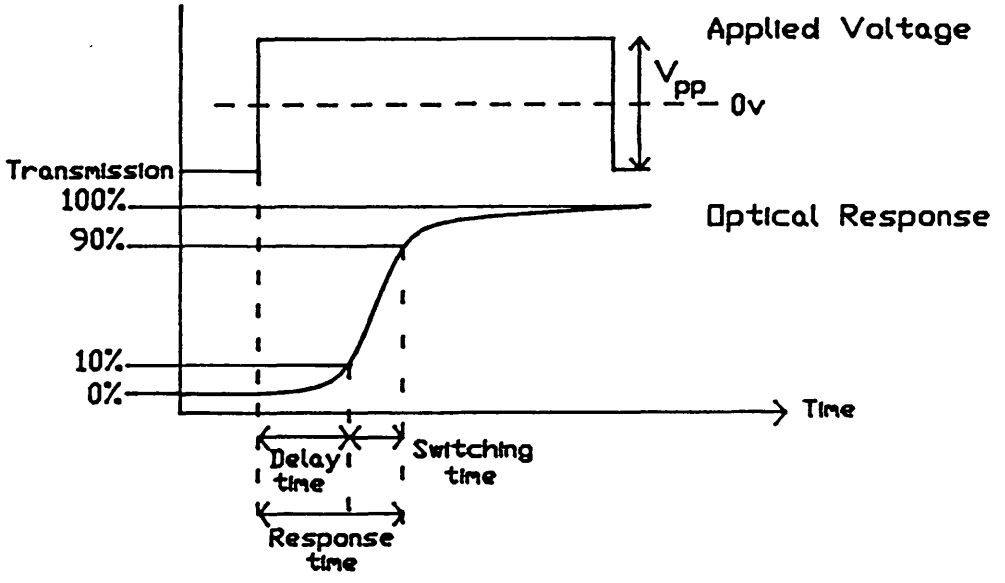

b. Using the pulsed technique
R_t = minimum t to retain transmission of latched states

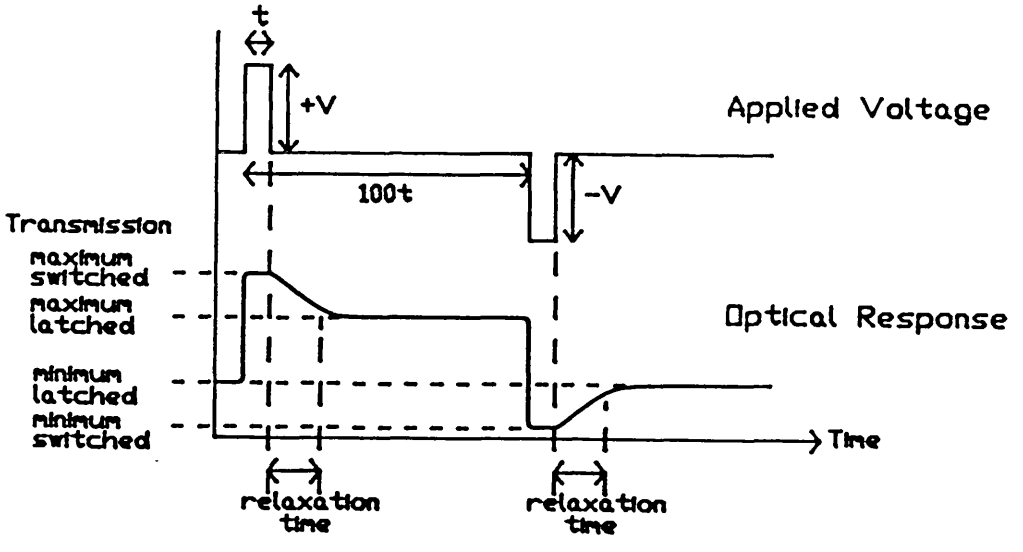

measuring R_t could be more useful than a square wave technique because it measured the minimum pulse time needed to fully switch and latch the device. However it was still limited because the R_t depended on the state the FLC was in just before the measurement pulse was applied and this depended on the pulses applied before the measurement pulse. For example bipolar pulses could double the response time and a continuous square wave could increase it by upto ten times that of unipolar pulses. For certain applications where continuous switching is required the square wave technique should be used for measuring R_t.

The relaxation time was determined by measuring the time taken for the device to relax to the intermediate state after a unipolar pulse was applied. This was useful to know for displays since a relaxation time of >40 ms would be greater than the frame time and the device could be considered as bistable.

The unipolar pulse technique of measuring R_t also simultaneously measured the bistability and contrast ratio (C_R). Qualitatively the bistability was seen by how little difference there was between the transmission levels when the pulse was applied (switched level) and when the pulse was removed (relaxed level) (Figure 4.3b). Quantitatively the bistability was defined as

$$\text{bistability} = \text{relaxed } C_R / \text{switched } C_R$$

where, C_R = maximum transmission level/minimum transmission level.

4.2 Polyimide Alignment

In this section the affect of the processing of the polyimide layer is investigated. An initial experiment was carried out which varied the rubbing pressure on the polyimide. This produced no difference to the alignment or electro-optic properties of any of the materials tried. This is because the director does not move at the surface therefore the strength of alignment is not important and because polyimide does not just form grooves when rubbed but also produces an electrostatic or chemical interaction with the FLC so that the rubbing pressure is not critical on alignment strength.

The next experiment was to investigate the importance of the surface pretilt angle on the electro-optic and alignment properties of SS devices [Bowry et al 1988]. For nematic liquid crystal (NLC) the pretilt angle can be varied from 0.1° to 6° by the processing conditions of the polymer [Mosley et al 1987, Gass et al 1987].

a. curing at 200°C is the normal treatment for NLC and gives a 1° surface pretilt.
b. curing at 300°C gives a higher surface pretilt of 6°.
c. reheating at 200°C after rubbing gives a 0.1° pretilt.

It was assumed that FLC also had a similar pretilt angle on these surfaces. (A selective pre-tilt angle of FLC when aligned on rubbed polymers has also been observed by Shingu et al [1988]). By aligning devices with the rubbing directions parallel (↑↑) and antiparallel (↑↓) two different device geometries could be produced which showed the importance of the pretilt angle (the higher the pretilt the larger the difference between the two devices). The materials used in this

experiment were SCE1, SCE2, ZLI3488 and ZLI3080. These materials do not have compensated pitches in the N^* phase and have short S_C^* pitches, they were therefore more difficult to align than the materials used in Section 4.3. However, this did make it easier to observe differences due to the pretilt angle.

The results are shown in Table 4.1. For comparison, the results for the same materials aligned in an HTA device are also shown. The alignment of the FLC depended on the size of the pretilt angle at the surface. For SCE1 and SCE2, which have the smallest N^* pitches, the higher pretilt layers produced bad alignment, (the pitch was sensitive to the pretilt angle). When the FLC was not aligned there was no bistability and the response time was slow. When the FLC aligned well the bistability, response time and cone angles were not affected by the pretilt angle but the alignment quality was.

One of the most important observations is that for materials with an S_A phase there was a difference in the number of zig-zags formed between parallel and antiparallel aligned devices. The parallel aligned devices produced few zig-zag defects and the antiparallel devices produced many zig-zags. Figure 4.4 shows the two possible layer and director configurations for the parallel and anti-parallel aligned cases when there is a pretilt angle. The anti-parallel case has two equi-energetic states, which form in equal amounts and many zig-zags appear where they meet. The parallel case has two unequal energetic states so that one state will dominate, there will be less boundaries and therefore less zig-zag defects.

Table 4.1: The affect of pretilt angle on alignment

Material	Alignment	Nominal pretilt (°)	Texture	Bistability	Response time (μs)
SCE1	reheat ↑↑	0.1	few zz	some	
	reheat ↑↓	0.1	many zz	some	
	200°C ↑↑	1	E.F.C.	none	250
	200°C ↑↓	1	E.F.C.	none	250
	300°C ↑↑	6	E.F.C.	none	
	300°C ↑↓	6	E.F.C.	none	
	HTA	30	F.C.	none	300
SCE2	reheat ↑↑	0.1	few zz	some	690
	reheat ↑↓	0.1	many zz	some	780
	200°C ↑↑	1	few zz	some	850
	200°C ↑↓	1	many zz	some	750
	300°C ↑↑	6	E.F.C.	none	1150
	300°C ↑↓	6	E.F.C.	none	1050
	HTA	30	F.C.	none	960
ZLI3488	reheat ↑↑	0.1	few zz	some	256
	reheat ↑↓	0.1	many zz	some	256
	200°C ↑↑	1	few zz	some	240
	200°C ↑↓	1	many zz	some	280
	300°C ↑↑	6	few zz	some	352
	300°C ↑↓	6	many zz	some	335
	HTA	30	V.small E.F.C.	some	642
ZLI3080	reheat ↑↑	0.1	E.F.C.	none	246
	reheat ↑↓	0.1	E.F.C.	none	198
	200°C ↑↑	1	small E.F.C.	none	165
	200°C ↑↓	1	small E.F.C.	none	190
	300°C ↑↑	6	V.small E.F.C.	none	206
	300°C ↑↓	6	V.small E.F.C.	none	250
	HTA	30	Uniform, no zz	excellent	158

zz = zig-zag, F.C. = focal conics, E.F.C. = elongated focal conics, V. = very
Response time measured using square waves at 30 Vpp, 100 Hz

Figure 4.4: Structure of the parallel and anti-parallel aligned SSFLC devices with a small surface pretilt

a. Parallel

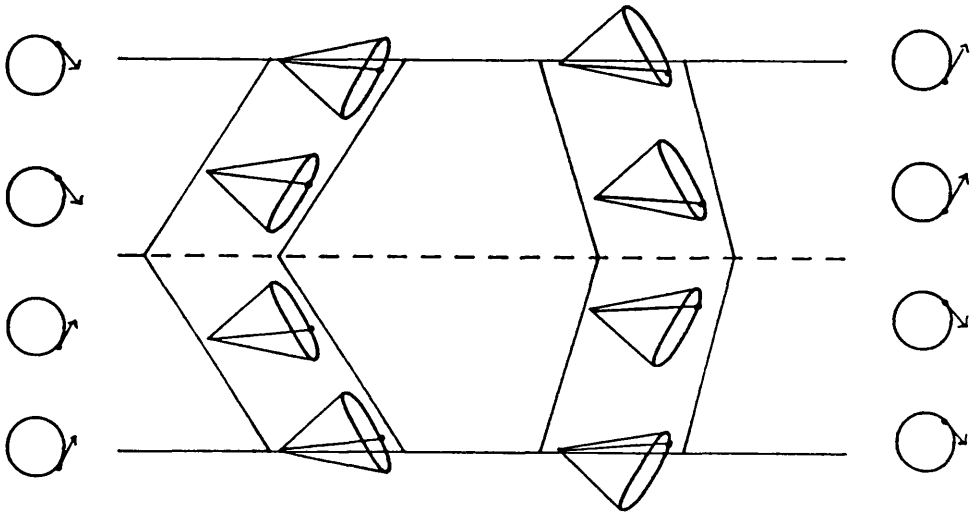

b. Antiparallel

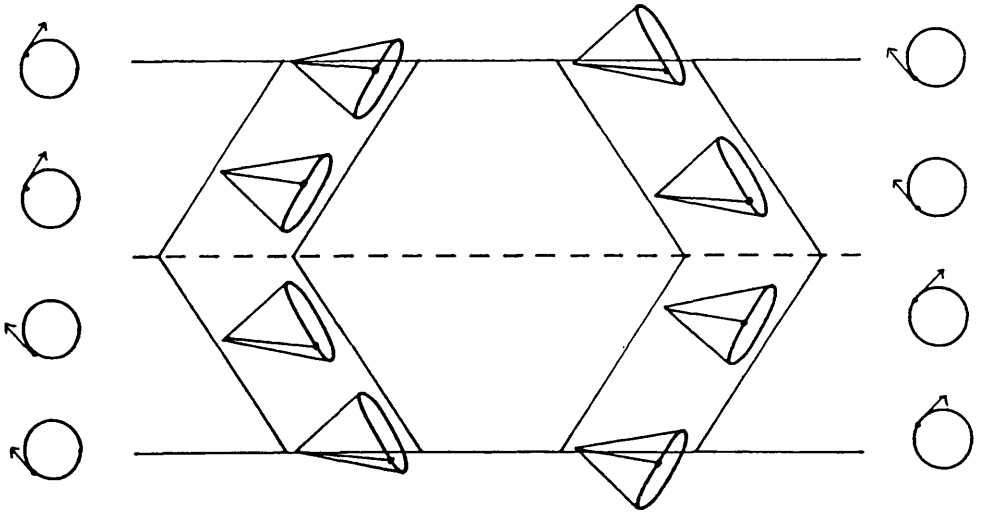

The material without an S_A phase ZLI3080 showed no difference between parallel and anti-parallel aligned polyimide devices because the material was not restricted to chevron layer structures and more than two states formed. However the pretilt angle did affect the alignment. The higher pretilt angles disrupted the alignment to produce small focal conics. It is worth noting that the ZLI3080 in the HTA device produced excellent alignment and bistability and a fast response time. However this material can no longer be used due to the crystallisation of one of the dopants. All the materials with an S_A phase produced bad alignment and bad electro-optic results in the HTA devices because the small pitch of the materials disrupted the alignment.

4.3 SiO Alignment

This experiment was designed to investigate the HTA geometry and compare it with the SS geometry. The HTA cells were constructed using SiO aligning layers evaporated at 5° to the surfaces with the evaporation direction of the top and bottom plates aligned parallel (5°SiO↑↑). To determine whether it was the geometry that was important rather than a 30° pretilt angle, the HTA cell was compared to a cell also with 5°SiO aligning layers but with the evaporation direction aligned antiparallel (5°SiO↑↓). Two surface stabilised alignments were compared with the HTA cells. One cell type used rubbed polyimide aligning layers with the rubbing direction aligned parallel (PI↑↑). This is the most common method of producing SS devices. The other cell type used SiO aligning layers evaporated at 30° to the surfaces with the evaporation directions aligned parallel (30°SiO↑↑). This gave a zero pretilt of the LC at the surfaces. If the behaviour of such SS devices was purely due to the geometry then these two cell types (PI↑↑ and 30°SiO↑↑) would produce the same results but they did not.

Plain ITO was also looked at but it produced a non-uniform homeotropic alignment for all the materials used, even when the ITO was rubbed.

Each alignment layer was studied when the FLC cooled slowly from the isotropic phase both with and without a d.c. field applied. The d.c. field could have two affects: (a) it could produce better alignment especially for materials with no S_A phase above the S_C^* phase, (b) the layer and director structure could be different when aligned in a field which could be used to help analyse the cell.

Four FLC materials were studied in each of these alignments, two supplied from BDH, SCE12 and 16042, and two from Merck, ZLI3654 and 87-703, in each case consisting of a material with and without an S_A phase above the S_C^* phase. Two manufacturers were used because they use different hosts; BDH use MBF esters and Merck use NCBs. These two host materials behaved differently in similar cell types. This showed that a FLC device is not only alignment layer dependent but it is also material dependent. All the cells were 2 μm thick. The results are presented for each material.

4.3.1 SCE12

SCE12 is a BDH material (MBF ester) with a phase sequence I-N^*-S_A-S_C^*. This material was placed in cells of all four types (5°SiO↑↑, 5°SiO↑↓, 30°SiO↑↑ and PI↑↑) and aligned both with and without a d.c. electric field. The results are presented in Table 4.2. The cells that were aligned without a d.c. field will be discussed first.

The first thing to note is that the textures produced on all four alignments were different (Figure 4.5). Both SS devices had many

Table 4.2 The Affect of Alignment Layer on SCE12

Alignment	Texture	Cone angle			Response Time			Bistability		Contrast Ratio	
		cone angle (with E)	relax angle (No E)	layer tilt	30 Vpp square (μS)	30V pulses (μS)	relax time (μS)	Qualitative	latch C_R / switch C_R	Switch $\frac{T_{max}}{T_{min}}$	Latch $\frac{T_{max}}{T_{min}}$
PI↑↑	Planar 2 domains few ZZ	23	±10	0	240	12	900	I	0.13	15	2
PI↑↑+dc	Planar 1 domain Few ZZ	21.5	±10	0	254	13	100	I	0.11	16	1.8
5° SiO ↑↑	Blue state domains Planar No Z.Z	22	±20	0	310	330	-	P	1	6.3	6.3
5° SiO ↑↑+dc	Planar No Z.Z	23	+22	0	250	250	-	P	1	7.4	7.4
5° SiO ↑↓	lots small black and blue domains No Z.Z	25.5	±25.5	0	104	80	-	P	1	4.6	4.6
5° SiO ↑↓+dc	As with no d.c	25	+20 -30	-5	220	175	-	P	1	3.2	3.2
30° SiO ↑↑	lots Z.Z. Only 1 domain Planar	21.5	+7 -8	-0	184	22	2 ms	I	1	10	10
30° SiO ↑↑+ dc	Planar lots Z.Z	19.5	±19	-4.5	600	110	-	P	1	11	11

zz = zig-zags, T_{max} = maximum transmission level, T_{min} = minimum transmission level, E = applied electric field, P = perfect bistability, I = relaxes to intermediate states

Figure 4.5 The textures of SCE12 on different alignments at 2 μm thickness

SCE12

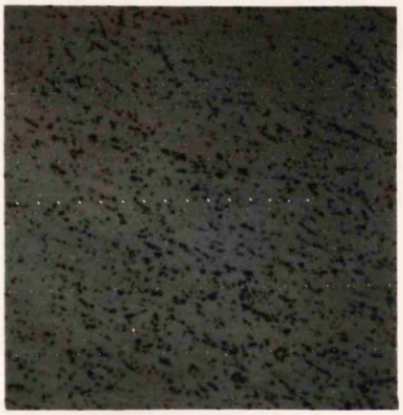

Polyimide

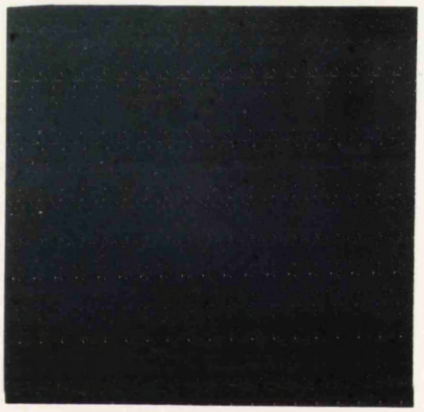

5 SiO ↑↑

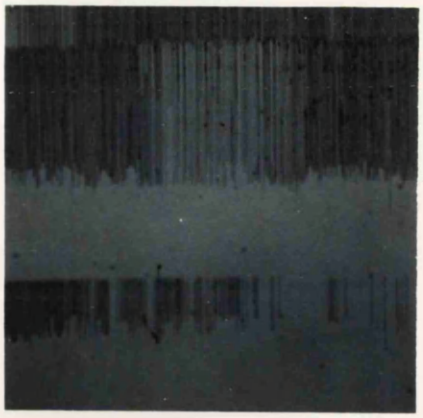

30 SiO ↑↑

5 SiO ↑↓

zig-zag defects although the 30°SiO produced a lot more than the PI, but neither of the 5°SiO devices had any zig-zag defects. Both 5°SiO alignments had twisted high tilt states as well as the two relaxed states but the 5°SiO↑↑ had a larger domain size than the 5°SiO↑↓ making it appear better aligned.

These results could be explained by considering the layer structure within each cell type. As shown in Section 3.3 the SS cells could develop two degenerate layer structures. Where these two layer structures meet, a discontinuity would form as a zig-zag. The PI cell had less zig-zags than the 30°SiO because it had a surface pretilt of ~1° whereas the 30°SiO had no pretilt. Therefore in the PI case one layer would be more energetically favourable and would predominate, so there would be less discontinuities where the different layer structures met and less zig-zags. The 30°SiO had zero pretilt angle so both layer structures would have equal energy causing many zig-zags to form. The 5°SiO cell types would both have only one possible layer structure with the layers lying perpendicular to the substrates. Since there was only one layer direction possible there can be no zig-zag defects.

One surprising result was that all the SiO aligning layers induced perfect bistability. Prior to this experiment it was believed that the bistability depended purely on the director configuration being able to be in two stable stables. These results show that the situation is more complex than this. In the case of the 5°SiO cell types there was only one straight layer structure. The director configuration of these two cell types when fully switched was very similar (Figure 3.8). Since most of the director was uniform and there was no strain due to the layers, there was no force acting on the director to make it relax

towards the surface directors. This allowed both 5°SiO cells to be bistable and to behave in a similar manner. In the case of the 30°SiO, it was only bistable when a large field had been applied and a lined texture appeared. The bistability was probably due to the large number of line defects pinning the director and preventing nucleation.

The response time (R_t) of SCE12 was not only a function of the material but it was extremely dependent on the alignment used and the measurement technique used. For the 5°SiO cell types there was little difference in R_t for the two measurement techniques used but for the SS devices the R_t became shorter when measured using the pulsed technique. The SS devices relaxed into an intermediate state after a pulse so that the next pulse needed only to switch the FLC from the intermediate state to the switched state. In the case of the 5°SiO cells there was no relaxation so each pulse had to switch the FLC from one switched state to the other switched state.

To compare the R_t of different cell types a square wave measurement was used so that the FLC was always being switched between the two switched states. The most striking feature about these R_t measurements was that the 5°SiO↑↓ cell was faster than both the PI and 5°SiO↑↑ cells even though one would expect both 5°SiO cells to take longer to switch because of the extra domain nucleations due to the appearance of the twisted high tilt states. However, this could be explained by the fact that 5°SiO↑↓ cells had smaller domain sizes which meant that it had more nucleation sites. Nucleation of new domains is a quicker switching process than the growth of domains. Therefore if the 5°SiO↑↓ cell nucleated a lot more small domains than the other cell types it would also have a faster R_t. The 5°SiO↑↑ cell type was slower than the PI

because although they had similar domain sizes and would nucleate just as quickly, the 5°SiO↑↑ cells would nucleate through the twisted high tilt states which would make the process slower.

The cone angle and contrast ratio measurements also depended on the alignment. The 5°SiO cells had larger measured cone angles than the SS devices. This may be explained by assuming that the high surface pretilt was less restricting on the director configuration in the bulk i.e. a surface director of 30° pretilt would be more likely to have some flexibility in movement than a 0° pretilt. This would allow the bulk of the LC to move towards the true cone angle of the material when a field was applied. This may also be why the bistability was better.

Although the cone angle was larger in 5°SiO cells the contrast ratio (C_R) was smaller. This could be attributed to the out of plane tilt of the surface director reducing the overall contrast. The 5°SiO↑↓ cell had the lowest C_R because it had a cone angle larger than the optimum of 22.5° therefore the optics was unmatched to the polarisers and the C_R was reduced. The 30°SiO cell had a lower C_R than the PI cell because of the large number of zig-zag defects present.

Adding a d.c. field to the FLC as it was cooling did not make any significant difference to the texture nor electro-optic properties of any of the alignments unless the field induced another texture to form as with the 30°SiO. The layers form in the S_A phase and in this phase the d.c. field would make no difference to the director alignment. As the FLC cools into the S_C^* phase the d.c. field would make the director tilt to the cone angle but because the layer structure is purely related to the pitch of the layers, the chevron structure would form

independently of the field. If the field was too high the layers would distort to form the lined texture and the behaviour of the cell became different.

4.3.2 16042

10642 is a BDH material that is similar to SCE12 except that it has a phase sequence of I-N^*-S_C^*. The electro-optic results of this material when placed in cells of all four types are shown in Table 4.3 and photomicrographs of the textures are shown in Figure 4.6. The alignment of 16042 was very different to SCE12 due to the fact that 16042 has no S_A phase (this caused most of the observed electro-optic differences). In the 16042 material both the layers form and the director tilts at the N^*-S_C^* transition. This allows the layers to form at an angle to the alignment direction rather than chevron layers having to form (also observed by Hatano et al [1986]). The layers are equally likely to tilt at either a positive or negative angle to the alignment direction and so the layers form in two directions. The layers formed at an angle to the alignment direction (7°-13°) which was less than the cone angle (27°) and despite the layers being free to form with the director at any angle on the cone, only two layer directions develop. This can be explained by realising that the layers form at the N^*-S_C^* transition. This transition is first order and there will be a discontinuous jump in the cone angle from 0° to a finite value. However, this value will be less than the measured θ_C at room temperature because the transition occurs at 63.3°C. At this temperature the cone angle is <20°. Therefore at the N^*-S_C^* transition the layers form at an angle <20°. Once the layers have formed they are unlikely to move and the layers could then chevron to accommodate the cone angle as with the SS states.

Table 4.3 The Affect of Alignment Layer on 16042

Alignment	Texture	Cone angle			Response Time			Bistability		Contrast		Comment
		Cone angle (with E)	relax angle (no E)	layer tilt	30 Vpp square (μs)	30V pulses (μs)	relax time (μs)	Qualit-ative	$\frac{latch\ C_R}{switch\ C_R}$	$Switch\ \frac{Tmax}{Tmin}$	$Latch\ \frac{Tmax}{Tmin}$	
PI↑↑	S_A lines 2 layers tilts	(1) 28 (2) 26	-2 +2	+13 -12	-	-	-	-	-	-	-	layer tilts prevent measurement
PI↑↑ + dc	1 layer tilt S_A lines	23	-3	+19	600	220	2.25 ms	None	-	17.3	-	
5° SiO ↑↑	Planar- 2 layer tilts	(1) 31 (2) 27	+21 -41 -16 +38	 -10 +11	400	10 ms	1 ms	None	-	5.7	-	
5° SiO ↑↑ + dc	Planar-1 layer tilt	27	+11 -44	-16	338	382	-	P	1	32	32	
5° SiO ↑↓	Lot of texture 1 domain dominates	(1) 31 (2) 31	+14 -12	+7 -8	740	24 (switch only)	360	None	-	2.2	-	
5° SiO ↑↓+dc	Texture of 45° to evaporation Planar	28	+40 -16	+12	394	235	-	P	1	10	10	
30° SiO ↑↑	Planar lots S_A lines	(1) 25 (2) 24	+14 +10 +24 +20	-7 +2	1.5 ms	34 (switch only)	1 ms	None	-	8.5	-	
30° SiO ↑↑ + dc	S_A lines but more uniform background	20	+2	+16	1 ms	87 (switch only)	1 ms	None	-	15.3	-	

zz = zig-zags, T_{max} = maximum transmission level, T_{min} = minimum transmission level, E = applied electric field, P = perfect bistability, I = relaxes to intermediate states

Figure 4.6 The textures of 10642 on different alignments at 2 μm thickness

16042

Polyimide

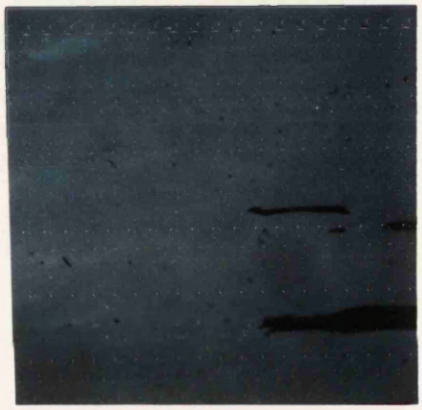

5 SiO ↑↑

30 SiO ↑↑

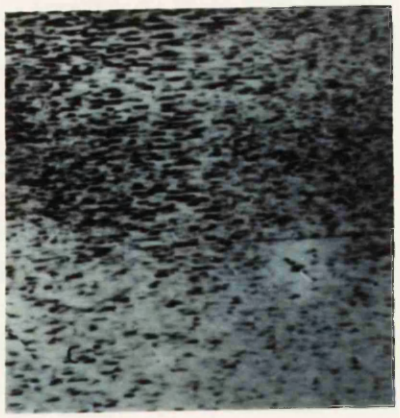

5 SiO ↑↓

One strange property of the material was that in the HTA cell, two layer directions also formed whereas previous results using ZLI3080 showed that this need not happen and theory predicted that it should not happen. The splitting of the layers into two directions in HTA cells may be due to the cone angle being a lot less than the pretilt angle at the N^*-S_C^* phase transition. In this case the layers would not be able to form perpendicularly to the surfaces so they must either chevron or tilt with respect to the aligning direction. Forming tilted layers would be energetically favourable over chevron layers. Therefore to get good alignment in a material with no S_A phase (as with ZLI3080) it must have a first order transition that has a large cone angle at the N^*-S_C^* transition.

It was essential to remove the degeneracy of the layers in 16042 before any measurements were taken because the two layer directions have different optical contrasts which destroy any electro-optic properties (unlike the chevron layers of the SS states). This was achieved by aligning the FLC with a d.c. field applied. The field would switch the director to one side of the cone so that only one layer direction could form. The rest of this discussion will be based on the alignments when a d.c. field was applied.

One obvious result of not having an S_A phase was that no zig-zag defects formed in any of the cell types. Although there were two layer structures in the cells each layer tilt would form an elongated domain (Figure 4.6) with domain walls where the two structures met instead of zig-zags. However, another texture also appeared called the lined texture. These lines were similar to elongated zig-zags.

The R_t of 16042 was slightly longer than for SCE12 but again it was very dependent on the alignment used. Both the SS devices had a long R_t when measured with a square wave. This was similar to the situation with SCE12. However, the 5°SiO cells both had a similar R_t and are not much slower than SCE12 on 5°SiO. The R_t was also dependent on the measuring technique for the SS devices. No relaxation occurred in 5°SiO cells therefore the R_t was similar using both techniques.

Both SS devices had no bistability at all because the layer tilt favoured one director configuration over the other (Figure 4.7). The cell would therefore always relax back to the alignment direction. On the other hand the 5°SiO alignments both had good bistability even though there was a large layer tilt. Again this may relate to the flexibility of the surface director when there was a large surface pretilt angle.

The measured cone angle of 16042 was different for the four alignments but the trend was the same as for SCE12. The 5°SiO alignments had higher cone angles than the SS devices. This could be related to the flexibility of the surface director as with the SCE12 material.

The contrast ratio was similar in both SS devices (and are similar to SCE12 SS devices), but unlike SCE12, the HTA device had a lot higher C_R than both SS devices because the alignment quality was better.

4.3.3 ZLI3654

The material ZLI3654 from Merck has the phase sequence I-N^*-S_A-S_C^*. The results from the alignment studies are shown in Table 4.4 and the textures are shown in Figure 4.8. This material behaved in a similar

Figure 4.7: A layer tilt causes only one director configuration to be stable

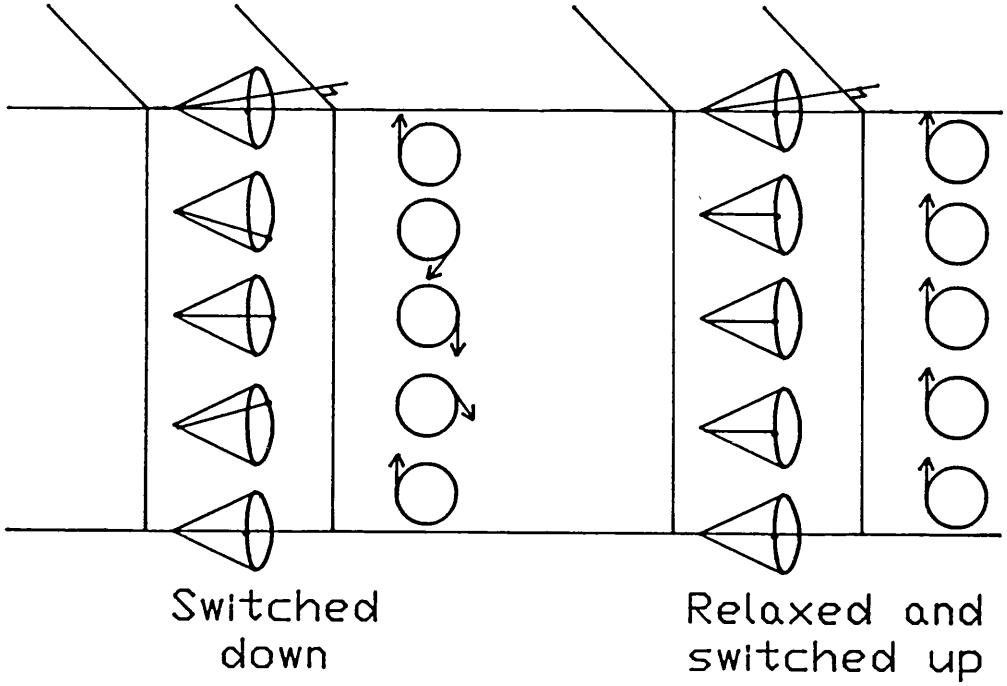

Table 4.4 The Affect of Alignment Layer on ZLI3654

Alignment	Texture	Cone angle			Response Time			Bistability		Contrast		Comment
		cone angle (with E)	relax angle (No E)	layer tilt	30 Vpp square (μs)	30V pulses (μs)	relax time (μs)	Qualit-ative	$\frac{\text{latch } C_R}{\text{switch } C_R}$	Switch $\frac{Tmax}{Tmin}$	Latch $\frac{Tmax}{Tmin}$	
PI↑↑	Planar few zz	19	±18	0	142	35	820	I	0.25	23.3	5.7	
PI↑↑+dc	Planar few zz	19	-8	0	176	37	484	I	0.41	14	5.75	
5° SiO ↑↑	Planar blue states No zz	21.5	±21.5	0	80	37	-	P	1	22.8	22.8	
5° SiO ↑↑+dc	Planar No zz	-	-	-	51	32	-	P	1	-	-	Blew up when took θ_c measurements
5° SiO ↑↓	Planar No zz	19	±19	0	40	40	-	P	1	3.5	3.5	
5° SiO ↑↓+dc	Planar No zz	-	-	-	64	44	20 ms	one state more stable	0.37	7.5	2.8	Blew up when took θ_c measurements
30° SiO ↑↑	S_A lines	19	+15	0	67	41	-	P	1	7	7	
30° SiO ↑↑+ dc	S_A lines	21.5	-21	0	83	59 (switch only)	1.5 ms	I	0.7	2	1.4	

zz = zig-zags, T_{max} = maximum transmission level, T_{min} = minimum transmission level, E = applied electric field, P = perfect bistability, I = relaxes to intermediate states

Figure 4.8 The textures of ZLI3654 on different alignments at 2 μm thickness

ZLI3654

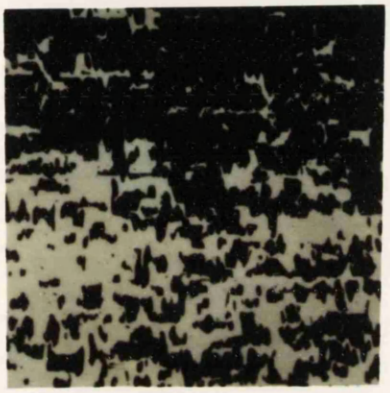

Polyimide

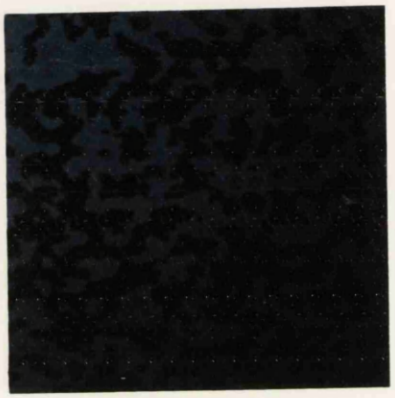

5 SiO ↑↑

30 SiO ↑↑

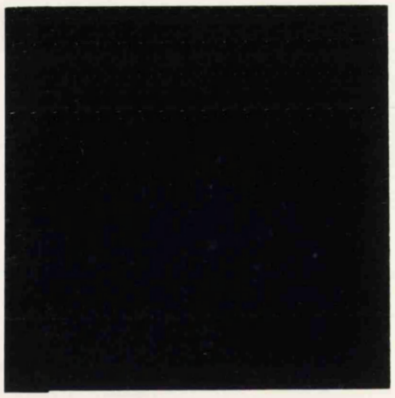

5 SiO ↑↓

manner to SCE12 in all the cell types except that in the HTA cells ZLI3654 had a faster response time and a higher contrast ratio than SCE12.

The R_t of ZLI3654 in all the SiO cells (30°SiO↑↑, 5°SiO↑↑ and 5°SiO↑↓) was faster than SCE12. Yet the quoted R_t from the manufacturer for this material is slower than SCE12 because a rubbed polymer alignment is used for the measurement and ZLI3654 switches comparatively slowly when aligned on a polymer. This difference in R_t is very important when using an HTA device where a material like ZLI3654 would be preferable because it switches faster. The reason for the difference in behaviour between the two materials is not clear. Material properties such as P_s, pitch, $\Delta\epsilon$ and θ_c have been varied but none have given this type of alignment dependence of the R_t. The conclusion drawn is that the difference is due to the chemical interaction between the FLC material and the surfaces but a clearer understanding of these effects needs to be acquired.

The contrast ratio (C_R) is another property that was different for ZLI3654 than for SCE12. In the case of ZLI3654 both the PI and HTA alignments had high C_R and the 5°SiO↑↓ and 30°↑↑ had low C_R. The HTA device had the highest C_R because it had a cone angle most suited to the optimum of 22.5°.

One other observed difference between SCE12 and ZLI3654 was found in the 30°SiO cell. This cell formed an alignment texture without any zig-zag defects but with a lined texture instead because this cell was slightly thinner than the others (1.5 μm) which prevented the zig-zags forming (see Section 4.4). This did not appear to affect the cone angle,

bistability or response time (ZLI3654 switched quickly on all the SiO alignments). However this alignment texture may reduce the contrast especially since the cell was only 1.5 μm thick.

Aligning the cells with a d.c. field produced little change on the alignment and electro-optic properties (as with SCE12). The most noticeable change was the reduction in bistability of the 5°SiO↑↓ and 30°SiO↑↑ cells. This affect was due to charge migration that switched the director into the opposite state to the aligning d.c. field.

The other effect that Table 4.4 shows is that 5°SiO cells were more susceptible to dielectric breakdown of the FLC than the SS alignments. The PI and 30°SiO are continuous planar layers that can act as an insulating layer whereas the 5°SiO has a loose, column structure that can allow charge injection from the electrodes. This could be overcome by adding an insulating barrier layer between the ITO electrode and the 5°SiO layer.

4.3.4 87-703

The material 87-703 from Merck has a phase sequence I-N^*-S_C^*. The alignment results are shown in Table 4.5 and the textures are shown in Figure 4.9. This material behaved in a similar manner to 16042 except in two details;

(1) The R_t for 87-703 (in all alignments) was quicker than for 16042 and was comparable to ZLI3654. As discussed in Section 4.3.3, the reason for this was probably due to the chemical interaction between the FLC and the surfaces.

Table 4.5 The Affect of Alignment Layer on 87-703

Alignment	Texture	Cone angle			Response Time			Bistability		Contrast		Comment
		cone angle (with E)	relax angle (No E)	layer tilt	30 Vpp square (μs)	30V pulses (μs)	relax time (μs)	Qualit-ative	latch C_R / switch C_R	Switch $\frac{T_{max}}{T_{min}}$	Latch $\frac{T_{max}}{T_{min}}$	
PI↑↑	lined texture	27	0	-2	160	24 (switch only)	1.2 ms	none	-	14.6	-	
PI↑↑+dc	lined texture	28	+2	-12	135	28 (switch only)	0.9 ms	none	-	10	-	
5° SiO ↑↑	Planar 2 layer tilts 2 twisted states	(1) 25 (2) 25	+13 -28 +24 -16	-8 +5	-	-	-	-	-	-	-	2 layer tilts prevent measurements
5° SiO ↑↑+dc	Planar	26.5	-13 +38	+12.5	40	66	-	P	1	4.5	4.5	
5° SiO ↑↓	Planar 2 layer tilts 1 twisted state	(1) 28.5 (2) 29	+24 -29 +29 -23	-2.5 +4	67	67	-	P	1	1.3	1.3	
5° SiO ↑↓+dc	Planar	29	+21 -37	-8	82	82	-	P	1	2.6	2.6	
30° SiO ↑↑	lined texture	24	±7	+1	55	17 (switch only)	720	none	-	14.5	-	
30° SiO ↑↑+ dc	lined texture	24	-24 -37	-14	57	240	700	I	0.75	11.3	1.75	

zz = zig-zags, T_{max} = maximum transmission level, T_{min} = minimum transmission level, E = applied electric field, P = perfect bistability, I = relaxes to intermediate states

Figure 4.9 The textures of 87-703 on different alignments at 2 μm thickness

87-703

Polyimide

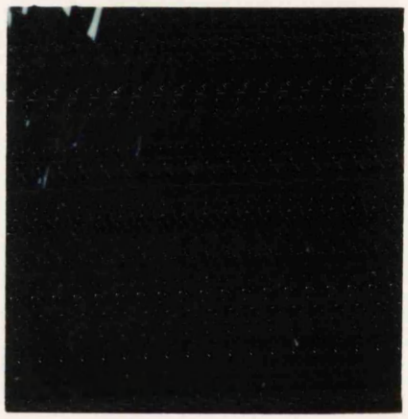

5 SiO ↑↑

30 SiO ↑↑

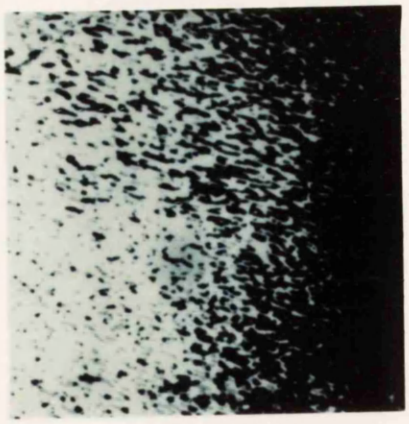

5 SiO ↑↓

(2) The C_R was lower for 87-703 (in all alignments) than for 16042 and had the highest value for 30°SiO rather than the HTA cell. This was probably due to θ_C being nearer the optimum of 22.5° for 30°SiO than the other alignments.

4.3.5 Summary of alignment considerations

One of the most surprising results was that the alignment and electro-optic properties of the 5°SiO↑↓ cells were similar to the 5°SiO↑↑ (HTA) cells. Neither cell type gave zig-zag defects and both gave perfect bistability and, for the Merck materials, fast response times could be obtained. This showed that the geometry was not as important as originally predicted by theory. The director configurations of the two alignments were not that dissimilar and the position of the surface director was less important than originally thought.

The phase sequence of the FLC material was extremely important in determining the behaviour of the device. Of the two types used, a material with the phase sequence I-N^*-S_A-S_C^* is preferable to use in all cell types tested. These materials easily produce good alignment and can produce good electro-optic behaviour. When such a material was aligned in a 5°SiO cell excellent bistability could be obtained with no zig-zag defects and a fast switching speed (for Merck materials anyway). The materials with the phase sequence I-N^*-S_C^* were more difficult to align and required a d.c. field to be applied whilst cooling from the isotropic phase. Surprisingly HTA cells also produced two tilted layer directions as did the SS cells. This may be related to the pretilt angle at the surface being larger than the cone angle at the N^*-S_C^* transition therefore the layers tilt as in the SS case. When a d.c.

field was applied whilst aligning a material with an S_A phase no change in alignment was obtained because the layers form in the S_A phase so there was no advantage in doing this.

For a display device it was very significant that a 5°SiO alignment could produce excellent bistability with no zig-zag defects. The zig-zag defects are visible in a display and are not only unattractive but can also reduce the contrast. The excellent bistability is important in order to achieve a good contrast when multiplexing a display. These two facts make it very attractive to use a 5°SiO alignment. The 5°SiO↑↑ cell is slightly better to use for displays because it has a higher contrast but in some applications the 5°SiO↑↓ would be preferable because it switches slightly faster.

The measured R_t was very dependent on the alignment and the FLC material used. For the PI alignment the BDH materials gave the fastest switching but for the 5°SiO alignments the Merck materials were fastest. This has been attributed to chemical interactions between the FLC material and the surfaces. The R_t also depended on the measurement technique used. For the SS alignments that have a relaxation process it made a big difference if the cell was allowed to relax into the intermediate state before measuring the R_t (pulsed technique) or delay time (square wave technique). For the 5°SiO alignments that have little or no relaxation the two techniques of measuring R_t produced similar results. The technique to be used should be dictated by the application that the R_t is being tested for.

The measured cone angle of the materials was also a function of the alignment. The 5°SiO cells produced a higher measured cone angle than

the SS cells. This has been attributed to the ability of the surface director to move in the 5°SiO cells towards the direction of the bulk director. This increased the measured cone angle.

The contrast angle depended on the birefringence, cone angle, device thickness and alignment quality. It was therefore unwise to read too much into comparisons of this property. However, the 30°SiO and 5°SiO↑↓ alignments did produce low contrasts and the materials with no S_A phases produced high contrasts. The reason for this may purely relate to the alignment quality and cone angle optimisation.

The results in this section have shown that there is not just one FLC device but four different sorts that depend on the alignment layer and the phase sequence of the FLC material. The 5°SiO alignments produced a different device from the SS alignments and the materials with an S_A phase produced a different device from the materials without an S_A phase. The detailed properties of each device could be modified by changing the material host or the type of layer used for the alignment. Unfortunately not enough is known about how the device is affected by these parameters to be able to predict the properties. This section has also highlighted the fact that it is always important to quote the alignment and measurement technique used for any quoted result if it is to be useful, this includes R_t, θ_c, C_R and bistability.

4.4 Layer Thickness

The performance of a FLC device is not only determined by the material and alignment used but also on the device parameters such as thickness and temperature. The device thickness (d) is particularly important in determining many properties and is investigated here. The device must

be sufficiently thin to unwind the helix. Clark and Lagerwall [1980] proposed that the S_C^* pitch (P_o) is unwound when d < pitch. The device also has to be thin enough to induce bistability even when d<< pitch. However, the thicker the device, the easier it is to fabricate. The chosen device thickness is therefore a trade-off between these requirements.

The affect of pitch on the alignment was investigated by using wedge cells (0-6 μm) to observe the change in texture and the onset of the pitch forming. The affect of thickness on bistability was studied using cells of different thicknesses and observing the changes in the electro-optic properties. Both the surface stabilised alignment using rubbed polyimide and the high tilt alignment were used with the material SCE12. The measurements were made at room temperature at a constant field (15 V/μm). Photographs of the textures seen in the wedge cells at different thicknesses are shown in Figure 4.10a and b and the electro-optic results are shown in Table 4.6.

4.4.1 Texture

For thicknesses $\geq$ 1.8 μm the polyimide cells all had a similar planar texture with a few zig-zags. For thinner polyimide cells a lined texture appeared in the background and the zig-zags disappeared. For such thin cells the cone angle was less therefore the chevron structure of the layers must have had less of a tilt. The layers may in fact have been arranged in a tilted layer fashion rather than a chevron. This would remove the zig-zag defect but there would be two layer tilts which would give the lined texture. The HTA cells had two twisted states (pale domains that did not extinct) and two untwisted states (which did

Table 4.6 The Affect of Layer Thickness on Device Performance Using SCE12

Align	thickness (μm)	Texture	Cone angle		Response time			Bistability		C_R		Colour
			θc switched	θc relaxed	R_t square 15V/μm (μs)	R_t pulses 15V/μm (μs)	Relax time (ms)	Qualitative	$\frac{C_R \text{ latch}}{C_R \text{ switch}}$	Switch	Latch	
PI↑↑	0.7	lined	+13 -15	0	98	39	0.14	none	0.21	4.7	1	black/blue
	1.8	Uniform, two domains, no zigzags	+23 -24	+14 -4	197	21	1	I	0.38	6.1	2.3	black/yellow
	3	Uniform, two domains, few lines	±26	+15 -17	173	36	1.5	I	0.18	7.6	1.4	black/pink
	5.5	Uniform, two domains, few zigzags	±27	±5	183	21	3	I	0.28	7.2	2	black/blue
	7	Uniform, two domains, few zigzags	±27	0	188	30	5	I	0.43	5.8	2.5	green/pink
5° SiO ↑↑	1	Uniform, two domains	+24 -23	±20	292	745	-	P	1	9.2	9.2	black/grey
	1.5	2 blue domains 2 yellow/black domains Uniform	+26 -24	±22	275	340	-	P	1	5.9	5.9	black/pale yellow -
	3.1	2 blue states (twisted) 2 black/yellow domains	+30 -27	+30 -29	285	312	-	P	1	5.6	5.6	black/green
	4.5	2 pink domains (twisted) 2 green/black domains	+30 -29	+30 -29	215	275	-	P	1	5.5	5.5	black purple/green
	6.5	background of 2 yellow domains (twisted)and 2 purple/pink domains	±23	+19 -14	210	300	-	P	1	5.6	5.6	blue/pink

p - perfect bistability, I - relaxes to intermediate states

Figure 4.10a The textures of SCE12 aligned in an HTA wedge cell 0-6 μm

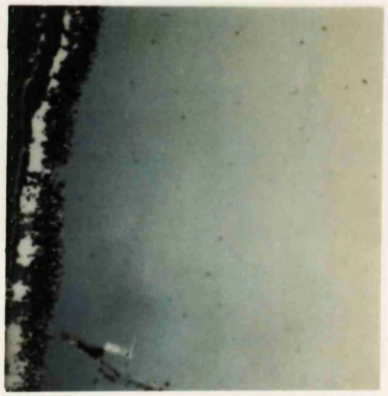

1 μm

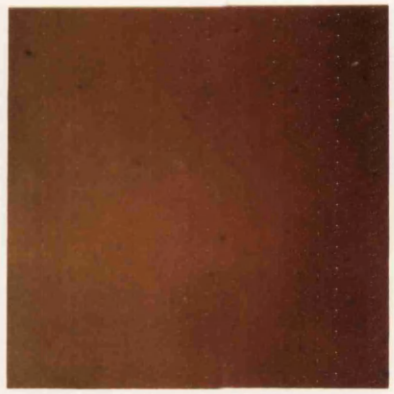

2 μm

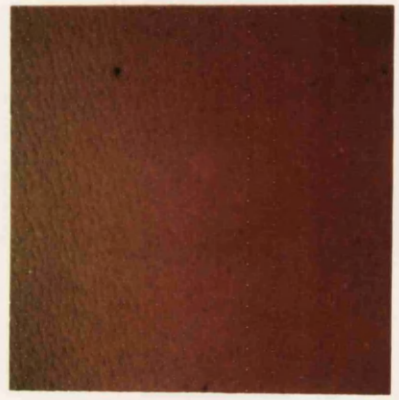

3 μm

4 μm

5 μm

6 μm

Figure 4.10b The textures of SCE12 aligned in a polyimide wedge cell 0-6 μm

2 μm

3 μm

4 μm

5 μm

6 μm

extinct) except for the cells < 1.5 μm. In the thin SiO cells the boundary conditions were strong enough to produce only the untwisted states.

The HTA cells also had a faint lined texture in the background of the thin areas. These lines grew to form elongated focal conics in the thick areas (Figure 4.10a). Pitch lines formed in both the HTA and SS wedge cells but they formed with a more distinct boundary in the polyimide cells than the HTA cells (this was also found to be true for ZLI3654). In the HTA cell there was a tendency for the alignment to be disrupted and focal conics to form when the pitch started to appear. The texture also deteriorated more rapidly in HTA cells than SS cells and pitch lines started to form from the apex's of the focal conics. This is because the HTA device is more sensitive to helical pitch. The distinctive S_C^* pitch can be seen in Figure 4.10b in the SS cell at 6 μm. In the SS cells the thickness at which the S_C^* pitch formed was 6 μm and in the HTA cells it was 4-5 μm. The S_C^* pitch of SCE12 is 2.4 μm and the N^* pitch is compensated.

4.4.2 Cone Angle

For both SS and HTA cells the measured cone angle got bigger as the cell got thicker until about 3 μm when it reached a plateau. (The thick (6.5 μm) HTA cell had a smaller measured cone angle than the thin cells due to the colours of the cell). The stronger boundary conditions in the thinner cells clearly had a strong influence on the degree of freedom that the director had and therefore on the cone angle.

4.4.3 Bistability

For both the SS and HTA cells a difference could be seen between the

long term bistability, shown by the relaxation of the cone angle, and the short term bistability, shown by the measurement of bistability using a continuous train of pulses with a pulse to gap ratio of 1:10. The SS cells all showed short term intermediate bistability except the very thin 0.7 μm cell which showed none. In this case the boundary conditions were strong enough to always pull the director into the alignment direction with a very fast relaxation time. The best long term bistability in SS cells occurred at 3 μm, when there was the least relaxation of the cone angle. However, both the thick cell (7 μm) and the thin cell (0.7 μm) relaxed into the alignment direction given enough time. Clearly the condition for bistability required that the boundary forces to be neither too strong nor too weak. If they were too weak then degeneracies in the director configuration were allowed and the bistability was disrupted and if they were too strong the director was pulled into the alignment direction.

In the HTA case the short term bistability was always perfect even at 1 μm thick, but there was a long term relaxation as shown by the few degree change in the cone angle. As with the SS case the long term relaxation occurred in thick and thin cells and the best bistability was obtained in cells 3-4.5 μm thick. It should be noted that the fact that perfect bistability could be obtained in 4.5 μm cells was a very significant result for the production of devices and even thicker cells could be used if some relaxation was allowed.

4.4.4 Response time

The HTA cells were all slower than the SS cells because the FLC material used was SCE12. The two methods of measuring response time (R_t) gave similar results for HTA cells (no relaxation) but different results for

the SS cells (relaxed between pulses). The SS cells all gave similar results (i.e. R_t was independent of thickness) except for the 0.7 μm cell when measured with a square wave. The response time was twice as fast because the cone angle was half the value of the other cells so the director had to switch less distance. The 0.7 μm cell when measured using the pulsed technique gave a longer R_t than the other thicknesses maybe because the cell relaxed into a more stable position between each pulse, i.e. was not moving when the pulse was applied. The relaxation time for the SS cells increased with increasing thickness (Figure 4.11) reflecting the weaker boundary forces as the thickness increased.

The HTA cells measured using 15V/μm pulses all gave similar R_t except for the 1 μm cell which as for the SS cell gave a longer measurement. For the square wave measurements there was a slight trend to get faster as the cell got thicker. If the R_t of HTA cells was dominated by nucleation then the thinner cells which have stronger surface forces would be slower. For SS cells nucleation is less important so this effect would not be so obvious.

4.4.5 Contrast and appearance

The contrast ratio (C_R) did not vary systematically with thickness but in general the HTA cells had a higher contrast ratio when switched andcertainly had a higher contrast ratio when latched because they were perfectly bistable. From an appearance viewpoint the best cells for SCE12 were when 1.5 μm $\leq$ d $\leq$ 5.5 μm. Less than 1.5 μm then the brightest state started to become darker and the perceived C_R was reduced. Thicknesses greater than 5.5 μm had coloured states instead of black and the perceived C_R was reduced. The exact thickness suitable

Figure 4.11: The affect of thickness on the relaxation time of SSFLC devices (SCE12)

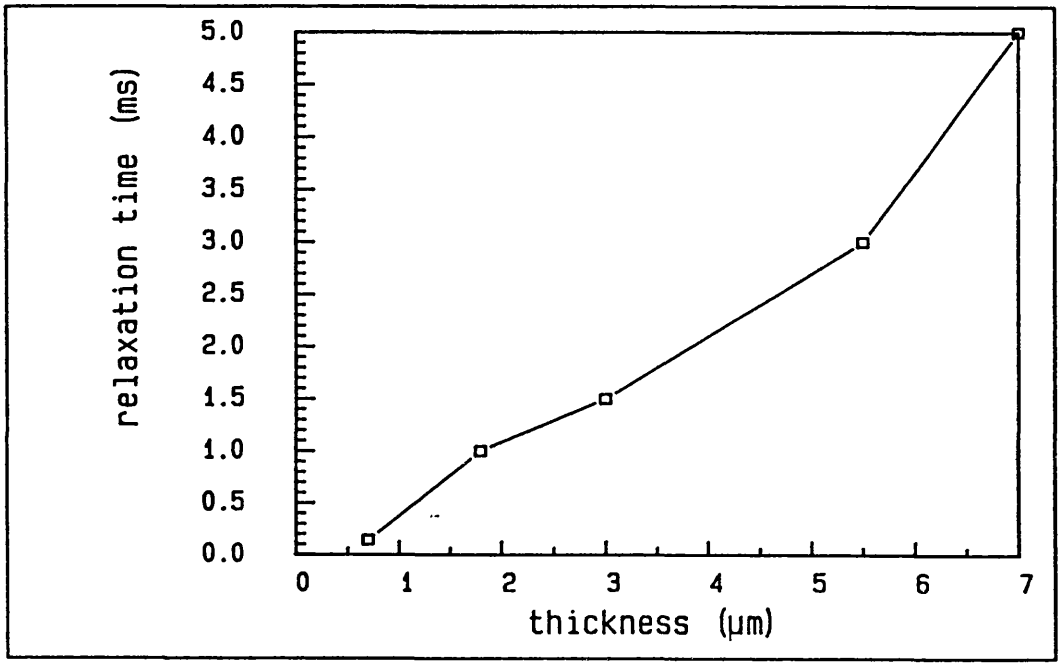

for a display would be when a black and white display is achieved with maximum C_R, which would depend on the birefrigence, Δn, of the material and must match

$$\frac{\Delta n d}{\lambda} = \frac{1}{2.}$$

For SCE12, $\Delta n = 0.18$, giving the optimum thickness for black and white switching as $d = 1.4\ \mu m$ which is close to the value for the optimum appearance although the C_R was starting to reduce at this thickness. For ZLI3654 $\Delta n = 0.12$ which has an optimum thickness of $d = 2.1\ \mu m$ which is the thickness used in production at present.

4.4.6 Summary of thickness considerations

The influence of the boundaries imposed on the FLC were very important to the cell behaviour. If the cell was too thin, the boundary forces were too strong and the director could not move to its natural position so that θ_c was reduced, bistability was lost or reduced and the R_t was altered. If the cell was too thick, the boundary forces were not strong enough and the director configuration became degenerate, this also reduced θ_c and bistability. For SCE12 the optimum electro-optic properties were at 3-4 μm for both the HTA and SS cells. However it is important to note that for HTA cells the electro-optic properties were still very good at 6.5 μm thick and perfect bistability was still observed.

When choosing the appropriate thickness for a device there are several factors to take into account which can be conflicting.

(1) The appearance of the device. For a display a high contrast is required with black and white switching. The colour depends on the Δn which for current materials is between 0.12-0.2. Even for materials of $\Delta n=0.12$, a thickness of 2 μm or less is required for black and white switching. To be able to use thicker devices either the Δn of the material must be reduced or a second order white must be used. This will occur at a thickness of 3 μm-3.5 μm.

(2) The voltage applied to the device. To drive FLC devices quickly with large voltages requires complex electronics because of the stringent requirements on rise times. If the cell can be driven with a voltage less than CMOS level (18V) then this becomes easier. Thinner cells are better for this requirement since $E \alpha 1/d$.

(3) The capacitance of the device. For displays it is important to be able to put very short (~30 μs) pulses across a pixel. In order to reduce the transmission line problem it is necessary to have a small capacitance. Thicker devices are therefore better for this requirement.

(4) A FLC device must be bistable. For SS devices this limits the device to $\leq$3 μm but for HTA devices a 6.5 μm device can easily be used.

(5) Ease of manufacture. It is far easier to manufacture 10 μm cells (nematic LC technology) than 2 μm cells (current FLC technology). The thicker the cell the easier and therefore cheaper it will be to make the display.

To choose an appropriate thickness for a display is therefore a trade off between ease of manufacture with a small capacitance (large thickness) and good optical properties achieved with low voltages (small thickness). At present 2 μm thickness is the accepted for FLC technology using SS technology but if materials with low Δn were made ($\Delta n = 0.07$) then a 3.5 μm HTA cell would be a better compromise between all the factors.

4.5 Material Considerations

It was shown in Section 4.3 that the phase sequence of the material is important in determining the properties of both the SS and HTA devices. The materials with an S_A phase were shown to be better than the materials without an S_A phase for both alignments although there were differences between the Merck materials and the BDH materials especially between the response times. However Section 4.2 showed that the material ZLI3080 which has no S_A phase could have excellent electro-optic properties in an HTA cell. This highlighted the fact that the chemical composition of the FLC material was also very important in determining the device properties. To explore the affect of different chemical compositions was difficult because most commercially available materials are eutectic mixtures and contain a host plus many dopants. Some experiments were carried out using materials made at RSRE for two different hosts NCB and MBF esters. A series of three were made for each host where the percentage of one of the dopants was varied to make

one with an S_A phase, one without an S_A phase and one on the border between the two. Both series behaved the same where the materials with an S_A phase behaved like SCE12 and the materials without an S_A phase behaved like 16042.

The affect of S_C^* pitch and P_S were also investigated by having materials with the same host but different material properties. Again there was little difference between the alignment and electro-optic properties of these materials. Changing the P_S value from 2 $nC/\mu m^2$ to 20 $nC/\mu m^2$ did change the R_t in proportion to the P_S as expected but the bistability and alignment remained the same.

In order to find out why ZLI3080 and ZLI3654 behave differently than the NCB and MBF esters on the HTA cells it is important to look further at the chemical compositions of all these materials and in particular to make a material similar to ZLI3080 that does not contain a dopant that crystallises. Other host materials should also be looked at.

To summarise the 5°SiO alignment was very good at producing bistability in thick cells with no zig-zag defects. In order to have a fast response time a Merck material was required and ideally a material similar to ZLI3080 in chemical composition. If a material with a $\Delta n = 0.07$ was produced then good optical characteristics could be achieved for a 3.5 μm cell which would make the displays easier to fabricate. The HTA cells also had the added advantage of being very robust. A suitable material is one with a long N^* pitch for good alignment and a high P_S (~20 nC/cm^2) so that the response time is small.

The affect of S_C^* pitch seems to be unimportant. The phase sequence is important but whether the material should have an S_A phase or not depends on the host FLC material.

CHAPTER 5

FERROELECTRIC LIQUID CRYSTAL DISPLAYS

In previous chapters small test cells have been used to study the alignment of ferroelectric liquid crystal and the effect of the alignment on their optical and electro-optical properties. The scaling up of these laboratory test devices to a working display is not a trivial task. The two most difficult problems to be considered in scaling up are (1) fabrication of a large 2 μm thick device with a ±10% tolerance and (2) individually addressing the elements of a highly complex display (e.g. 1000 x 1000 elements). This chapter starts with investigating the addressing of FLC displays with different alignments using simulated driving schemes on laboratory test devices. It then goes on to describe the production of two 3" x 3", 92 x 92 line displays using both the HTA and SS alignments. The optical and electro-optic characteristics of these displays are presented along with some of the problems.

5.1 Introduction

The addressing of any LC display can be achieved by directly connecting a voltage source to each picture element (pixel) of the display. This direct drive technique is used in simple displays such as the 4-10 digit twisted nematic displays used in watches and calculators. For more complex displays, such as the 600 x 400 line displays required for computer or video terminals, there are too many pixels for a direct drive technique to be practical and the drive electronics would become prohibitively complex and expensive. The problem is reduced by matrix addressing the display. The pixels are made up from column electrodes

which supply the data voltage (V_D) and (usually orthogonal) row electrodes which when time-multiplexed supply the scanning voltage (V_S) (Figure 5.1). This reduces the number of connections from n+1 to $2\sqrt{n}$ for an n pixel display. If the row electrodes always have a voltage applied to them it is called static matrix addressing. This has the disadvantage that only restricted patterns can be shown e.g. a closed figure with a hollow centre cannot be displayed [Needham 1983]. To overcome this problem a time-multiplexing technique can be employed by sequentially scanning the row electrodes a line at a time. The data voltage (V_D) is synchronised with the scanning voltage (V_S) so that the only pixel that changes is where these two lines meet.

All the pixels in a column have the data voltage applied but only the pixel that has V_S+V_D applied must switch. A single pixel has a voltage of V_S+V_D applied for a short period of time, T/N, where T is the frame time and N is the number of rows, and then a voltage of V_D for the rest of the time, T(1-1/N), for which it must not switch. (It is important to note that the voltage applied across the pixel is the difference between the voltages applied to either side of the LC layer and not the sum of them.) The time taken for V_S to address one row is called the line address time, the time taken to scan all the rows is called the field time and the time taken to be able to change the data of all the elements is called the frame time, which is often the same as the field time.

The time-multiplex addressing of nematic devices is a well understood technique. It was analysed by Alt and Pleshko [1974] for a dynamic scattering device but the principles are the same for twisted nematic (TN), electrically controlled birefringence (ECB) and supertwist

Figure 5.1: Schematic diagram showing time multiplexing of a display

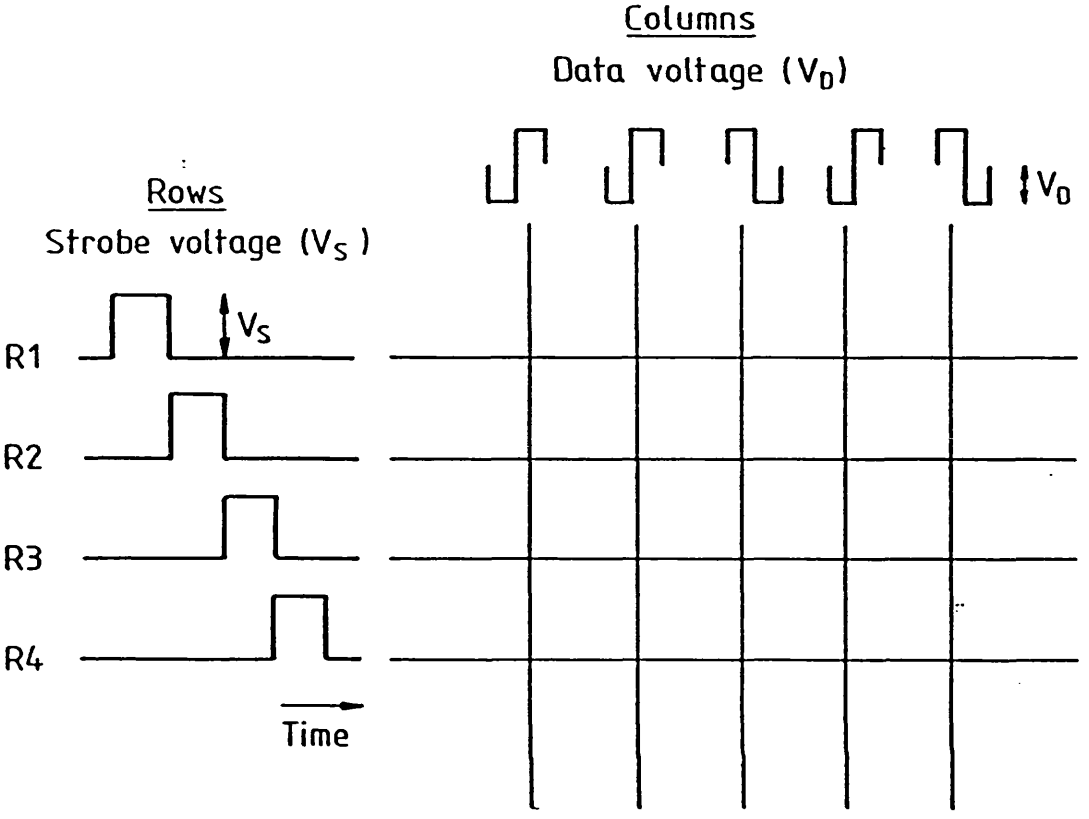

birefringence effect (SBE) displays, the differences in performance being due to the threshold characteristics and response speeds of the relative devices. Nematic devices respond to the rms voltage applied and not to the sign of the voltage. It is this rms behaviour that limits the scanning capability of nematic devices. Alt and Pleshko [1974] showed that the maximum number of scanning lines N_{max} is

$$N_{max} = \frac{[M^2 + 1]^2}{[M^2 - 1]^2}$$

where the voltage discrimination ratio M = V_{on}/V_{off}

V_{on} = threshold voltage for when display is acceptably ON

V_{off} = threshold voltage for when display is acceptably OFF

It can be seen from this that the duty ratio (N_{max}) becomes larger as M becomes sharper. This imposes a severe limitation on rms responding materials. The maximum limit for a dynamic scattering nematic display as calculated by Alt and Pleshko was ~45. Many years of optimisation of material and device parameters has led to twisted nematic displays with duty ratios of 240 being produced. However the viewing characteristics (contrast and viewing angle) become progressively worse as the duty ratio is increased. To overcome these problems nematic displays with sharper thresholds have been produced (SBE and ECB). These displays also have a 240 duty ratio but they retain acceptable viewing characteristics. These displays have found a market in alphanumeric computer terminals but there is still a need for more complex displays for graphic terminals and TVs.

Unlike nematic LCs, FLCs respond to the sign, amplitude and length of a single pulse and not to the rms voltage, and they are also bistable. This makes it possible to address as many rows as required before readdressing the first row, therefore the duty ratio is theoretically unlimited (>1000) and independent of the sharpness of the threshold curve. In practice the duty ratio is limited by the response time of the FLC since

frame time (T) = line address time x number of rows (N).

A video display needs to be driven at $\geq$25 Hz frame rate so for a 625 line display the minimum line address time needs to be <64 μs. This is a very stringent requirement. Other conditions also exist in order to obtain high contrast ratios whilst multiplexing which do depend on the threshold voltages. These are discussed in Section 5.2.

5.2 Multiplexing Scheme Requirements For FLC Displays

The aim of any multiplexing scheme is to:

(a) Individually address each element.
(b) Permit a high duty ratio.
(c) Generate a high contrast ratio.
(d) Use as low a voltage as possible at video frame rates.

These requirements are not only dependent on the multiplexing scheme but are also dependent on the liquid crystal material used and the device configuration, as will be seen later (Section 5.8). It was found that particular multiplexing schemes suit some materials better than others.

Any multiplexing scheme needs to provide:

(i) A positive selection pulse that will latch the device on.

(ii) A negative selection pulse that will latch the device off.

(iii) No overall d.c. bias across the device. A d.c. bias leads to decomposition of the liquid crystal over long periods of time. In addition, charge build up on the surfaces of the device can produce anomalous switching.

(iv) Minimal crosstalk when the data voltage is applied to an element when it is not selected (this occurs for all multiplexing schemes).

The simplest possible driving scheme to meet requirements 1 and 2 has two fields for each frame and is shown in Table 5.1, scheme 1. (Table 5.1 shows all the schemes discussed in this Chapter). One field turns the device to 0 (data 0 can be on or off depending on the orientation of the polarisers) with a positive pulse and the other field turns the device to 1 with a negative pulse. The data is either negative, $-V_D$, and adds to $+V_S$ to switch it to 0 or the data is positive, $+V_D$, which adds to $-V_S$ to switch it to 1. However, this scheme will put a d.c. bias across an element which is dependent on the data applied, e.g. if a column is all at data 0 then the data voltage seen by an element will be a continuous negative d.c.. A scheme which overcomes this problem was proposed by Harada et al [1985] and is shown in scheme 2. This scheme is similar to scheme 1 but there is an equal and opposite pulse in front of each pulse to immediately cancel the d.c. component. One frame requires each element to be addressed by four pulses therefore it is called a four slot scheme. This scheme can be considered as the standard scheme with which to compare other addressing schemes too.

Table 5.1: Multiplexing schemes for FLC displays

Scheme No.	Strobe voltage (V_S)	Data	Data voltage (V_D)	$V_S - V_D$	Comments
1	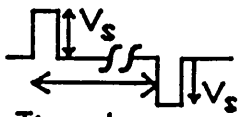	0	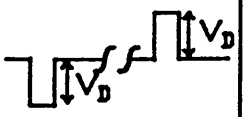	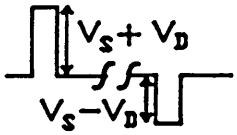	Adds D.C. across elements
		1	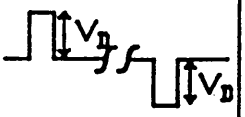	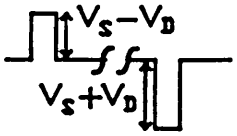	
2	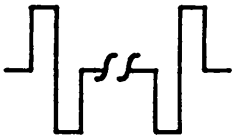	0	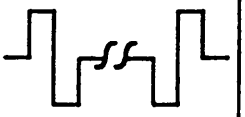	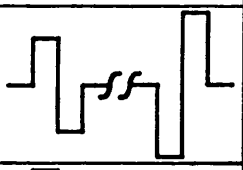	The standard scheme
		1	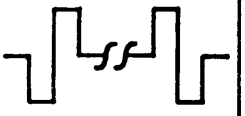	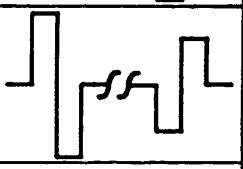	
3	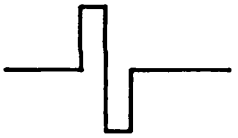	0	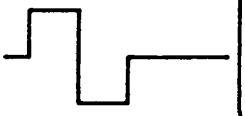	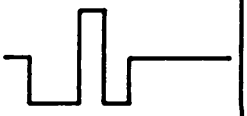	Data pulses twice as long than necessary
		1	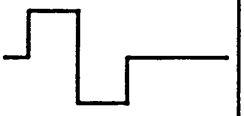	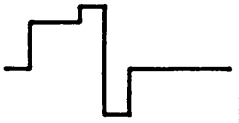	
4	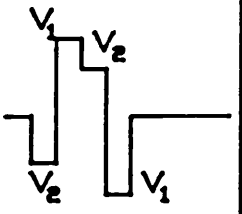	0	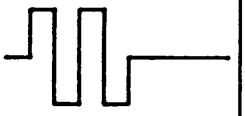	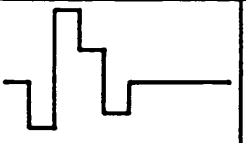	Where $V_1 > V_2$ or $V_2 > V_1$ or $V_1 = 0$ or $V_2 = 0$
		1	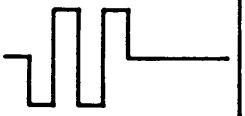	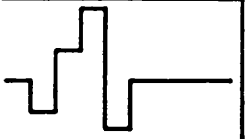	
5	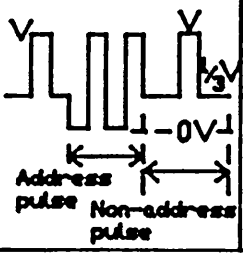	0	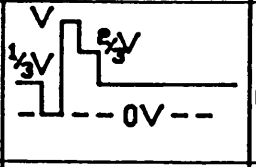	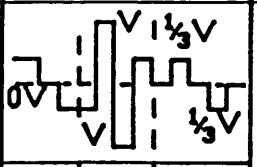	no negative voltage applied
		1	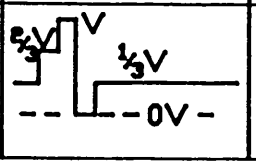	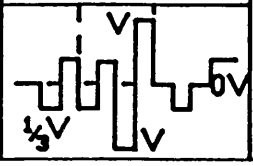	

Table 5.1:

Scheme No.	Strobe voltage (V_S)	Data	Data voltage (V_D)	$V_S - V_D$	Comments
6	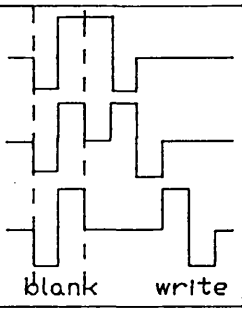	0	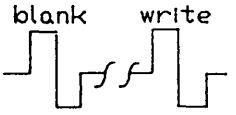	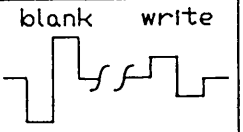	Blanks n lines first then writes the data
		1	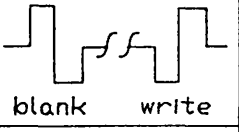	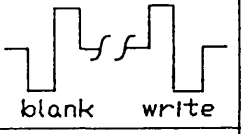	
7	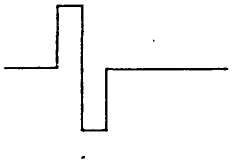	0	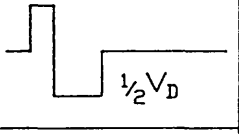	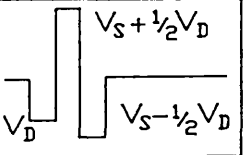	3 slot scheme Either adds d.c. on the 0 data or can only use ½V_D
		1	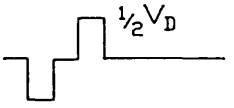	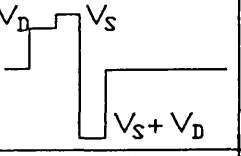	
8	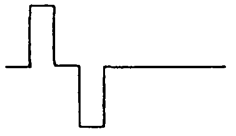	0	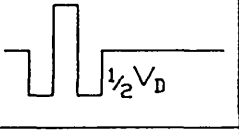	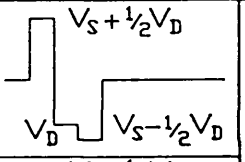	3 slot scheme Adds d.c. or uses only ½V_D
		1	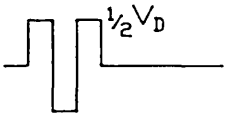	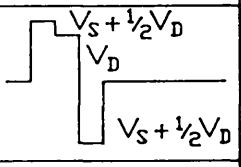	
9	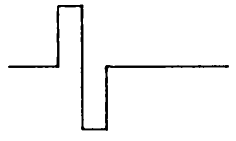	0	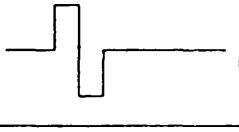	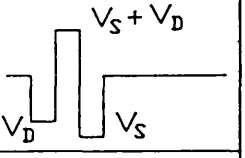	3 slot scheme
		1		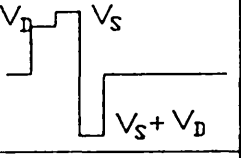	
10	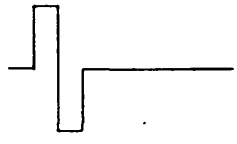	0	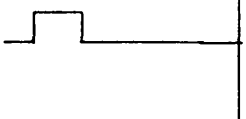	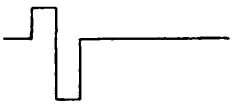	2 slot scheme Adds d.c. and data pulses are twice as long
		1		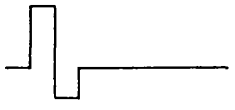	

Table 5.1:

Scheme No.	Strobe voltage (V_S)	Data	Data voltage (V_D)	$V_S - V_D$	Comments
11	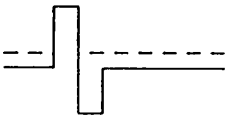	0	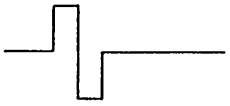	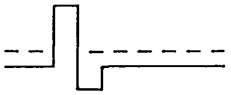	Uses a blanking pulse technique
		1	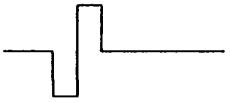	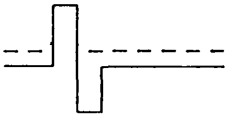	
12	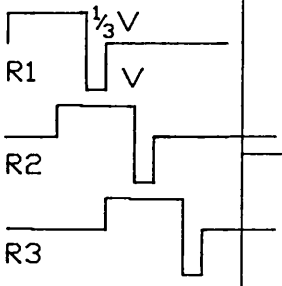	0	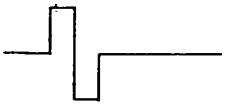	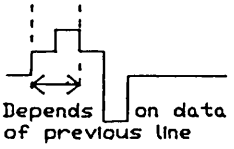	Interlaces a 4 slot scheme so that it becomes a 2 slot scheme
		1	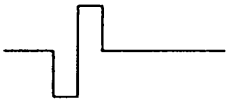	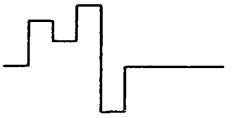	
13	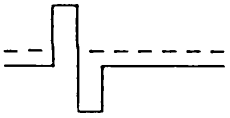	0		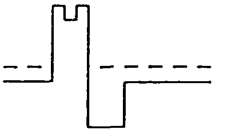	A 'split data pulse' technique There is no limit on the no. of data pulses
		1	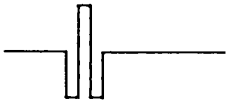	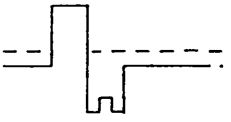	
14	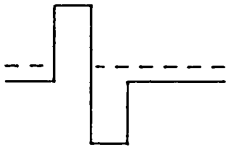	0		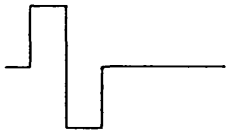	Split data pulse technique (2)
		1	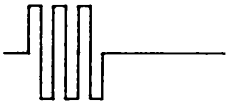	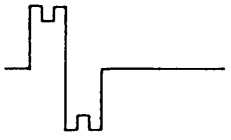	
15	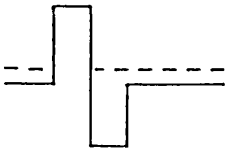	0	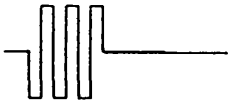	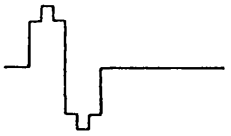	Split data pulse technique (3)
		1	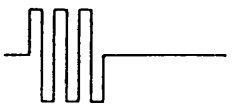	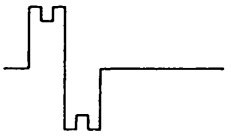	

Table 5.1:

Scheme No.	Strobe voltage (V_S)	Data	Data voltage (V_D)	$V_S - V_D$	Comments
16	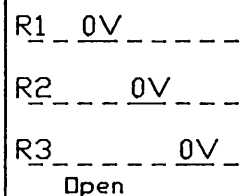	0	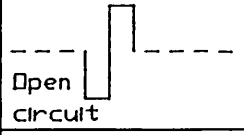	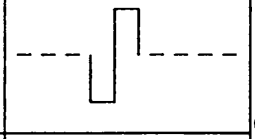	Uses an open circuit addressing technique
		1	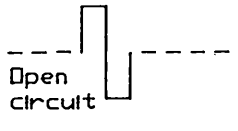	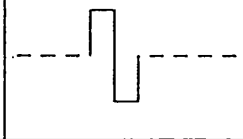	
17	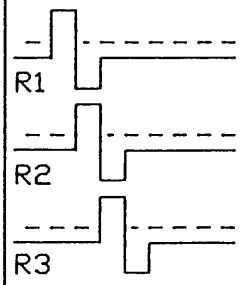	0		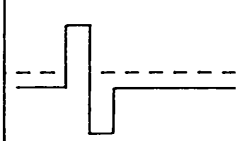	a 1 slot scheme
		1	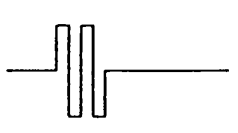	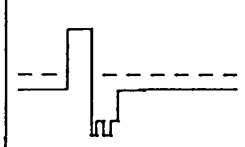	
18	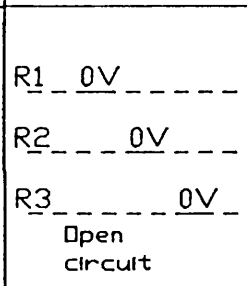	0	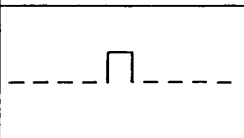	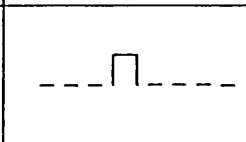	A 1 slot scheme Requires non-sequential addressing to remove d.c.
		1	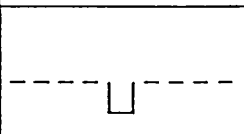	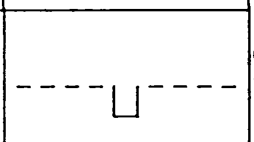	
19	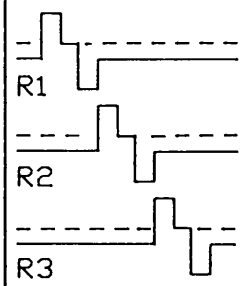	0	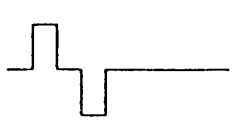	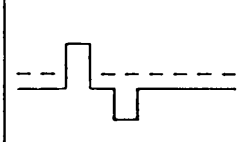	Adding zero voltage pulses can improve contrast
		1	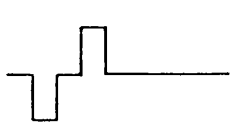	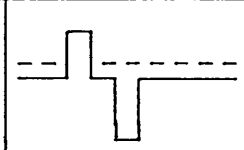	
20	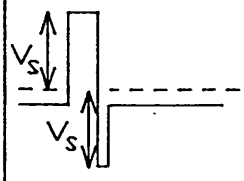	0	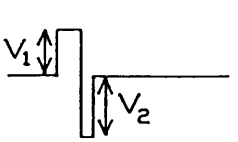	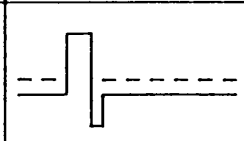	Varying the timing of pulses can reduce the line address time
		1	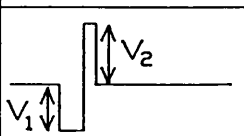	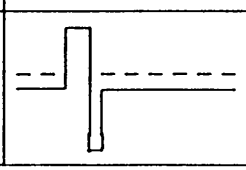	

Scheme 2 will work as long as it satisfies various conditions required to reduce the crosstalk. For a fixed pulse length;

(a) The switching threshold (V_{Sth}) must be greater than the data voltage (V_D) so that there is no crosstalk; $V_{Sth}>V_D$.

(b) The 100% latching threshold (V_{Lsat}) must be less than the selecting pulse (V_S+V_D) so that the pixel switches and latches when addressed; $V_{Lsat}<V_S+V_D$.

(c) The 0% latching threshold (V_{Lth}) must be greater than the non-selecting pulse (V_S-V_D) so that the pixel does not latch when addressed (the display can be switched by the non-select pulse if necessary but it must not latch); $V_{Lth}>V_S-V_D$.

(d) The threshold condition for good multiplexing is: $V_{Lsat}-V_{Lth}\leq 2V_{Sth}$.

Not many materials meet these requirements. The biggest problem is that the contrast ratio is reduced by the data crosstalk. This can be seen in Figure 5.2 which shows the materials ZLI3774 and ZLI3654 in HTA cells being multiplexed using scheme 2 with a duty ratio of 8. Although there are two distinct on and off levels the contrast is reduced because the FLC is being switched by the data voltage between the selecting pulses. This is because most FLC materials have little or no switching threshold, therefore will always be switched by the data voltage. The alignment, FLC material and driving mode affect the threshold voltages, so that different devices can have less crosstalk and therefore a higher contrast ratio (see Section 5.4).

Figure 5.2: Transmission response of ZLI3774 and ZLI3654 in HTA cells when multiplexed using scheme 2. Crosstalk due to the data voltage is clearly seen.

1: 0.5V/div 2: 50V/div t: 2 ms/div

ZLI3774

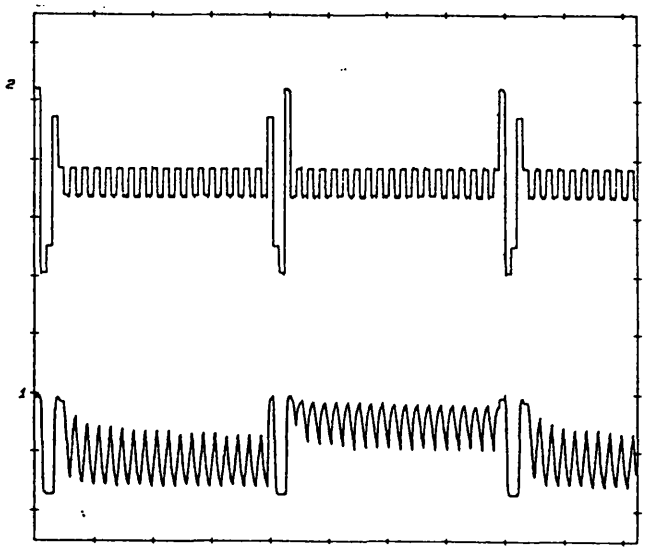

1: 0.1V/div 2: 50V/div t: 1 ms/div

ZLI3654

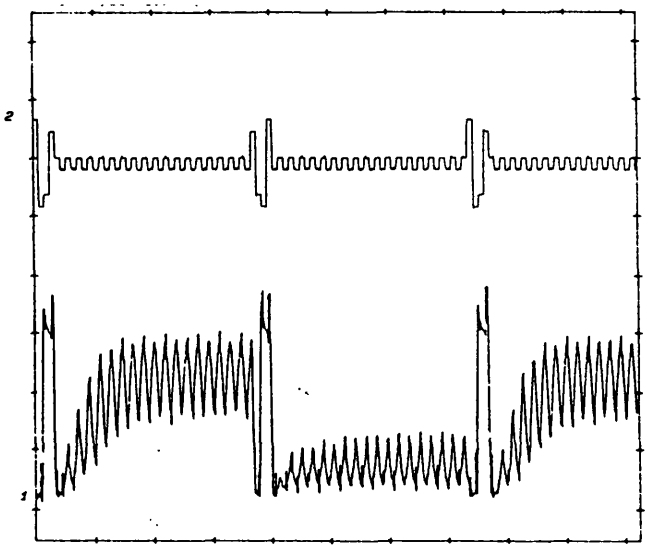

The two major aims in studying multiplexing of FLCs is to reduce the crosstalk and to reduce the frame time. These two aims can be met by the following:

(i) Change the material and the alignment to improve the threshold voltages and reduce the response time.

(ii) Improve the multiplexing scheme to reduce the crosstalk.

(iii) Decrease the frame time by reducing the number of time slots of the multiplexing scheme.

(iv) Add an a.c. stabilising field which will induce a dielectric dipole and hold the director in the switched state. This increases the switching threshold and reduces the level of crosstalk.

5.3 Experimental Technique

The experimental apparatus and the test cells used in these experiments were similar to that in Chapter 4 (Figure 4.2). The work used a polarising optical microscope so that the texture could be analysed at the same time as the optical response. White light was used with a photomultiplier detector. Two 175 Wavetek arbitrary function generators were used to create the scan voltage (V_S) and data voltage (V_D). This allowed the amplitude of the two waveforms to be varied separately with the frequencies synchronised. The two signals were added together through 10 MΩ resistors then amplified by a Burr Brown 354 amplifier (±150V). One side of the cell was earthed and the other side supplied both the V_S and V_D signals. (A true multiplexed device has V_D on one

substrate and V_S on the other). The Waveteks were controlled using a BBC microcomputer via an IEEE interface. Programs were written to enable any waveform required to be entered into the Waveteks for quick and easy manipulation of the multiplexing schemes and experiments. The signals from the Gould 4050 digital storage oscilloscope (DSO) could also be stored or manipulated if required. The DSO monitored the applied signal and the transmission through the cell.

5.4 Threshold Voltages

The threshold voltages are a measure of the force required to switch and to latch the liquid crystal director. The switching threshold V_{Sth} is defined as the absolute voltage at which the FLC just starts to change from the condition of no switching to having a small switching response. The latching threshold V_{Lth} is similarly defined as the voltage at which the FLC just starts to change from no difference between the positive and negative latched levels to a small difference between the latched levels. The voltages required to produce the maximum switched and latched levels are called the saturated switching threshold V_{Ssat} and the saturated latching threshold V_{Lsat} respectively. These four threshold voltages are different when the FLC switches from positive to negative and from negative to positive. This hysteresis is a measure of the bistability of the device. Typical hysteresis plots for latching and switching are shown in Figure 5.3. This shows that $V_{Sth}=0$ and that the curves are not quite symmetrical. Only one side of the loop will be quoted when examining the dependency of the thresholds on other parameters. There are two ways of displaying the threshold sharpness, either as a ratio (V_{Lsat}/V_{Lth}) or as a difference ($V_{Lsat}-V_{Lth}$). It is the absolute voltage values that are important for multiplexing FLC displays so the difference is quoted here.

5.4.1 The Affect Of The Measuring Waveform

The problem with measuring threshold voltages was that they varied not only with the expected parameters such as temperature, pulse length, alignment and liquid crystal material but they also depended on the method of measurement and the type of waveform used (i.e. the sequence of pulses). Figure 5.4 shows the transmission change with voltage for ZLI3654 aligned on polyimide when three different measuring waveforms were used. Each waveform had two pulses. The first pulse was a blanking pulse, V_B, the voltage of which was fixed to ensure that the FLC always started in the same state. The second pulse was the probe pulse, V_P, which was varied for the measurements. Waveform 1 had the two pulses together, waveform 2 had a zero voltage gap between the pulses and waveform 3 had a small square wave applied between the two pulses which simulated the V_D crosstalk in a multiplexing scheme.

Figure 5.4 shows several important features. Waveforms 2 and 3 produced lower and sharper thresholds than waveform 1 because the FLC could relax between the blank and probe pulses. This was not necessarily an advantage because they also produced no switching thresholds therefore they did not meet the multiplexing condition. However waveform 1 did produce a switching threshold which allowed the multiplexing condition to be met if a small amount (10%) of transmission was allowed. The small amount of crosstalk introduced in waveform 3 produced slightly higher threshold voltages which was opposite than expected. It was therefore better to use a multiplexing scheme with two pulses applied together in order to increase the switching threshold.

The results were taken in a single shot measurement [Kondo et al 1988, Patel and Goodby 1988]. This was a more reliable technique than a

Figure 5.3: Typical hysteresis plots of ZLI3488 when SS aligned for the switched and latched states

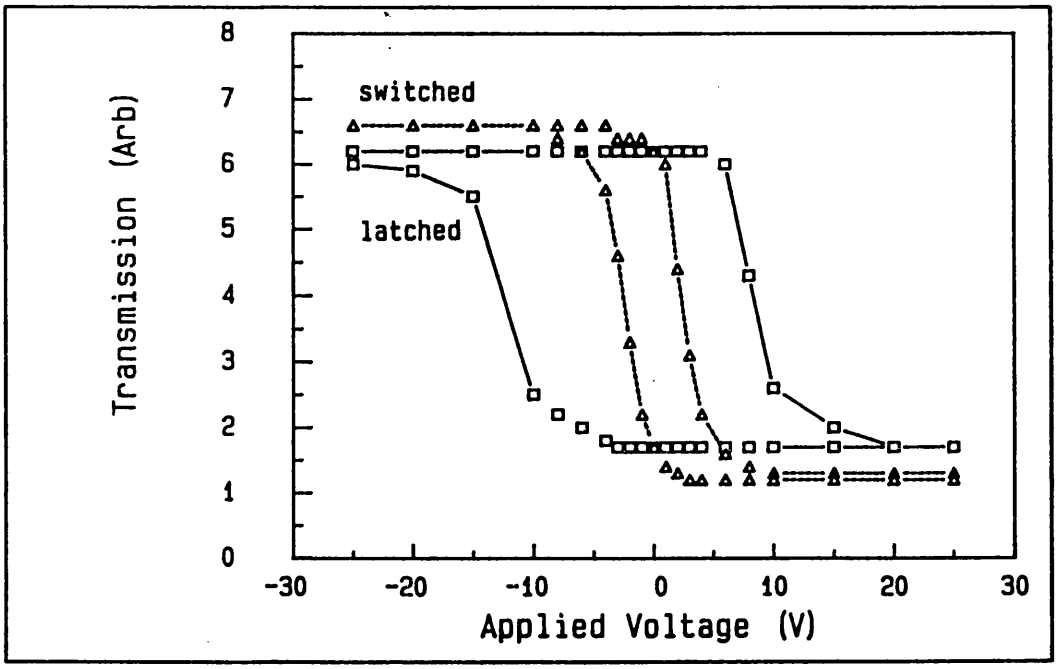

Figure 5.4: Transmission as a function of voltage for the switched and latched states using three different measuring waveforms (ZLI3654 on polyimide)

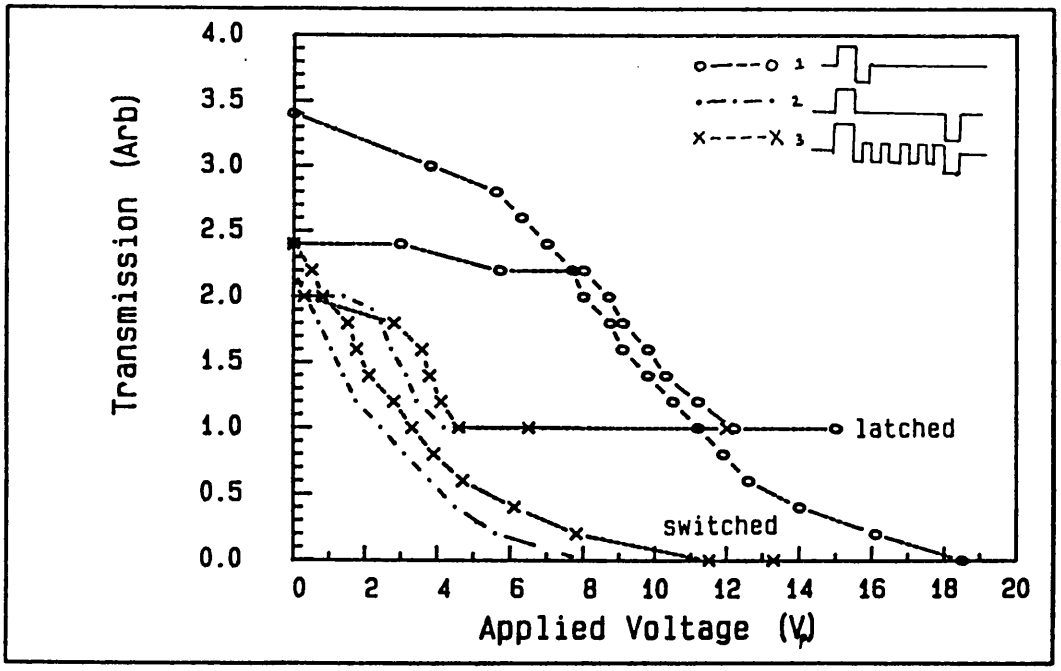

continuous signal because if there was any overall d.c. applied across the device by the waveform then a space charge could build up over many cycles of the applied waveform which altered the transmission levels of both the latched and switched states. Therefore not only were the transmission levels different but the measurements could only be taken when a steady state was reached. If the same waveform was applied as one shot only then the charge could dissipate between measurements so that the overall d.c. did not affect the results. This charging effect can be seen in Figure 5.5 which shows waveform 2 with different voltage levels of the probe pulse, V_P, for single shot measurements. When $V_P=0$ the charging effect was very evident. The charge built up in the blank pulse, V_B, switched the FLC into the opposite state once V_B had been removed. This effect remained until Vp was large enough to fully switch the FLC into the opposite state.

Figure 5.6 shows how the sequence of pulses affected the latching levels when a continuous signal was applied. Figure 5.6 a and b show the bistability of the device when the positive and negative pulses had equal voltages but a had a shorter pulse width which did not fully switch the FLC. Figure 5.6c shows the case when the probe pulse was not as long as the blanking pulse which provided a charge build up so that the blanked latched state was less than it should be. Figure 5.6d shows the case when the d.c. due to the longer blanking pulse was cancelled out by an equal but opposite pulse being applied just before it. This provided an overall d.c due to the probe pulse which switched the probed latched state to a transmission level greater than it should be. Figure 5.6e shows the case when the waveform shown in Figure 5.6c was reversed after each application. This meant that no overall d.c. was applied and the latched levels were the same as in Figure 5.6b.

Figure 5.5: Transmission of ZLI3654 aligned on polyimide when switched using pulses. Charging effects can be seen.

Blank pulse: 1 ms, 15V
Probe pulse: 200 μs, V
Scale: 2: 1 mV/div, t: 2 ms/div

(a) V = 0 (t: 5 ms/div)

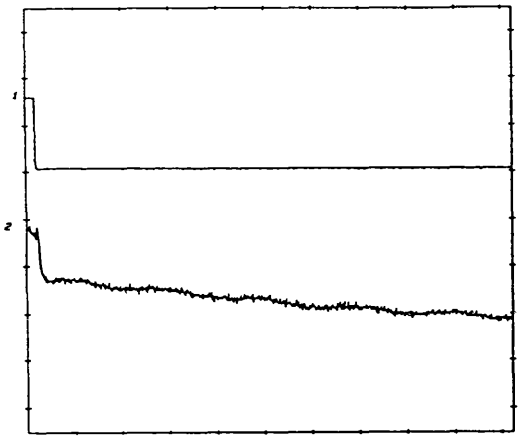

(b) V = 2.17V

(c) V = 2.5V

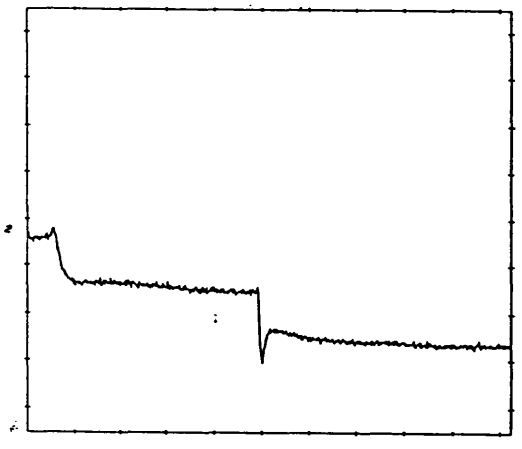

(d) V = 15V

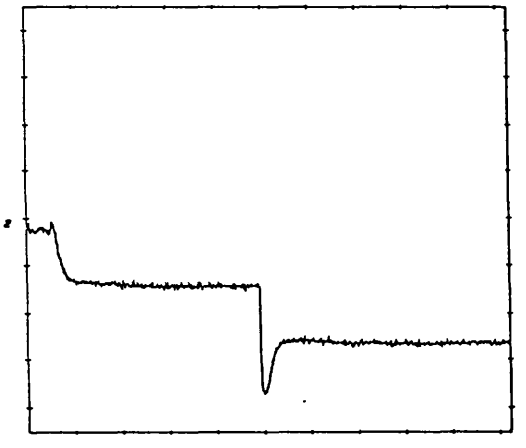

Figure 5.6: Transmission of ZLI3654 aligned on polyimide showing how the sequence of pulses affect the latched levels when a continuous waveform is applied.

Scale: 1: 10V/div, 2: 1 mV/div, t: 0.5 ms/div

(a) 16V, 25 μs
Not fully switched

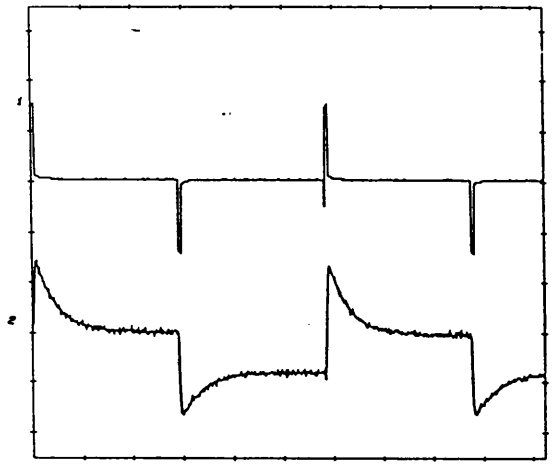

(b) 16V, 125 μs
Fully switched

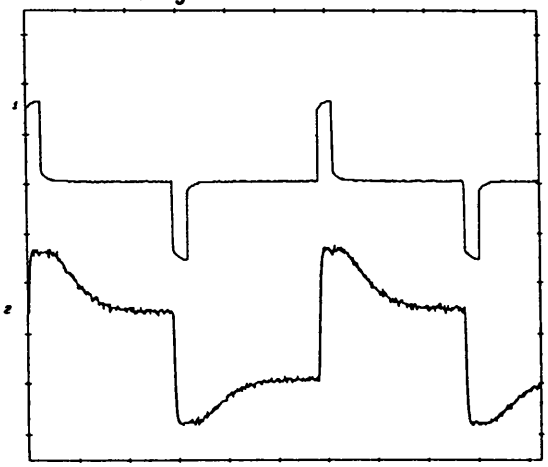

(c) Positive charging effects

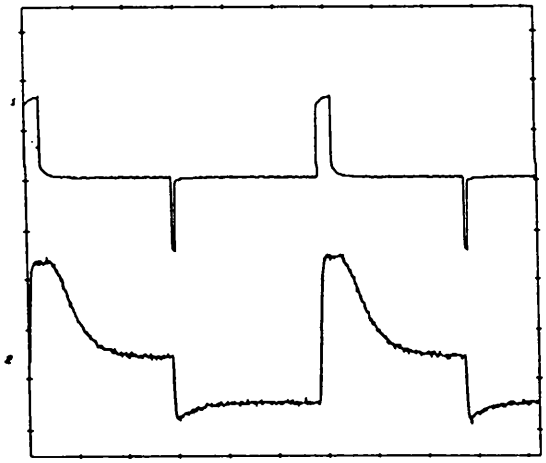

(d) Negative charging effects

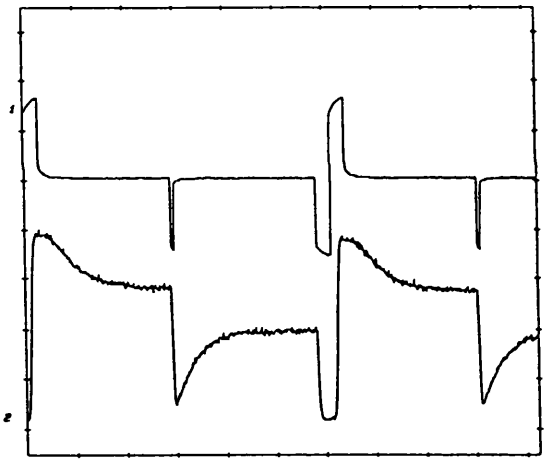

(e) No charging effects

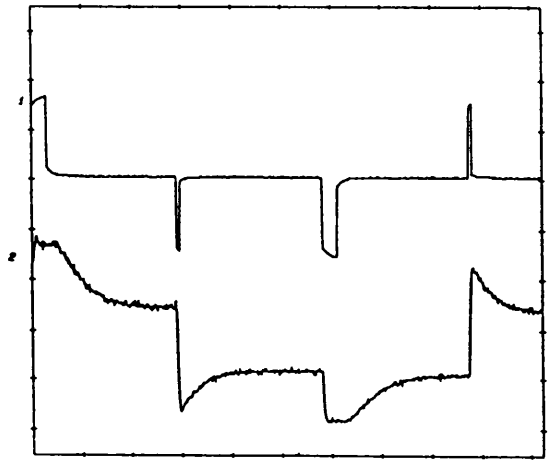

To measure threshold voltages in order to compare multiplexing abilities, a continuous signal would be needed which would cause the problems as discussed above. Threshold measurements using a single shot technique are therefore not suitable for quantitative comparison with multiplexing results but they are suitable for analysing the qualitative affect of pulse width, temperature and alignment on the threshold voltages.

5.4.2 The Affect of Temperature

Figure 5.7 shows the transmission change with voltage for ZLI3654 aligned on polyimide at three different temperatures, 45°C, 35°C and 25°C measured using waveform 2. Increasing the temperature reduced the threshold voltages because of the decreased viscosity and reduced the transmission of the device because of the reduced cone angle. There was a small V_{Sth} at 25°C but it disappeared at higher temperatures. Therefore for this cell the contrast when multiplexing would be better at lower temperatures

5.4.3 The Affect Of Pulse Length

The affect of pulse length on the threshold voltages for ZLI3654 aligned on polyimide is shown in Figure 5.8 when measured at 25°C using waveform 2. The V_{Sth} was zero until the pulse length was <100 μs. Therefore the crosstalk should get less at pulse lengths <100 μs as long as $V_{Lsat}-V_{Lth} \leq 2V_{Sth}$. The $V_{Lsat}-V_{Lth}$ was constant until 100 μs then it reached a minimum at 40 μs then increased rapidly at 20 μs. Even though $V_{Lsat}-V_{Lth}$ was highest at 20 μs the multiplexing condition was best met at this pulse length because the V_{Sth} was the highest. Increasing the pulse length may enable the voltages to be reduced when multiplexing but it would not keep the contrast the same because the crosstalk would

Figure 5.7: Transmission as a function of applied voltage for the switched and latched states at different temperatures (ZLI3654 on polyimide)

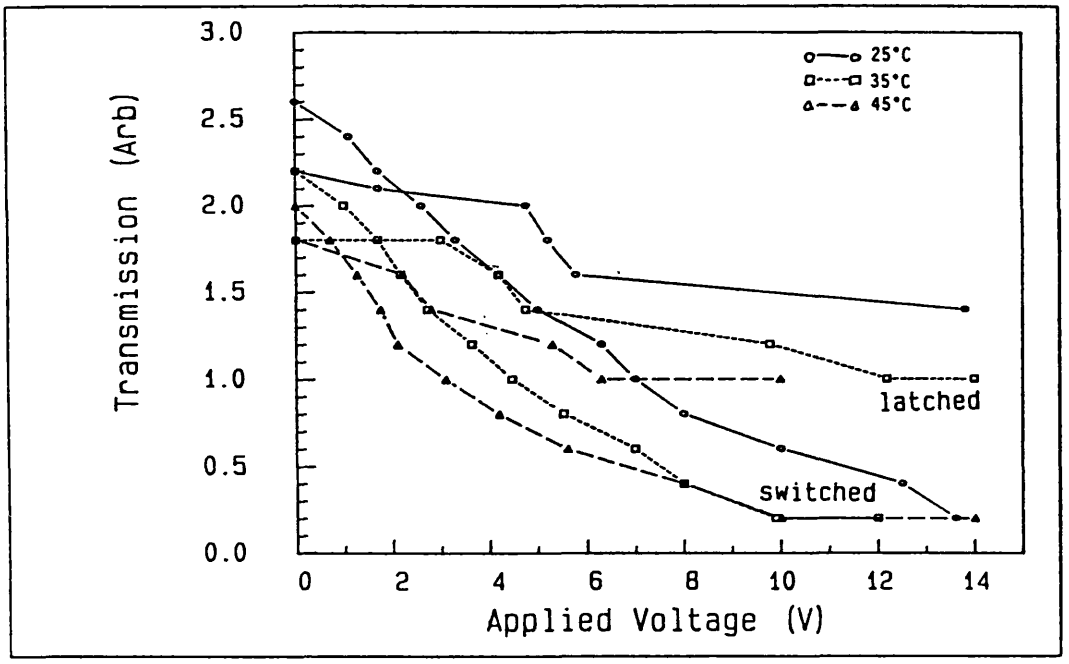

Figure 5.8: The four threshold voltages as a function of pulse width (ZLI3654 on polyimide)

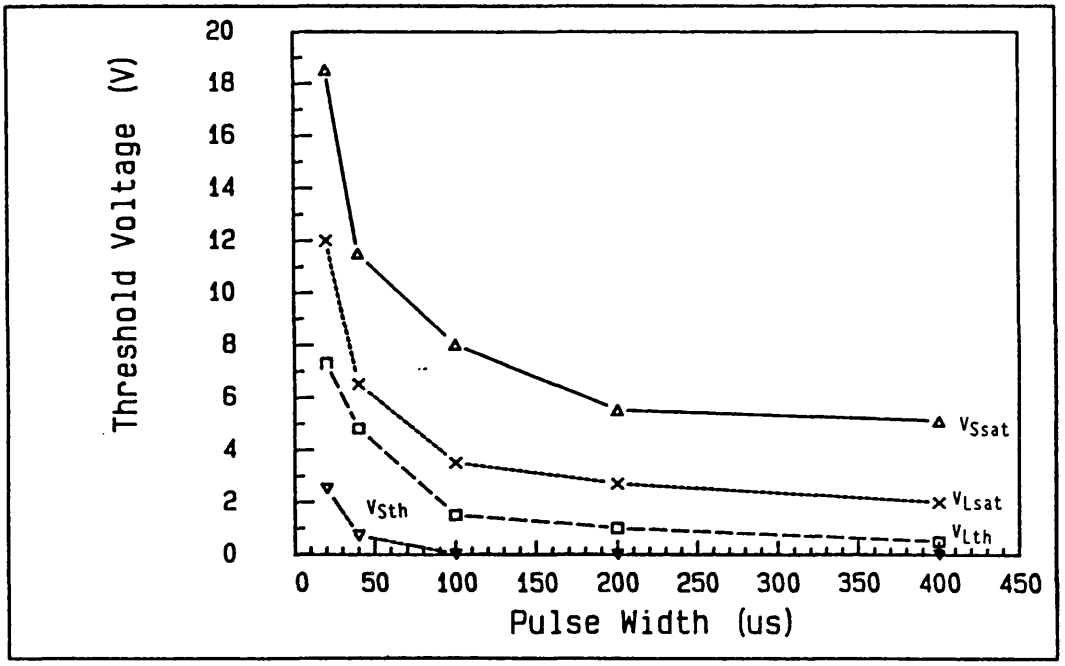

increase. Small pulse lengths are therefore best for multiplexing displays. If the temperature was increased these curves would shift towards shorter pulse lengths as the viscosity decreased.

5.4.4 The Affect Of Alignment

Table 5.2 shows the threshold voltages of three materials CS1014, ZLI3654 and SCE12 on different alignments. The threshold voltages are quoted at a pulse width of 100 μs at 25°C. This table shows that the high tilt alignments 5°↑↑ and 5°↓↑ produced higher threshold voltages than the low tilt alignments 30°↑↑ and PI↑↑. The reason for this is similar to the differences observed in response times. The high thresholds occurred in the high tilt devices because they were less prone to nucleation.

On polyimide alignment the material SCE12 had the lowest threshold voltage, then CS1014, then ZLI3654. SCE12 was the fastest material on polyimide therefore at 100 μs it was the easiest to switch. For the HTA alignment the ZLI3654 had the lowest threshold, then SCE12, then CS1014. Again this reflected the switching of these materials when aligned on 5°SiO. The best alignment to use for multiplexing in terms of threshold voltages was the HTA devices because they had a high switching threshold. The twisted high tilt states that exist in these devices could increase the V_{Lth} by upto three times when latching into these states rather than the fully switched states. These two facts combined to allow the high tilt devices to easily meet the multiplexing condition $V_{Lsat}-V_{Lth} \leq 2V_{Sth}$.

5.5 Multiplexing Schemes For FLC Displays

To improve on existing multiplexing schemes it is possible to rearrange

Table 5.2: The threshold voltages of CS1014, ZLI3654 and SCE12 on different alignments. (Results are quoted at 100 μs pulse length).

Material	Alignment	V_{Lsat}	V_{Lth} switched (white state)	V_{Ssat}	V_{Sth}	V_{Sth} 10%
SCE12	PI↑↑	4	3.2	2.9	0.07	0.63
	5°SiO↑↑	27.3	25.2	9.1	1.21	3.4
	5°SiO↑↓	23.1	15.4	16	1.75	5.2
	30°SiO↑↑	8.9	5.0	5.7	0.3	1.2
ZLI3654	PI↑↑	8.2	5.2	5.6	0.2	1.7
	5°SiO↑↑	15.4	11.3	5.6	1.8	3.8
	5°SiO↑↓	14.1	7.8	5.75	0.35	1.75
	30°SiO↑↑	7.6	3.7	3.5	0	1.1
CS1014	PI↑↑	7.5	5.4	5.25	0.25	1
	5°SiO↑↑	41.5	15.4	28.7	1.4	6.6

the pulse sequence and amplitude of the individual pulses in scheme 2 and also to reduce the number of pulses per frame. This section categorises the multiplexing schemes investigated by the number of scan pulses required per frame starting with four slot schemes.

When considering multiplexing schemes there are three important pulses:

(a) The amplitude of V_D

(b) The amplitude and position of the selecting pulse with respect to other pulses in the scanning sequence.

(c) The amplitude and position of the non-selecting pulses in the scanning sequence with respect to the selecting pulse.

Ideally V_D will be small and the selecting pulse will be large and always at the end of the sequence of scan pulses. However in practice if the positive selecting pulse is at the end of the scanning sequence then the negative selecting pulse cannot be. The aim is then to make the negative selecting pulse the penultimate one followed by a small positive non-selecting pulse. However this conflicts with the requirement for the positive selection when the ultimate pulse must be large. Figure 5.9a shows the effect of having the selecting pulse always at the end of the sequence (which cannot be realised in a multiplexing scheme) and Figure 5.9b the effect of having one of the selecting pulses as the penultimate pulse. The C_R achievable was higher and the data crosstalk was less for Figure 5.9a.

5.5.1 Four Slot Schemes

Scheme 2 has four pulses which can be made contiguous. When $+V_D$ is

added the selecting pulse is at the end of the sequence as required but when $-V_D$ is added it is at the second pulse. This scheme can be improved by making the two selecting pulses contiguous and removing the first two pulses to give scheme 3. The data pulses are now twice as long as the scan pulses which makes V_{Sth} less and the data crosstalk more likely to occur (Figure 5.10).

An alternative is to make scheme 2 contiguous and to vary the voltages. A simple variation is shown in scheme 4 [Bowry et al 1987b] where $V_1>V_2$ or $V_2>V_1$ or $V_1 = 0$ or $V_2 = 0$. The best is when $V_1 = 0$ or $V_2>V_1$ (Figure 5.11). This makes the negative selecting pulse less than the positive one but because it is at the end of the sequence of pulses the threshold for the positive pulse is less than for the negative pulse. The advantage of scheme 4 is that the negative non-selecting pulse will delatch the positive selecting pulse less than in schemes 2 or 3.

It is also possible to generate multiplexing schemes that do not apply negative voltages to either the strobe or data lines. The negative fields are produced from the difference between V_D and V_S. This was demonstrated by Wahl et al [1987] and is shown in scheme 5. This scheme has the advantage that the selecting pulses are as close to the end of the sequence as possible and that the non-selecting pulse is always V_D. Also the data voltage has a zero voltage period between pulses which helps to reduce V_{Sth} and increase the contrast. The disadvantage with this technique is that the ratio $V_S+V_D:V_D$ is fixed at 3:1. The other four slot schemes can have much larger ratios therefore decreasing the probability of crosstalk.

Figure 5.9: The affect of having the select pulse always at the end of the multiplexing sequence for ZLI3080 in an HTA cell

(a) Select pulses at end of sequence
1: 50V/div, 2: 1V/div, t: 2 ms/div

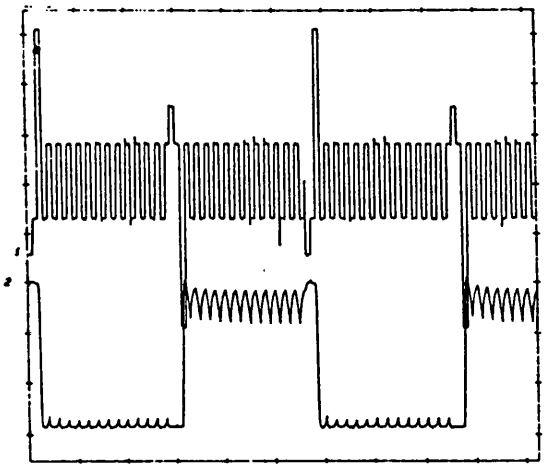

(b) True multiplexing
1: 50V/div, 2: 1V/div, t: 5 ms/div

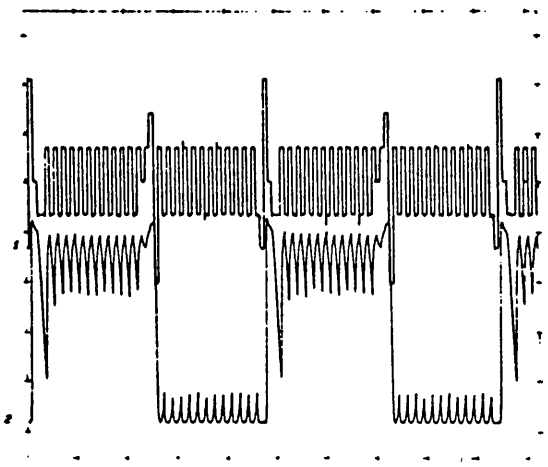

Figure 5.10: ZLI3080 in an HTA cell being multiplexed using scheme 3. The data voltage is twice as long as for scheme 2 therefore the crosstalk is more.

Scale; 1: 50V/div, 2: 1V/div, t: 5 ms/div

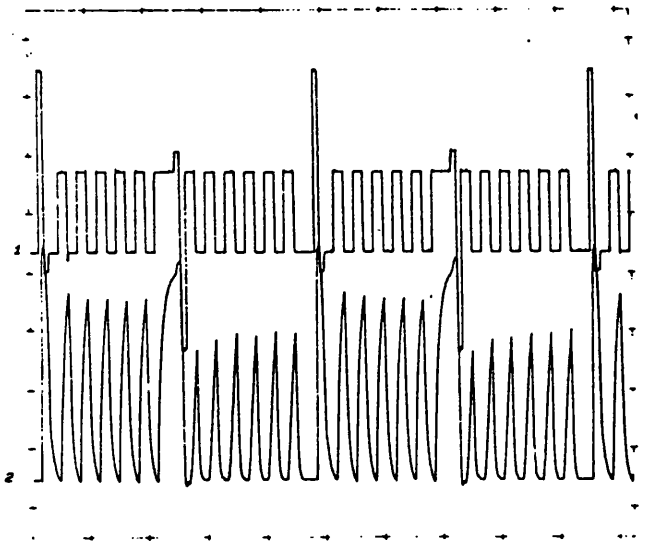

Figure 5.11: Optical response of ZLI3654 in an HTA cell when multiplexed using scheme 2 and scheme 4

(a) Scheme 2
1: 0.1V/div, 2: 10V/div, t: 2 ms/div

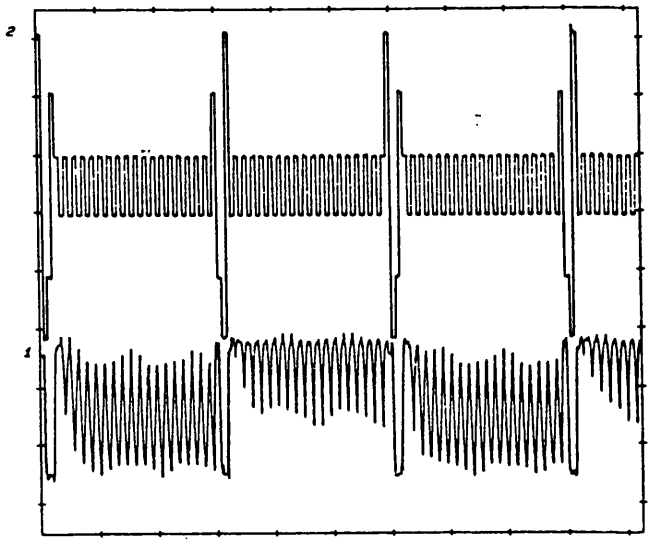

(b) Scheme 4
1: 0.1V/div, 2: 20V/div, t: 2 ms/div

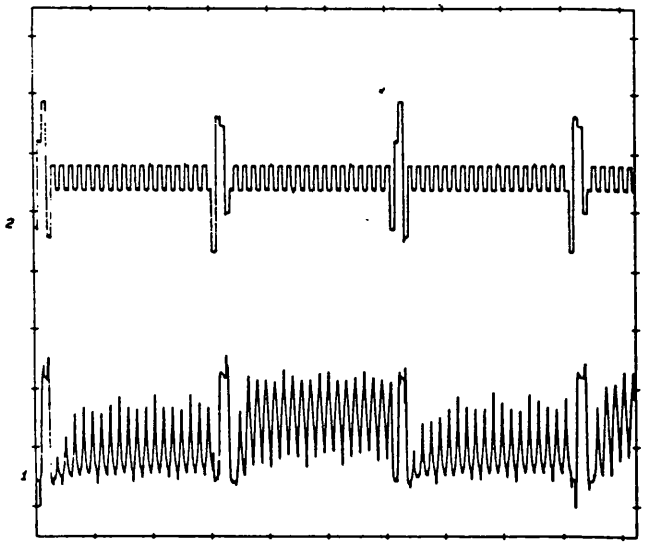

5.5.2 Three slot schemes

For a given material and alignment a reduction in the line address time can be achieved by reducing the number of pulses needed to address each pixel. Although three slot schemes have a faster line address time than the four slot schemes, they are not as good because the contrast ratio is reduced. Three slot schemes have the disadvantage that the non-selecting pulse is equal to the selecting pulse minus V_D whereas in the four slot schemes the non selecting pulse has at least $2V_D$ difference. This makes the threshold voltage requirements more stringent for the three slot schemes and the crosstalk due to the data signals is more. For three slot schemes, there are seven different types of signal that can be used for the strobe, data (1) or data (0) voltages. These signals are shown in Figure 5.12. Some possible combinations of these signals are shown in schemes 7-9 [Bowry and Mosley 1989a].

5.5.3 Two Slot Schemes

The simplest two slot scheme is shown in scheme 10. However this is not suitable for a display because V_D puts d.c. across the cell which is dependent on the data applied. This d.c. will not only switch the cell but will induce surface charges that can produce anomalous switching. One scheme that can overcome the d.c. problem is shown in scheme 11 which is based on a blanking technique [Bowry et al 1987b]. The first strobe pulse is a blanking pulse, V_B, that latches the pixel into the positive state regardless of the data voltage. The second strobe pulse is a write pulse, V_W, set so that $+V_D$ latches the cell into the negative state and $-V_D$ leaves the pixel unchanged in the blanked positive state.

Figure 5.12: Different possible signals for the strobe, data (1) and data (0) voltages when using a three slot scheme

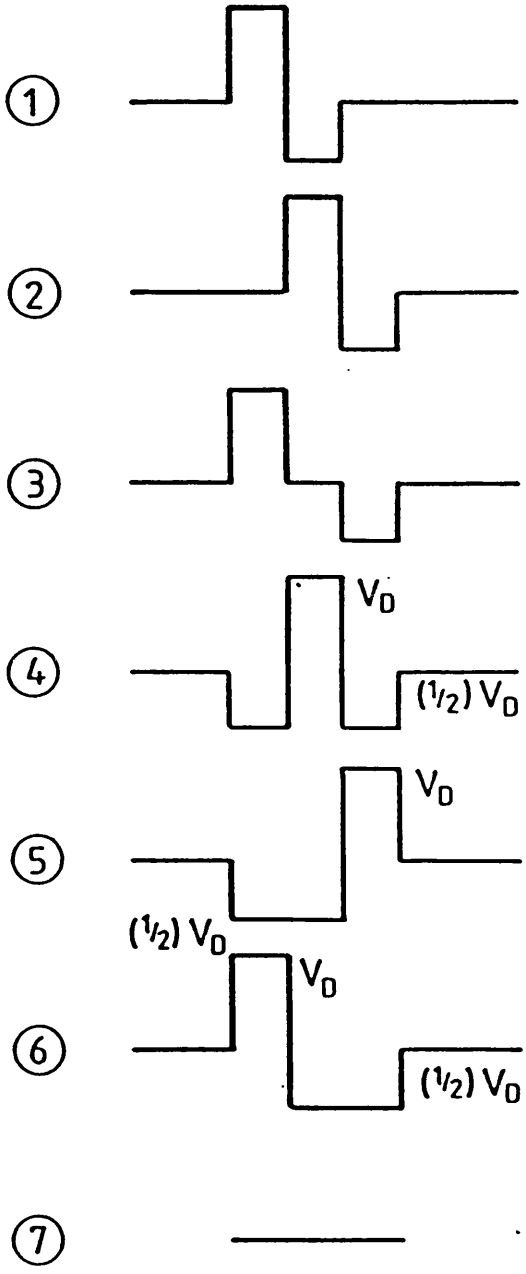

The difference between the blank and write strobe pulses is compensated by a negative d.c. voltage, V_{dc}, being applied to the strobe line between addressing pulses. This d.c. is small since

$$V_{dc} = \frac{V_B - V_W}{N - 1}$$

where N = number of lines. As N increases V_{dc} gets smaller and therefore has less effect. It has been shown that 128 lines is sufficient to make V_{dc} negligible (see Section 5.9). This scheme is very flexible because the selecting pulse can be set independently of the non-selecting pulse (this is not possible in other schemes). It was also found that this scheme can work with a small V_D and therefore good contrasts can be obtained (Figure 5.13). This two slot scheme can be modified in order to remove the d.c. voltage by inverting all the voltages after each frame has been written.

Scheme 11 can also be reduced to less than two slots by blanking several rows at once and then writing them with a scanning write voltage. This is quicker but may lead to more flicker. An example of a four slot scheme using such a technique is shown in scheme 6 [Kanbe and Katagiri 1985].

Maltese et al [1988] proposed an alternative method for producing a two slot scheme. This is a four slot scheme that is interlaced so that it appears as a two slot scheme (scheme 12). The second row starts being written before the first row has completed writing. This requires that

Figure 5.13: Optical response of CS1014 in an HTA cell multiplexed using scheme 2 and scheme 11.

Scale: 1: 1 mV/div, t: 50 ms/div

(a) Scheme 2

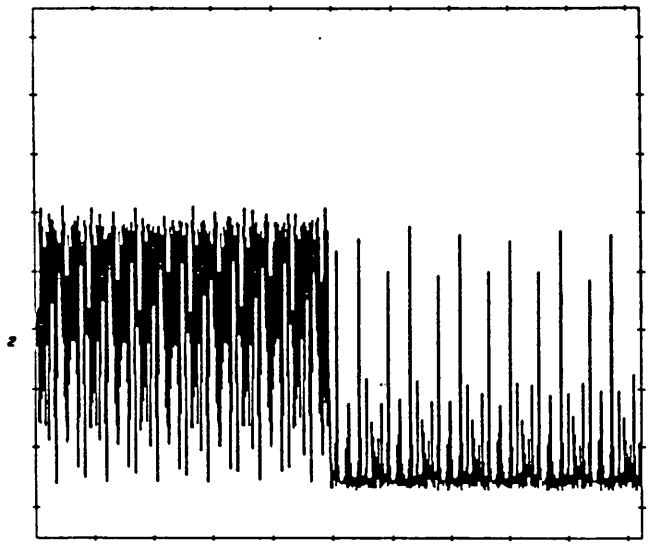

(b) Scheme 11

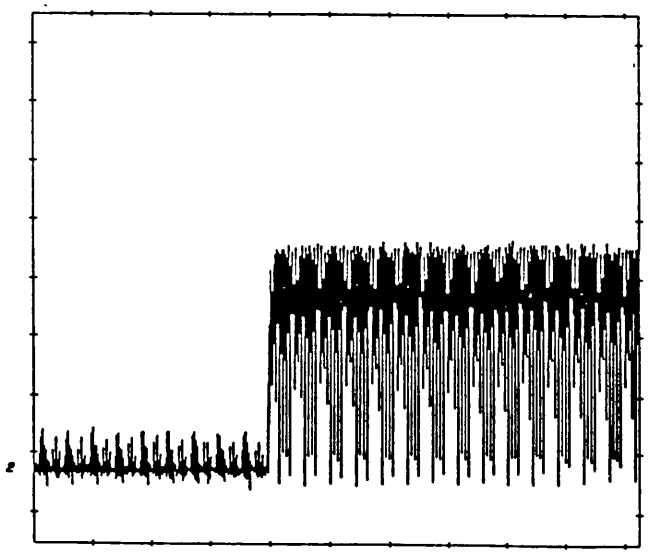

V_D consists of only two pulses whereas V_S can consist of four (or more). It also requires that the two strobe pulses that are not synchronised with the data pulses must be independent of the data being 0 or 1.

Two other methods for reducing the crosstalk will now be discussed. The first is a variation of scheme 11 but can also be used with other schemes if necessary. The idea is to make the V_D pulses also act as an a.c. stabilising signal, this will increase the V_{Sth} and prevent switching. Several possibilities are shown in schemes 13, 14 and 15 [Bowry et al 1989c]. Figure 5.14 shows SCE4 on polyimide driven by such a scheme. The advantage is that V_D is now an a.c. signal inducing a dielectric stabilisation effect and aiding bistability (i.e. keeps the pixel switched in the required state). This technique is referred to as split data pulses. Figure 5.14 shows that the number of pulses required to induce an a.c. effect are ≥ 4 per strobe pulse. The problem with this scheme is that high data (~60 Vpp) voltages are required in order to induce a.c. stabilisation and d.c. switching.

Another technique to stop V_D crosstalk totally was demonstrated by Matuszczyk [1987] and Wahl [1988]. This technique produces an open circuit (high impedance) across the pixel when it is not being addressed, therefore the pixel never has any data voltage applied across it when not being addressed (scheme 16). To prevent an overall d.c. being built up across the pixel V_D consists of a positive and negative pulse therefore it is a two slot scheme. The disadvantage with this technique is that a capacitative crosstalk can occur between pixels which will reduce the contrast. (A capacitative crosstalk will occur for

Figure 5.14: Optical response of ZLI3488 aligned on polyimide when multiplexed using scheme 14.

Scale: 1: 0.2V/div, 2: 20V/div, t: 2 ms/div

(a) 1 data pulse/strobe pulse
V_D = 11 Vpp

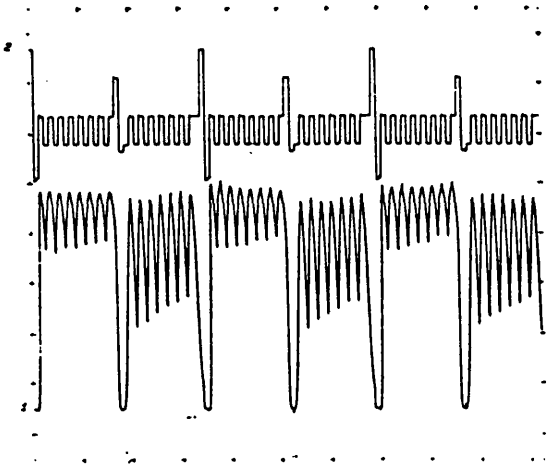

(b) 3 data pulses/strobe pulse
V_D = 64 Vpp (max)

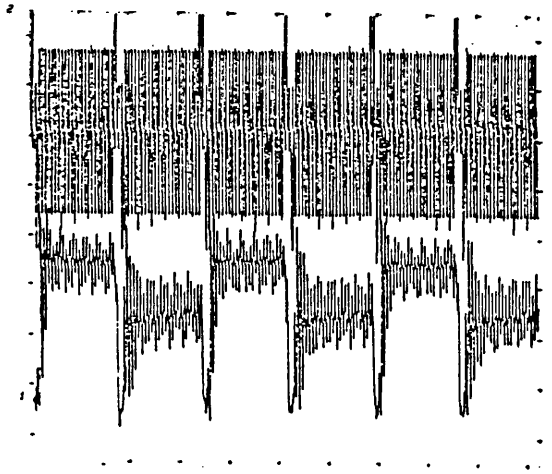

(c) 4 data pulses/strobe pulse
V_D = 64 Vpp (max)

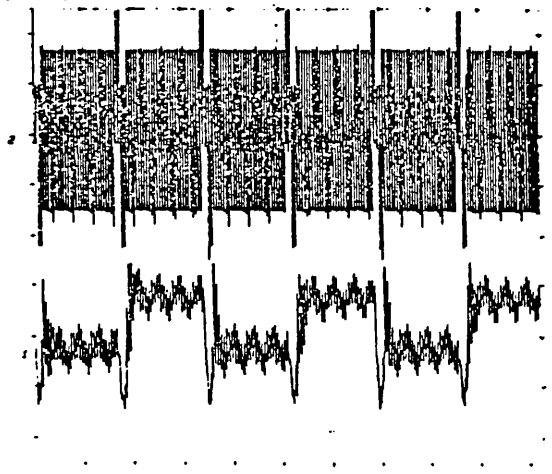

all driving schemes but it will be more acute for scheme 16). The advantage is that the switching will be as good as the bistability of the device.

5.5.4 One Slot Schemes

Interlacing can be used to make scheme 13 into a one slot scheme as shown in scheme 17 [Bowry and Mosley 1989b]. V_D is a pulse of a.c. that lasts for the length of the write pulse only. The blank pulse can therefore be applied to the second row while the first row is being written. A plot of this scheme working is shown in Figure 5.15.

Scheme 16 can also be used in a one slot scheme as shown in scheme 18. This applies a single d.c. pulse across the pixel when addressed and is open circuit at all other times. This will put an overall d.c. across the pixel unless non-sequential addressing is used. Non-sequential addressing has the pixel addressed only when the data needs changing and not continually. The pixel will be switched on as many times as it is switched off so that over a period of time the overall d.c. is always zero. Other schemes such as scheme 10 can not be used in non-sequential addressing to remove the d.c. component because the data voltage is applied to all the pixels in the column all of the time. Scheme 15 gets around this because it is open circuit to all the pixels in the column except the one being addressed.

5.5.5 Other Multiplexing Techniques

There are certain techniques that can improve the performance of a device when addressed by any of these schemes:

Figure 5.15: Optical response of CS1014 in an HTA cell when multiplexed using split data pulse schemes including a one slot scheme

(a) Scheme 13
1: 1 mV/div, t: 50 ms/div

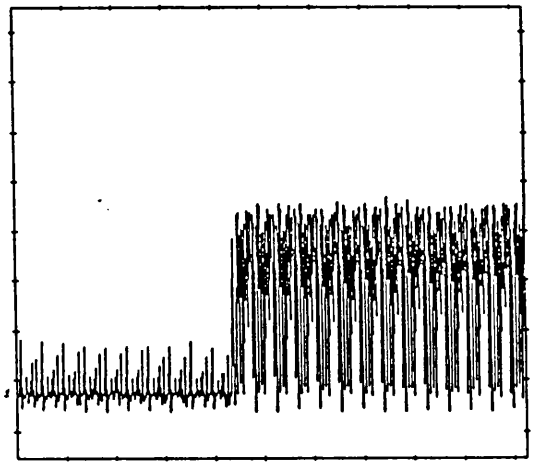

(b) Scheme 14
1: 1 mV/div, t: 20 ms/div

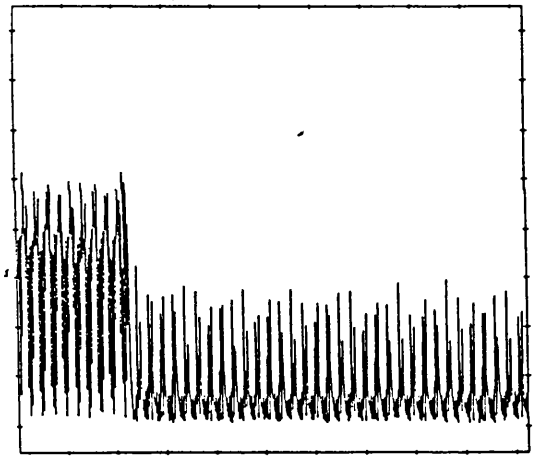

(c) Scheme 17
1: 1 mV/div, t: 50 ms/div

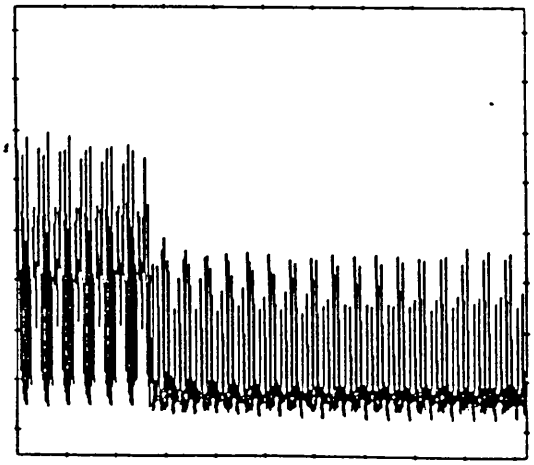

(i) Superimposing a high frequency a.c. field onto the row or column signal can improve the contrast ratio of the polyimide aligned cells by inducing dielectric stabilisation. It is found that if a high frequency field is superimposed on the low frequency pulses, then the switching threshold voltage is increased. The consequence of this is that the elements on the non-addressed rows do not respond to the data signals leading to a reduction in crosstalk and hence to an increased contrast. This is shown in Figure 5.16 for the material ZLI3488 aligned on polyimide. The HTA displays do not a.c. stabilise because there is no relaxation in the first place.

(ii) If a period of zero field is applied to the liquid crystal after a pulse [Ayliffe et al 1985], then the FLC domain has time to establish itself which leads to a reduction in the latching threshold. This situation is more suitable for multiplexing and the contrast ratio is increased. This technique does increase the line address time unless an interlaced scheme is used. An example of this technique is shown in scheme 19. This is more suitable for polyimide aligned cells than HTA cells because they relax between pulses.

(iii) In order to reduce the line address time, and hence the frame time, it is desirable to use the smallest pulse width possible but commensurate with the maximum voltage available from commercial display driver chips. For some schemes it may be advantageous to make all the pulses the same amplitude and vary the width of the pulses. An example of this technique is shown in scheme 20 for the two slot scheme 11.

Figure 5.16: Optical response of ZLI3488 aligned on polyimide showing a.c. stabilisation

(a) Scheme 11
1: 20V/div, 2: 0.1V/div, t: 2 ms/div

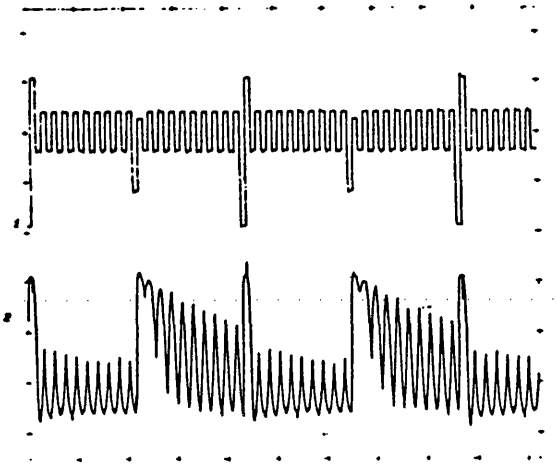

(b) Scheme 11 plus a.c.
1: 20V/div, 2: 0.1V/div, t: 2 ms/div

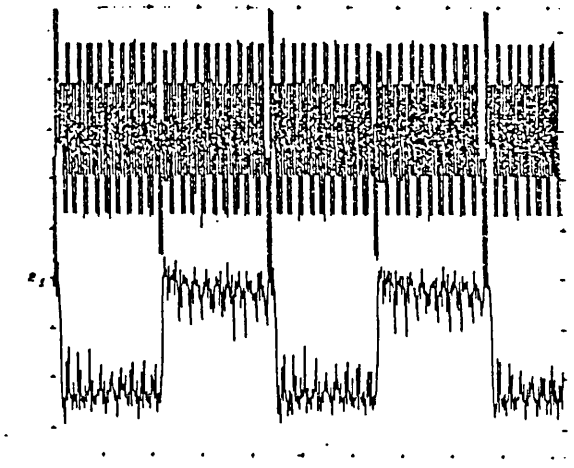

(c) Affect of a.c. on bistability
1: 0.2V/div, 2: 10V/div, 3: 0.2V/div, t: 1 ms/div

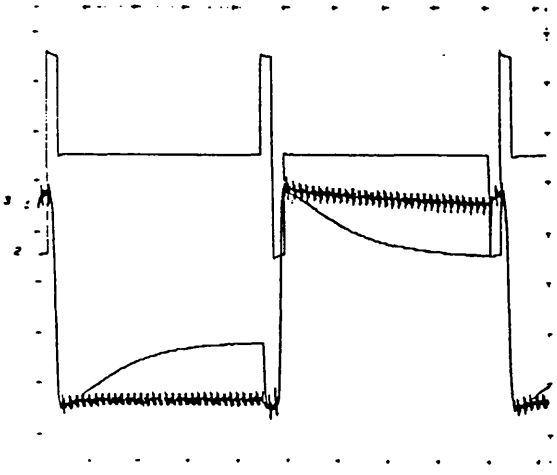

5.6 Results From Different Multiplexing Schemes

Six different multiplexing schemes have been investigated, schemes 2,4,11,13,14,17 from Section 5.5. Scheme 2 was included as a standard for comparison and the other schemes were developed for this work. The waveforms were produced using a specially designed multiplexing box that had a maximum voltage of ±36V for both the strobe and data lines. The minimum pulse width was 20 μs which increased in steps of 12 μs. For this experiment the duty ratio was limited by the box to always be 8 which was small but was still useful for comparing the driving schemes. The material used in this experiment was CS1014 aligned in an HTA cell. This alignment allowed a twisted high tilt state to be seen when the multiplexing was not quite strong enough to switch into the white state. Table 5.3 shows the results including the minimum achievable pulse length, the maximum achievable contrast (not necessarily at the minimum pulse length) and the voltages required to multiplex the cell at a fixed pulse length of 192 μs, (this pulse length was chosen because this was the minimum to achieve maximum contrast for schemes 13 and 17). For maximum contrast the angle of the cell between crossed polarisers was 20° from the alignment direction (for all schemes). This was slightly less than the cone angle (22°) because of the switching from the crosstalk.

Table 5.3 shows that schemes 2,4 and 11 were better to use than schemes 13,14 and 17. For scheme 13 the data voltage was about three times larger than for schemes 2,4 and 11. There were three data pulses per strobe pulse in scheme 9 therefore the pulse length per data pulse was three times less than the other schemes so to switch the FLC the voltage needed to be three times larger. This meant that these split data pulse schemes only switched the FLC in the last pulse applied and was purely a

Table 5.3 Results from using different multiplexing schemes with CS1014 aligned on 5°SiOtt(HTA)

Scheme	Min P_w	Max C_r	V_B	V_w	V_D	colour of states	Comments
Scheme 17 (1 slot)	92 μs	14:1	19.6	15.3	±36.4	blue/black	
Scheme 14 (2 slot (1))	92 μs	14.:1	24.5	14.7	±26.9	blue/black	
Scheme 13 (2 slot (2))	68 μs	20:1	32	11.3	30pp (±15)	white/black	
Scheme 11 (2 slot (3))	32 μs	20:1	33.7	11.9	9.8pp (±5)	white/black blue/black	at 185 μs at 32 μs
Scheme 4 (4 slot)	44 μs	20:1	V_1 24.6	V_2 16.4	12.4 pp (±6.2)	white/black	Excellent C_R over whole area
Scheme 2 (4 slot standard)	32 μs	20:1	±17.3	-	10.5pp (±5)	white/black	

d.c. field effect, it did not have an additive effect and because this was an HTA cell the a.c. field had no stabilisation effect. The minimum pulse length for the split data pulse schemes was longer than for the other schemes because the strobe and data voltages were limited to ±36V. Schemes 14 and 17 have four data pulses per strobe pulse and the minimum pulse length was correspondingly longer. The contrast ratio was less for schemes 14 and 17 because the difference between the latching pulses was only V_D whereas in all the other schemes the difference was $2V_D$. This made the multiplexing less strong and they switched between the twisted blue state and the black state rather than the white and black states which gave a contrast of 14:1 rather than 20:1.

The best scheme was scheme 11 which required similar voltages to scheme 2 and the same minimum pulse length but because it was only a two slot scheme it had a faster line address time. However, the contrast at 32 μs pulses was less than scheme 2 because it switched into the blue twisted state rather than the white switched state. This showed that the multiplexing was less strong. Scheme 4 did not appear better than scheme 2 because it required higher voltages and had a longer minimum pulse width, but it had the advantage that it was easier to set up than scheme 2 because there were more independent variables. There was also less variation in contrast due to thickness so that the cell looked as if it had a better contrast when addressed with scheme 4 than with all the others.

To increase the multiplexing ability of scheme 11 it would be necessary to add pulses in front of the blanking pulses to disrupt the FLC domain

structure before the blanking pulse, making switching easier and the multiplexing stronger. The lines could be interlaced as in scheme 12 so that the scheme remained a two slot scheme.

With all these schemes it was important to have a variable d.c. level. This was used to counteract any overall d.c. that may have been applied to the cell. Even with scheme 2 it could not have been guaranteed that the multiplexing box gave out exactly the same positive and negative voltages.

One of the problems when multiplexing FLC displays was that when the pulse length was >100 μs the display started to whistle. The director was being continuously switched by the applied field causing a piezoelectric effect. The cell acted as a transducer to produce a sound. The pitch of the whistling could be controlled by the frequency of the applied electric field. Increasing the frequency such that the pulse length was <100 μs increased the pitch until it was inaudible. The movement of the FLC director could also be seen in the hydrodynamic motion of the pixel as it was multiplexed. These could be seen as rolls forming in the pixel like Williams domains which changed size and shape with frequency.

5.7 Reverse Multiplexing

When multiplexing certain SSFLC devices using scheme 2, the contrast could be increased by reducing the pulse length to below that required for latching. The resulting picture had a reverse contrast to the picture obtained at the longer pulse length even though the voltages remained the same. This is referred to as reverse multiplexing. It was caused by the bistability of the cell inverting when the pulse length

Figure 5.17: Bistability of SCE4 aligned on polyimide at 700 μs and 240 μs pulse lengths showing reversing of the bistability

(a) Normal bistability (700 μs)
1: 20V/div, 2: 50 mV/div, t: 5 ms/div

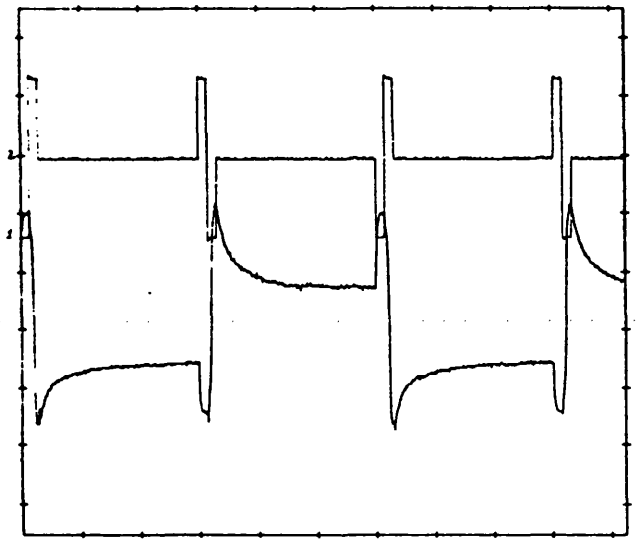

(b) Reverse bistability (240 μs)
1: 20V/div, 2: 50 mV/div, t: 2 ms/div

was reduced. Figure 5.17 shows the bistability of SCE4 on polyimide for two different pulse lengths. At 700 μs there was normal bistability but at 240 μs the pulses were not long enough to fully switch the cell and it switched into the intermediate states. The first pulse switched from a negative intermediate state to a positive switched state. The second pulse switched from the positive switched state to the positive intermediate state. The second pulse switched the cell less than the first pulse because the voltage required to switch out of the switched state was higher than to switch out of the intermediate state. It was this difference that produced the reverse bistability.

In order to get reverse multiplexing the cell must have intermediate states and suitable threshold voltages. The HTA cells do not have intermediate states therefore they do not produce reverse multiplexing. Only polyimide cells are suitable and in particular cells containing BDH materials. The Merck materials do not have suitable thresholds and require very small pulse widths and very high voltages to produce reverse multiplexing making it difficult to use.

For a fixed voltage of the strobe and data lines the reverse multiplexing mode could be driven at faster pulse widths than the normal mode. This was an advantage for achieving video frame rates and also enabled the contrast to be higher because the data voltage did not produce as much crosstalk switching. Figure 5.18 shows SCE4 on polyimide being driven using scheme 2. The voltages were fixed at V_S=37Vpp and V_D=17.5Vpp, the duty ratio was 128 and the pulse width was varied. At 700 μs there was normal multiplexing which reduced to no multiplexing at 600 μs when the bistability was lost. The reverse multiplexing appeared at 500 μs with better contrast than at 700 μs and

Figure 5.18: Optical response of SCE4 aligned on polyimide when multiplexed using scheme 2. The voltages are fixed and the pulse length is reduced, leading to reverse multiplexing

Scale: 1: 50 mV/div, t: 200 ms/div

(a) 700 μs
Normal multiplexing

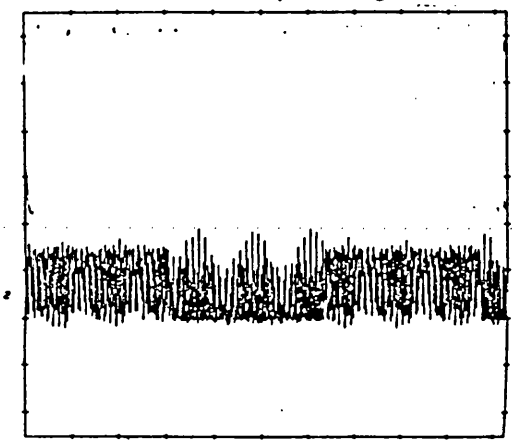

(b) 600 μs
No multiplexing

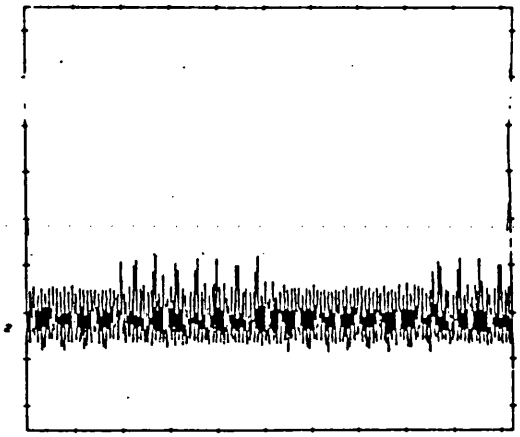

(c) 550 μs
Reverse multiplexing

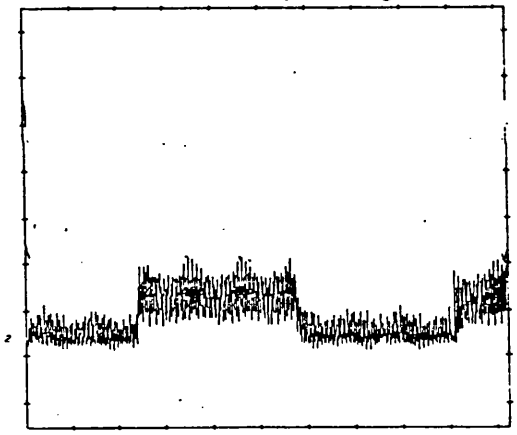

(d) 400 μs
Change time is increasing

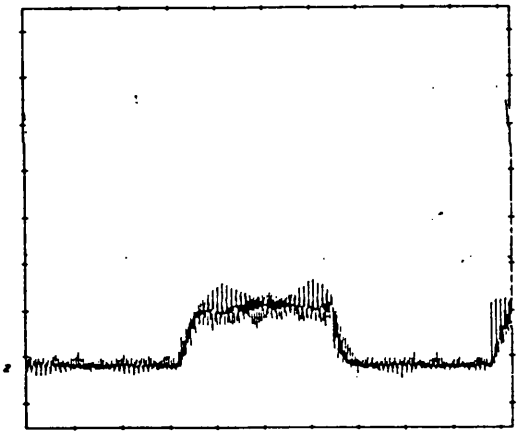

(e) 250 μs
Change time very long

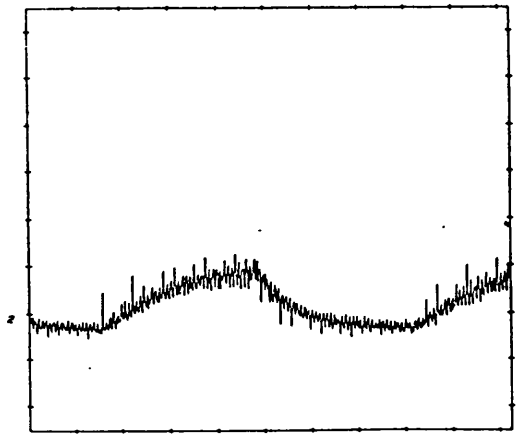

(f) 200 μs
No multiplexing

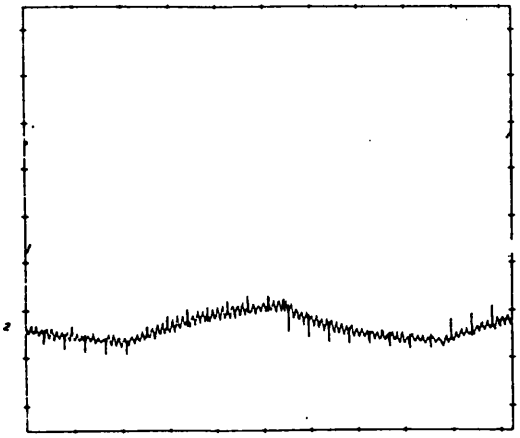

the contrast continued to improve as shown at 400 μs although the time taken to change states was getting longer. At 250 μs the multiplexing was beginning to disappear and the change time between on and off states was becoming very long.

The reverse switching mode was excellent to use for polyimide cells and although a four slot scheme had to be used rather than a two slot scheme the resulting frame time was about the same because the pulse width could be reduced. The advantage was the improved contrast ratio achieved using this technique.

5.8 The Affect of Alignment on Multiplexing

This section discusses the multiplexing of different FLC materials and alignments when driven using schemes 2 and 11. The results are shown in Table 5.4 for a duty ratio of 128. The minimum pulse width possible for each scheme and cell are shown along with the voltages required (the maximum voltages available were ±37V for the strobe and data lines and the minimum pulse width available was 32 μs). The maximum contrast shown was the maximum that could be produced for that cell at any pulse width. The angle between the alignment direction and the polarisers to obtain maximum contrast is also shown.

The first thing to note is that none of the 87-486 cells multiplexed because this material has no S_A phase and the cells had no bistability and relax quickly into one intermediate state.

The materials ZLI3654, CS1014 and SCE12 multiplexed when they were aligned on PI, 5°SiO↑↑ or 30°SiO↑↑ but they did not multiplex when aligned on 5°SiO↑↓.

Table 5.4 The multiplexing of different FLC materials and alignments at a duty ratio of 128 using a four slot scheme (2) and a two slot scheme (11)

Material	Alignment	Multiplexing scheme	Extinction angle	Minimum pulse length (μs)	Maximum contrast ratio	V_{strobe} (V_{blank}) (V)	V_{write} (V)	V_{data} (Vpp)	Comments
SCE12	PI↑↑	11	8°	32	5:1	31.8	19.9	9.6	Has persistance
		2	9°	32	5:1	36	17	10	
SCE12	5°SiO↑↑	11	0	200	18:1	37.9	16	7.35	No persistance
		2	0	155	18:1	±36	-	15	
SCE12	5°SiO↑↓	11&2	-	-	-	-	-	-	Not multiplex
SCE12	30°SiO↑↑	11	8°	100	3:1	32.5	13.6	7.7	
		2	12°	124	3:1	±22	-	15	
CS1014	PI↑↑	11	11°	32	5:1	28.7	7.4	17	
		2	10°	32	4:1	±27	-	11	
CS1014	5°SiO↑↑	11	20°	32	15:1	31	13	11.5	Blue/black switching
		2	20°	32	30:1	±25	-	15.7	White/black switching
ZLI3654	PI↑↑	11	12°	32	3:1	29	17	10	
		2	14°	32	3:1	±27	-	14	
ZLI3654	5°SiO↑↑	11	21°	64	5:1	34.6	11.5	9.6	Persistance is very strong: is not useable
		2	21°	32	9:1	±19.7	-	16	
ZLI3654	5°SiO↑↓	11&2	-	-	-	-	-	-	Not multiplex
ZLI3654	30°SiO↑↑	11	6°	68	4:1	35:7	5	8	
		2	6°	54	3:1	±15	-	8	zig-zags less after multiplexing
87-486	PI↑↑	11&2	-	-	-	-	-	-	Not multiplex
87-486	5°SiO↑↑	11&2	-	-	-	-	-	-	Not multiplex
87-486	30°SiO↑↑	11&2	-	-	-	-	-	-	Not multiplex

The polyimide aligned materials had a contrast ratio and an extinction angle when multiplexed that was the same as the relaxed states. This gave the cells a low contrast but a fast switching speed because to change from on to off the pixel needed to be switched from the intermediate state only. All three materials (ZLI3654, CS1014 and SCE12) multiplexed in a similar manner when aligned on polyimide.

The SCE12 and CS1014 HTA cells (5°SiO↑↑) also multiplexed with a contrast ratio and extinction angle that was as good as the bistability of the device. Since there was no relaxation in HTA cells the contrast was good (upto ten times that of the PI cells). The ZLI3654 HTA cell had a contrast ratio only slightly higher than the PI cell. This cell had long persistance and appeared to have anomalous switching maybe due to charging effects. Although the SCE12 HTA cell had a slow switching speed when multiplexed the CS1014 and ZLI3654 did not, the switching speeds were comparable to the PI cells. This behaviour followed the response times of these materials in HTA cells.

The 30°SiO↑↑ cells behaved similarly to the PI cells in that they produced contrast ratios that reflected the relaxed states. However the switching speeds when multiplexed were longer than the PI cells and were similar to the HTA cells. These cells therefore are both slow and have a low contrast ratio.

The best display to use was a CS1014 HTA device driven using the two slot scheme (scheme 11). This gave a fast switching speed and high contrast with the flexibility of varying all the voltages to optimise the performance. However the HTA cells tended to have a greater

persistance of the image than the PI cells i.e. the cell had to be addressed many times before the picture changed because they were more bistable and had higher latching thresholds.

5.9 Ferroelectric Liquid Crystal Displays

Two large area displays have been produced using both the HTA and SS alignments. Both displays were 2 μm thick, 6 cm x 6 cm in size and had 92 x 92 lines with a track pitch of 0.7 mm. The FLC material used (SCE6) was the same for both displays and they were driven using a two slot multiplexing scheme (scheme 11).

Photographs of these displays are shown in Figures 5.19 and 5.20. Figure 5.19 shows colour photographs of both the HTA and SS displays with three different pictures and Figure 5.20 shows black and white photographs of the HTA display with the same three pictures. Both displays were yellow and black (or blue and white if the polarisers were rotated) but the HTA display was less coloured. The HTA display had better contrast and viewing angle than the SS display.

One of the limitations in producing displays that looked good was the difficulty in fabricating large area cells with uniform thickness. Although fabrication is not central to this discussion it is necessary to mention the problems of shorting between electrodes and filling the cell with the FLC since these affected the appearance of the displays. The line shorts between the electrodes on the front and back plates of the cell were overcome by placing an insulating organic polysiloxane layer over the electrodes. However some shorts can still be seen especially on the earlier SS display (Figure 5.19b and e).

Figure 5.19: Photographs of FLC displays

HTA display (5°SiOtt)

a.

SS display (PItt)

b.

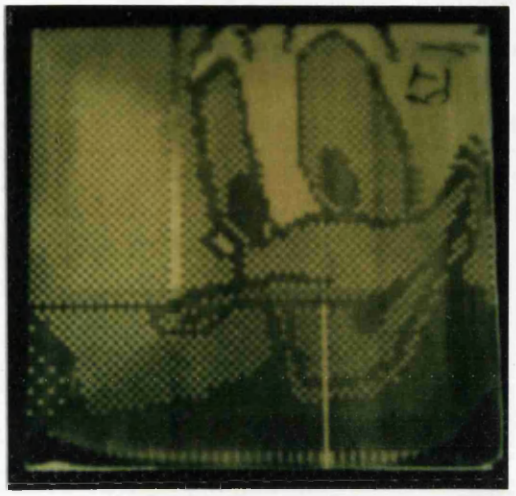

c.

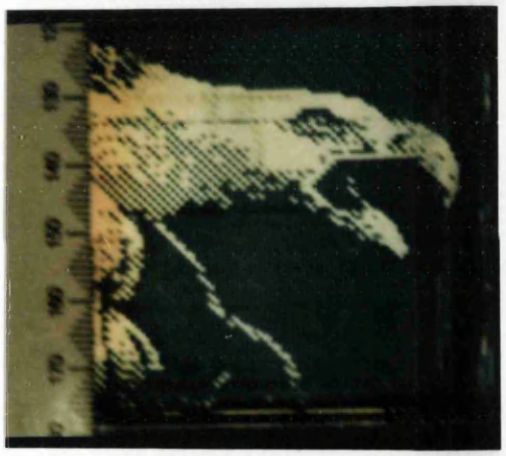

d.

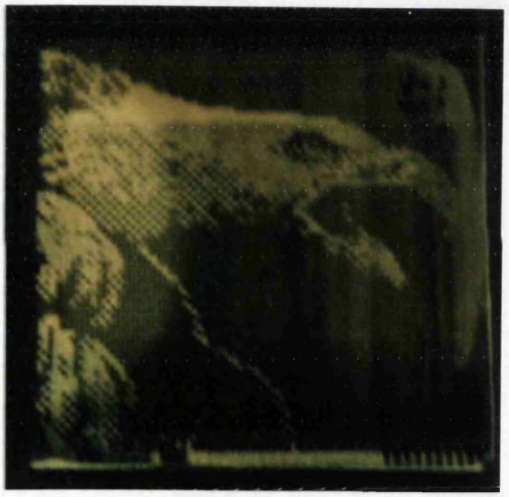

e.

f. Display has misaligned, especially the bottom quarter

Figure 5.20: Photographs of an HTA FLC display

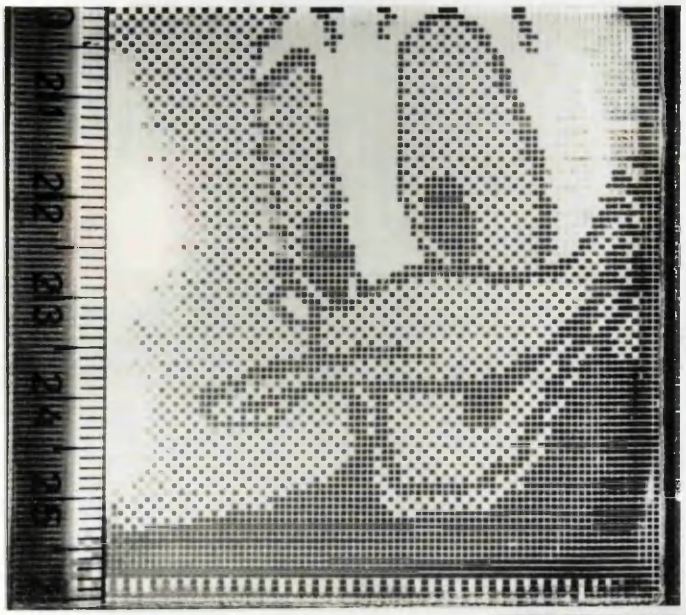

a.

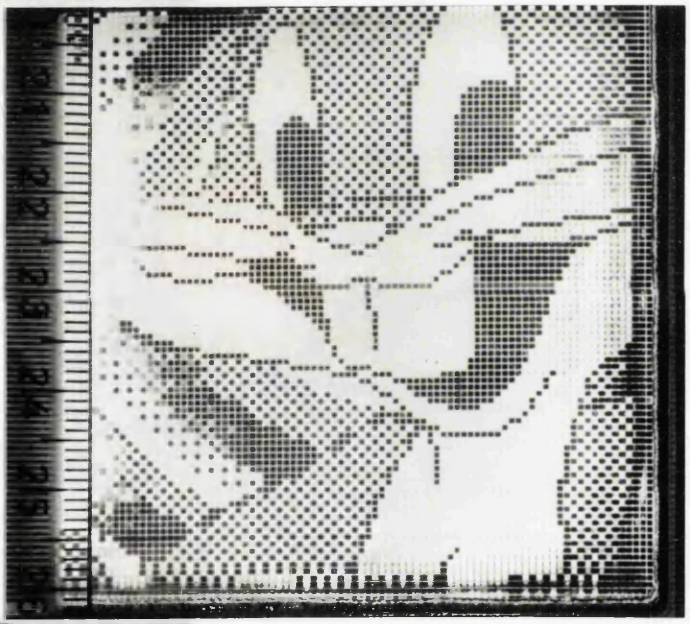

b.

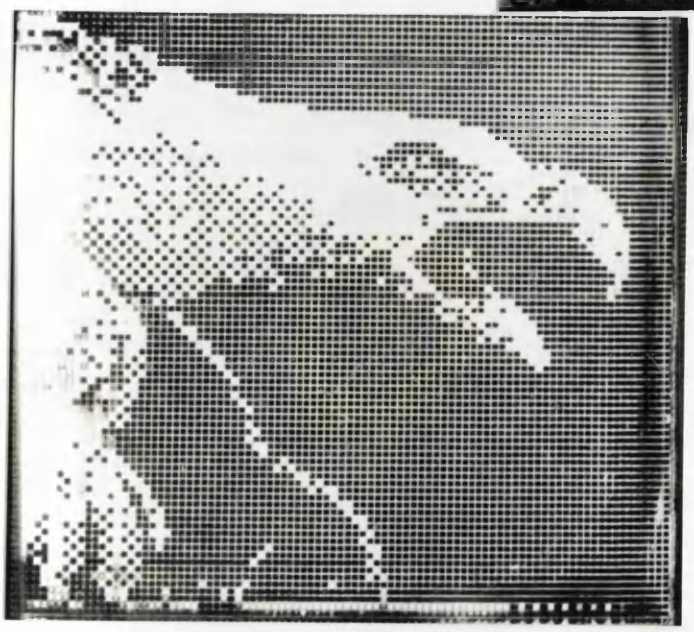

c.

When the cells were filled the FLC was at an elevated temperature (isotropic phase) in a vacuum for several hours. This caused the dopants to separate around the fill hole which produced a region that had a different birefringence (and therefore colour) and multiplexed differently. This was seen in both displays as a dark yellow region on the left hand side of the photographs. The problem was less acute when other materials were used but improvements in the material stability are still required.

Essential to the generation of a viable display was the specification of the requirements for the electronics to drive the display. A number of problems were encountered, chiefly the slew rate of the high voltage pulses and the low impedance output to drive the high capacitance load of the display. The availability of suitable prototype high voltage driver chips enabled these problems to be overcome whilst retaining a compact size. The driver chips, HV60, were designed by Leti to produce high voltage pulses upto 90 Vpp and are manufactured by Supertek. The power supply and computer interface were contained in one box and the driver chips were placed on a PCB along with the display. The display was connected to the driver PCB via flexible connectors which had conducting strips the same pitch as the display and were connected via anisotropic conducting adhesive.

The specifications of the drive electronics were:

Blank pulses:	+60V (generally kept less than +30V to prevent destroying the display)
Write pulses:	-30V
Data pulses:	±15V (generally kept to 5 Vpp)

d.c. offset on strobe line:±2V

a.c. field on strobe line: ±20V (not used because it would destroy the chips)

Pulse length: 32 μs to 1000 μs

Slew rate (to 90 Vpp): 8 μs

Pictures could be transferred from the computer to the display. A moving picture of 8 frames could be viewed by showing the stored images sequentially.

The switching speed of the HTA display was slower (~200 μs) than the SS cell which could be driven at video frame rate (32 μs) once the backlight had heated it above 30°C. The HTA also had persistence of the image which the SS did not. One way of reducing the persistence would be to reverse the blank pulse each cycle, i.e. reverse the whole sequence, so that the overall d.c. was not in one direction which would help the image to change more quickly. Finding a material with a faster response time that multiplexed well in an HTA device would also reduce this problem.

The HTA display had several advantages over the SS display other than the viewing characteristics which made it very attractive. The display was more stable to mechanical pressure and electrical spikes. The larger the cell was, the more flexible it became. This made the larger area SS displays very susceptible to zig-zags forming when pressed e.g. when connected to the driving board, when polarisers were put on or even to sudden electrical spikes when turned on or off (Figure 5.21e and f). The display then required realigning before it could be used again. The

HTA display was very stable and could be handled and moved without risk of destroying the alignment. This is very important when the displays are being manufactured.

Another advantage of HTA displays is that they can be made thicker and still retain good alignment, multiplexing and viewing characteristics. Fabrication would be made easier if a 3.5 μm display was used instead of 2 μm. To take advantage of this a low Δn material would be needed to produce a non-coloured display.

Multiplexing a PI or 30°†† cell moved the zig-zags off the electrode area to produce an almost zig-zag free switching region surrounded by a non-switching region of dense zig-zags (Figure 5.21c). The continual switching induced layer movement which resulted in the layer alignment being homogenised and the switching being made easier. Applying large electric fields to a FLC display would also rearrange the layer structure. The resulting texture is referred to as 'fatigued' and is shown in Figure 5.21a and d for a SSFLC device. The layers broke up to form a texture which was lined at 60° to the layer normal. This fatigue destroyed the multiplexing in SSFLC displays.

The 5°SiO†† cells also produced the fatigue texture on the electrode area when they were being switched (Figure 5.21b). The layer break up was not as strong and rather than destroying the multiplexing it appeared to improve the switching speed. The layer breakup could have been providing nucleation sites which speeded up the switching and therefore improved the multiplexing.

Figure 5.21 Distorted textures

Electrical Distortion

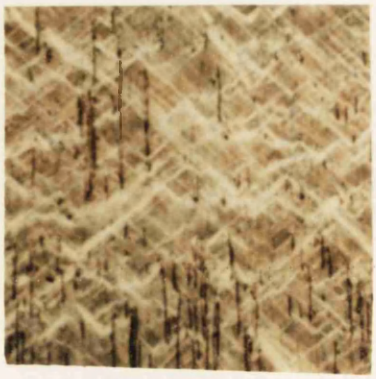

(a) Polyimide

(b) HTA

After Multiplexing

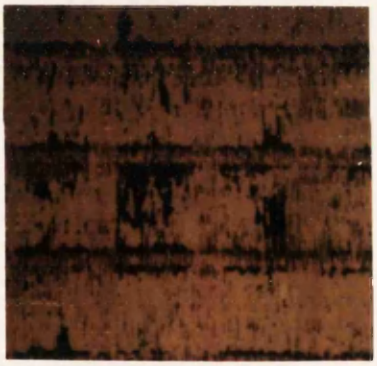

(c) zigzags moved

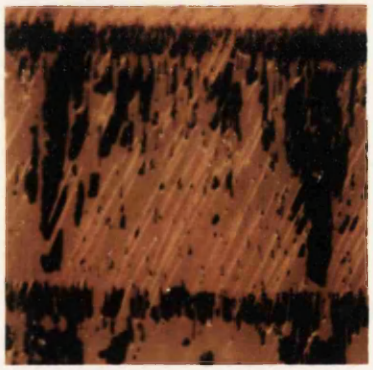

(d) Fatigue

Mechanical Distortion

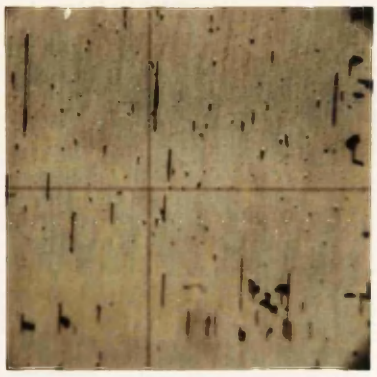

(e) Before

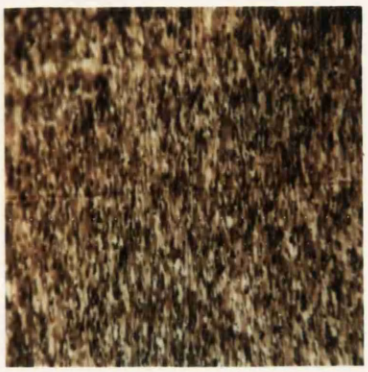

(f) After

5.10 Future Work and Greyscale

Two ferroelectric displays have been presented and compared. The SS display produced a fast frame time but a poor contrast and the HTA display produced an excellent contrast with a slow frame rate. The HTA display also had persistence of the image which was not as acute in the SS display and related to the relative switching speeds of the two devices. A more detailed investigation is necessary to determine methods to reduce this persistence. The starting place would be to use the two slot multiplexing scheme 11, with the voltage reversed each frame. This would stop any d.c. effects and would not give a preference to one state as at present. The major advantage of the HTA display over the SS display was that it was very mechanically stable. This made it easy to handle, for example to put polarisers or connectors onto the display, and it also was more resistant to electrical spikes or mechanical shocks.

In order for the HTA display to become attractive to use in video displays it is necessary to increase the speed. The reverse multiplexing technique that could be used in the SS displays to increase the speed could not be used for the HTA displays because they were totally bistable. The speed must therefore be improved by changing the material or the multiplexing scheme. The difference in switching speed between Merck and BDH materials was far greater than the difference in multiplexing rate for different multiplexing schemes. It is therefore necessary to do further work on improving the FLC material to suit an HTA display. A pyrimidine or NCB material is required with good temperature stability, large S_C^* and N^* pitches and one that can

multiplex well. More work is needed to relate the chemical composition of the FLC materials to its threshold voltages and to its multiplexibility.

Work on improved FLC materials is also necessary to facilitate easier cell fabrication techniques. An HTA display can be made over 6 μm thick if required although 3.5 μm is the optimum when taking into account voltage and capacitance. This would still be enough to make fabrication of a display easier and cheaper and is very desirable. The problem at present is that the current FLC materials have a high birefringence which demand a cell thickness between 1.5 μm and 2 μm in order to obtain black and white switching. The synthesis of FLC materials with a birefringence of 0.07-0.08 would enable 3 μm to 3.5 μm thick displays to be used.

At present the best displays are fabricated by using spacers that are grown up to 2 μm thick and are regularly placed. This is difficult and expensive. A cheaper technique is to randomly scatter plastic spacers of the required thickness between the two substrates. For 2 μm thick displays it is very difficult to achieve a uniform thickness over large areas using this technique although it is possible (the displays shown here use this technique). However, at 3 μm thickness this method of spacing becomes significantly easier.

The next major goal in FLCD research is to obtain greyscale. However this is not easy to do because FLCDs switch by nucleation and are field dependent. There are four methods of obtaining greyscale that are currently being investigated:

(1) voltage controlled.

(2) using the electroclinic effect

(3) spatial dither

(4) temporal dither

Voltage controlled greyscale is the most desirable because it is easy to implement electronically without losing speed or resolution. Unfortunately it is the most difficult to achieve in a multiplexing display. Greyscale can easily be shown in a single pixel of a FLCD when addressed using single pulses of different voltages. This is particularly easy in HTA displays because they are bistable. The different greylevels obtained are due to the size and number of domains. The problem is that each pixel will nucleate and grow domains in a different way so that at a fixed voltage different pixels will have different greylevels. To control the nucleation of domains is extremely difficult because they are affected by perturbations and defects in the alignment which are random. The situation is made more complex when the display is multiplexed. The crosstalk due to the data voltage switches the pixel into a greylevel that is determined by the history of the pixel and therefore the greylevel is dependent on the data being applied. It has been found that applying an a.c. stabilising field can minimise this effect [Maltese et al 1988] but it is still a problem. Alternative techniques to voltage controlled greyscale are therefore being sought.

One such technique is to use the electroclinic effect. Using this effect the cone angle of the FLC can be controlled by varying the voltage levels and therefore the greylevel can be controlled. However, there are many foreseeable problems; the cone angle is very small except when

extremely large voltages are used, the whole effect is very temperature dependent and, most importantly, the device is no longer bistable and therefore it is difficult to see how such a display will be multiplexed.

Spatial and temporal dithering are two techniques that are well known in other applications. Spatial dithering is used in newspaper pictures and is based on an array of sub-pixels to make up one pixel. The number and pattern of sub-pixels that are switched on at any moment in time determine the perceived greylevel of the pixel. The biggest problems with this technique are that the resolution decreases and the number of connections increases. However by having four different sized sub-pixels it is possible to obtain 16 greylevels with only four sub-pixels the total size of which are not much bigger than a single pixel.

Temporal dithering switches the pixel fully on or fully off but it addresses the pixel for different lengths of time in order to vary the perceived greylevel. If the display is addressed using five fields for each frame and each field has a different line address time e.g. 8,10,12,14 and 16 μs it is possible to obtain 25 greylevels at a frame rate of 26 Hz for a 625 line display. The length of time the pixel is on is made up of different combinations of the five addressing fields. This would require a 4 μs switching speed for a two slot multiplexing scheme. This is not only difficult to obtain from the display but is also difficult for the electronics.

In practice a combination of both spatial and temporal dither will be used on the first FLC displays. Using 16 greylevels obtained from

spatial dithering and 4 from temporal dithering (requiring a 12 μs response time and only two addressing fields), a total of 64 greylevels can be obtained which is sufficient for many displays.

The future of FLC displays will depend on the ability to obtain greyscale. The present state-of-the-art FLC display will replace the supertwist LCD as an alpha-numeric display e.g. for portable computers. If adequate greyscale can be obtained then the FLC display could replace the active matrix LCD as a video or graphics terminal.

CHAPTER 6

LIQUID CRYSTAL ALL-FIBRE OPTIC DEVICES

The use of light in communications and sensor applications is becoming increasingly important. The advantages of using light in telecommunications are its resistance to electromagnetic interference (EMI), its increased data rate and distance of transmittance over electrical signals, low weight and decreasing cost. The use of fibre optic waveguides for transporting light is an essential part of realising these applications. Most fibre optic waveguides are used as passive optical components, but in optical systems there is a need for active devices such as switches or modulators. These could be achieved by combining bulk optical components with fibre optics, however, this can result in high losses, high cost and low stability. It is therefore desirable to have active devices that are purely fibre-optic. Many different all-fibre optical devices have already been realised such as directional couplers (to replace the bulk optical beam splitter), phase controllers (to replace the bulk electro-optic phase modulator), polarisers, polarisation controllers and wavelength multiplexers.

One approach to realise all-fibre optic components is to use the evanescent field of the guided signal therefore allowing most of the power to remain in the fibre unless deliberately removed. Over the last ten years devices based on evanescent field interactions have been demonstrated showing that low losses can be achieved using this technique. The principle of evanescent field devices is that the decaying tail of the field that exists outside of the fibre core

interacts with an appropriate overlay such as a metal film [Eickoff 1980], birefringent material [Bergh et al 1980], other fibres etc.

The work here uses the approach where the overlay is a liquid crystal. Liquid crystals (LC) have the necessary large birefringence and large electro-optic effect to produce good polarisers and modulators with the added advantage that they can be chemically engineered to the required refractive indices. The intrinsic uniaxial nature of LCs makes them suitable for polarisation sensitive devices although this is not always desirable. Polarisation desensitised LC modulators have been reported [Kashyap et al 1987].

The first reports of combining LCs with waveguides used the LC as an active planar waveguiding layer [Channin 1973, Kobayashi et al 1982]. The large scattering and optical absorption of the LC gave the device a large propagation loss. More recent reports on LC modulators have used evanescent field coupling of fibre optic waveguides. These modulators have the electrodes placed either side of the fibre core [Goldburt and Russell 1986, Liu et al 1986] which has the cladding removed by polishing to allow access to the evanescent field. The NLC is placed on top of the exposed core.

This chapter demonstrates a simple nematic LC evanescent field all-fibre optic polariser and modulator using a LC with appropriately low refractive indices [Ioannidis et al 1988]. The extinction ratio, losses and modulation frequency are given and the temperature stability is determined. FLC fibre optic devices are also presented. These use LC materials that have high refractive indices which are not optimum for this application therefore low modulation depths are obtained. However

fast modulation is demonstrated and the potential for future devices is discussed.

This work was carried out jointly with Z. Ioannidis whose expertise is in waveguides and fibre optics. He set up the equipment and characterised all the half couplers used in this work. The liquid crystal experience, alignment and interpretations were contributed by myself. The measurements were mostly taken jointly although Z. Ioannidis concentrated on the nematic liquid crystal devices and I concentrated on the FLC devices.

6.1 Evanescent Field All-Fibre Optic Couplers

For an optical fibre to guide light the core must have a higher refractive index than the surrounding medium. This can be achieved either by a fibre whose refractive index varies continuously in the radial direction (a square law is commonly used) or by a stepped index fibre which has a distinct core with a cladding of different but homogeneous refractive index (Figure 6.1). Cladded single mode fibres are used in this work. It is not essential to have a cladding on such fibres to produce waveguiding since air provides $n_2 = 1 < n_1$, but a cladding is important for two reasons:

(1) Evanescent fields exist outside the core and the surrounding medium of the fibre would distort this field.

(2) For a given frequency a fibre can support a finite number of modes which depend on the core radius, a_1 and the ratio n_1/n_2. If $a_1 > \lambda n_1/n_2$ then many modes can be supported. In many applications (e.g. long distance telecommunications, coherent

sensors etc) it is desirable to have single mode operation. The larger n_1/n_2 is, the smaller a_1 must be for single mode operation. It is easier to produce fibres with large cores (e.g. >5 μm) therefore it is preferable to have n_2 only slightly less than n_1.

In order to transfer light from one fibre to another it is desirable to use a directional coupler. The devices investigated here couple the optical power between two waveguides via the evanescent field that extends outside the core. To achieve this it is necessary to remove some of the cladding to expose the evanescent field and then bring the two fibres into close proximity. Several fabrication techniques have been reported to produce coupling; a fusion method [Ozeki and Kawsaki 1976, Veilleux et al 1986], a chemical etching method [Shemm and Giallorenzi 1979], a mechanical polishing method [Bergh et al 1980] and a D fibre method [Dyott and Schrank 1982].

The mechanical lap and polish technique was used to produce the devices in this work. A single-mode fibre was bonded with optical adhesive along a curved slot cut into a fused silica block. The cladding was first ground and then polished to within a few microns of the core. This is called a half coupler block. When another block is placed so that the two cores are in close contact, a full coupler is made. An index matching oil is placed between the two blocks. This also acts as a lubricant to allow one half coupler to be slid over the other (generally achieved by placing in a holder equipped with micrometers) thereby changing the core-to-core separation and the net coupling. Figure 6.2 shows how the coupling can change as the core-to-core distance changes [Digonnet and Shaw 1982]. At 0 μm the light recouples

Figure 6.1: A stepped index optical fibre showing the field distribution

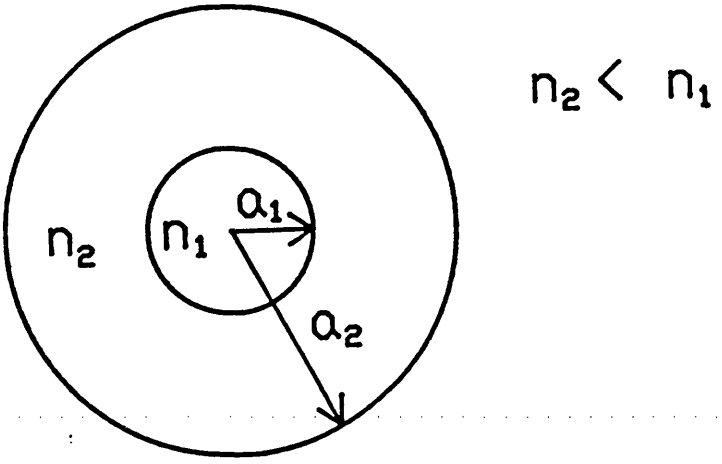

Figure 6.2: Coupling between two fibres as the core-to-core distance is varied

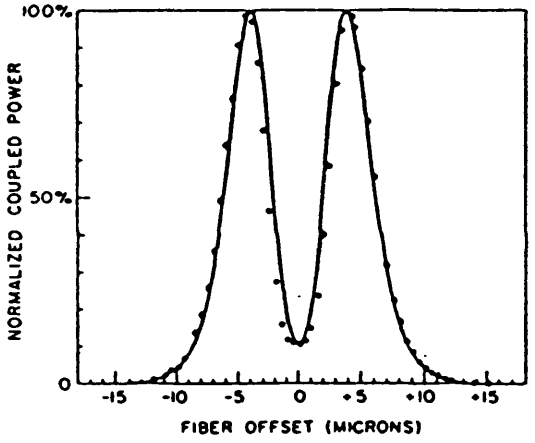

Figure 6.3: Characteristic refractive index response of the half coupler used in Section 6.3.1

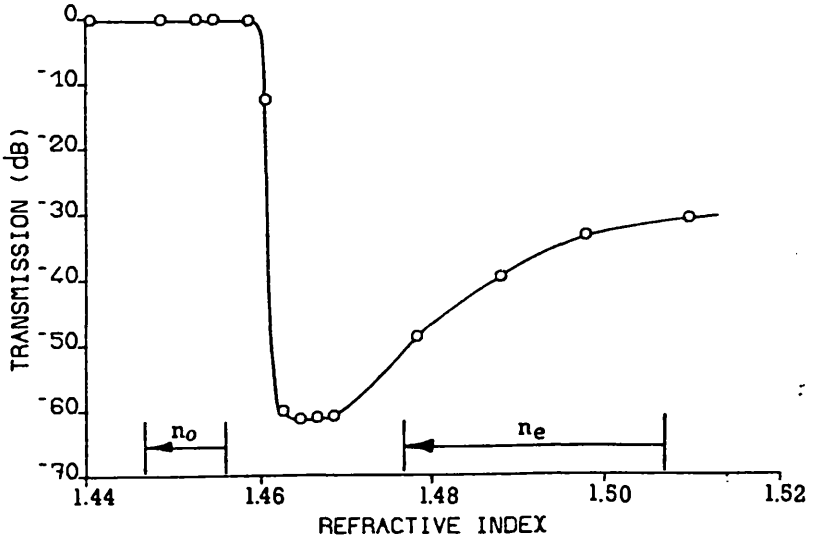

back into the original fibre, at ±3 μm the light couples into the second fibre and at ±10 μm the light couples out of the original fibre but does not couple into the second fibre. The exact shape of this curve is affected by the coupling length and coupling coefficient. When a LC is placed in the coupler the refractive index can be varied by applying a field. This electrically alters the coupling efficiency replacing the need to move the fibre cores with respect to each other.

The optical characteristics of the half couplers are determined by the depth of polishing. Therefore each half coupler needs to be characterised individually by measuring its transmission as a function of the refractive index of the overlay. Oils of different refractive indices are placed on the exposed fibre core and the transmission of light along the fibre is monitored. A characteristic curve is shown in Figure 6.3. (This block was used to produce the NLC polariser).

When the overlay has $n<n_{silica}$ the light remains guided in the core. When the overlay has $n>n_{silica}$ the light couples out of the core and the transmission along the fibre drops sharply. As the refractive index of the overlay increases the coupling efficiency decreases due to the mismatch between the core and the LC. This causes the transmission to slowly increase again. The polishing depth determines the rate of this increase. A highly polished fibre produces a small increase in transmission but the losses can be greater because more of the evanescent field is leaving the fibre. A lightly polished fibre has a large amount of cladding remaining which reduces the effect of the overlay. This produces a rapid increase in transmission for $n>n_{silica}$.

6.2 Experimental Technique

The experimental setup is shown in Figure 6.4. It consisted of a chopped He-Ne beam detected by a photodiode and lock-in amplifier. The beam was launched into the fibre through a 50 dB polariser which passed through an all-fibre polarisation controller and two splices before reaching the half coupler. A splice is a method of joining two fibres. The jacket was removed from the cladding (by a flame or chemical etch) and the two cores were aligned then melt fused together using a high voltage corona discharge. The two splices joined the coupler and the polarisation controller and the fused coupler was used to take out a reference signal.

The polarisation controller was made by bending a fibre into two loops [Lefevre 1980]. This induced linear birefringence in the fibre through the photoelastic effect. When the loops were twisted, circular birefringence was induced. By having two such loops, each of $\lambda/4$, that could be twisted independently all polarisation states could be realised. The linear polarisation in the plane parallel to the loop encountered a higher refractive index than did the polarisation perpendicular to the plane of the loop. By using a 50 dB analyser at the output it was determined that the extinction ratio achieved by the controller was in excess of 45 dB.

Two measurements were made on the LC polarisers; the extinction ratio and the losses. The extinction ratio measured the difference in transmission when the polarisation state was adjusted from maximum to minimum transmission. This was measured as a function of temperature (the temperature dependence of the refractive index of fused silica is very small ($dn/dT = 11.9 \times 10^{-6}$ /°C) and can be neglected). The loss

Figure 6.4: Experimental setup

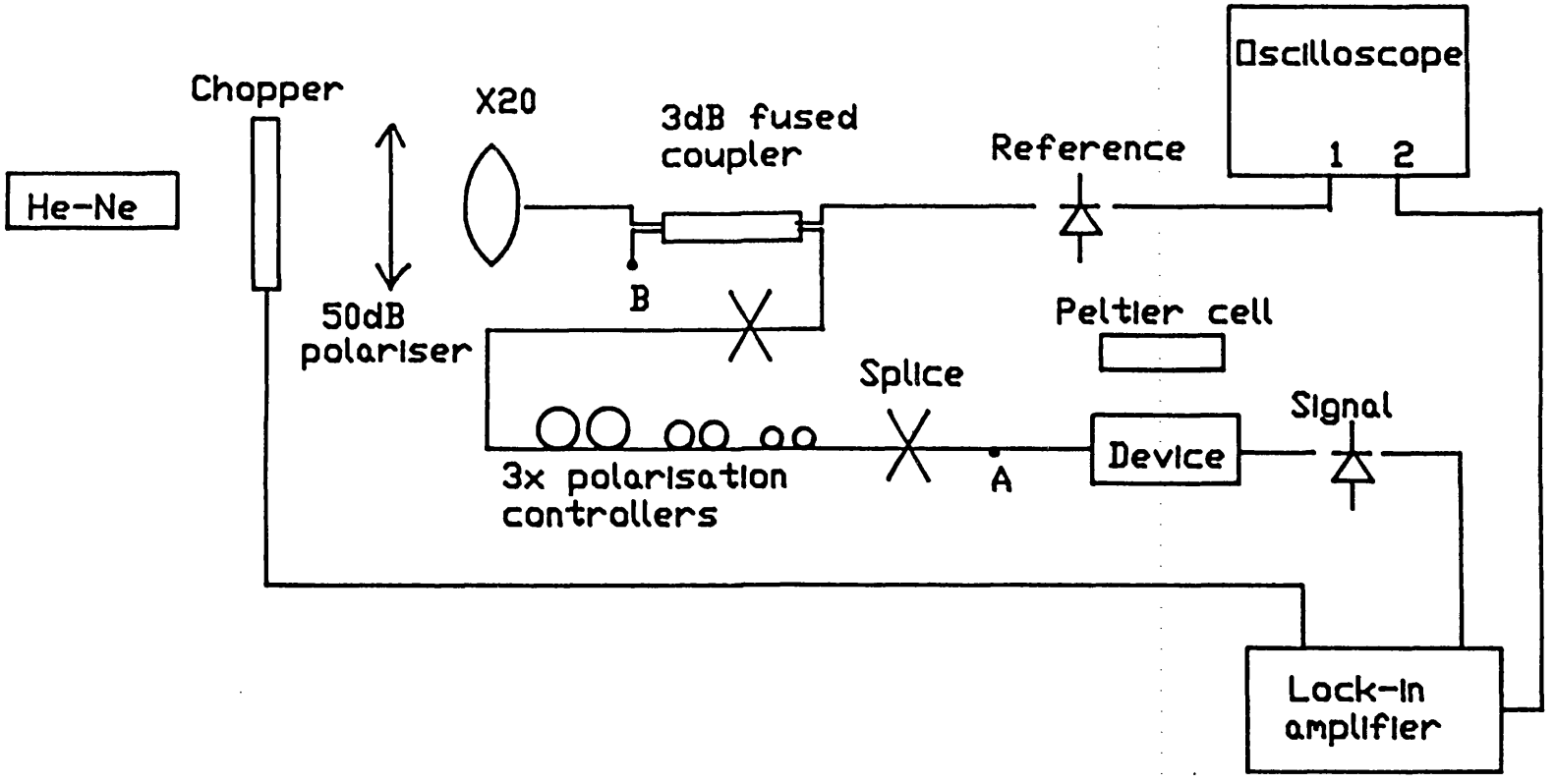

was a measure of the difference between the transmission with and without the LC, oil or aligning overlay. The loss of the coupler was determined by breaking the fibre after the splice (point A, Figure 6.3). The losses normally ranged between 0.2 and 2 dB for a half coupler. All measurements are quoted in dB for example;

$$\text{Loss} = 10 \times \log_{10} \left(\frac{\text{maximum transmission with overlayer}}{\text{maximum transmission without overlayer}} \right) \text{ dB}$$

For the LC modulators the modulation depth, the maximum modulation frequency and the losses were measured. The modulation depth measured the difference between the maximum and minimum transmission for a particular polarisation state when the LC was being switched.

The effects produced by using a LC overlayer on a coupler half were polarisation dependent due to the uniaxial nature of the LC. How the TE or TM mode were affected by the LC depended on the alignment geometry (Figure 6.5). For a nematic LC homogeneously aligned perpendicular to the fibre ($\theta = 0°$), the TM mode would see a refractive index of n_o which ideally would be less than n_{silica} and the light would remain in the core. The TE mode would see n_e which ideally would be greater than n_{silica} and would couple out of the fibre to produce a polariser. For the LC modulator switching would cause the LC to become homeotropic and the TE mode would see n_o and the TM mode would see n_e so that both polarisation states would be modulated but they would be 180° out of phase. It was important to adjust the input polarisation for the maximum and minimum transmission levels when any measurements were made.

6.3 Nematic Liquid Crystal All-Fibre Optic Devices

The performance of previously reported nematic liquid crystal (NLC) fibre optic devices has been limited by the refractive indices or the transition temperatures of the NLC material. This work used a new NLC material, 14616, developed by BDH [Sage and Chaplin 1987] that has a nematic phase between 10°C and 53°C and refractive indices where for λ = 633 nm, $n_o < n_{silica}$ and $n_e > n_{silica}$ over the whole nematic temperature range. This material was therefore well suited to make a practical polariser with low loss, a high extinction ratio and good temperature stability. For this particular NLC material it was best to have a half coupler which was highly polished so that at high values of n_e, i.e. low temperatures, the extinction ratio remained high. To produce a polariser the nematic LC could be aligned homogeneously or homeotropically. To produce a polarisation modulator the LC had to be aligned homogeneously to suit the positive $\Delta\epsilon$ of the NLC used. (A negative $\Delta\epsilon$ material with suitable refractive indices is produced by BDH, but was not used in this work).

6.3.1 A nematic fibre optic polariser

Four different alignments have been studied; three homogeneous alignments produced by rubbing the surface of the fibre and block with a cloth in the required direction and one homeotropic alignment that was produced by coating the fibre surface with lecithin (1% solution in IPA). The characteristic refractive index response of the half coupler used is shown in Figure 6.3 along with the refractive indices of the NLC, 14616. This block without any overlay had a loss of <0.1 dB. When the NLC overlay was placed over the fibre the loss of the device was

Figure 6.5: Alignment of the nematic LC with respect to the fibre axis showing the TE and TM modes

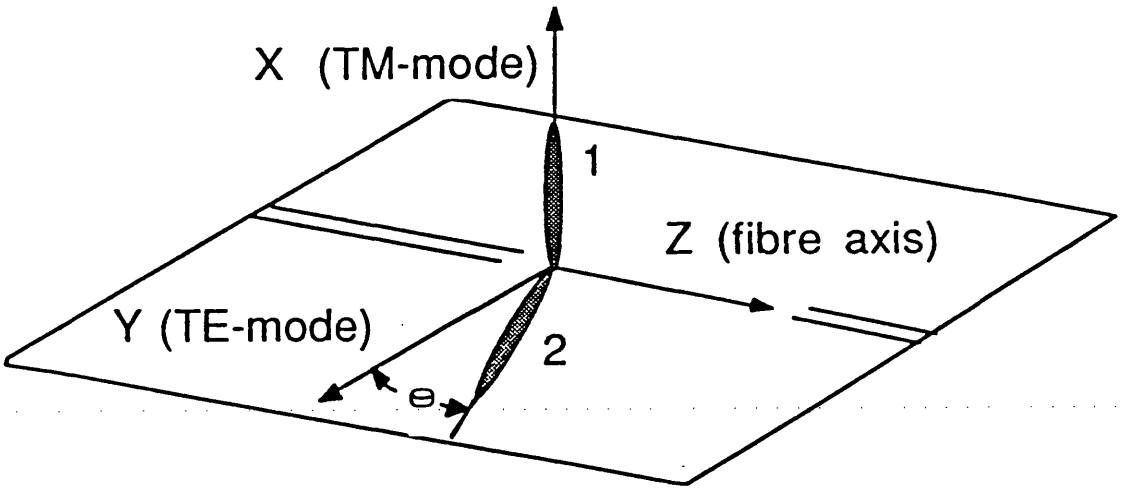

Figure 6.6: Variation of the measured extinction ratio with temperature for a nematic LC polariser homogeneously aligned perpendicular to the fibre axis (case 1)

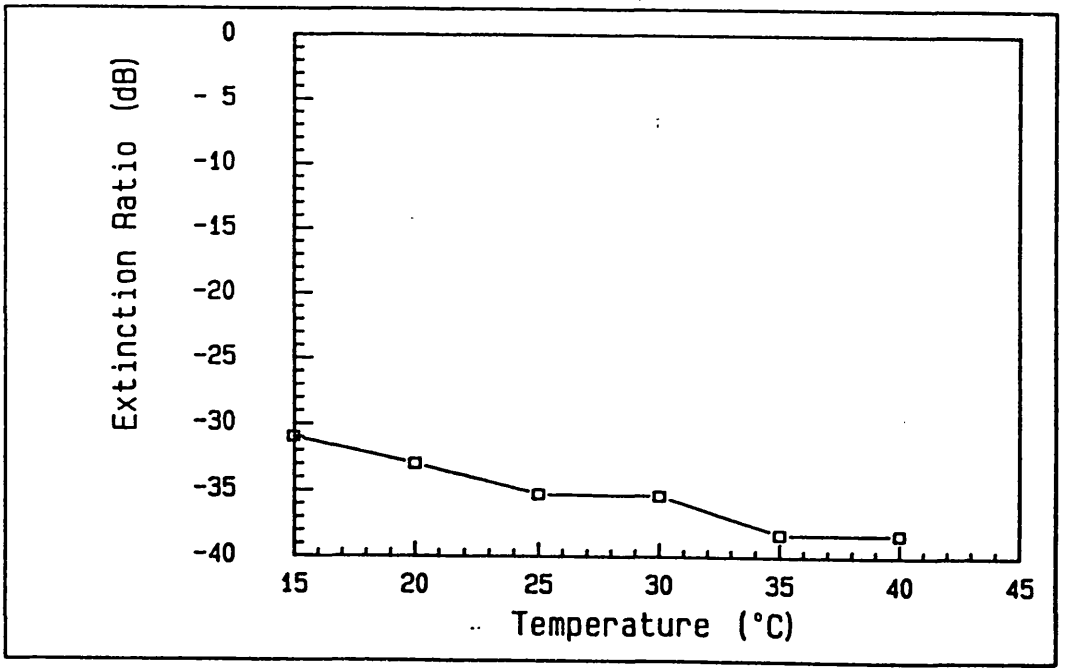

independent of the alignment used and varied between 0.2 dB and 0.36 dB. The loss varied due to the alignment quality but was independent of temperature between 15°C and 45°C.

Case 1

The director was homogeneously aligned perpendicularly to the fibre (Figure 6.5 for the case when θ=0°). This alignment produced a TM polariser. The TM mode saw a refractive index of n_o and remained guided in the fibre. The TE mode saw a refractive index of n_e and radiated out of the fibre. At room temperature a drop of NLC on the rubbed fibre produced an extinction ratio of 44.3 dB. A 12 μm thick cell was produced using 12 μm mylar for spacing. The measured extinction ratio as a function of temperature is shown in Figure 6.6. The minimum transmission level was varying periodically due to the light waveguiding in the NLC layer (at 12 μm thickness the NLC would act as a multimode waveguide). The resulting extinction ratio was a combination of matching the refractive indices and waveguide coupling. The unstable transmission levels made measurements difficult and the results shown are an average of the observed values.

Case 2

The director was homogeneously aligned parallel to the fibre (Figure 6.5 for case 2 when θ = 90°). Both TE and TM modes saw a refractive index of n_o and there should have been no polarising effects. The observed extinction ratio was very small as expected and varied between 0.02 dB and 0.06 dB. However a small change in transmission with polarisation was seen because the director was not exactly aligned with the fibre.

Case 3

The director was homogeneously aligned at an angle of 45° to the fibre to produce a TM polariser. Aligning the director at an angle θ allowed optimisation of the extinction ratio by lowering the effective refractive index seen by the TE mode, where:

$$n_{TE} = n_e n_o \left(n_o^2 \cos^2\Theta + n_e^2 \sin^2\Theta\right)^{-1/2}$$

$$n_{TM} = n_o$$

An extinction ratio of 50 dB at room temperature was observed. The theoretical and measured extinction ratio as a function of temperature are shown in Figure 6.7. The signal was unstable because the measurements were at the limit of the polarisation controllers. However, the extinction remained between 45 dB and 50 dB for the whole temperature range which corresponded to the reproducible limits of the polarisation controller and input polariser. It is reasonable to assume that the two isolated measurements at higher temperatures which were less than 45 dB were also limited by the polarisation controller.

Case 4

The director was homeotropically aligned with respect to the fibre surface (Figure 6.5, case 2). This produced a TE polariser. The TE mode saw n_o and remained guided but the TM mode saw n_e and was radiated out of the fibre. At room temperature an extinction ratio of 32.85 dB was obtained which was less than the values obtained for the optimised homogeneous alignment at θ=45°. The theoretical and measured extinction ratio as a function of temperature are shown in Figure 6.8.

Figure 6.7: Theoretical and measured extinction ratio of a homogeneously aligned NLC polariser (at 45° to the fibre axis) at different temperatures

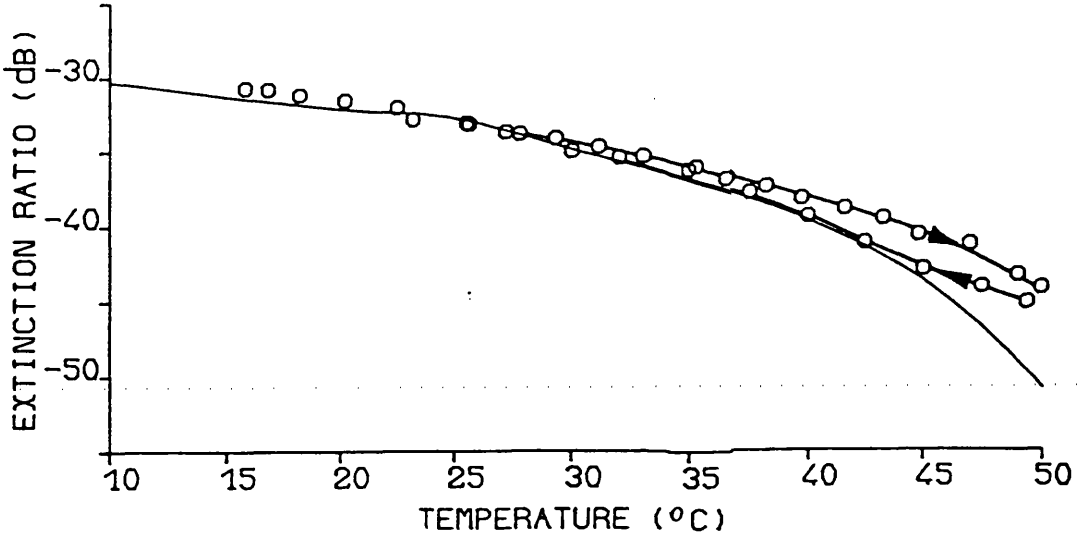

Figure 6.8: Theoretical and measured extinction ratio of a homeotropically aligned NLC polariser at different temperatures

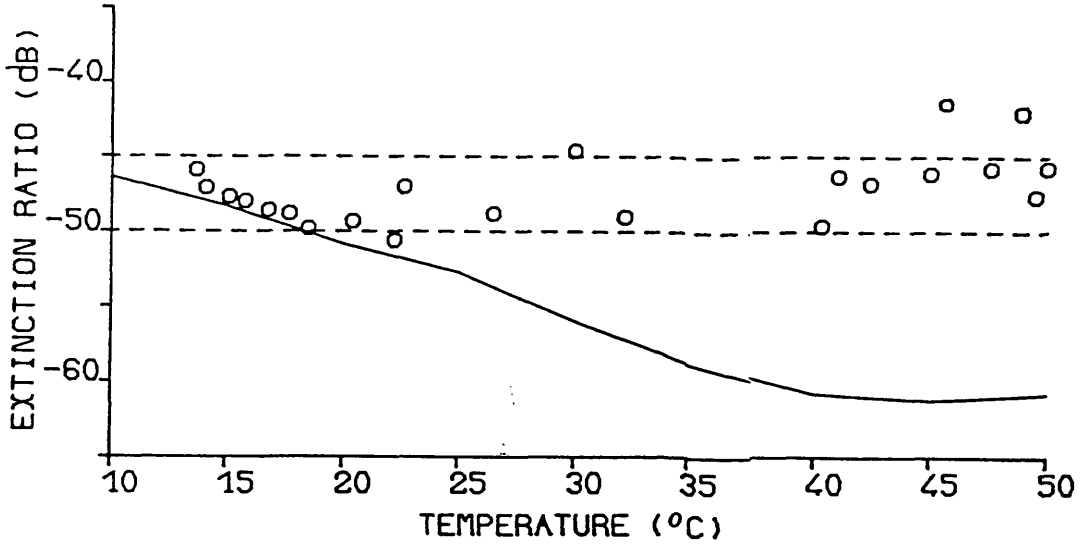

There was good agreement between the experiment and expected response except close to the nematic to isotropic transition temperature. The proposed explanation for this discrepancy is that the surface forces induce a higher degree of alignment near the surface than in the bulk. Since the evanescent field is exponentially decaying in the NLC, the interaction with the material is concentrated very close to the surface so the effective n_e seen by the light is greater than the bulk measured n_e. This discrepancy could also be due to director fluctuations being less at the surface than in the bulk producing the same effect as described above. A hysteresis was also observed which was attributed to a temperature lag in the system.

Best Alignment

It was best to use a homogeneous alignment for a nematic liquid crystal fibre optic polariser. The alignment was easier to control and produced a higher extinction coefficient. It was also possible to vary the angle between the director and fibre axes to optimise the extinction ratio. A totally temperature independent polariser could be produced by using a tilted homeotropic alignment [M G Clark 1988] where the tilt angle could be altered to suit the temperature by applying a field. A similar system could be used with a homogeneously aligned FLC in the S_A phase where the applied field would vary the angle between the director and fibre axes in the plane of the device. However both these devices would require electrodes and a continuous field to be applied which would make them more complex to produce and less attractive to use.

6.3.2 A nematic Hi-Bi fibre optic polariser

A high birefringence (hi-bi) fibre retains the polarisation state of the input light either by having a non-circular core or by having

anisotropic stress applied. Hi-bi fibres are more stable to bending or external influences than ordinary single-mode fibres. A hi-bi fibre is produced by stressing the core, for example by placing two lobes of material either side of the core that have different thermal coefficients than the cladding. When the fibre is cooled the lobes stress the core (Figure 6.9) to produce a birefringent waveguide. Such a 'bow tie' fibre was used in this device. This type of fibre is useful because the polarisation state passing through the coupler is known. When making a hi-bi coupler it is essential that the fibre is aligned with one of the polarisation axis in the plane of the block surface so that the maximum extinction ratio can be achieved.

Although a hi-bi fibre has two distinct polarisation axes, there is some polarisation mixing. The extent to which the two modes can remain separate is called the isolation of the fibre and can be as high as 45 dB. When making a coupler the isolation is decreased to ~25 dB because of the misalignment of the fibre axes and polishing induced birefringence. The extinction ratio of the polariser is limited by the isolation of the fibre.

To test the hi-bi coupler a polarisation controller was unnecessary but the polarisation state of the launched light was very important. To aid the alignment of the polarisation state with the fibre axes a $\lambda/2$ plate was used to rotate the plane of polarisation of the laser light which was also polarised. The efficiency of the $\lambda/2$ plate was only 30 dB so another polariser was added to increase this to >50 dB. In order to take the measurements the polariser and $\lambda/2$ plate were rotated to launch light along either of the two orthogonal polarisation axes which would

also change the launching conditions. Therefore the extinction ratio, R, had to be measured in a different way than for normal single-mode fibres. The extinction ratio was defined as

$$R = 10 \times \log_{10} \left(\frac{\text{loss of TE mode}}{\text{loss of TM mode}} \right) \text{ dB}$$

The half coupler used for this polariser was lightly polished to produce the characteristic refractive index response shown in Figure 6.10. The refractive indices of the NLC are shown on the graph. The losses were measured without an output polariser. The TE losses were 0.14 dB and the TM losses were 0.15 dB. The isolation of the coupler was measured as the (TM output)/(TE output) when TE light was launched in the coupler with no overlayer. This was measured to be -27.6 dB.

The nematic LC was aligned homeotropically. The theoretical extinction ratio as a function of temperature for this block with NLC on top is shown in Figure 6.11, along with the experimental results. The measured extinction could only be as good as the isolation of -27.6 dB. This limit was below the theoretical value and the measured value of extinction remained constant at all temperatures. The hi-bi polarisation coupler therefore had low loss (0.14 dB) with a >-22 dB extinction ratio for temperatures between 10°C and 50°C.

6.3.3 A nematic fibre optic modulator

To make a NLC modulator the same alignment techniques could be used as in Section 6.3.1 with electrodes added. The use of gold electrodes plated either side of the fibre was reported by Liu et al [1986] and Goldburt and Russell [1986] (Figure 6.12). If the gold was placed over

Figure 6.9: A hi-bi optical fibre

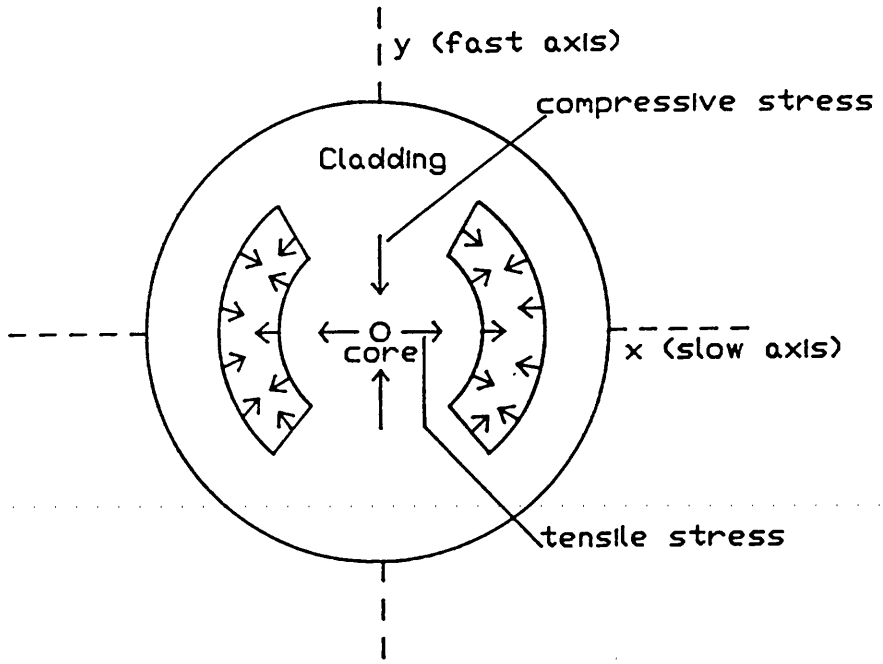

Figure 6.10: Transmission of the hi-bi coupler used in Section 6.3.2 as a function of refractive index of the overlayer

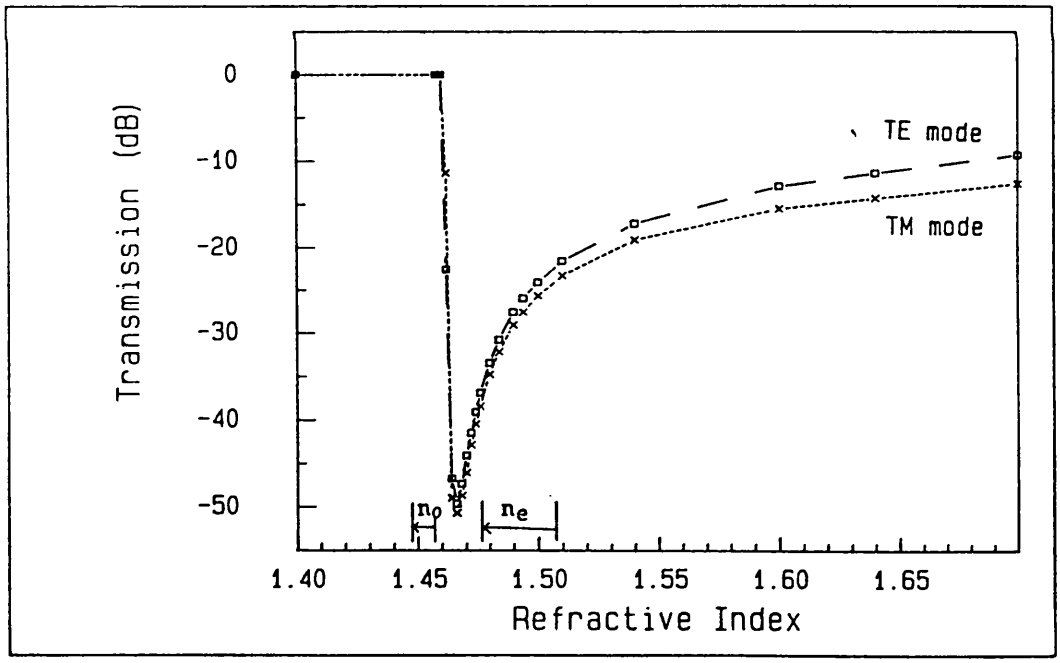

Figure 6.11: Theoretical and measured extinction ratios for a nematic LC hi-bi TM polariser homogeneously aligned at 55° to the fibre axis at different temperatures

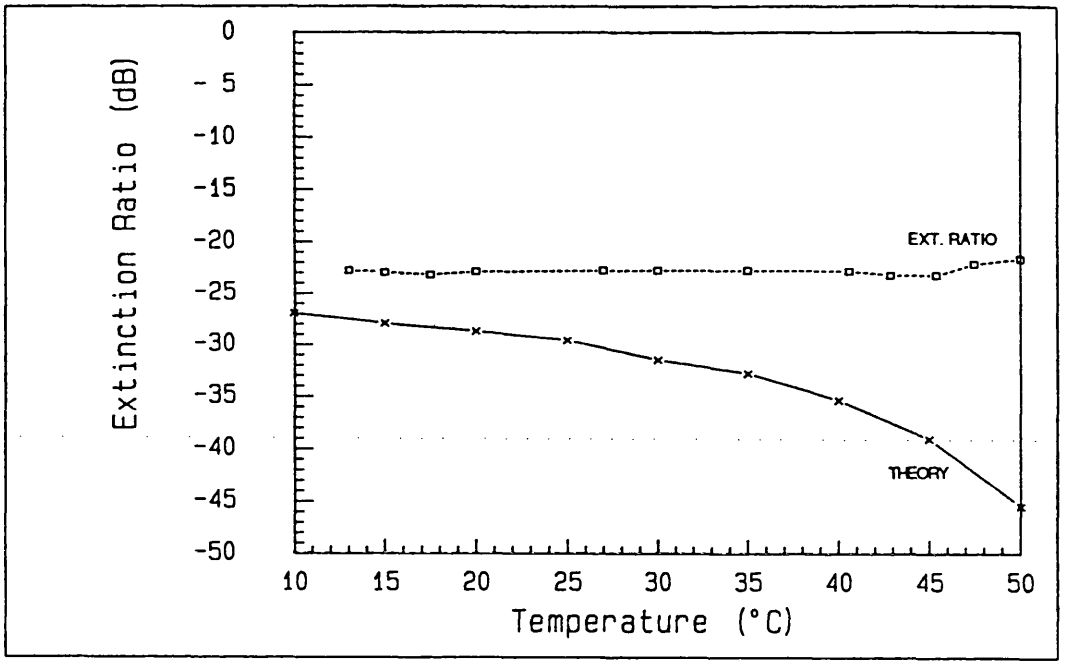

Figure 6.12: All-fibre optic nematic LC modulator used by Goldburt and Russell [1986]

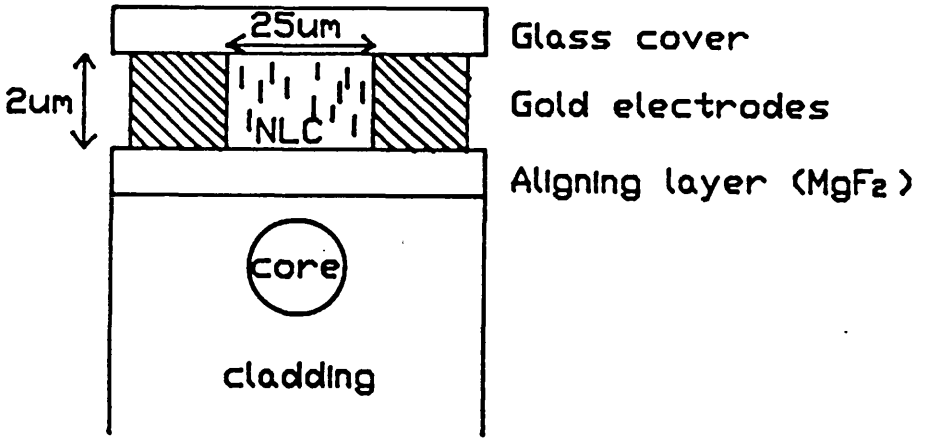

the fibre it would interact with the light to produce absorption effects. A similar device was constructed for this work with a gap between the gold electrodes of 50 μm which were 2 μm thick (the thickest the gold could be plated). A homeotropic alignment was needed for such an electrode arrangement (14616 has a positive $\Delta\epsilon$). An aligning layer of either chrome complex or lecithin was put down over the electrodes and the NLC placed on top. The first few attempts showed no observed effect when the field was applied. The resistance between the electrodes was always infinite even with the NLC overlayer. The lack of switching was probably due to the aligning layer lying between the electrodes rather than the NLC. (It should be noted that Liu et al [1986] used a layer of MgF_2 as an aligning layer which was beneath the electrodes). A later experiment showed slight switching but at extremely high voltages (~150 Vdc).

Our approach was to use an ITO electrode evaporated over the fibre. ITO has a positive optical dielectric constant and should not produce surface plasmon effects. The arrangement is shown in Figure 6.13. This had several advantages over the gold electrodes; it was easy to coat ITO onto the fibre, the ITO was very tough and was not scratched easily like gold and the NLC, 14616, could be aligned homogeneously which was more reliable than the homeotropic alignment. The use of ITO as an electrode for a waveguiding coupler switch was shown by Okamura et al [1984] however their setup used a prism coupling planar waveguide rather than a fibre. The biggest advantage with this approach was that low voltages could be used for switching (an order of magnitude less than previously).

Figure 6.13: All-fibre optic nematic LC modulator used in Section 6.3.3

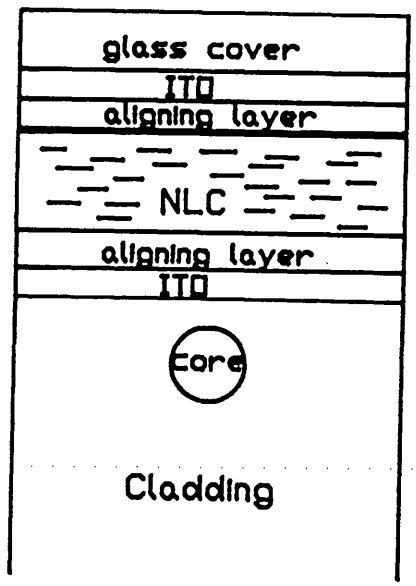

Figure 6.14: The characteristic refractive index response of the half coupler used in Section 6.3.3 with an ITO overlay

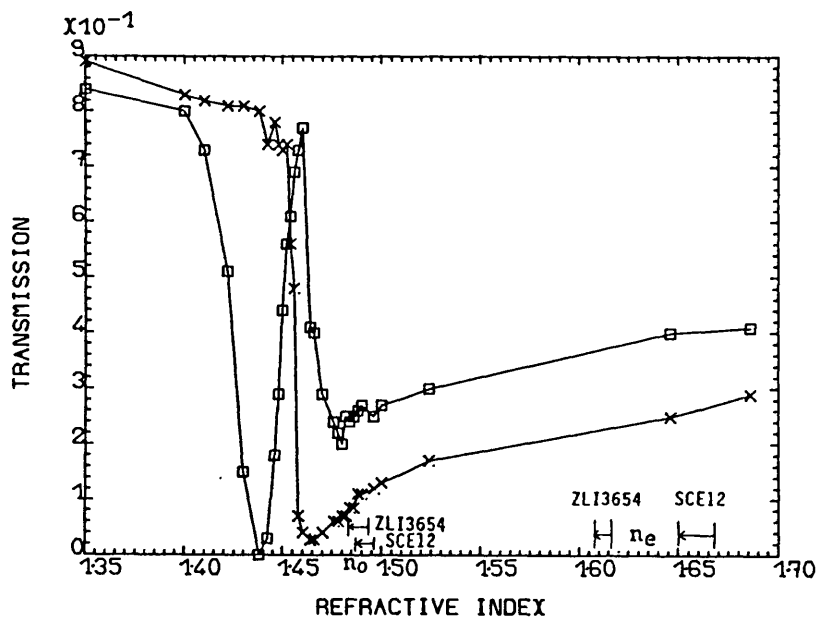

The characteristic refractive index response of the coupler half with 15 nm ITO coated as an overlayer is shown in Figure 6.14 along with the refractive indices of the NLC. A distinctive dip in the TE mode (similar to a surface plasmon resonance) was observed just before $n = n_{silica}$ and the TE mode and TM mode have separated i.e. there was a polarisation effect. This was a waveguiding resonance of the coupler. The ITO had a high refractive index of 1.7 and either side of it were low refractive index media (the fibre and the NLC). Normally the differences between these refractive indices would be too large for waveguiding to occur, however because the ITO was very thin only the fundamental TE and TM modes could be supported which were very close to cut-off. The effective refractive index of the ITO was therefore very close to the cladding (~1.46) and waveguiding could occur [Ioannidis 1989]. By adjusting the refractive index of the upper cladding (NLC) the effective refractive index of either the TE or TM mode was 'fine' adjusted to match that of the fibre mode and therefore the fibre mode coupled to the lossy planar ITO waveguide. In this experiment the variation of the upper cladding refractive index was such as to reveal only the TE mode resonance but both modes could be made apparent in other devices. The losses of the coupler with the ITO layer were 0.33 dB and the losses of the device with a NLC overlay were 1.44 dB.

The NLC was aligned homogeneously by rubbing with a tissue along the direction of the fibre axes so that both the TE and TM modes would see n_o. The extinction ratio at room temperature was 19 dB because n_o was on the resonance dip for the TE mode but at maximum transmission for the TM mode. The 19 dB corresponded to an $n_o = 1.455$ which was close to the quoted value at room temperature of $n_o = 1.452$. When a field was applied the NLC switched to homeotropic so that the TE mode continued to

see n_o and was therefore not modulated but the TM mode saw n_e. The modulation of the TM mode with applied voltage is shown in Figure 6.15. There was also modulation of the TE mode but this was small (30% maximum). Both modes had a threshold voltage of ~6V. The modulation of the TE mode was probably due to the director not being aligned exactly along the fibre when homogeneously aligned. Not much change in n was required to produce a large modulation of the TE mode because the variation in n was about the resonance dip. The maximum modulation depth of the TM mode was 37.8 dB which was stable at 25V.

The periodic variation was the effect of waveguiding. For such a thick NLC layer (12 μm) there would be many possible waveguiding modes in the NLC layer itself (~10). As the director switched the propagation constant of the NLC waveguide changed and scanned through the matching conditions for many of these modes to produce the modulation. This modulation was only small because the NLC was a poor waveguide and it is difficult to couple between two different waveguides anyway. There was more waveguide modulation at low voltages because matching was best when n was low and the LC tilt angle was small.

The modulation frequency for a NLC depends on the relaxation time of the LC which is independent of the field applied. For this material the relaxation time was 200 msec which limited the modulation frequency to 5 Hz if the maximum modulation depth was required. Table 6.1 shows the affect of the applied voltage on the switching and relaxation times and the modulation depth for the TM mode.

Figure 6.15: Transmission of the TM mode as a function of applied voltage for a nematic LC modulator with ITO electrodes. Waveguiding effects produce a periodic oscillation

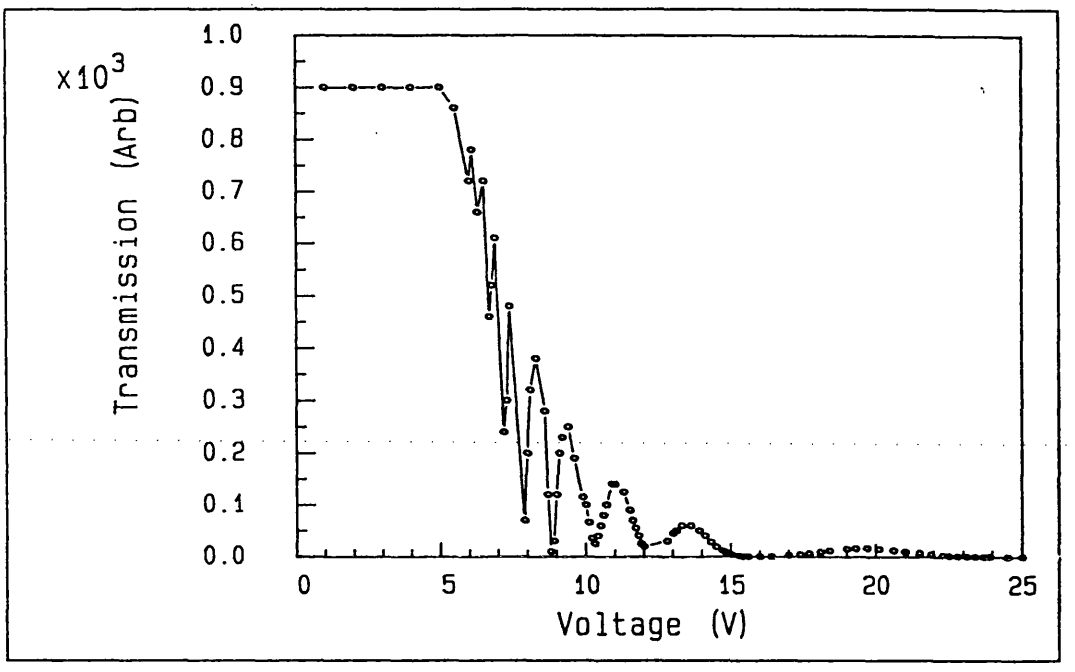

Figure 6.16: The modulation depth of a nematic LC modulator as a function of frequency for a sine wave of 10 Vpp

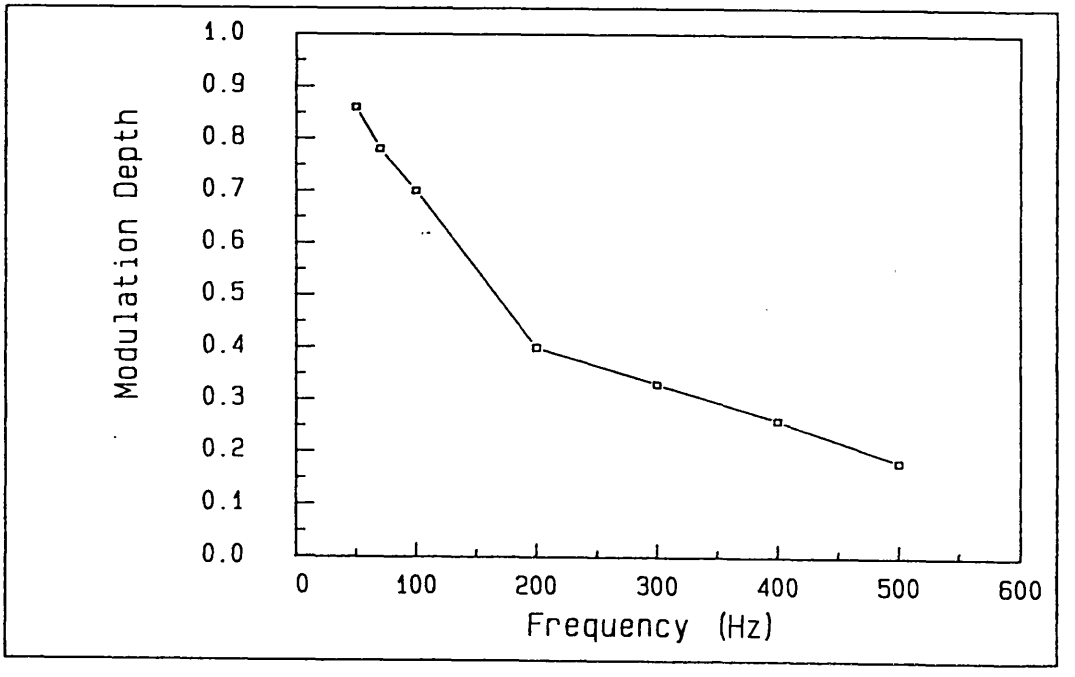

Table 6.1: The rise and fall times of a nematic LC modulator for three different voltages

Voltage (Vpp)	Rise time (ms)	Fall time (ms)	Modulation depth (dB)
10	50	200	-23.3
15	10	200	-23.3
20	5	200	-31.1

Figure 6.16 shows the modulation depth as a function of frequency for a non negative sine wave. 100 Hz was the maximum frequency that was useable whilst retaining a reasonable modulation depth. This was very slow but could be improved by increasing the elastic constants (k_{11}) or decreasing the viscosity (η) of the NLC since

$$(\text{relaxation time}) \alpha (\eta/k_{11}).$$

Photographs of the switching behaviour of the NLC device are shown in Figure 6.17. The difference between the switch and relax times can be seen in Figure 6.17a. When relaxing the modulation showed waveguiding effects similar to Figure 6.15 (static response). The waveguiding effects could not be seen for the switched response because it was too fast. At 10 Hz the periodic behaviour due to waveguiding could be seen (Figure 6.17b) but at faster frequencies (50 Hz) only the initial large drop was observed (Figure 6.17d) and the transmission modulated with an apparent lag to the applied voltage but without any perturbations.

Figure 6.17: The switching characteristics of a nematic LC fibre modulator showing waveguiding effects

(a) Square wave response (switch and relax)

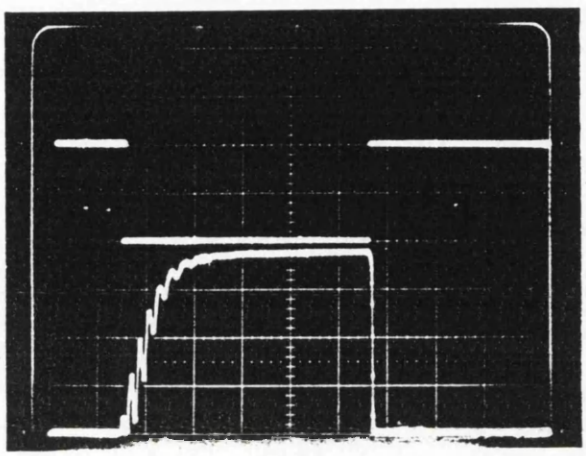

(b) Sine wave response 10 Hz

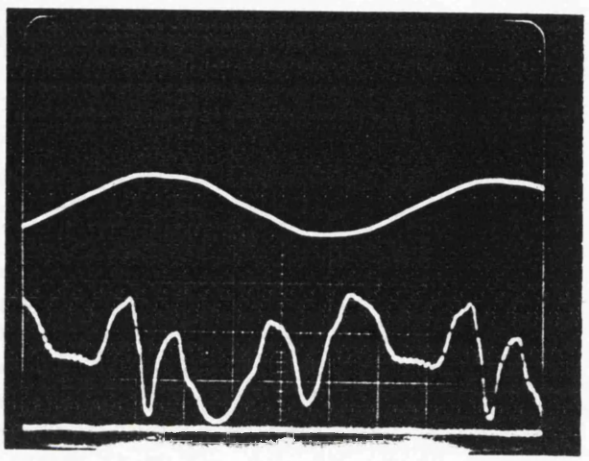

(c) Sine wave response 20 Hz

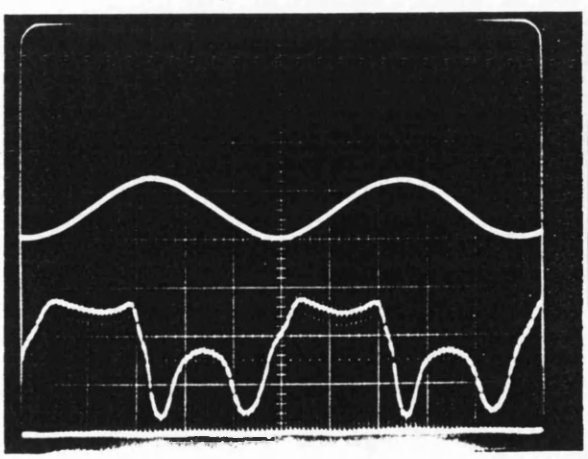

(d) Sine wave response 50 Hz

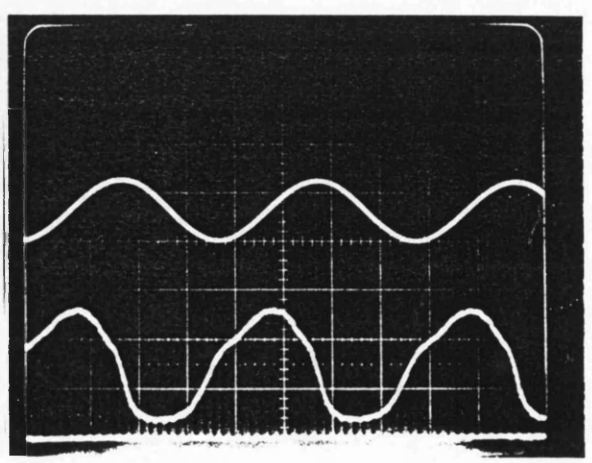

6.4 Ferroelectric liquid crystal all-fibre optic devices

Ferroelectric liquid crystals (FLC) are more suitable materials to use in modulators than nematic liquid crystals (NLC) because they can switch upto a thousand times faster. The main problem with using FLC with fibre optics at the present time is that the refractive indices are too high to produce large modulation depths. This situation can be improved by using a lightly polished coupler so that the coupling efficiency drops off rapidly as the n of the overlayer increases above n_{silica}. The simplest device configuration uses ITO electrodes coated over the fibre and homogeneously aligned FLC. When switched the FLC will move in the plane of the fibre. The same lightly polished block was used for both devices in this section. The characteristics of the block are shown in Figure 6.18 along with the refractive indices of ZLI3654 and SCE12, the two FLC materials used. The maximum theoretical extinction ratio for either material was ~8 dB. The polarisation effect and the waveguiding resonance in the TE mode due to the ITO could be seen. The losses for the coupler with ITO were 0.33 dB and with the FLC overlayer the losses were 3 dB. The losses due to the FLC were greater than due to the NLC because it was more difficult to get a uniform, monodomain alignment of the FLC therefore more scattering was likely and also the refractive indices were higher.

6.4.1 A surface stabilised aligned fibre optic modulator

The alignment used for this device is shown in Figure 6.19. A rubbed polyimide aligning layer was used with an unoptimised rubbing direction at 55° to the fibre axes. When a field was applied the director switched by θ_C either side of the rubbing direction. The FLC material SCE12 was used because it has a large birefringence and good alignment properties.

Figure 6.18: The characteristic refractive index response of the half coupler used in Section 6.4 which is lightly polished and has an ITO overlay

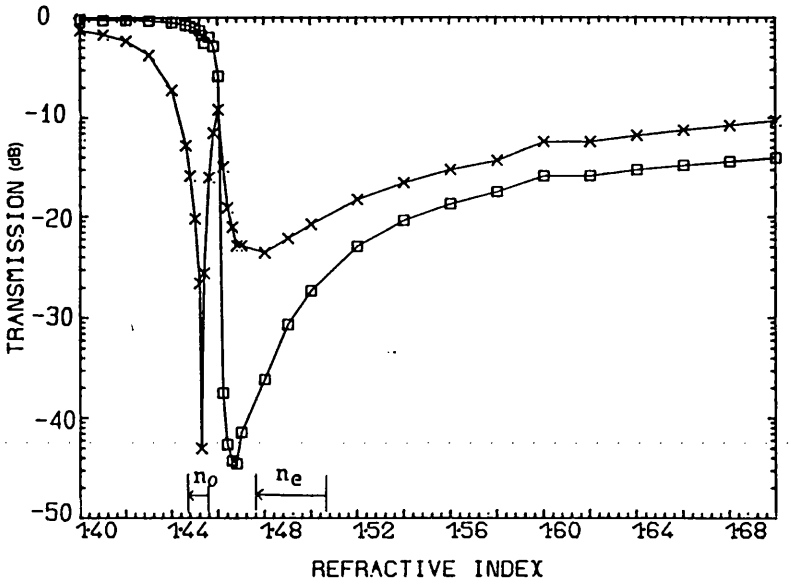

Figure 6.19: A schematic diagram of the SSFLC fibre modulator

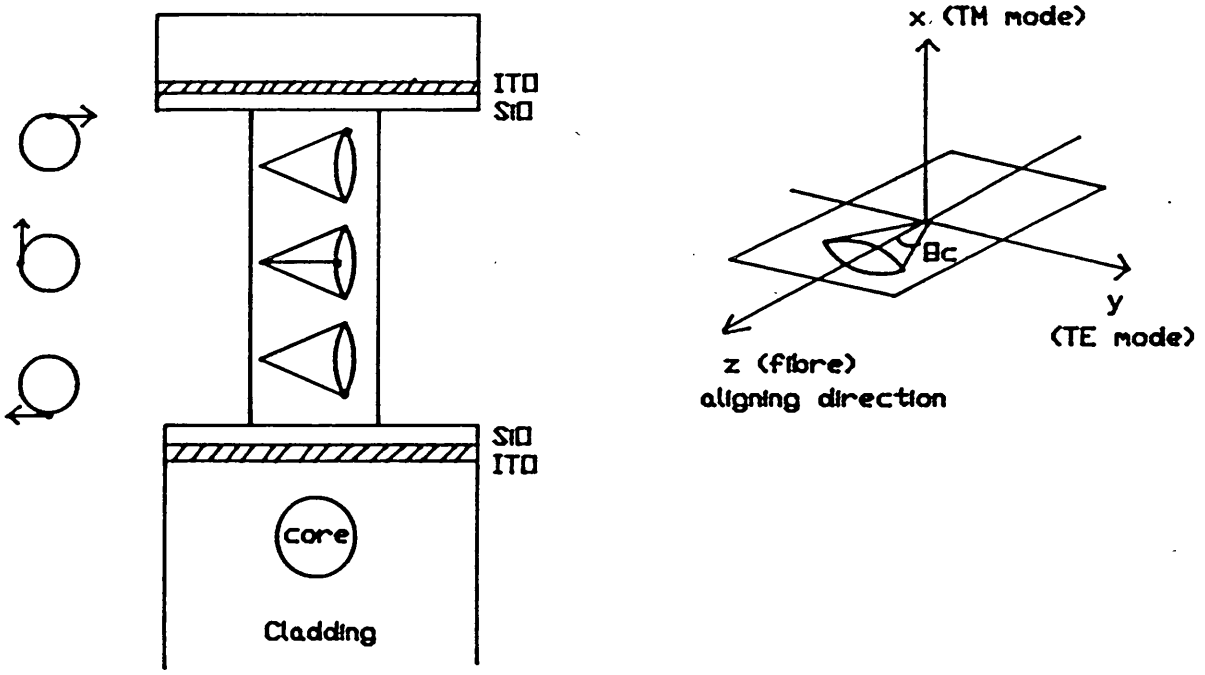

Other methods of aligning the FLC were also tried. Rubbed PVA and PTFE were coated over the ITO layer and then a drop of FLC was placed on top. A glass slide with similar coatings of ITO and rubbed polymer was placed on top of the block and pressed together. However, this technique produced devices which were too thick to align the FLC therefore a sealed device was made using rubbed polyimide.

Figure 6.20 shows the change in transmission of the TE and TM modes as the SSFLC modulator was heated from 20°C to 45°C. The TE mode varied very little and since n_e varied by only 0.001 between 20°C and 60°C it would be reasonable to assume that the TE mode was very stable upto 60°C. The transmission of the TM mode varied by 25% between 20°C and 45°C. The TM mode saw n_o which like n_e also varied by 0.001 from 20°C to 60°C but n_o was lower than n_e and was on a steeper part of the curve (Figure 6.18) therefore this small variation in n could cause a larger variation in the transmission. The SSFLC modulator was found to be extremely stable at all temperatures and the responses produced by applying a field were very reproducible. The change in transmission of the device as a d.c. voltage was applied is shown in Figure 6.21.

The switching behaviour of the SSFLC modulator when a square wave voltage was applied can be seen in Figures 6.22a for the TE mode and Figure 6.22b for the TM mode. Both modes had some modulation contrary to expectations. The TE mode had a large modulation (50%) and smoothly switched from one state to the other as expected. There were some peaks in the optical response which were unexpected. The most likely explanation for this is that the out of plane switching that occurred

Figure 6.20: Transmission as a function of temperature for the TE and TM modes of the SSFLC fibre modulator when relaxed

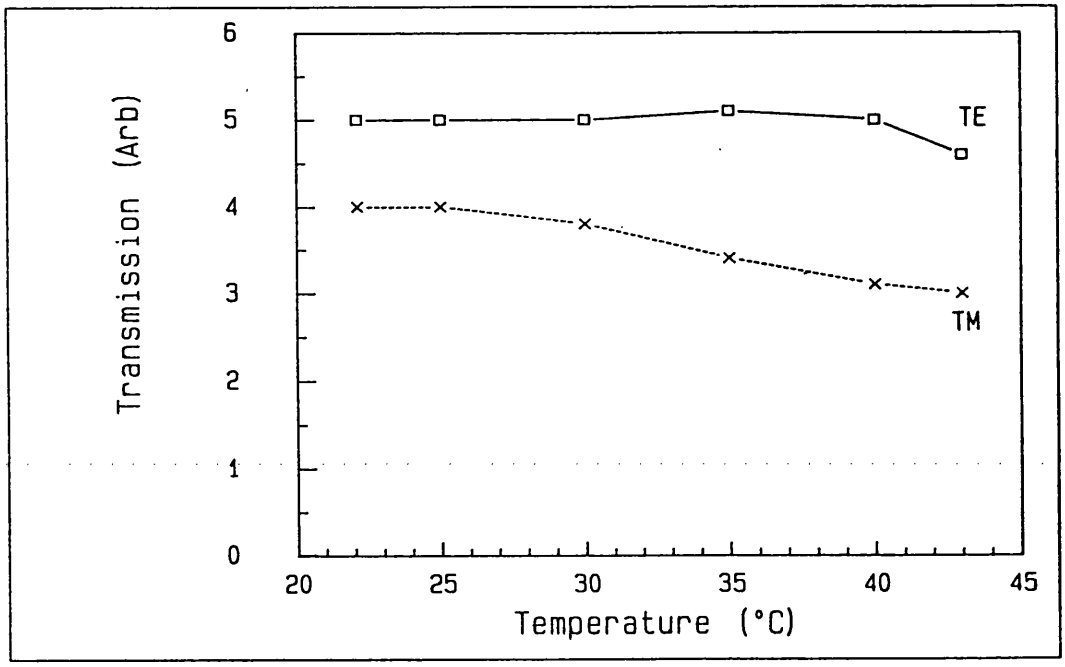

Figure 6.21: Transmission change for the TE mode of a SSFLC modulator when a d.c. voltage is applied (c.f. Figure 6.22c)

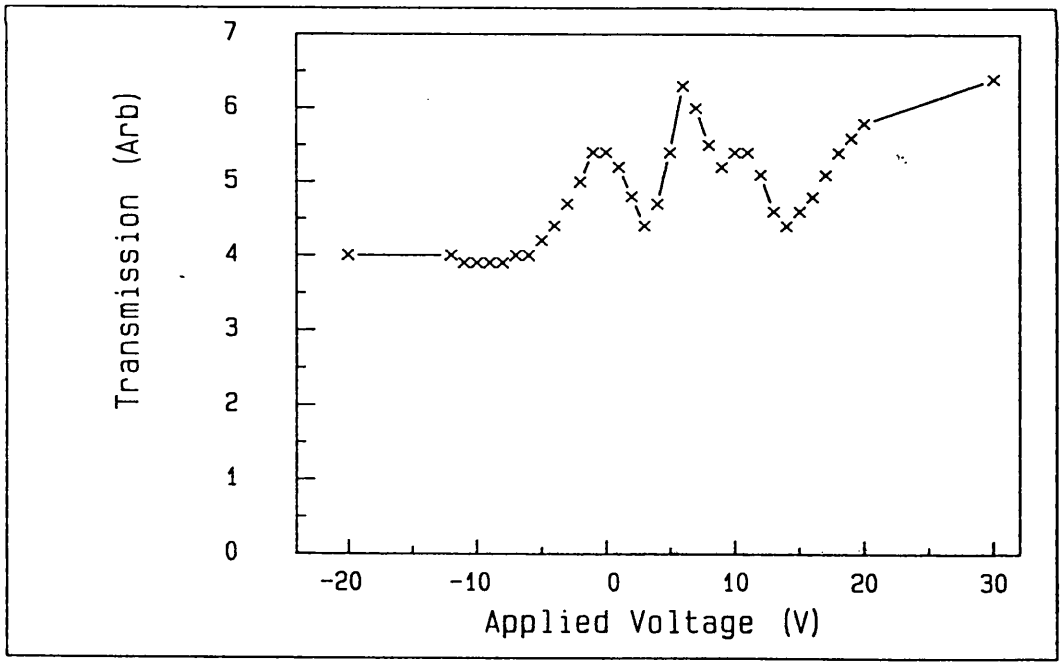

Figure 6.22: The switching characteristics of a SSFLC fibre modulator

(a) Square wave response
100 Hz, 10 Vpp, TE mode

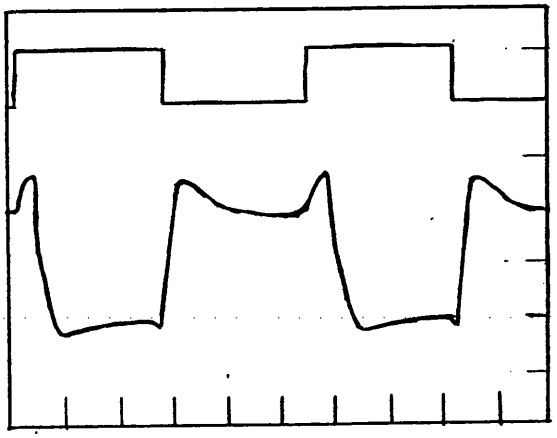

(b) Square wave response
100 Hz, 10 Vpp, TM mode

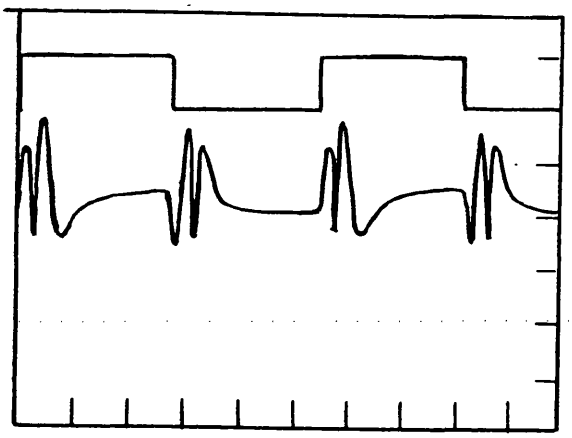

(c) Square wave response
200 Hz, 20 Vpp, TE mode

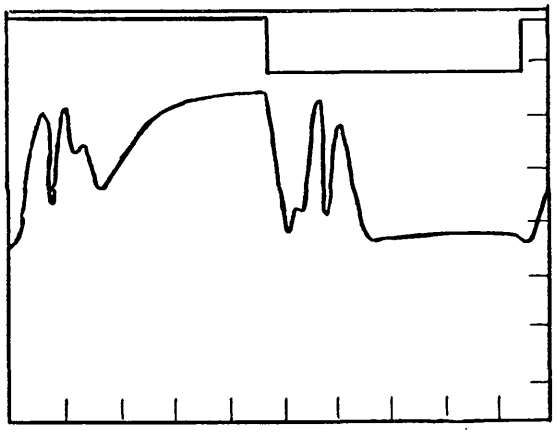

(d) Response to pulses
100 μs, ±35V, TE mode

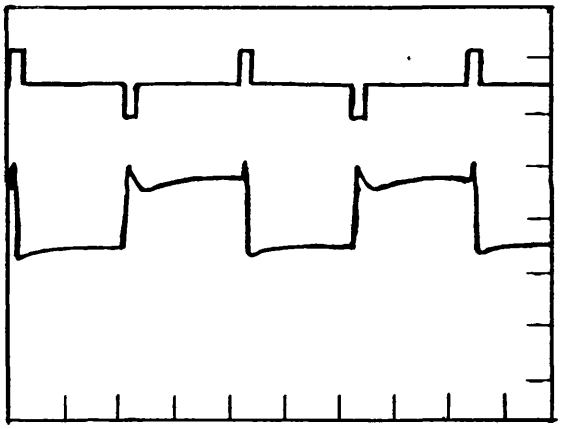

(e) Square wave response
2.5 kHz, 50 Vpp, TE mode

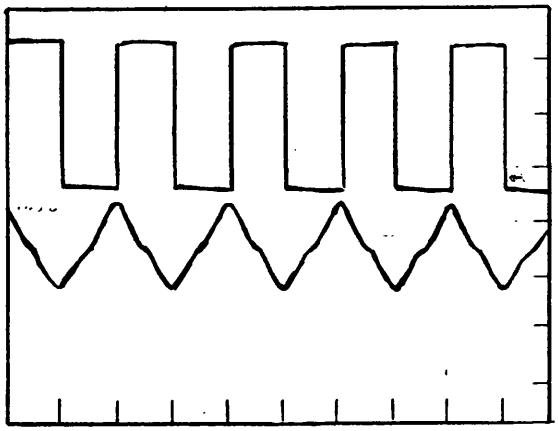

whilst the director switched around the cone caused some waveguiding. (The cone angle was too small for these peaks to be due to the director switching beyond the fibre axis).

The TM mode had the two switched levels the same, which gave zero overall modulation as expected. However during the reorientation process between the two switched states there were four peaks and troughs in the transmission level. One peak would be expected due to the increase in n as the director switched around the cone out of the plane of the block. These other peaks must have been due to waveguiding as the n changed due to this out of plane switching. The waveguiding effects were seen more for the TM mode because it saw a lower n than the TE mode. The 'ringing' in the TM mode was not a dynamic effect due to flow (as can be seen in twisted nematic devices). This can be shown by comparing Figures 6.22c, the dynamic response for a certain polarisation state, and Figure 6.21, the static response for the same polarisation state. These two graphs have the same number of peaks and troughs and similar transmission levels. This effect was therefore not dynamic and was reproducible and stable.

When the polarisation state was changed from the TE mode to TM mode the modulation was inverted by a small amount (~10%) (Figure 6.22b). There were also two different polarisation states for which zero modulation could be obtained but they were at different transmission levels again by ~10%. This could be the affect of waveguiding.

The bistability of the SSFLC modulator is shown in Figure 6.22d for the TE mode when 35V, 100 μs bipolar pulses were applied. The bistability of the device was very good but the switched modulation was less than

when a square wave was used (Figure 6.22a). The transmission of the switched and relaxed levels as a function of voltage are shown in Figure 6.23 for the TE mode. Good bistability was observed which was fairly stable after 4V. The TM mode had no bistability as expected because the two switched levels were the same to start with.

The TE mode remained bistable even when 35 μs, 50V pulses were applied. The quoted response time from BDH of 25 μs could be obtained by heating the device to 30°C and applying 50V pulses. Figure 6.24 shows the minimum pulse width required to obtain bistability as a function of temperature. It can be seen that at 40°C using 50V pulses the device could switch and remain bistable in 16 μs. However to use a FLC fibre optic modulator as a switch it would be necessary to apply a square wave to the device rather than pulses. This produced slower switching and different transmission versus voltage characteristics. This is shown in Figure 6.25. For a 60 Vpp square wave a change in transmission of 30% (as good as the device could be) could be obtained at 2.5 kHz. Modulation could still be observed at 10 kHz although the modulation depth had been reduced by 75%. This switching was 100 times faster than the nematic device. Modulation when a 50 Vpp square wave at 2.5 kHz was used is shown in Figure 6.22e.

Figure 6.26 shows the TE and TM modulation at 100 Hz, 30 Vpp at two wavelengths of light, 633 nm and 820 nm. At 820 nm the modulation depth of the TE mode was larger (85% rather than 50% at 633 nm) and the TM mode always had some modulation. This was due to the difference in the refractive index characteristics of the block plus ITO at the two

Figure 6.23: Transmission changes with applied voltage for the latched and switched states when 1 ms bipolar pulses are applied to the SSFLC modulator for the TE mode

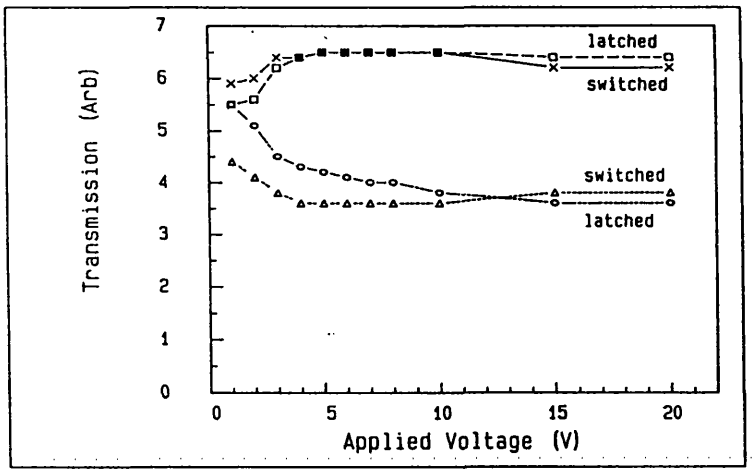

Figure 6.24: The affect of temperature on the minimum pulse length required to maintain bistability using ±50V pulses

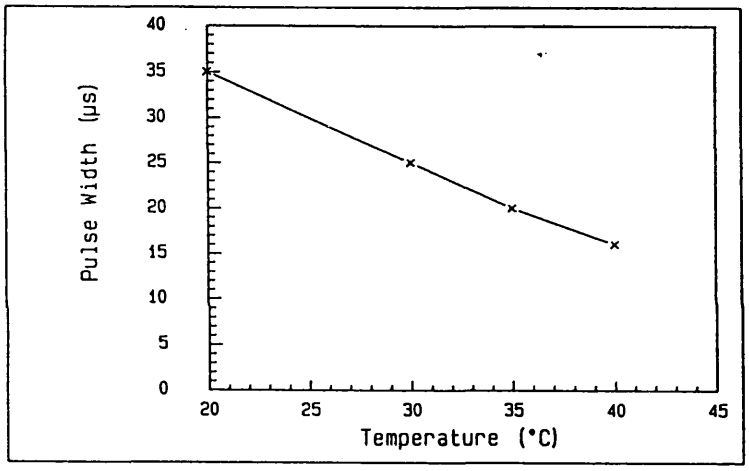

Figure 6.25: Transmission changes with pulse length for the TE and TM modes of a SSFLC fibre modulator

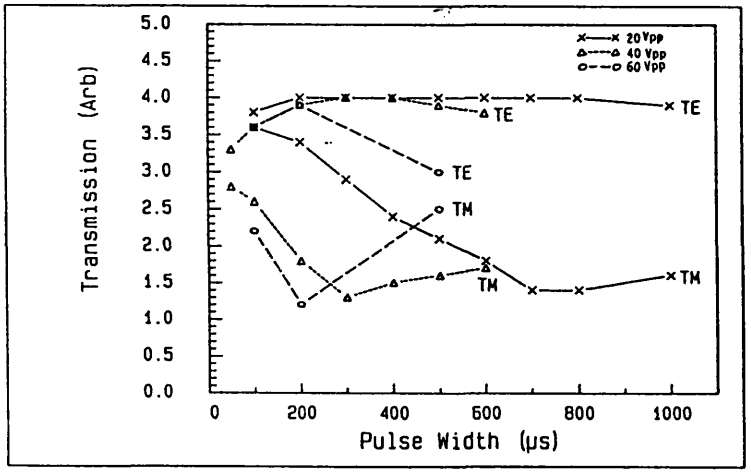

Figure 6.26: The switching characteristics of a SSFLC fibre modulator at 633 nm and 820 nm for a square wave at 100 Hz, 30 Vpp

(a) 633 nm, TE mode

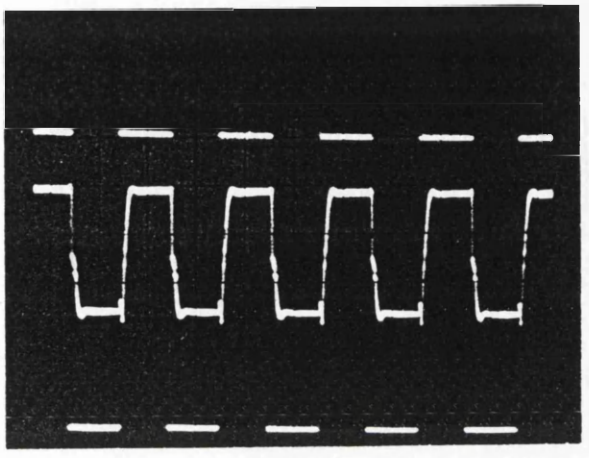

(b) 633 nm, TM mode

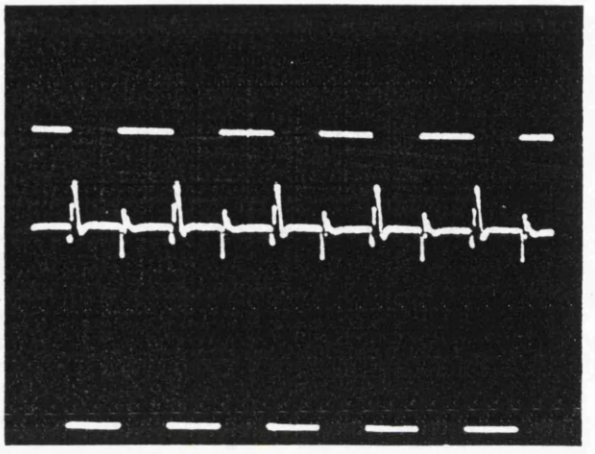

(c) 820 nm, TE mode

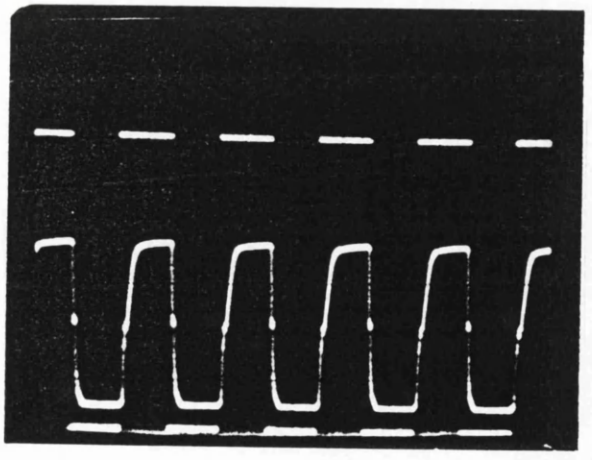

(d) 820 nm, TM mode

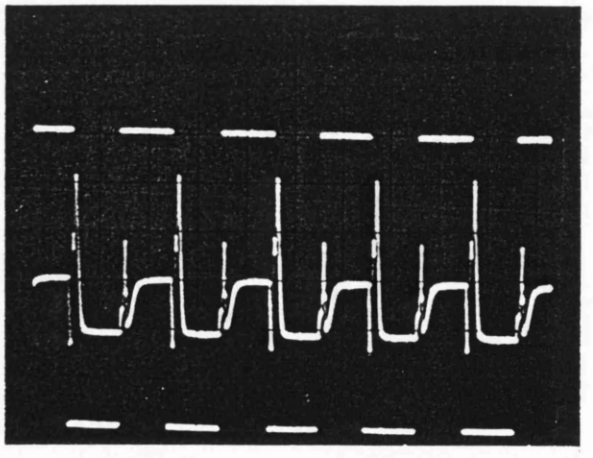

different wavelengths. At 820 nm the block had a higher transmission overall but a steeper difference in transmission at the n_e and n_o values of SCE12.

The alignment direction of the SSFLC modulator was determined by observing the reflected light shining through the FLC using a polarising microscope. The rubbing direction was approximately 55° from the fibre axis and the cone angle was 30°. The switching characteristics observed through the microscope were as expected for 2 μm SCE12 on a polyimide cell. There was no 'ringing' of the optical response when switching, as observed when measuring the output of the fibre. Any ringing observed in earlier experiments must therefore have been due to waveguiding.

6.4.2 A high tilt aligned fibre optic modulator

This device used SiO aligning layers evaporated at 5° to produce a high tilt alignment. The FLC material used was ZLI3654. Although ZLI3654 has a low birefringence it was chosen because it has a fast response time to a square wave when aligned on 5° SiO. The alignment direction of the SiO was along the fibre so that the director switched by an angle θ_c either side of the fibre axis (Figure 6.27). Although this geometry was not ideal it could be used to determine the modulation frequency and to detect any out of plane tilting of the director.

The variation of the maximum transmission as a function of temperature is shown in Figure 6.28 for several heat and cool cycles. The transmission was fairly constant upto about 50°C after which the light started to couple out. The variations in the heat and cool cycles show that the device was not very stable. The device was probably thicker than the SSFLC modulator and could support more waveguiding modes. The

Figure 6.27: Schematic diagram of the HTA FLC fibre modulator

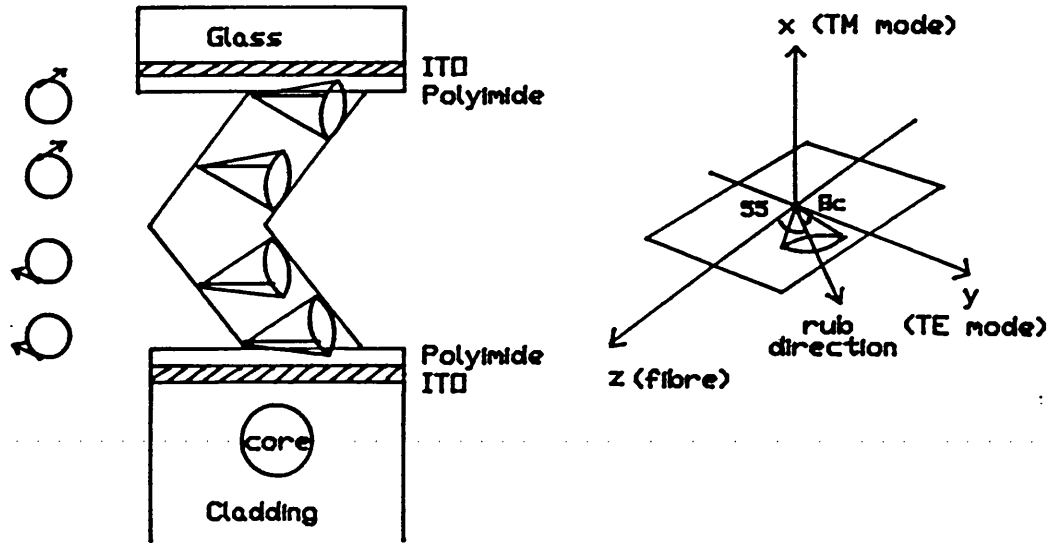

Figure 6.28: Transmission as a function of temperature for a HTA FLC fibre modulator

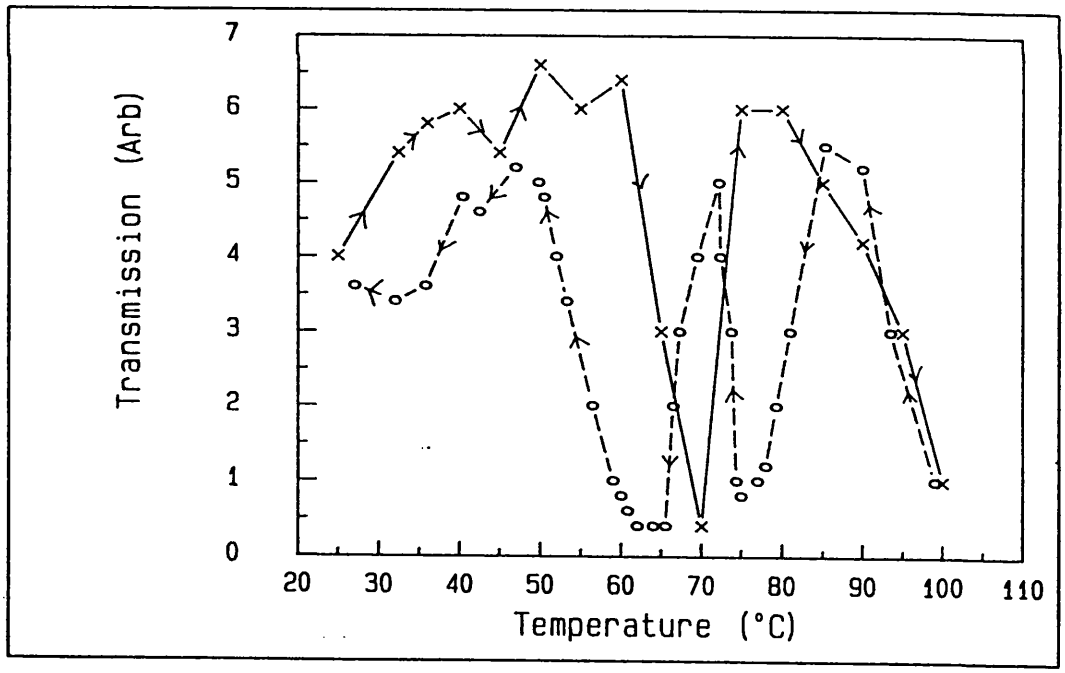

Figure 6.29: The switching characteristics of an HTA FLC fibre modulator to an 8 Vpp square wave at different frequencies

(a) 100 Hz, TE mode

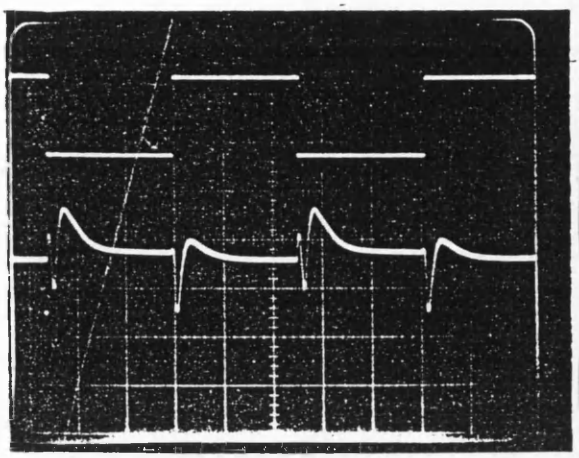

(b) 100 Hz, TM mode

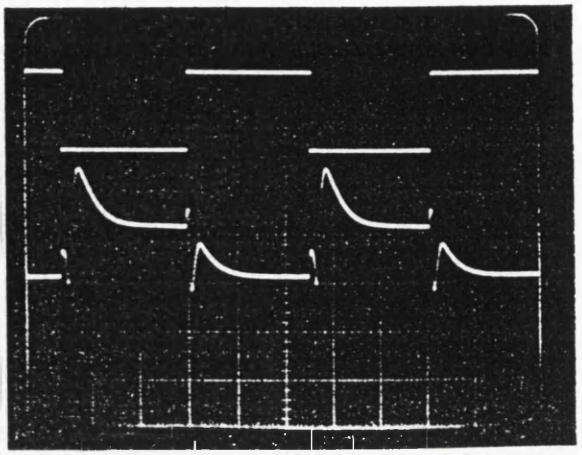

(c) 500 Hz, TE mode

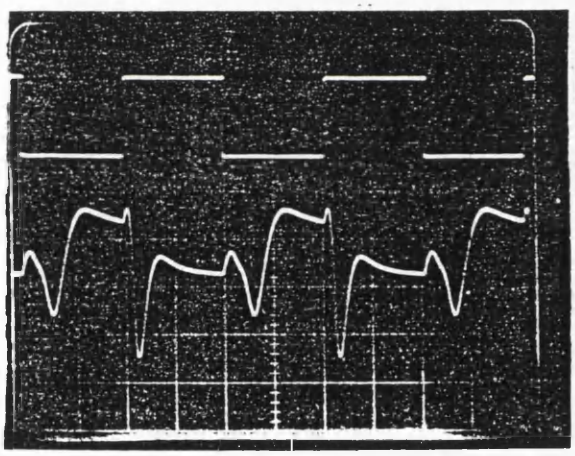

(d) 500 Hz, TM mode

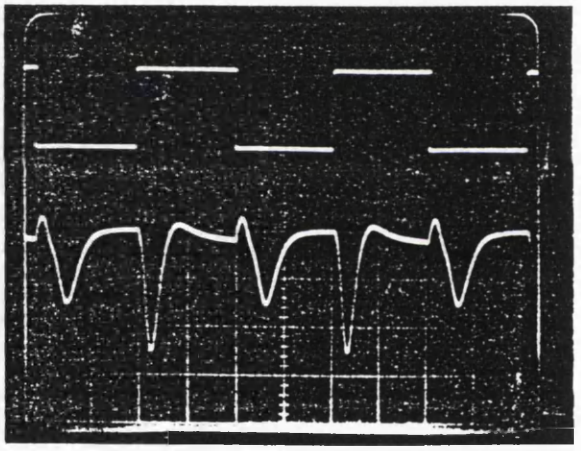

(e) 1 kHz, TE mode

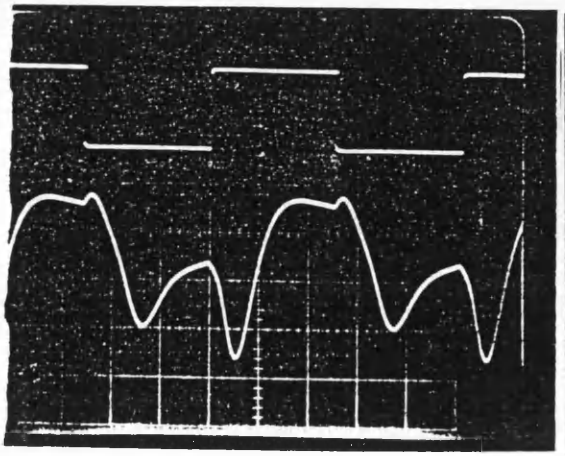

(f) 1 kHz, TM mode

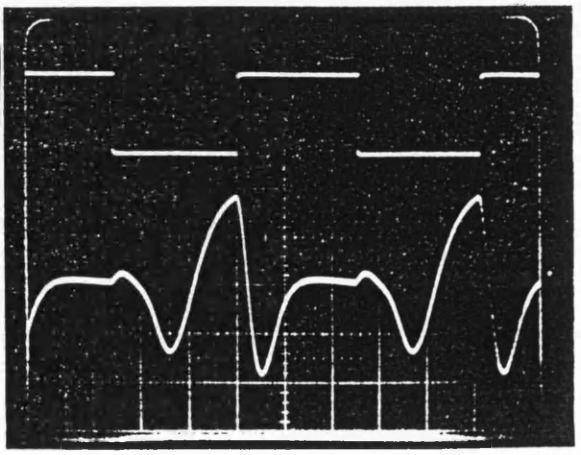

refractive indices of ZLI3654 are also more temperature dependent than SCE12 which would enhance any guiding effects and instability seen as the temperature was increased.

The switching characteristics of the HTA modulator to an applied square wave at 8 Vpp are shown in Figure 6.29. Both the TE and TM modes were modulated as the director switched from one state to the other as did the SSFLC. The TM modulation was due to the change in the out of plane tilt as the director switched around the cone. Since this tilt was the same for both switched states there was no change in TM transmission once full switching had been achieved. As the frequency was increased the FLC did not have time to complete its switching process before the end of the pulse and the TM mode appeared to have a high modulation depth or even an inverted modulation compared to the TE mode. However the modulation did not invert as the polarisation state changed.

The modulation depth of the TE mode was not large because the director switched about the fibre axis. In fact the axis of switching symmetry was 4° from the fibre axis. This was determined by looking through the LC device between crossed polarisers whilst it was switching. The optical transmission of the FLC is shown in Figure 6.30 and the case when θ = -4° was very similar to the TE mode switching in Figure 6.29a. This shows that the peaks were due to the unoptimised alignment rather than waveguiding effects.

Figure 6.31 shows the modulation depth as a function of frequency for an applied square wave of different voltages. At low voltages the curves varied a lot because the FLC was not fully switching and the waveguiding effects were being observed. At 15 Vpp however this had disappeared so

Figure 6.30: Optical response of ZLI3654 on the HTA FLC fibre modulator when polarised light is shone through the device.
15 Vpp, 100 Hz square wave applied.

Scale; 1: 10V/div, 2: 1 mV/div, t: 2 ms/div
θ = angle of polariser to fibre axis

(a) θ = -4°

(b) θ = 24°

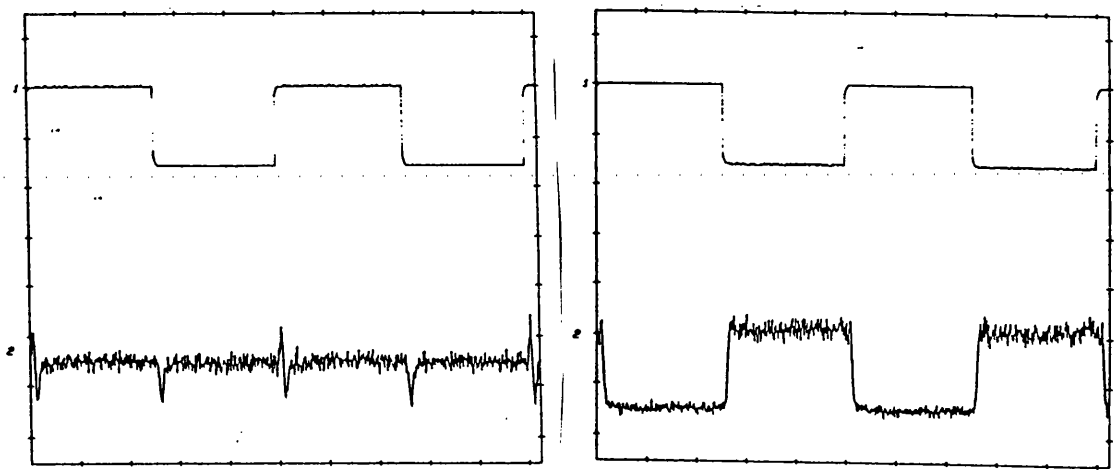

Figure 6.31: Transmission as a function of frequency at different voltages for the TE and TM modes of an HTA FLC fibre modulator

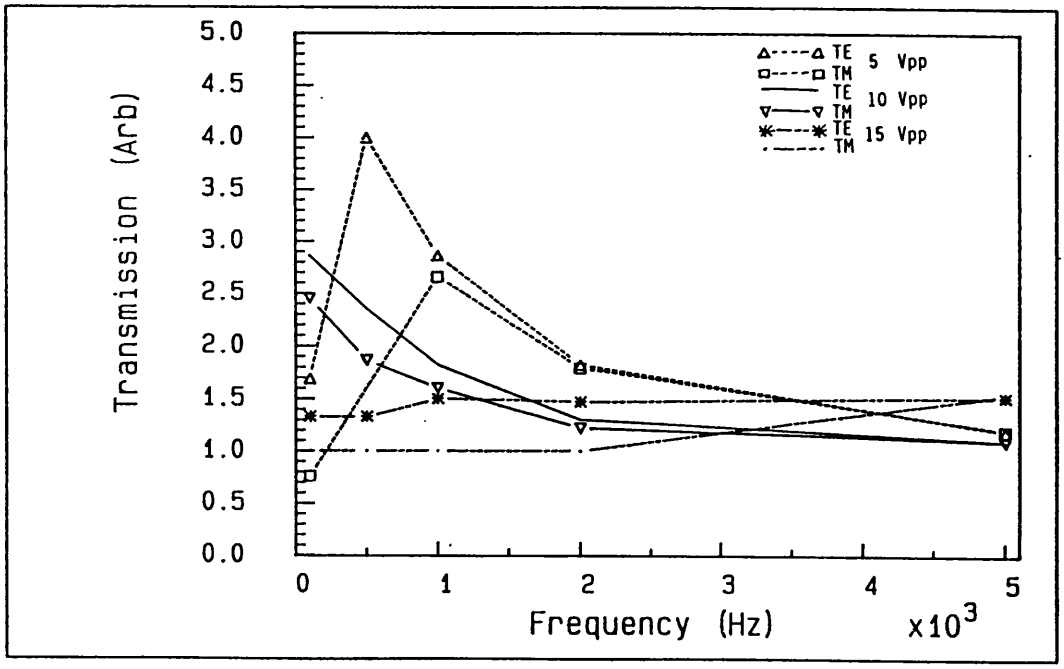

Figure 6.32: The switching characteristics of an HTA FLC fibre modulator to a 40 Vpp square wave at different frequencies

(a) 100 Hz

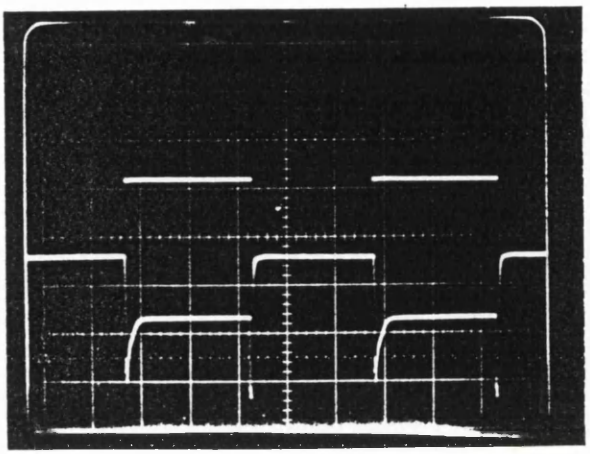

(b) 1 kHz

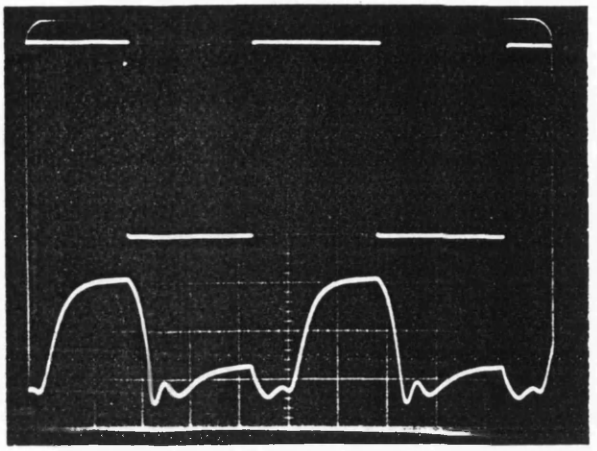

(c) 5 kHz

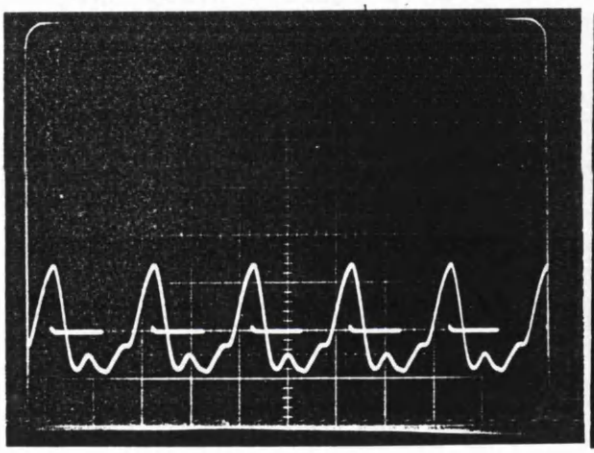

(d) 10 kHz

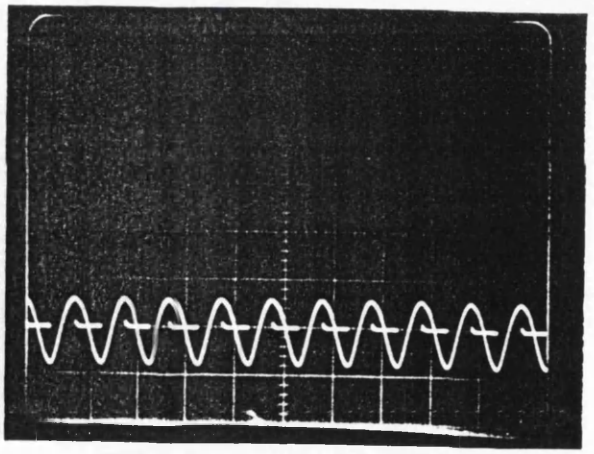

(e) 20 kHz

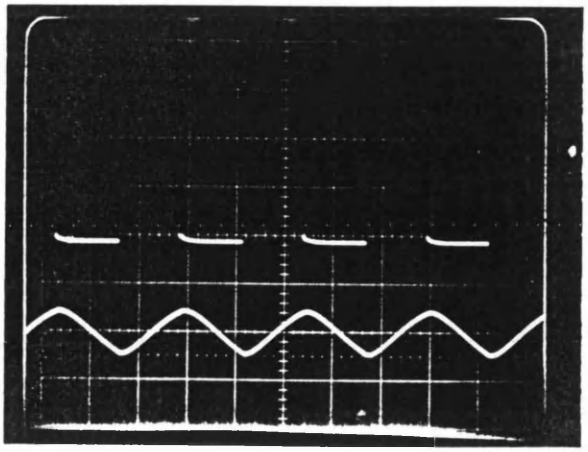

(f) 50 kHz

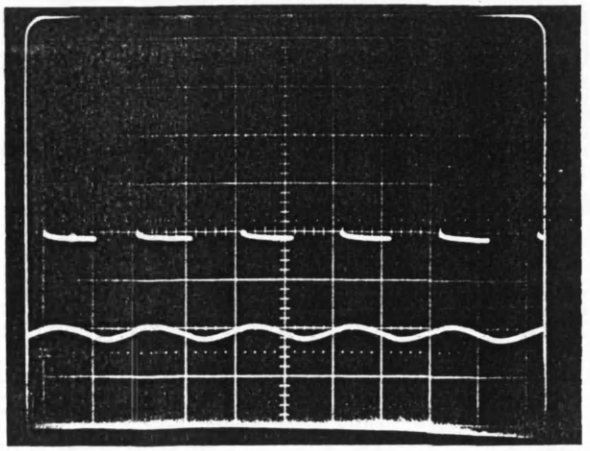

that the TM mode had no modulation and the TE mode had only a small modulation as expected. At this voltage it was possible to still maintain the modulation depth at 5 kHz and a reasonable modulation depth (~50% of maximum) at 10 kHz. This was faster than the SCE12 SSFLC modulator because the FLC material responded faster to a square wave. The response of the modulator to a 40 Vpp square wave is shown in Figure 6.32 for different frequencies. It can be seen that at 10 kHz reasonable modulation was maintained and at 50 kHz some modulation could still be seen.

6.5 Discussion

It has been shown that a nematic liquid crystal (NLC) fibre optic half coupler could produce a polariser with a 45 dB extinction ratio with losses as small as 0.2 dB. The best geometry was found to be a homogeneously aligned NLC with the director at an optimised angle θ to the fibre axes. However, the alignment technique used to produce the polariser would not be a robust device. Sealing the device, as for displays, would be necessary to make it less prone to environmental effects. The temperature stability of the NLC polariser was very good and it had a >45 dB extinction ratio between 10°C and 50°C.

Good all-fibre optic polarisers are important in advanced optical telecommunications and sensors, such as the optical fibre gyroscope, where a strict definition of the polarisation state is essential. The polariser must have a high extinction ratio, be stable to temperature and pressure, have low losses and must be cheap and reliable. The nematic liquid crystal polariser produced here satisfies all these requirements. The existing coiled polarisers are not as good because the losses are higher.

The polarisers produced by resonance absorption through surface plasmons are also not as good as the NLC polariser because they are very temperature dependent. The main competitor to the NLC polariser are the fibre blocks coated with a metal absorber (not a surface plasmon effect). These are very stable to temperature and can produce low loss devices with high extinction ratios.

The NLC modulator that was studied in this work produced a good modulation depth (37.8 dB) but was too slow (100 Hz) to be useful as a modulator. It may be useful as a low speed re-routing switch in telecommunications (if another half coupler is added) where 100 Hz switching is adequate. The losses of this device were 0.33 dB but they could be <0.1 dB when optimised. If a glass slide (or another half coupler) is placed on top of the NLC the losses increased to 1.44 dB but again they could be optimised to <0.4 dB.

The ferroelectric liquid crystal (FLC) devices were shown to produce modulation in excess of 10 kHz but they had low modulation depths. This was due to the high refractive indices of the materials used. New materials can be molecularly engineered to have a lower n_0 in which case the extinction ratio should be as good as for the NLC. The FLC switch is also useful as a re-routing switch in telecommunications (if another half coupler is added) and the faster switching speeds will enable the device to be used in a wider variety of applications than the NLC. Bistability will also be a significant advantage. Some sensor applications need low frequency modulation (kHz), e.g. heterodyne systems, where FLC modulators would be useful.

The SSFLC modulator presented here had fast switching, >2.5 kHz with a square wave applied or 35 μs with pulses, which was as fast as the quoted response time of SCE12 on polyimide. The modulation depth was poor (maximum was 85%, 8.2 dB) because the FLC had unsuited refractive indices. The device had good bistability but the modulation depth decreased for both the switched and latched states when pulses were applied. Out of plane switching could be clearly observed in the TM mode as the director moved around the cone.

The HTA modulator had a faster response time than the SSFLC because it was a faster material when switched with a square wave. However the modulation depth was smaller than for the SSFLC device because the alignment direction was along the fibre rather than at θ_C to the fibre axis. The HTA device was not as stable as the SSFLC because the refractive indices varied more with temperature and the device was probably thicker. The out of plane switching could also be detected in the TM mode of this device. The TM mode could be made to modulate and invert for both FLC devices by increasing the frequency of the applied waveform. This was an artifact of the experiment and was due to waveguiding effects.

The technique of using ITO as a conducting layer coated over the fibre produced excellent modulation results and was a more reliable and robust method than previously reported devices such as Liu et al [1986] where gold electrodes were used. It was also an easier, production compatible technique for producing fibre optic switches and it required lower voltages (~10V) than the other techniques (~100V) because they used a

25 μm separation of the electrodes rather than a 2 μm to 5 μm thickness. The losses due to the ITO were small but the polarisation effects did affect the device properties.

The devices studied in this chapter are only a few of the possible LC fibre optic devices. The electro-clinic effect is particularly important for use in fast switching devices and if used in a FLC fibre optic modulator, switching speeds of >1 GHz may be possible. This device would then be attractive for use as a data modulator. Using LCs as temperature or pressure sensors and biosensors in fibre optics is also possible.

A non-polarisation sensitive modulator could be made using the dynamic scattering effect. If the LC director was aligned along the fibre both TE and TM modes would see n_o. When a field was applied the LC would become random and both the TE and TM modes would see $f(n_e,n_o)$ therefore both modes would modulate in the same way. The losses of this device may be large making it un-useable as a switch.

It has been shown here that LCs are important materials for use in all-fibre optic devices as replacements for the bulk optic components of polariser and modulator. There is need for improvements on the devices demonstrated, (although very little extra work is needed to make a good nematic polariser) and there are other devices that need to be looked at. The limit on the number of existing LC materials with low refractive indices is restricting at present but hopefully more will be produced in the future, in particular suitable FLC materials.

CHAPTER 7

CONCLUSIONS

The aim of this work was to compare the alignment, electro-optic characteristics and device performance of the traditional surface stabilised (SS) alignment to the new high tilt alignment (HTA). This has been done using three different devices; (a) small test cells, (b) large area displays, (c) all-fibre optic modulators.

The internal structure of a surface stabilised cell has been the subject of much discussion. This stems from the observation that there is always some relaxation of the liquid crystal director when the electric field is removed. This has led to the chevron layer structure being proposed by Rieker and Clark [1987]. This relaxation has advantages and disadvantages. It has been shown in this work that when multiplexing SS devices the contrast was only as good as the bistability. In fact it was always less because the SS devices had little or no switching threshold so that there was always some switching due to crosstalk when multiplexing, which reduced the contrast. However the relaxation into an intermediate state allowed the cell to be driven in a reverse bistability mode. This could be used to an advantage when multiplexing because the multiplexing speed was increased and the contrast was improved because the crosstalk was reduced. SS cells also produced very fast response times if pulses were used for the measurement. The cell can relax into an intermediate state during zero voltage after the pulse was applied, therefore less time (or voltage) was needed to switch the

cell out of that state than if it was fully switched. When a square wave was applied, the measured response time could be greater than ten times longer.

It was shown in Section 4.2 that the polyimide aligned FLC had a small pretilt angle at the surface. This made a difference for parallel and antiparallel aligned cells. The chevron layer structure in SS devices meant that zig-zag defects formed where two opposite layer bends met. The antiparallel aligned cells had two equal energy states and therefore had many zig-zags but the parallel aligned cells have unequal energy states and very few zig-zags. The SS display in Section 5.9 was aligned parallel on polyimide. The display could be driven at video frame rates at 30°C and had acceptable viewing characteristics and contrast. However the display was very sensitive to mechanical pressure and electrical spikes. The degeneracy of the chevron structure meant that zig-zags formed very easily. When subject to mechanical or electrical shock the SS displays developed dense zig-zag defects that prevented the display from operating until realigned by heating into the isotropic phase.

The novel high tilt alignment (HTA) presented in this work had many interesting features. It had no zig-zag defects because it had only one layer structure (there was no degeneracy). It was bistable with no relaxation process, and there were two stable 'twisted' states that formed when first aligned.

To examine the importance of the geometry for the high tilt alignment the parallel aligned cells were compared to antiparallel aligned cells. Surprisingly the antiparallel cells also had excellent bistability with

no zig-zags but with only one 'twisted state'. Therefore the geometry was not critical for producing bistability in the high pretilt cells. The bistability was probably related to the surface nucleation and the increased freedom of movement of the surface director.

The parallel aligned high tilt cells multiplexed well to produce excellent contrast since there was no relaxation. Also these cells had higher switching thresholds than the SS cells so that the crosstalk was less. The HTA cells could not be driven in the reverse multiplexing mode because there was no relaxation. The antiparallel high tilt cells did not multiplex at all.

An HTA display was presented which had an excellent contrast ratio and viewing angle. The display was also very mechanically stable because there was no degeneracy of the layers so that zig-zags did not form when the display was pressed. Thicker HTA displays could be manufactured than SS ones. The bistability of HTA cells was retained even up to 6 μm. The optimum thickness for improving the ease of manufacture but retaining low voltages would be 3.5 μm thick, however lower birefringent FLC materials would be required (0.07). The FLC material used in the HTA device was very important. The BDH materials all produced very slow response times in the HTA cells whereas the Merck materials produced similar response times in both the HTA and the SS cells.

In order to produce a FLC display it was necessary to develop new multiplexing schemes with increased flexibility and faster line address times than previously. A novel two slot scheme was developed that was successfully used with both the HTA and SS displays.

The use of liquid crystals with all-fibre optic devices has also been investigated. The refractive indices of existing FLC materials are not well suited to this application therefore a suitable nematic LC was investigated first. An excellent polariser was produced using this nematic LC with a 45 dB extinction ratio and 0.3 dB loss over a 15°C to 55°C temperature range. A novel electrode structure using ITO coated over the fibre was then investigated in order to produce a LC modulator. Although this electrode arrangement produced a good modulation depth (37.8 dB) with low loss (0.4 dB) at low voltages (~10V) the nematic LC limited the modulation speed to <100 Hz.

A FLC modulator was then produced in order to increase the speed. As expected the modulation depth of the FLC modulator was low (85%) because the refractive indices were too high. However a modulation frequency of 10 kHz was obtained from the HTA device and 5 kHz from the SS device when a square wave was used. Effects due to waveguiding in the LC layer could be seen when switching the FLC and advantage could be taken of this to increase the switching speed. In order for FLCs to be used in fibre optics it is necessary to produce FLC materials with $n_o < 1.46$ and $n_e > 1.46$.

This study into the different alignments of FLC materials has shown that there is not one type of device but many. The differences in behaviour between the low tilt alignments and high tilt alignments are analogous to the difference between a twisted nematic display and a supertwist display - they both use the same liquid crystal material but the display performance is different and the material optimisation needs to be different. The choice of alignment to be used will depend on the required application.

REFERENCES

Adamson, A., 1976, 'Physical Chemistry of Surfaces', Pub. John Wiley p246

Alt, P.M. and Pleshko, P., 1974, IEEE Trans. on Electron. Devices, ED-21 p146

Ayliffe, P.J., Davey, A.B. and Zelisse, J.K., 1985, UK Patent No. 2173337A

Bahr, C.H. and Heppke, G., 1987, Mol. Cryst. Liq. Cryst. 150b p313

Beresnev, L.A., Blinov, L.M., Baikalov, V.A., Pozhidayev, E.P., Purvanetskas, G.V. and Pavluchenko, A.I., 1982, Mol. Cryst. Liq. Cryst. 89 p327

Bergh, R.A., Lefevre, H.C. and Shaw, H.J., 1980, Opt. Lett. 5 p479

Berreman, D.W., 1972, J. Opt. Soc. Am., 62 p502

Berreman, D.W., 1983, Phil. Trans. Roy. Soc. London A309 p203

Bishop, D., Jenner, J.A. and Sage, I.C., 1986, Presented at 11th Inter. Liq. Cryst. Conf., Berkeley

Bos, P.J. and Koehler, K.R., 1988, Ferroelectrics 85 p15

Bowry, C., Clark, M.G., Mosley, A. and Nicholas, B.M. 1987a, Proc. Eurodisplay '87, London, p33

Bowry, C., Mosley, A. and Nicholas, B.M., 1987b, Proc. Eurodisplay '87 p152

Bowry, C., Mosley, A., Nicholas, B.M., Letexier, F., Boyer, J.Ph., Le Pesant, J.P., Clerc, J.F., Dijon, J. and Ebel, C., 1988, Ferroelectrics 85 p31

Bowry, C. and Mosley, A., 1989a, UK Patent No. 2208741A

Bowry, C. and Mosley, A., 1989b, UK Patent No. 2208740A

Bowry, C., Mosley, A. and Nicholas, B.M., 1989c, UK Patent No. 2208739A

Bradshaw, M.J., Brimmell, V. and Raynes, E.P., 1986, Liq. Cryst. 2 p107

Brunet, M. and Williams, C.L., 1978, Ann. Phys. 3 p237

Busch, G. and Scherrer, P., 1935, Naturwissenschaft 23 p737

Byrne, J., Kuo, K. and Marsh, H., 1987, Presented at Brit. Liq. Cryst. Soc. Conf., Hull

Castellano, J.A., 1984, Liq. Cryst. Ordered Fluids 4 p763

Chandrasekhar, S., 1977, 'Liquid Crystals', Pub. Cambridge Univ. Press

Chandrasekhar, S., 1983, Phil. Trans. Roy. Soc. London A309 p69

Chan, L.K.M., Gray, G.W., Lacey, D. and Toyne, K.J., 1988, Mol. Cryst. Liq. Cryst. 158B p209

Channin, D.J., 1973, Appl. Phys. Lett. 22 p365

Ciferri, A., Krigbaum, W.R. and Meyer, R.B., 1982, 'Polymer Liquid Crystals', Pub. Academic Press

Clark, M.G., 1988, Private communication

Clark, M.G., Bowry, C., Nicholas, B.M. and Mosley, A., 1987, Presented at Brit. Liq. Cryst. Soc. Conf., Hull

Clark, N.A. and Lagerwall, S.T., 1980, Appl. Phys. Lett. 36 p399

Clark, N.A. and Lagerwall, S.T., 1984, Ferroelectrics 59 p25

Cox, J.S.G., Woodard, G.D. and McCrone, W.C., 1971, J. Pharm. Sci. 60 p1458

Crossland, W.A., Bone, M. and Ross, P.W., 1987, Proc. Eurodisplay '87, London p29

Crossland, W., Morissey, J.H. and Needham, B. 1976, J. Phys. D. Appl. Phys. 9 p2001

Curie, J. and Curie, P., 1880, C.R. Acad. Sci. Paris 91 p294

De Gennes, P.G., 1974, 'The physics of liquid crystals', Pub. Oxford Sci.

Digonnet, M.J.F. and Shaw. H.J., 1982, IEEE J. Quantum Electron. QE-18 p746

Dijon, J. and Ebel, C., 1988, Ferroelectrics 85 p441

Dyott, R.B. and Schrank, P.F., 1982, Electron. Lett. **18** p980

Eickoff, W., 1980, Electron. Lett. **16** p762

Eidenschink, R., Hopf, R., Sheuble, B.S. and Wachtler, A.E.F., 1986, Presented at 16th Freiberg Liq. Cryst. Conf.

Etherington, G., Leadbetter, A.J., Wang, X.J., Gray, G.W. and Tajbakhsh, A., 1986, Liq. Cryst. **1** p209

Friedel, G., 1922, Annl. Phys. **18** p273

Garoff, S. and Meyer, R.B., 1977, Phys. Rev. Lett. **38** p848

Gass, P.A., Mosley, A., Nicholas, B.M., Brown, J.T., Edwards, C.P. and McDonnell, D.G., 1987, Presented at SID Conf., New Orleans

Geary, J.M., 1985, SID Inter. Symp. Digest **16** p128

Goldburt, E.S. and Russell, P.St.J., 1986, Appl. Phys. Lett. **48** p10

Goodby, J.W., 1983, Ferroelectrics **49** p275

Goodman, L.E., McGinn, J.T., Anderson, C.H. and DiGeronimo, F., 1977, IEEE Trans. Electron. Devices **ED-24** p795

Gray, G.W. and Goodby, J.W., 1976, Mol. Cryst. Liq. Cryst. **37** p157

Gray, G.W. and Goodby, J.W., 1984, 'Smectic liquid crystals: texture and structures', Pub. Hill

Gray, G.W., Harrison, K. and Nash, G., 1973, Electron. Lett. **9** p130

Guyon, E., Pieranski, P. and Boix, M., 1973, Lett. Appl. Eng. Sci. **1** p19

Handschy, M.A. and Clark, N.A., 1982, Appl. Phys. Lett. **41** p39

Handschy, M.A. and Clark, N.A., 1984, Ferroelectrics **59** p69

Harada, T., Taguchi, M., Iwasa, K. and Kai, M., 1985, Proc. SID Inter. Symp. Digest **16** p131

Hartshorne, N.H. and Stuart, A., 1970, 'Crystals and the polarising microscope', Pub. Arnold p509

Hatano, T., Yamamoto, K., Takezoe, H. and Fukuda, A., 1986, Jap. J. Appl. Phys. **25** p1762

Hiji, N., Ouchi, Y., Takezoe, H. and Fukuda, A., 1988, Jap. J. Appl. Phys. 27 pL1

Ioannidis, Z.K., 1989, Private communication

Ioannidis, Z.K., Giles, I.P. and Bowry, C., 1988, Electron. Lett. 24 p1453

Ishikawa, K., Ouchi, Y., Uemura, T., Tsuchiya, T., Takezoe, H. and Fukuda, A., 1985, Mol. Cryst. Liq. Cryst. 122 p175

Jannings, J.L., 1972, Appl. Phys. Lett. 21 p15

Jones, J.C., Raynes, E.P., Towler, M.J. and Sambles, J.R., 1989, Presented at Brit. Liq. Cryst. Soc. Conf., Sheffield

Kanbe, J. and Katagiri, K., 1985, UK Patent No. 2156131A

Kashyap, R., Winter, C.S., Nayar, B.K., White, K.I. and Rush, J.D., 1987, Conf. Digest, 'lasers and electro-optics', Opt. Soc. Am. paper WD5

Kobayashi, M., Kawachi, M. and Noda, J., 1982, IEEE J. Quantum Electron. QE-18 p1603

Kondo, K., Nagae, Y., Isogai, M., Kitamura, T. and Mukoh, A., 1988, Jap. J. Appl. Phys. 27 p464

Lefevre, H.C., 1980, Electron. Lett. 16 p778

Lines, M.E. and Glass, A.M., 1977, 'Principles and applications of ferroelectrics and related materials', Pub. Oxford Sci. pl

Liu, K., Sorin, W.V. and Shaw, H.J., 1986, Opt. Lett. 11 p180

Luzzati, V., 1963, Proc. Nucl. Acid. Res. 1 p347

Maltese, P., Dijon, J., Leroux, T. and Sarrasin, D., 1988, Ferroelectrics 85 p265

Martinot-Lagarde, Ph., 1977, J. Physique Letts. 38 pL17

Matsumoto, S., Marayama, A., Hatoh, H., Kinoshita, Y., Hirai, H., Ishikawa, M. and Kamagami, S., 1988, Digest SID '88, Anaheim p41

Matuszczyk, T., 1987, Presented at Rank Prize Symp. on Liq. Cryst., Malvern

McMillan, W.L., 1973, Phys. Rev. A. 8 p1921

Meyer, R.B., Liebert, L., Strzelecki, L. and Keller, P., 1975, J. de Physique 36 p69

Mosley, A., Nicholas, B.M. and Gass, P.A., 1987, Displays 9 p17

Needham, B., 1983, Phil. Trans. Roy. Soc. London. A309 p179

Nesrullaev, A.N., Rabinovich, A.Z. and Sonin, A.S., 1980, Sov. Phys. Tech. Phys. 25 p1445

Nishiyama, S., Ouchi, Y., Takezoe, H. and Fukuda, A., 1987, Jap. J. Appl. Phys. 26 pL1787

Okamura, Y., Kitatani, K. and Yamamoto, S., 1984, J. Lightwave Tech. LT-2 p292

Ostrovskii, B.I., Rabinovich, A.Z., Sonin, A.S., Strukov, B.A. and Chernova, N.I., 1977, J.E.T.P. Lett. 25 p70

Ouchi, Y., Takezoe, H. and Fukuda, A., 1987a, Jap. J. Appl. Phys. 26 p1

Ouchi, Y., Takano, H., Takezoe, H. and Fukuda, A., 1988, Jap. J. Appl. Phys. 27 p1

Ouchi, Y., Takano, H., Takezoe, H. and Fukuda, A., 1987b, Jap. J. Appl. Phys. 26 pL21

Ozeki, T. and Kawasaki, B.S., 1976, Electron. Lett. 12 p151

Parmar, D.S. and Martinot-Lagarde, Ph., 1978, Ann. Phys. 3 p275

Patel, J.S. and Goodby, J.W., 1986, J. Appl. Phys. 59 p2355

Patel, J.S. and Goodby, J.W., 1988, J. Appl. Phys. 63 p80

Patel, J.S., Leslie, T.M. and Goodby, J.W., 1984, Ferroelectrics 59 p137

Pieranski, P., Guyon, E. and Keller, P., 1975, J. Phys. Paris 36 p1005

Prost, J., 1980, 'Liquid crystals of one and two dimensional order', Ed. Helfrich, W. and Heppke, G., Pub. Springer-Verlag p125

Raynes, E.P., 1987, Private communication

Reinitzer, F., 1888, Mh.Chem. **9** p421

Rieker, T.P., Clark, N.A., Smith, G.S., Parmar, D.S., Sirota, E.B. and Safinya, C.R., 1987, Phys. Rev. Lett. **59** p2658

Ross, P.W., 1988, Proc. 1988 Inter. Display Res. Conf. p185

Sage, I. and Chaplin, D., 1987, Electron. Lett. **23** p1192

Sakurai, T., Mikami, N., Higuchi, R., Honma, M., and Yoshino, K., 1988, Ferroelectrics **85** p469

Saupe, A., 1972, Mol. Cryst. Liq. Cryst. **16** p87

Shemm, S.K. and Giallorenzi, T.G., 1979, Opt. Lett. **4** p29

Shimizu, K., Tanaka, Y., Sekikawa, K., Inove, K. and Hori, H., 1986, Proc. Japan Display Conf. p484

Shingu, T., Tsuchiya, T., Ouchi, Y., Takezoe, H. and Fukuda, A., 1986, Jap. J. Appl. Phys. **25** pL206

Small, D.M., 1969, 'Liq. Cryst. 2 Part 1', Ed. Brown, G.H., Pub. Gordon and Breach p209

Uemoto, T., Yoshino, K. and Invishi, Y., 1979, Jap. J. Appl. Phys. **18** p126

Valasek, J., 1920, Phys. Rev. **15** p537

Veilleux, C., Lapierre, J. and Bures, J., 1986, Opt. Lett. **11** p733

Wahl, J., 1988, Ferroelectrics **85** p207

Wahl, J., Matuszczyk, T. and Lagerwall, S.T., 1987, Mol. Cryst. Liq. Cryst. **146** p143

Williams, R. and Heilmeier, G., 1966, J. Chem. Phys. **44** p638

Wulf, A., 1975, Phys. Rev. A **11** p365

Zaschke, H., 1975, Jour. Prac. Chem. **317** p617

Appendix 1: Manufacturer's Data for FLC Materials

All measurements at 20°C unless stated

Company	Material	Host material	Transition temperature				Pitch	
			K-S_C^*	S_C^*-S_A	Smectic-N^*	N^*-I	N^*(μm)	S_C^* (μm)
BDH	MBF ester	SCE1	-3	70	102	126		~10
		SCE2	-7	63	105	131		
		SCE4	-20	57	88	122	>30	
		SCE6	-9	63.4	80.4	120	>30	2.2 (25°C)
		SCE12	-20	66.3	80.8	118	>100 (81°C)	2.4 (25°C)
		16042	<-5	-	63.3	130		
Merck	NCB	ZLI3488	-20	61	66	85	+50 (70°C)	+10
		ZLI3489	-20	65	71	87	-20 (70°C)	+4
		ZLI3654	-20	62	76	86	-60 (80°C)	-5
		ZLI3774	-20	62	76	86	+80	-4
		ZLI3080	5	-	59.5	84.5		16.5
		87-486	-20	-	57	80	65 (63°C)	
		87-703	<-20	-	65	83	+70 (72°C)	+6
Chisso	NCB/pyrimidine	CS1014	0	56				5

Appendix 1: Manufacturer's Data for FLC Materials (Continued)

All measurements at 20°C unless stated

Company	Host material	θ_c	P_s (nC/cm^2)	R_t (μs) (15V/μm)	Δn (589 nm)	$\Delta\epsilon$	Comments
BDH	SCE1		25		0.15	<0	
	SCE2	25	11.8		0.15	<0	
	SCE4	23	6.1	165 (30°C) (10V/μm)	0.19	-1.5	
	SCE6	23.5	15.5	115 (10V/μm)	0.18	-1.7	
	SCE12	20.5	+17.1	74	0.18	-1.8	
	16042	27	19.1				ΔH=0.21J/g (S_C^*-N^*)
Merck	ZLI3488	25.5	+9.7	140	-	-2.2	
	ZLI3489	29	+32.7	90	-	-2.2	inverts pitch at 85°C
	ZLI3654	25	-29	44	0.13	-1	
	ZLI3774	25.5	-28.9	54	0.13	-1	
	ZLI3080	26.9	7.7			+1.7 (65°C)	inverts $\Delta\epsilon$ (probably -ve at 20°C) ΔH~2J/g(S_C^*-N^*)
	87-486	27.5	11.2	145		<0	
	87-703	27	+14.4	65			
Chisso	CS1014	21	5	350 (20Vpp)			Results at 25°C

LIST OF PUBLICATIONS

Ferroelectric Liquid Crystals

Bowry, C., Clark, M.G., Nicholas, B.M. and Mosley, A., 1987, Presented at Brit. Liq. Cryst. Soc. Conf., Hull. "The effects of surface alignment on the electro-optic characteristics of ferroelectric liquid crystal devices".

Bowry, C., Clark, M.G., Mosley, A. and Nicholas, B.M., 1987, Proc. Eurodisplay '87, London p33. "A thick bistable ferroelectric liquid crystal display".

Bowry, C., Mosley, A. and Nicholas, B.M., 1987, Proc. Eurodisplay '87, p152. "Four slot and two slot multiplexing schemes for ferroelectric liquid crystal displays".

Bowry, C., Mosley, A., Nicholas, B.M., Letexier, F., Boyer, J.Ph., Le Pesant, J.P., Clerc, J.F., Dijon, J. and Ebel, C., 1988, Ferroelectrics, **85**, p31. "Alignment treatments for surface stabilised ferroelectric liquid crystals".

Clark, M.G., Bowry, C., Nicholas, B.M. and Mosley, A., 1987, Presented at Inter. Ferroelectric Liq. Cryst. Conf., Bordeaux. "Alignment and electro-optic performance of a 5 μm bistable ferroelectric liquid crystal device".

"A new theory to explain the director and layer alignment in ferroelectric LCDs".

Ioannidis, Z.K., Giles, I.P. and Bowry, C., 1988, Electron. Lett., **24**, p1453. "Liquid crystal all-fibre optical polariser".

Polymer Liquid Crystals

Bowry, C., Presented at IEE Colloquium on Optics in Computing, November 1988, London. "Optical storage using liquid crystal polymers".

Parker, A., McArdle, C.B., Bowry, C. and Haws, C.M., To be published. "Laser-induced optical effects in side chain liquid crystal polymers".

Patents

Ferroelectric Liquid Crystal Devices

Bowry, C. and Mosley, A., 1989, UK Patent Nos. 2208741A and 2208740A

Bowry, C., Mosley, A. and Nicholas, B.M., 1989, UK Patent No. 2208739A

Bowry, C., 1989, Inter. Patent Appl. No. PCT/GB88/00669

Clark, M.G., Bowry, C., Mosley, A. and Nicholas, B.M., US Patent Appl. No. SN:62,159

Polymer Liquid Crystal Devices

Beck, W.R., Bowry, C., Clark, M.G. and McArdle, C.B., Patent Appl. No. 8903658.6

ADDENDUM

It has recently been shown by two different groups [1,2,3] that FLC devices with a high tilt alignment (HTA) have a chevron layer structure with layer angles the same as for low tilt aligned devices. This has important consequences for understanding the HTA device performance. The existence of the chevron structure makes it necessary to revise sections 3.3 and 3.4 and to reanalyse the HTA characteristics in terms of this new director and layer configuration.

Both combinations of a high surface pretilt device have been studied, parallel aligned (HTA) and antiparallel (uniform) aligned. The materials studied behave similarly (ZLI3654, SCE3, CS1014 and CS1013). The anti-parallel aligned device behaves as expected. In the S_A phase there is a single layer tilt of 20-25° (which may bend slightly as the layer pitch shrinks on cooling). In the S_C^* phase the layer tilts more until it reaches about 30-35° at room temperature. This shows that there is a surface pretilt in the smectic phases, of between 20 and 35°. However this surface pretilt is not seen in the parallel aligned high tilt devices. In the S_A phase a small chevron structure can exist with layer tilt angles between 0 and 15°. The exact angle obtained appears to be random because both boundary conditions cannot be satisfied simultaneously. The presence of a 15° layer tilt in the S_A phase means that there is a surface tilt present. In the S_C^* phase the chevron layer still exists with the layer angles increasing, however, they only increase to approximately 20° at room temperature which is identical to the low tilt (surface stabilised) case. There is therefore no evidence [illegible] the surface pretilt in the S_C^* phase. This must mean that the [illegible]face director moves around the cone to lie parallel to the substrate

surfaces. The anchoring energy of the high tilt SiO must therefore be very weak. Rieker et al [3] proposed that this occurs because SiO has a weaker polar interaction than the rubbed polymer. However, a lower anchoring energy need not be related to the polarity of the surface and since 30°SiO (low tilt) behaves similarly to rubbed polymer the polarity of the SiO is probably not important.

The chevron model can be used to easily explain the absence of zigzags because the surface pretilt gives a preference to one layer tilt direction therefore only one chevron layer forms. The increased stability of the HTA device is more understandable than if the layer was straight and perpendicular to the surfaces. As the HTA device is flexed the chevron layer may increase its layer tilt angle to accommodate the decrease in device thickness. Since only one chevron exists there is not the rapid formation of zigzags that occurs in low tilt devices. If the layer in the HTA device was straight then there is no possibility for accommodating the change in device thickness other than by chevron formation, which can tilt in either direction therefore zigzags would form.

The main advantage of the high surface pretilt devices is that they are truly bistable. This is not so easy to understand using either the straight layer or chevron layer models because the antiparallel and the parallel aligned devices both have excellent bistability. Since the director configuration of the HTA device must be similar to the low tilt device (the layers are the same), and the director and layer configuration of the antiparallel high tilt device is totally different, it cannot be the bulk director configuration that is determining the bistability. The excellent bistability must be determined by the

surface properties. The fact that the high tilt surfaces allow the director to move more freely implies that they can also stay parallel to the surface more easily therefore there is less force on the director to move out of the switched position and there is little or no relaxation. This will be true for both the parallel and antiparallel aligned cases. There is a force imparted at the chevron discontinuity in the HTA which will rotate the director around the cone slightly. This is observed experimentally since a relaxation of the cone angle of a few degrees can often be observed when the applied field is removed. If the surface director is parallel to the surfaces then the application of an a.c. stabilising field will make little difference to the director configuration (there may be a small reorientation at the chevron discontinuity) therefore a.c. stabilisation is not necessary.

The ability for the surface director to move easily has also been used by Rieker et al [3] to explain the difference in nucleation between HTA and surface stabilised devices when switching. They found that the surface domain switching is more important in the HTA case because there is a larger change in angle of the director around the cone. This gives a larger contrast between domains with a surface discontinuity then with a chevron discontinuity (opposite than for the surface stabilised case). They also found that the voltage to switch the surfaces was less in the HTA case than the surface stabilised case which would agree with the theory of the surface director switching more easily.

The twisted high tilt states (section 3.4) must be the deformed states that are seen when the surfaces nucleate. As observed, there is only one such state in the antiparallel aligned case and two states in the parallel aligned case (see ref [3]). The appearance of these states on

cooling from the isotropic phase or after not fully switching the device implies that the director can be stabilised either side of the cone even when there is a twist of the director around the cone.

The chevron layer structure found in the high tilt devices is surprising but does in fact explain the device behaviour very well. More evidence is now needed to show the necessary large director reorientation at the surfaces and also further study of the switching behaviour of these devices in terms of the low surface anchoring energy.

References

[1] Ouchi, Y., Lee, J., Takezoe, H., Fukuda, A., Kondo, K., Kitamura, T. and Mukoh, A., 1988, 27 (5) p L725

[2] Ouchi. Y., Lee, J., Takezoe, H., Fukuda, A., Kondo, K., Kitamura, T. and Mukoh, A., 1988, 27 (11) p L1993

[3] Rieker, T.P., Clark, N.A., Smith, G.S. and Safinya, C.R., 1989, Preprint

Additional to section 5.7

[4] Hughes, J.R. and Saunders, F.C., 1988, Liq. Cryst. 3 (10) p 1401